DESIGN & TEST OF A 100 AMPERE-HOUR NICKEL CADMIUM BATTERY MODULE

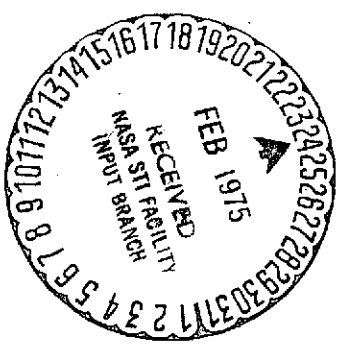

GRUMMAN

DESIGN AND TEST

OF A

100 AMPERE-HOUR NICKEL CADMIUM

BATTERY MODULE

S. Gaston, M. Wertheim, F. S. Burgess
D. Lehrfeld, A. Winegard
GRUMMAN AEROSPACE CORPORATION
Bethpage, N. Y. 11714

March, 1973
Engineering Report

Prepared for:

Manned Spacecraft Center
Houston, Texas 77058

GRUMMAN

NOTICE

This report was prepared as an account of Government sponsored work. Neither the United States, nor the National Aeronautics and Space Administration (NASA), nor any person acting on behalf of NASA:

A.) Makes any warranty or representation, expressed or implied, with respect to the accuracy, completeness, or usefulness of the information contained in this report, or that the use of any information, apparatus, method, or process disclosed in this report may not infringe privately owned rights; or

B.) Assumes any liabilities with respect to the use of, or for damages resulting from the use of any information, apparatus, method or process disclosed in this report.

As used above, "person acting on behalf of NASA" includes any employee or contractor of NASA, or employee of such contractor, to the extent that such employee or contractor of NASA, or employee of such contractor prepares, disseminates, or provides access to, any information pursuant to his employment or contract with NASA, or his employment with such contractor.

GRUMMAN

TABLE OF CONTENTS

TABLE OF CONTENTS (CONT'D)

LIST OF FIGURES

LIST OF FIGURES (CONT'D)

LIST OF FIGURES (CONT'D)

LIST OF FIGURES (CONT'D)

LIST OF FIGURES (CONT'D)

LIST OF TABLES

1.0 INTRODUCTION

This document fulfills a part of the requirement listed in NASA/MSC Contract NAS 9-11074, Exhibit "A", Statement of Work, Paragraph 5.0, Table I, Item 5, "Engineering Test Reports". Specifically, this report covers the design and test of the preliminary Engineering Test Unit of the 4-cell module containing 100 A.H. Nickel-Cadmium cells.

Other reports to be issued under the above-named documentation item include:

- o Cell Development Test Report
- o Battery Test Controller Report

Similar reports will be issued for the Parametric Cycle, Life Cycle, and Development Test Module tests.

This report covers the following technical material concerning Battery Module Development:

- o Review of Requirements
- o Materials Properties and Selection
- o Module Design
- o Module Tests
- o Systems Considerations

Conclusions drawn from the effort to date, and recommendations for the direction of remaining and future effort are also incorporated.

2.0 OBJECTIVE

The engineering model of the four-cell 100 A.H. battery module was fabricated and tested as an intermediate step in the design of qualifiable flight hardware. Specific primary objectives to be accomplished included:

- o Generation of thermal data as a check against design analysis
- o Proof of mechanical (stress) adequacy of design
- o Establishment of manufacturing procedures for the module

Other goals set for this effort included:

- o Check-out and verification of test controllers and data acquisition system preparatory to parametric cycle and life cycle testing
- o Generation of electrical data showing rough-order-of-magnitude dissipation, and voltage and pressure performance for 100 A.H. cells.

The module design was considered sufficiently flexible that information established during the construction and test period could be used to modify the design for the later Development Test Model. Indeed, this proved to be the case, both thermally and mechanically as noted in 7.2.1.2 (elimination of Kapton wrap and tightening cell dimension tolerances) and 6.2.3.1/7.5.1 (butt welded cell dividers).

3.0 SUMMARY

The work reported herein established the feasibility to design and build a flight-worthy replaceable battery module consisting of four (4) 100 A.H. Nickel-Cadmium rechargeable (secondary) cells for large manned space vehicles. This module will weigh less than 43 pounds, will be fully maintainable in a zero "g" environment by one man (without use of special tools), will be temperature controlled by an active environmental control system (as presently planned, and will be a building block for a battery complex with load capability to at least 25 KW.

4.0 REQUIREMENTS, GROUND-RULES AND ASSUMPTIONS

4.1 Thermal and Mechanical

The basic requirements used for module design are those called out in 2.1.1, 3.2.a, and 3.2.b of the Statement of Work, Exhibit A of NASA/MSC Contract NAS 9-11074. Additionally, certain ground-rules were applied as follows:

- o Minimize weight, with 40 lb. as a design goal
- o Minimize fabrication cost, assembly complexity
- o Minimize cell-to-coolant thermal gradient
  - Shortest path (least material minimizes weight)
  - Smallest number of interface elements
- o Avoid use of internal heat pipes unless no other practical alternative exists
- o Do not violate thermal control integrity by module removal/insertion
  - Coolant lines not to be parted
- o Implementation of Line Replaceable Assembly (LRA) module
- o Number of cells/module shall be four

The major assumptions and estimates used were:

- o Worst case orbital average heat generation (dissipation) rate shall be 16 watts/cell (See 5.2.2)
- o Maximum internal cell pressure shall be 100 psig
- o Capability required to incorporate instrumentation, monitor circuits for functional control and/or diagnosis by simple, external modification (See 3.2.c, Statement of Work)

4.2 Electrical

The functional requirements called out in 2.1.2, 3.2.a (25 KW system), and 3.2.c (as required) of the Statement of Work formed the

basis for the electrical design. Additional ground-rules and assumptions were:

- o Insulate each cell from every other cell within the module; in order to avoid cell-to-cell shorts via cell cases or through module structure
- o Maximum steady-state cell current ((4 cells in series) shall be 100 amperes (C-rate)

4.3 Maintainability, Human Factors and Safety

Except for such references as that relating to pressure control and inadvertent escape of electrolyte (3.2.b), the maintainability, human factors and safety requirements of this design are implied rather than explicitly stated in the Statement of Work. Conditions for design, then, have been taken from the Grumman proposal, and have been added to using information derived by coordination with Grumman's ongoing Space Station study group, and with the Space Station Phase B study contractors (McDonnell-Douglas, North American Rockwell). The ground rules thereby obtained and used were:

- o Minimize astronaut effort and time to repair/replace
  - Minimize special training required
  - Use captive mounting hardware
  - Avoid loose hardware in zero "g"
- o Minimize use of tools
  - Avoid application of unbalanced forces
  - Use no "special" tools
- o Design for handling by one man
  - Carrying handles
  - Weight limit (40-45 lb. on earth)
  - Maximum dimension limit (based on mass considerations)

- o Avoid generation of excessive gas pressure
  - No venting of gas (H_2, O_2) or electrolyte (KOH) to cabin
- o Prevent shock hazard to astronaut
- o Prevent damage to module from dropped tool

4.4 Miscellaneous Considerations

Several studies conducted, or in process, by Grumman and others have shown the desirability to design for maximum physical compatibility among the various electrical and electronic components used in Space Station build-up. Thus, it was decided early that, ideally, a complete battery with associated charge controller, circuit protection, and data handling equipment should be mounted together in a rack. Among the in-house programs whose outputs affected the module design in this way were:

- o NASA/MSC Contract NAS 9-10411 - Evaluation of New Approaches to Packaging of Power Assemblies for Use in a Space Environment
- o NASA/MSFC Contract NAS 8-24690 - Development and Verification Of Space Replaceable Housings and Packaging Criteria for Electrical and Electronic Hardware
- o NASA/MSFC Contract NAS 8-27775 - On-Board Monitoring and Management of the Space Shuttle Electrical Power System
- o Solid-State Power Management System - Grumman Advanced Development Program
- o Standard Modularized Power Conditioning Electronics - Grumman Advanced Development Program

Additionally, technical interchanges with the Phase B Space Station Study contractors supported this concept.

5.0 MATERIALS PROPERTIES

5.1 Packaging Materials

Primary consideration was given to:

- o Thermal properties
- o Structural properties
- o Weight limitations
- o Economical fabrication
- o Corrosion resistance
  - During manufacture
  - During integration and prelaunch
- o Compatibility with other materials
  - Electrochemical
  - Thermal expansion
- o Electrical insulation
  - Cell-to-cell
- o Potential safety and/or handling problems

5.1.1 Structural Materials

Candidates for the module structure were finally reduced to three classes:

- o Beryllium and its alloys (Lockalloy)
- o Magnesium alloys
- o Aluminum alloys

Of these, 6061-T6 aluminum was finally chosen based on the properties described below, and shown in Table 5.1-1.

5.1.1.1 Lockalloy

The beryllium alloy seriously considered was Lockalloy, an alloy of beryllium and aluminum. It combines the ductility of aluminum with the high strength of beryllium, resulting in good fabrication (machining, forming and welding) properties with a

strength-to-density ratio only 28% below that of pure beryllium. It exhibits the highest thermal conductivity-to-density ratio of any structural material considered.

The major disadvantages of Lockalloy are:

- o Safety hazards in fabrication
- o Limited availability in widely varied forms and sizes
- o High cost
- o Unknown and/or uncertain corrosion properties

Berylliosis, a chronic, severe lung disease, can be caused by inhalation of beryllium particles. These would be present during any machining or finishing operation, necessitating use of a controlled environment and, possibly, excessively costly shielding for the operator. Furthermore, Lockalloy is a fairly new material. As such, many properties are unknown, and, even where data have been published, changes are occurring constantly. This newness also results in availability limitations of forms and sizes, and high cost noted above.

5.1.1.2 Magnesium Alloys

The alloys evaluated (as listed in Table 5.1-1) are available in virtually all forms and sizes. Although lower in actual yield strength and thermal conductivity than the others, magnesium alloys have strength-to-density and thermal conductivity-to-density ratios comparable to those of the aluminum group. Fabrication and welding properties are generally good to excellent.

Major disadvantages are relatively poor corrosion characteristics, and the high activity level of magnesium (electromotive potential is -1.6 V, placing it at the anodic end of the galvanic series). The resultant requirements for special coatings for magnesium alloys, and prohibitions on coupling to other metals

TABLE 5.1-1

MATERIAL PROPERTIES DATA

Material	Alloy	Density Lb/In^3	Yield Strength KSI	Thermal Cond (K) Btu-Ft/Hr-Ft^2-$^\circ$F	Thermal Exp Coef, In/In-$^\circ$F X 10^{-6}	Yield Str / Density In X 10^3	Thermal Cond/Density, Btu-Ft-In^3/Lb-Hr-Ft^2-$^\circ$F	Machinability	Weldability	Max. Usable Temp., $^\circ$F
Magnesium	MN21A	0.0642	21.6	79.2 (@ R.T.)	14.5 (@ 200°F)	327.1	1233.6	Excellent	Good	700
	AZ31BF	0.064	24.0	44.0	16.0 (68-750°F)	375.0	688.0	Excellent	Good	600
Aluminum	6061 (T6 Cond)	0.098	35.0	96.7	13.0 (@ 200°F)	357.1	986.7	Fair	Excellent	300
	7075 (T73 Cond)	0.101	55.0	90.0	13.2 (@ 200°F)	544.6	891.0	Good	Not Weldable	225
	6101 (T6 Cond)	0.098	28.0	125.8	13.0 (68-212°F)	285.9	1282.0	Fair	Good	--
Beryllium	Leokalloy	0.0756	40.0	118.0	9.2 (77-300°F)	530.0	1560.0	Good	Good	600

(especially those below magnesium in the galvanic series) except aluminum make these alloys difficult to handle. Among other reasons for rejecting these alloys was the fact that the Lunar Module all-welded battery module, fabricated from cast magnesium, had fatigue failure problems.

5.1.1.3 Aluminum Alloys

While most aluminum alloys are more dense than either Lockalloy or the magnesium materials, heat treatment yields strength-to-density ratios similar to the latter, and often exceeding the former. Most of these alloys have good to excellent workability and weldability properties. Highly stable, adherent oxide films can be developed by an anodizing process, and provide excellent corrosion resistance and good dielectric properties, while retaining excellent thermal conductivity (which is better than magnesium in any case). Galvanic corrosion resistance is inherently high, since aluminum is less anodic than magnesium, resulting in safe interfacing with a variety of dissimilar metals.

The alloy chosen, 6061, in a T6 temper, exhibits an optimum combination of high strength, good corrosion resistance, high thermal conductivity, fair workability, and excellent weldability. Furthermore, a wealth of experience in handling this alloy is available, both in-house and elsewhere. Finally, although untreated aluminum is extremely susceptible to KOH (the electrolyte used in nickel-cadmium cells), hard-coat anodizing will prevent any serious corrosion problem from arising.

5.1.2 Encapsulants

The selected design utilizes a potting compound to encapsulate the cells within the module structure for two purposes:

- Provide high heat transfer efficiency between cell and structure

- Provide electrical insulation cell-to-cell to avoid intra-modular shorts and consequent destruction of the cells

The chosen material must fill all voids between the cell case and module structure, and, in addition have the following properties:

- Thermal conductivity $\geq$ 0.5 BTU/hr.-ft.-^{o}F
- Viscosity $\leq$ 30,000 centipoise (preferably less than 10,000 centipoise)
- Cure at 110^{o}F maximum
- Low outgassing and shrinkable
- Low coefficient of thermal expansion relative to aluminum
- Crew compatible, after curing, in a Space Station environment

Three candidate materials were subjected to detailed evaluation:

- Stycast 2850 FT (Emerson and Cuming Incorporated)
- Ableth erm 7-3 (Ablestick Lab, Incorporated)
- Delta Cast 153 (Wakefield Engineering, Incorporated)

Stycast 2850 FT was chosen based on its previous qualification on the Lunar Module program, and the evaluation results noted below.

A fixture and dummy cell were designed and fabricated to develop a reliable encapsulation procedure.

This fixture, shown in Figure 5.1-1, is a five-sided box made of clear plastic (plexiglas). Sides and base are bolted together for each test, and may be disassembled by unbolting. Mold release was used to coat the dummy cell and fixture inner walls to permit evaluation of the encapsulant after disassembly. Each compound and/or procedure was observed through the transparent walls for such qualities as flowability, leveling and bubble entrapment.

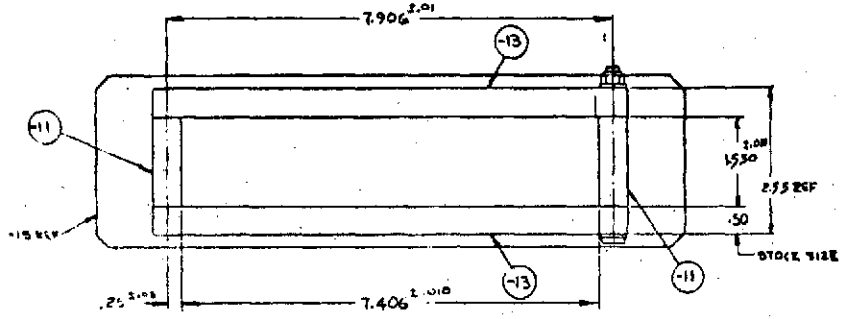

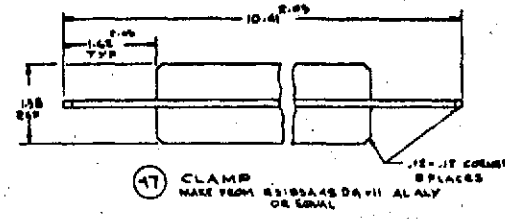

(-17) CLAMP
MAKE FROM 6061-T6 OR T-11 AL ALLY OR EQUAL

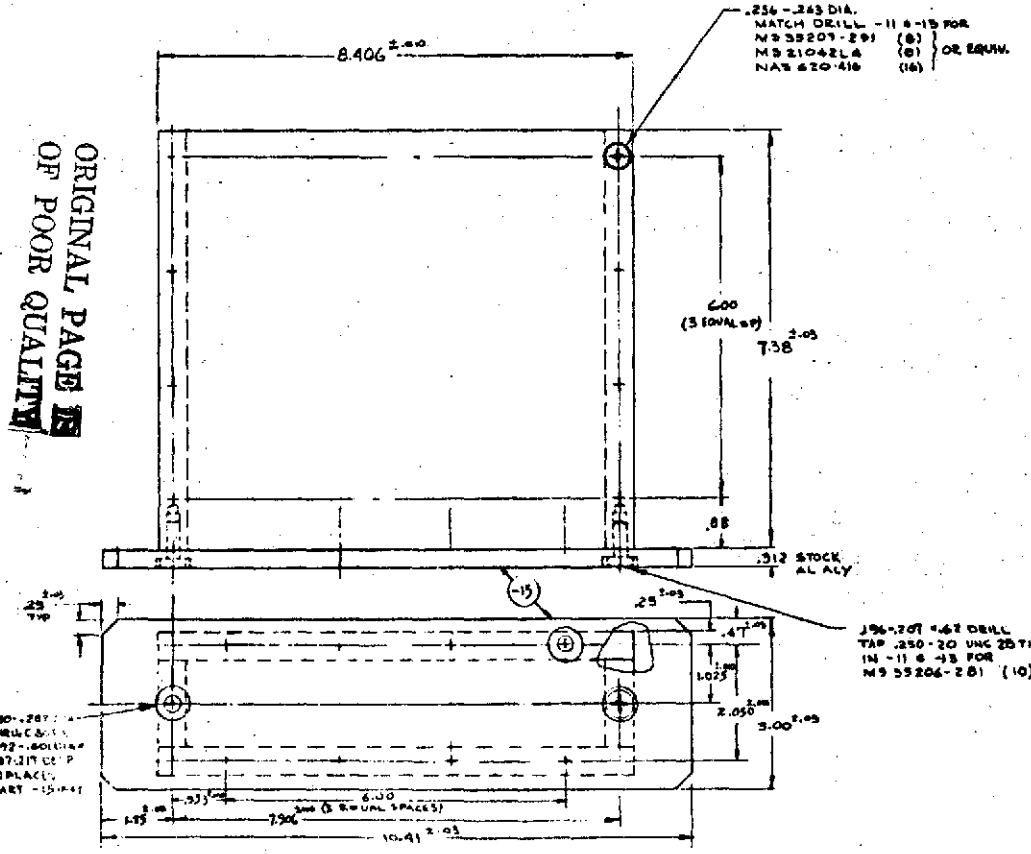

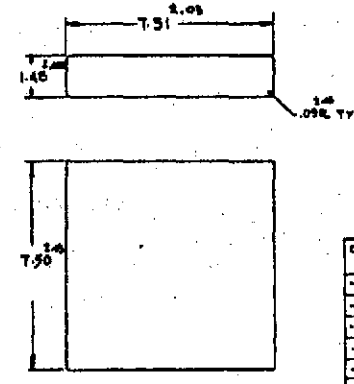

(-19) CELL SIMULATOR
MAKE FROM HARDWOOD
FINISH WITH VARNISH OR ACRYLIC
ALL DIMS ARE AFTER FINISH
(SCALE 1/2)

NOTES:
1- BREAK ALL EDGES ON PTS -15 & -17
2- PART -19 MAY BE MADE FROM ALUMINUM.

PARTS LIST

DASH NO	NAME	MAT'L	NO REQD
-11	END	[illegible]	2
-13	SIDE	[illegible]	2
-15	BOTTOM PLATE	AL ALLOY [illegible]	1
-17	CLAMP	[illegible]	1
-19	CELL SIMULATOR	WOOD [illegible]	1
—	SCREW	MS 35207-291	8
—	SCREW	MS 35206-281	10
—	WASHER	NAS 620-416	16
—	NUT	MS 21042L4	8

CELL POTTING FIXTURE
559-10BAV
SCALE: FULL
JOB NO. 249-901

F16 5.1-1

GRUMMAN AEROSPACE

5.1.2.1 Evaluation Results

Both Stycast 2850 FT and Delta Cast 153 performed very well. The former had good flow characteristics when catalyzed, outgassed well, and had a pot life of at least 30 minutes (long enough for the intended use). The Delta Cast was essentially identical.

Aside from the qualification for LM noted above, the following reasons were used to justify selection of 2850 FT over Delta Cast 153:

- o Flammability and outgassing requirements for manned space use is already proven
- o Actual data confirming thermal conductivity (0.5 BTU/hr.-ft.-^{o}F) is already available

While the manufacturer claims the same characteristics for Delta Cast 153, the claims are not currently supported by objective data or experience in another manned space program.

Ableth®erm 7-3 proved unacceptable. Pot life was only 8 to 10 minutes when the material was mixed and handled in accordance with the manufacturer's recommendations. This time was deemed insufficient for the intended use.

5.1.3 Cell Interconnections

The material chosen was high conductivity copper in accordance with Federal Standard QQ-C-576. The straps are nickel plated for optimum corrosion protection per QQ-N-292 CL2, Type VI.

The only alternate considered was aluminum. This was rejected as it could not be protected against KOH attack without some form of oxide coating, which is an electrical insulator.

5.2 Thermal Properties of Ni-Cd Cells

5.2.1 Physical Properties

A literature search was performed early in the program to determine the thermal conductivity and specific heat of nickel-cadmium cells. This information was needed to establish the cell thermal math model to be used in the packaging optimization studies (see Section 6.1). Since much experimental work had already been done in this field by other investigators, new testing under the scope of the present contract was not contemplated. Instead, it was decided to determine the magnitudes and variability of the numbers reported in the literature, and investigate their effect on the package optimizations making conservative assumptions wherever a choice was needed.

Table 5.2-1 (a) illustrates the range of thermal conductivity values reported for 6 to 20 AH prismatic Ni-Cd cells. As can be seen in the table, the variation from minimum to maximum is considerable illustrating both the difficulty in obtaining accurate test results and the variation of construction parameters from cell to cell. No values for thermal conductivity in the terminal to cell bottom direction are reported in the literature, due primarily to the experimental difficulty caused by the presence of the terminal on the cell's header. In the math model, it was assumed that the conductivity in this direction was equal to that in the "parallel to the plates" direction.

Table 5.2-1 (b) presents the range of values reported in the literature for the average specific heat of Ni-Cd cells. As can be seen, the reported values vary widely.

These large variations in the values reported for the thermal properties of Ni-Cd cells represent one reason for deciding to conduct the packaging optimization studies using steady state rather

TABLE 5.2-1(a)

Ni-Cd Cell Thermal Conductivity

Conductivity (cal/sec.-cm-^{o}C)

Direction	Min.	Max.	$\frac{\text{Max.}}{\text{Min.}}$ x 100
Normal	0.0020	0.0086	430%
Parallel	0.0055	0.126	2290%

Top to Bottom: not reported in literature

TABLE 5.2-1(b)

Ni-Cd Cell Specific Heat

Min. (cal/gm-^{o}C)	Max. (cal/gm-^{o}C)
0.20	0.38

than transient thermal analysis techniques.

5.2.2 Ni-Cd Heat Generation

Since the module design phase proceeded in parallel with the cell development phase of the program, no actual calorimetric data for 100 A-H size cells existed initially. It was decided to use extrapolated OAO cell (20 A-H) characteristic data to estimate the heat generation rates which could be expected from the 100 A-H cells.

Table 5.2-2 shows these average expected heat generation rates during charge and discharge vs. depth of discharge and type of charge control. Of particular interest is the 50% DOD, voltage limit charge control case. This case was selected as the design point for packaging optimization studies since it is at the most severe end of the operating range thermally.

A calorimetric test program, included in the scope of the cell development effort, was established to provide heat generation rate data for the final design cells. These data will be incorporated into Phase II of the module development program when they become available.

The rate at which heat is liberated during discharge corresponds to a dark period of 36 minutes. The charge period is 58 minutes. Since the selection of an optimum charge control scheme is another parallel effort to the cell packaging phase of the program, estimates for heat generation during charge were made for various generic types of charge control. "Auxiliary Electrode Signal Cutoff" implies that the signal from an auxiliary electrode is used to terminate charging at a state of charge less than 100%, precluding any operation whatsoever in the overcharge region. Such a scheme, were it feasible, would result in the lowest heat generation during charge. "Auxiliary Electrode Signal Limit" control implies that the signal from an auxiliary electrode would be used to indicate that 100% state of charge has been reached. This signal is presumed to be sensitive enough to limit operation in

the overcharge regime to a minimum. "Voltage Limit" implies that a predetermined maximum voltage vs. temperature and charge rate relationship exists which will permit cutting the charge rate back in preset increments whenever the limit voltage is reached.

The last case was conservatively assumed for the thermal studies. It was left to Phase II of the module development to re-examine this assumption in light of the performance data on third electrode charge control, which is expected to be available at that time.

TABLE 5.2-2

Estimated 100 A-H Ni-Cd Cell Heat Generation

Characteristics

Depth of Discharge %	Q Discharge, Watts	Q Charge, Watts		
		Voltage Limit	Auxiliary Signal Limit	Auxiliary Signal Cutoff
12	3.63	4.07	3.50	~0.
30	8.75	10.00	8.60	~0.
50	14.00	16.45	14.15	~0.

6.0 MODULE DESIGN

6.1 Thermal Design

The selected design is "Alternate Concept No. 2", Figure 6.1-19.(page 43). This design meets the desired maximum cell temperature (68°F) under the thermal environment conditions shown in 6.1.1 below. Cell to cell gradients are also minimized, and weight penalty attributable to thermal control is less than 6 lb.. Approaches,analytic techniques and candidates studied are given in 6.1.1 through 6.1.3 below.

6.1.1 Thermal Design Approach

The goal of the module's thermal design is to control the temperatures of the cells to no lower than 32°F (0°C) and no higher than 68°F (20°C) over the entire range of electrical operating regimes and thermal environments which can be expected in an Earth Orbital Space Station. In addition, the maximum variation of temperature among the cells should be less than 8°F (5°C).

The assumed module thermal environments were derived from Space Station prime contractor studies and are summarized below:

a. Pressure: 0 to 14.7 psia

b. Air temperature: 65 to 75°F

c. Bulkhead temperatures: 40 to 105°F

d. Active cooling for battery (water loop)

32°F (minimum)

40°F (nominal)

55°F (maximum)

30 pounds per hour per module

e. Gravity field: 0 to 1 g

Of the items in the list above, both the maximum coolant temperature and flow rate assumptions made for the study require further elaboration. Working under the original terms set forth in its proposal, Grumman proceeded with the design of the module assuming a maximum coolant

temperature of 40°F. Space Station studies at the time indicated that this was the maximum steady-state temperature to be expected in the battery portion of the ECLS system. Near the start of the study, cognizant NASA personnel advised Grumman that at this early stage of the Space Station's development, a module which could tolerate a wider range of acceptable inlet coolant temperatures would be more desirable. A thirty-pound-per-hour flow rate and 55°F inlet temperature was selected as the worst case conditions to be assumed for the purpose of a trade-off study of module design alternatives. 55°F was selected for two reasons:

a) it was the maximum coolant temperature which could be assumed and still achieve a reasonable package design with a constraint of 68°F on the maximum cell temperature, and

b) it was a temperature which should be well within the capability of the ECLS system.

Thirty pounds was selected as a nominal design flow rate since it was a value which kept the temperature rise in the coolant along the direction of flow to a moderate level. If the module is considered to be cooled by the average of the coolant inlet and outlet temperatures, it can be appreciated that too small a flow rate can cut drastically into the 13°F (68°F-55°F) available temperature gradient between the hottest cell and the coolant inlet.) The implications of these assumptions on the integration of the entire battery system into the station's ECLS system will be presented in Section 8.0.

These environments were combined with the electrical operating regimes to define "max. cold" and "max. hot" thermal conditions. Briefly, the "max. cold" case considers the battery to be in standby ("floating"), with 32°F inlet coolant temperature and 40°F bulkhead temperatures. Under these conditions, the 32°F minimum cell temperature

requirement is automatically met.

The "max. hot" case is the one which dictates the thermal design of the module. The module is assumed to be cycling to a discharge depth of 50% in a 14.7 psia, 75°F air environment in a 1 "g" field. Surrounding bulkhead temperatures are assumed to be 105°F and the coolant to the module is 55°F.

Presented below is a discussion of the trade-off study performed to select the recommended module design. The analysis technique used, the configurations examined and a comparison of the candidate designs is included.

6.1.2 Thermal Analysis Technique

Maximum use was made of a Grumman developed thermal analysis program, GTA-1. This is a Fortran IV program for the IBM 360/75 system for solving heat transfer problems by the "lumped parameter" (nodal analysis) technique. In this method, one makes the assumption that a heat transfer problem can be represented by an analogous network of thermal conductors and thermal capacitors. Within this network, the distributed heat capacitance of the object is concentrated or "lumped" at discrete nodes and the distributed conductance is concentrated in discrete conductors connecting the nodes. Any area which may be considered isothermal may be used as a node in such a network.

The solution of a heat transfer problem is thus reduced to the solution of its analogous network. The program performs a heat balance on each node and uses the numerical method of forward differences to determine the temperature distribution in the network at an incremental time in the future based on the present temperatures and heat generation sources within the network.

Depending on the problem requirements, one may obtain either a temperature history of each node or only the final temperature dis-

tribution. Hence, either "transient" or "steady state" heat transfer problems can be treated.

The approach taken in the packaging study was to create an analagous nodal network for each candidate configuration and investigate the effect on the cell case temperature distribution by varying the thickness of various thermal paths. By taking advantage of the symmetry of each configuration, only a fraction (typically $\frac{1}{4}$) of the four cell module required simulation. The math model given in the figures described below is for one of the early packaging concepts (subsequently discarded) but serves as an illustration of the method.

Figure 6.1-1 shows the portion of the module simulated by the model. Figure 6.1-2 gives the detailed nodal breakdown used in the analysis.

Nodes 1 through 6 represent the mass of one half cell #1 (excluding the case). The nodes are interconnected by thermal conductors whose value is based on the values of cell conductivity (parallel and normal to the plates) reported in the literature (see Section 5.2). At first, both the maximum and minimum values of conductivity were used to see their effect on the cell case temperature distribution. Those values which produced the worst distribution (minimum reported conductivities) were conservatively assumed in all later studies. The heat generated in the cell is assumed to be distributed in nodes 1 through 6 in direct proportion with their respective masses (nodes 1, 2 and 3 each represent 1/18 of the cell, while nodes 4, 5 and 6 each represent one ninth of the cell).

Nodes 7 through 30 represent the 0.031 inch thick 304 stainless steel cell case. The nodes are interconnected with conductors whose values are based on the conductivity of 304 stainless as reported in the literature. The case nodes are connected to the plate nodes by conductors calculated from the appropriate parallel-to-the-plates, or

FIGURE 6.1-1

MODEL of SIMULATED MODULE

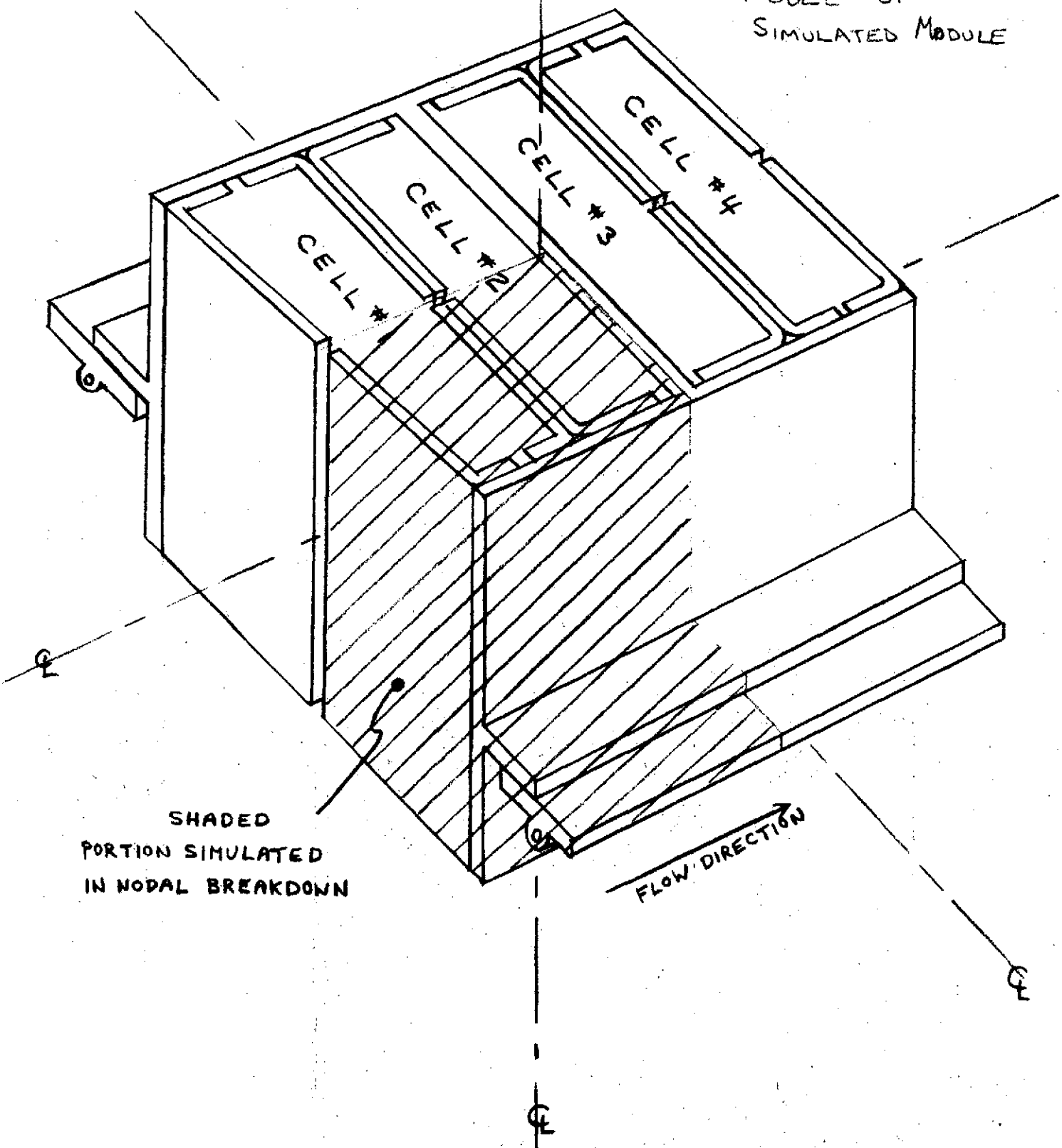

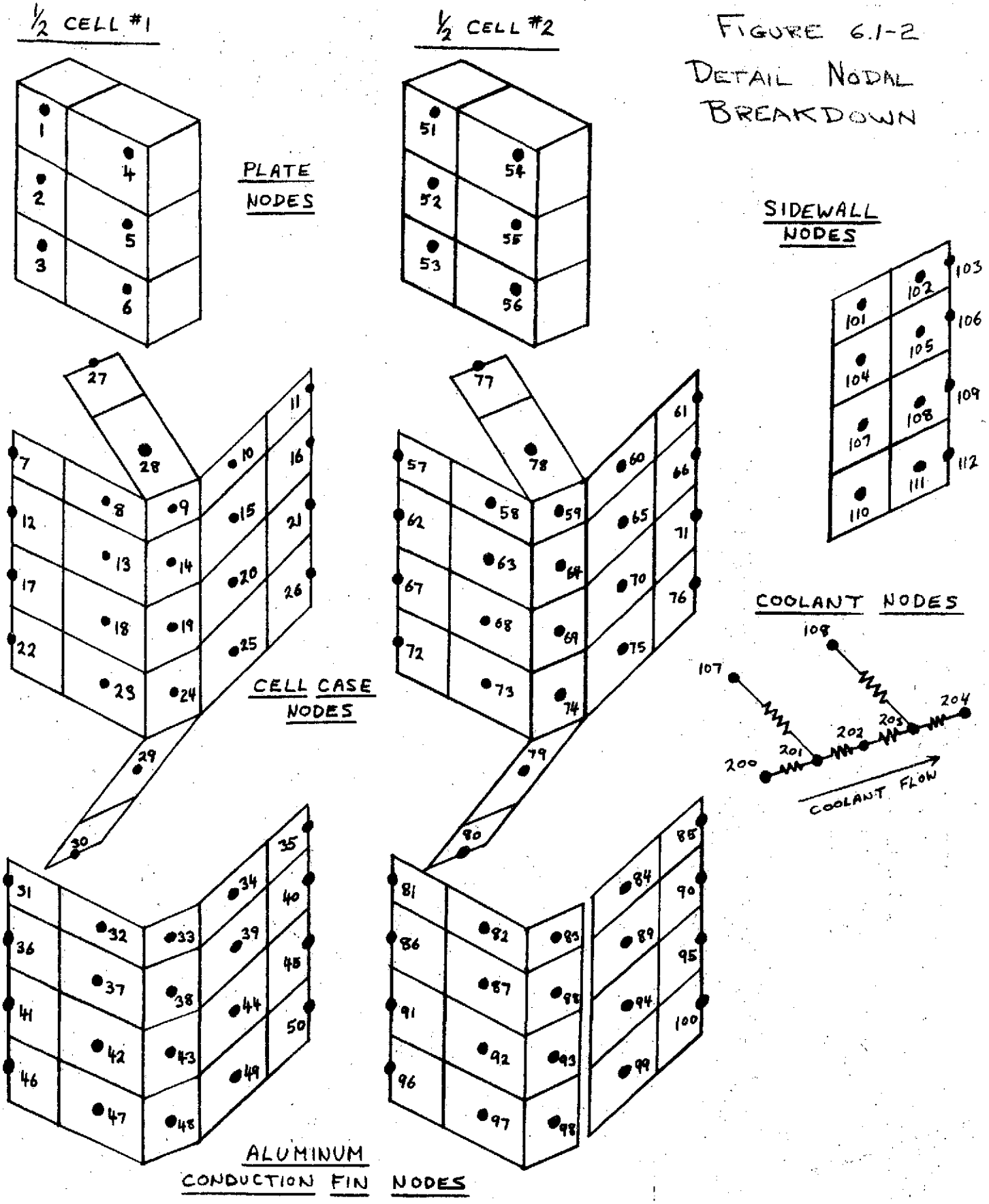

FIGURE 6.1-2
DETAIL NODAL BREAKDOWN

normal-to-the-plates cell conductivity. The heat path from the plates to the cell header through the tabs, terminal, ceramic seal, etc. was conservatively omitted.

Nodes 31 through 50 represent the aluminum conduction fin which carries heat from the broad side of the cell to the sidewall of the module. The nodes are interconnected by variable conductors whose initial value is calculated based on a material conductivity of 100 Btu/(hr.-^{o}F-ft.)and material thickness of 0.025 inches. These conductors are parametrically varied in subsequent runs by multiplying the initial values by a constant; thereby effectively varying the fin thickness. The fin nodes are connected to the cell case nodes by conductors whose values simulate the conduction across a Kapton tape and potting interface. A .001 inch layer of Kapton (k = 0.1 Btu/(hr.-^{o}F-ft.)) and .050 inch thick layer of potting (k = 0.5 Btu/(hr.-^{o}F-ft.)) was assumed.

Nodes 51 through 100 are the corresponding cell, cell case, and aluminum fin nodes for cell #2.

Nodes 101 through 112 represent the module's aluminum sidewall. They are interconnected by variable conductors whose initial values are based on a conductivity of 100 Btu/(hr.-^{o}F-ft.) and a thickness of 0.050 inches. The thickness can parametrically be varied by multiplying these conductors by constant values other than unity.

Nodes 200 through 204 represent the coolant (water) flowing in the module's cold rails. Node 200 was assumed constant at 55^{o}F and the flow rate was 15 pounds per hour per rail (design values).

Nodes 107 and 108 are connected, respectively, to nodes 201 and 203 by conductors representing the flange root to coolant conductance. The design value assumed for this conductance was 2.5(^{o}F-in.)/watt.

It was decided that the large variance in the reported material

property of Ni-Cd cells (cell conductivity, specific heat) and the lack of data on the orbital heat generation rate characteristics of 100 A-H size cells made it inadvisable to attempt transient thermal analyses of the candidate module configurations. Rather, a conservatively estimated average orbital heat generation rate was assumed (Section 5.2) and a steady state technique was utilized.

This approach permitted a comparison of the packaging designs on a equal basis and the timely selection of a recommended design. The assumption that a conservative, steady state analysis would be as stringent a requirement as a transient analysis was later verified during thermal tests on the engineering module.

6.1.3 Candidate Configurations

Both the limitations in allowable cell to coolant temperature rise ($13^{\circ}F$), and the desirability of minimizing intra- and inter-cell gradients within the module, limit the number of practical thermal control schemes available. Presented below are the schemes most seriously considered.

Figure 6.1-3 shows the original baseline design considered early in the program (its nodal model was used as an illustration in 6.1.2). Though only suitable for low temperature cooling ($40^{\circ}F$), and therefore no longer an adequate concept, it does serve to illustrate a discussion of the thermal problems which are confronted when attempting to package large size cells.

As can be seen in Figure 6.1-3, the heat generated within each of the four 100 A-H cells is transferred through the broad faces of the cell (across a thermal interface composed of dielectric tape and encapsulant material) to thermal fins adjacent to these faces. This heat is then transferred along the thermal fins to the sidewalls of the module (across a welded interface), along the sidewalls to the mounting flanges, and from the mounting flanges (through a bolted interface) to cold rails. In addition, part of the generated heat is transferred from the narrow faces of the cell (across a thermal interface composed of dielectric tape and encapsulant material) directly to the sidewalls. No use is made of the terminal (header) and bottom ends of the cells since the thermal path length from these surfaces to the cold rails is too long to be effective.

Using the analysis technique described in the preceding section, Figures 6.1-4 through 6.1-9 were generated to illustrate the relative contributions of the various thermal paths to the overall cell to coolant temperature gradient.

BASELINE MODULE THERMAL SCHEMATIC

FIGURE 6.1-3

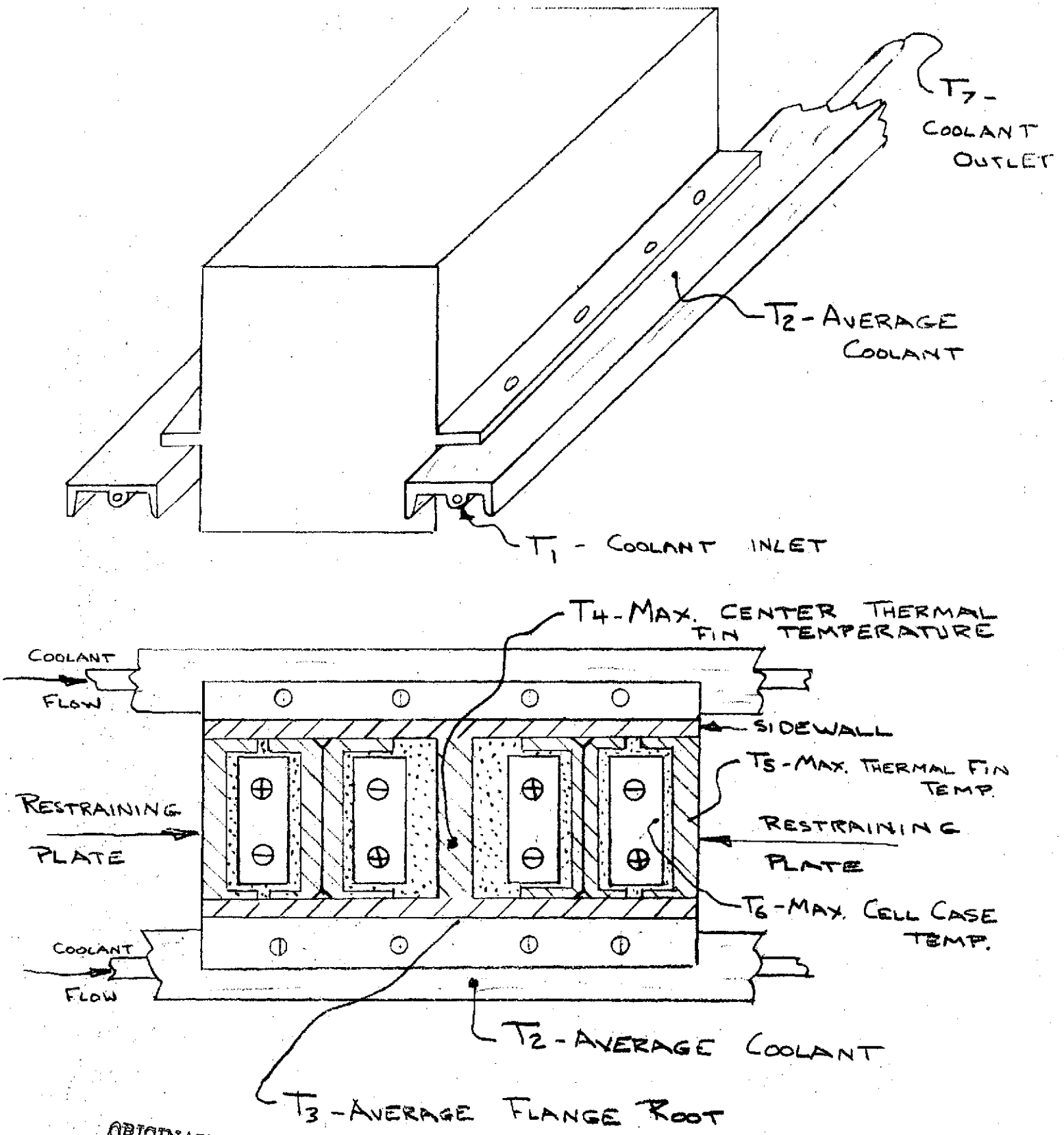

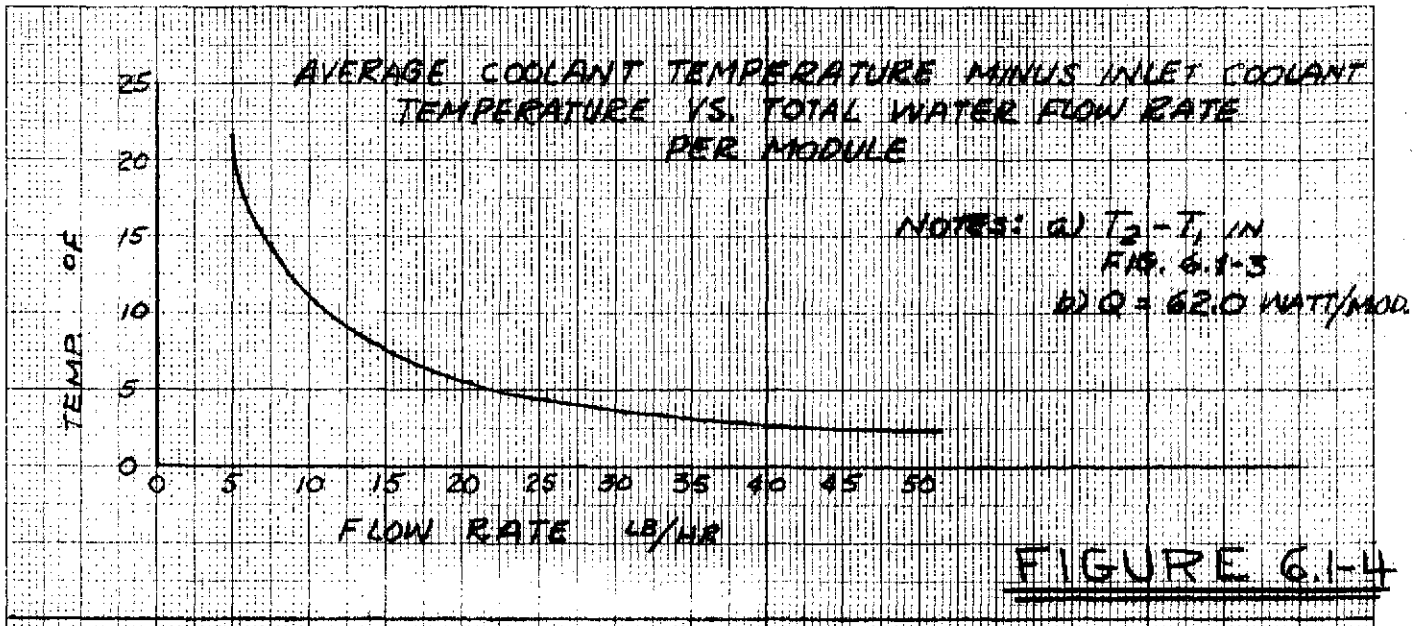

FIGURE 6.1-4

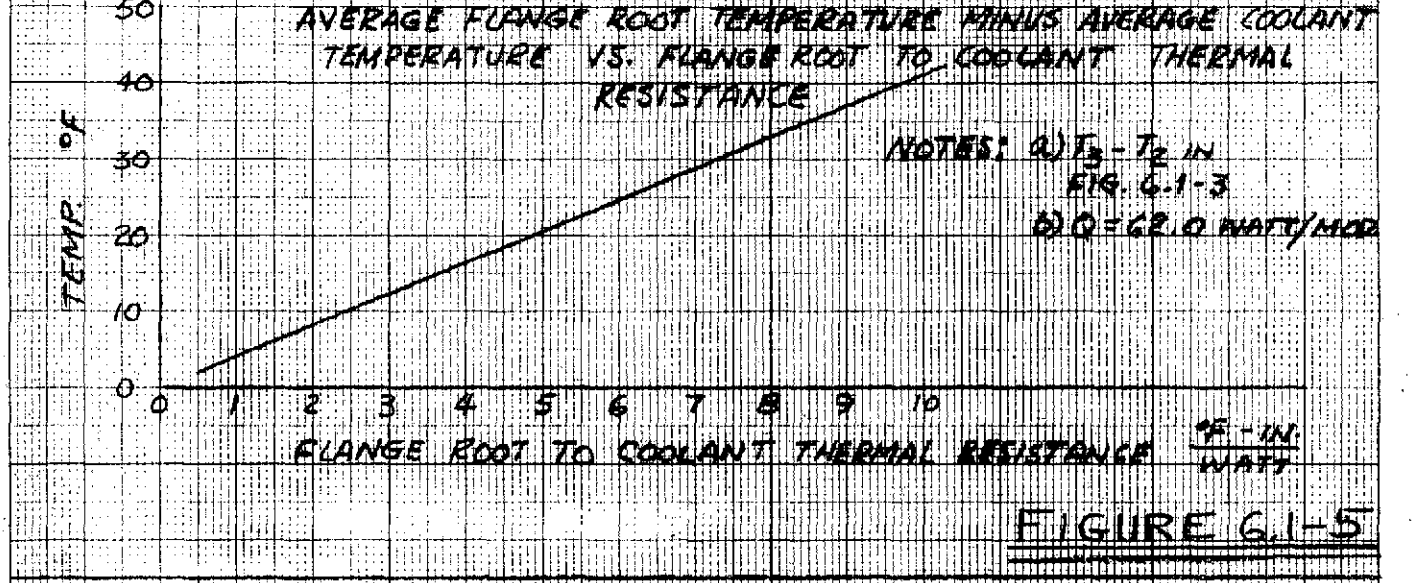

FIGURE 6.1-5

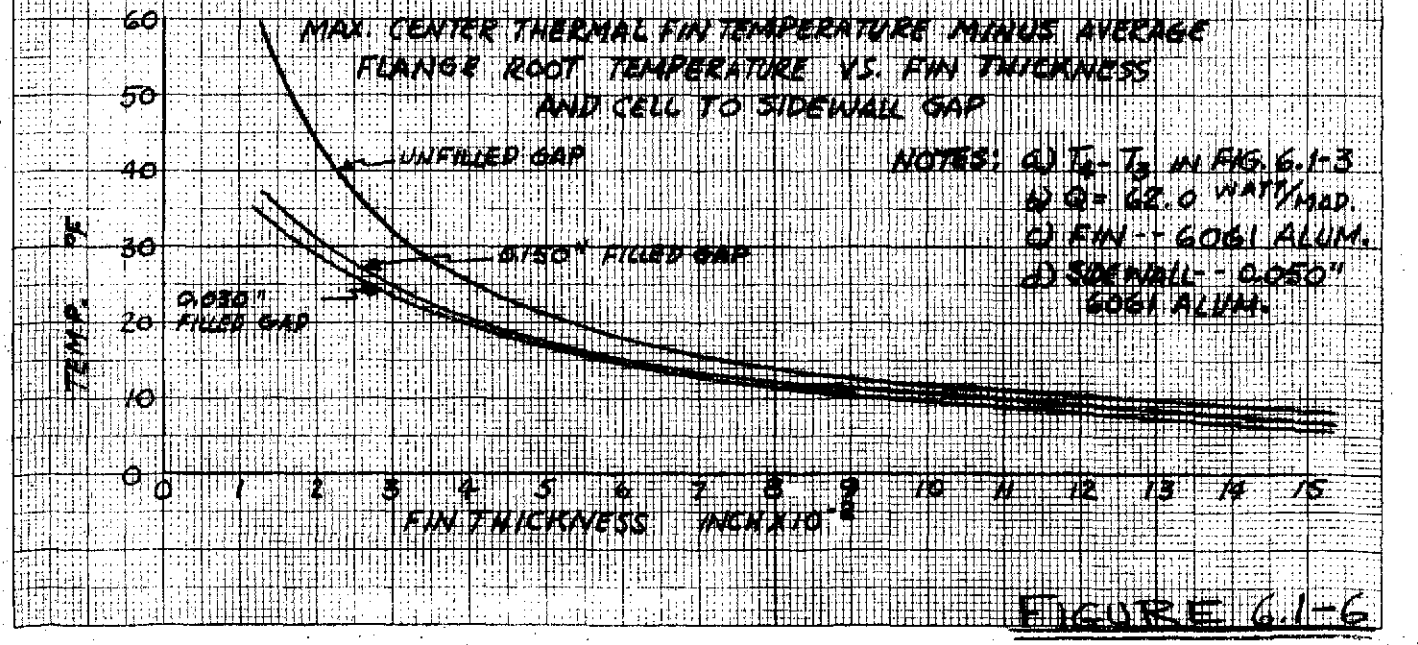

FIGURE 6.1-6

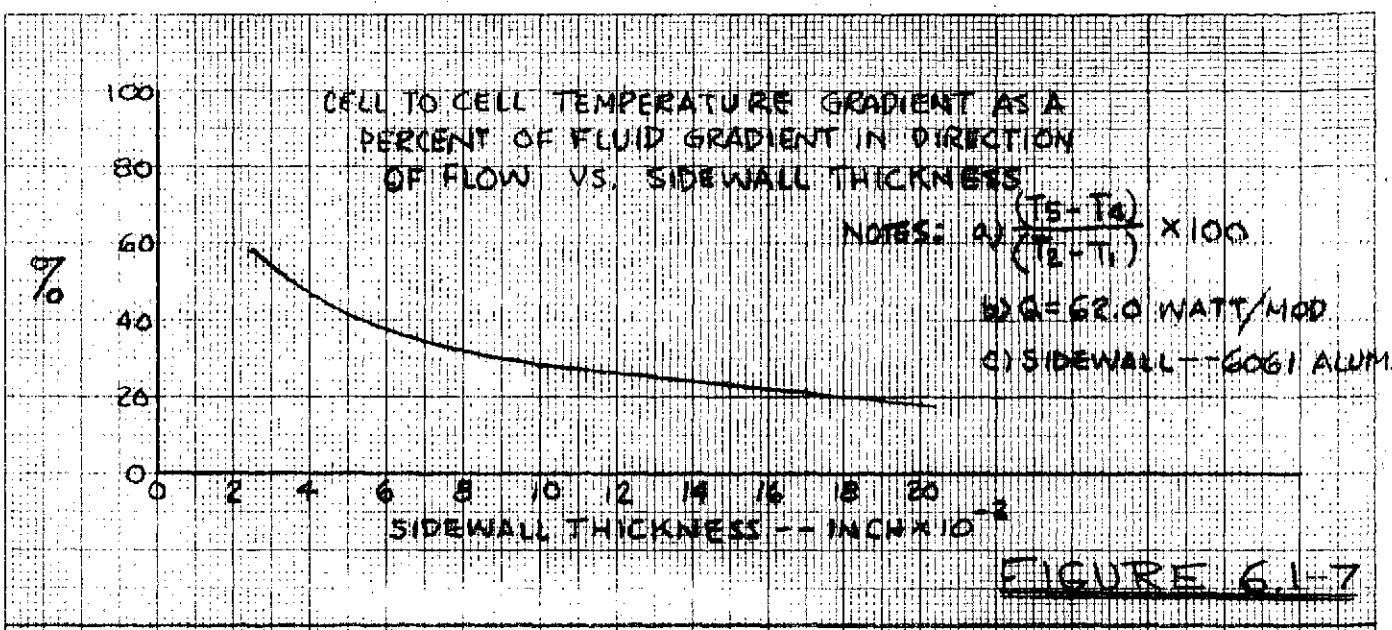

FIGURE 6.1-7

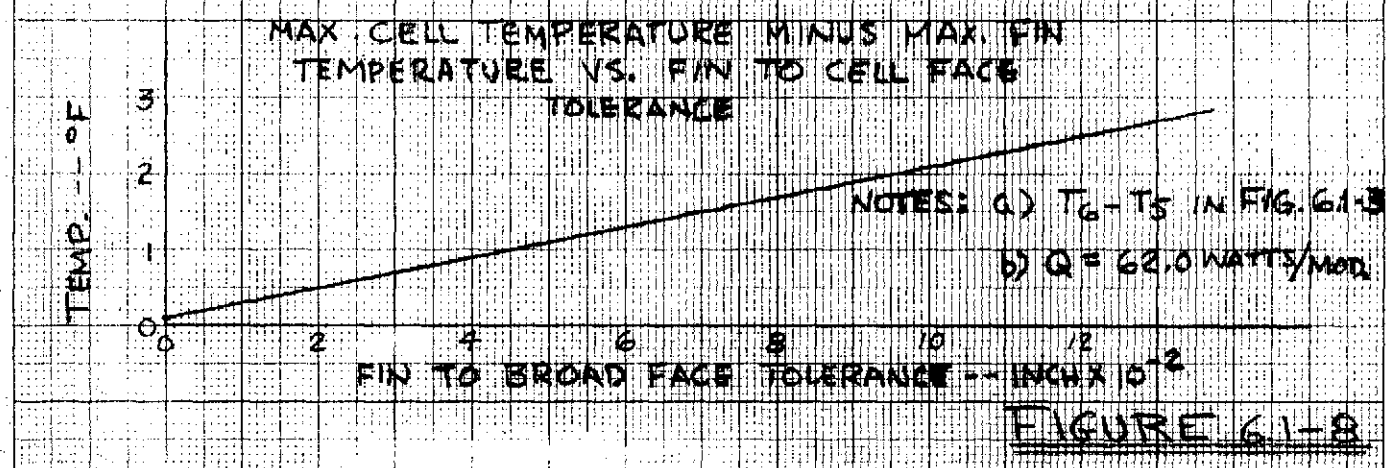

FIGURE 6.1-8

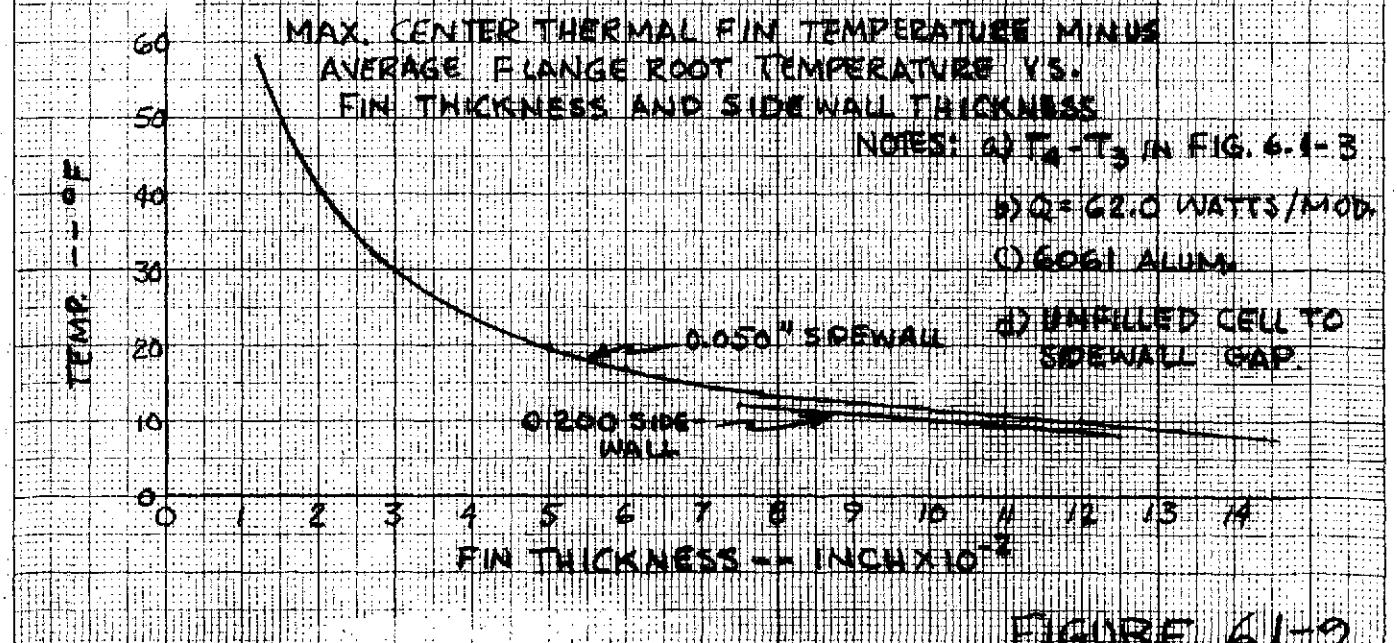

FIGURE 6.1-9

Figure 6.1-4 shows the effect of flow rate on the temperature rise in the coolant from the inlet to the cold rail to a point halfway down the cold rail ($T_2 - T_1$ on Figure 6.1-3). It can readily be seen that low flow rates can substantially cut into the total allowable maximum cell to inlet coolant gradient. As mentioned earlier, a 30 pound per hour module flow rate was assumed.

Figure 6.1-5 shows the effect of flange and cold rail design (as represented by the overall flange root to coolant unit thermal resistance) on the flange root to coolant gradient ($T_3 - T_2$ in Figure 6.1-3). This resistance is a function of the flange dimensions, flange material, flange flatness, flange surface roughness, bolt spacing, bolting torque, interface material, cold rail flatness, cold rail surface roughness, cold rail material, cold rail thickness, tube diameter and internal tube extended surface design. Within the scope of the present program, it was assumed that a LM type cold rail would be used. Assuming a reoptimized LM cold rail, silicone grease interface, flange flatness requirement of 0.010" per foot TIR, flange roughness of 63 μ inches, two-inch bolt spacing, and bolt torque of 35 in-pounds, a root to coolant resistance of 2.5°F-inch/watt should be obtainable. However, as can be seen in Figure 6.1-5, even a resistance of 2.5°F-inch/watt would result in a 10°F root to coolant gradient.

Figure 6.1-6 shows the effect of fin thickness and cell to sidewall tolerance gap on the gradient between the center thermal fin and the average flange root ($T_4 - T_3$ in Figure 6.1-3). In the analysis it was assumed that the tolerance gap would be filled with a thermally conductive (0.5 Btu/(hr.-ft.-°F)encapsulant material. As can be seen in Figure 6.1-6, the difference between even a large filled gap and any unfilled gap is quite substantial in terms of required fin thickness.

Figure 6.1-7 shows the effect of sidewall thickness on the axial gradient within the package. Assuming a 30 pound per hour flow rate, the inlet to outlet coolant gradient ($T_7 - T_1$ in Figure 1) would be approximately 7°F. For very thin sidewalls, this would mean the temperature variation from the inlet to outlet cell would be 7°F (since conduction through the cell stack itself is poor). At lower flow rates this cell to cell variation would become very large (see Figure 6.1-4). However, as can be seen in Figure 6.1-7, the percent of cell to cell gradient vs. coolant gradient rapidly falls off with increasing sidewall thickness.

Figure 6.1-8 illustrates the effect of cell case distortion on the maximum cell case to maximum thermal fin temperature gradient. The design of the thermal fins is such that the thermal effect of small variations in maximum overall cell thickness (broad face to broad face) can be eliminated. The problem that cannot be avoided is the residual distortion left in the face of a cell after welding and after packaging (applying compressive load to the cell stack). This distortion leaves gaps between the cell and fin which must be filled with encapsulant material, which, at best, is a poor thermal conductor. Figure 6.1-8 can thus be used to relate the degree of distortion in the cell face to increase in cell temperature. This in turn can be related to fin thickness (and weight) via Figure 6.1-6.

Figures 6.1-4 through 6.1-8 illustrate the effect of coolant flow rate, flange and cold rail design, fin thickness, side wall thickness, and dimensional tolerances on the thermal gradients within a battery module. The figures are, to a small degree, an oversimplification of the total effect of these parameters on the thermal gradients in the package since there are actually second order interactions between these parameters which have not been shown. For example, Figure 6.1-9

illustrates the second order interaction of sidewall thickness on the maximum fin to flange root gradient. This interaction was not shown in Figure 6.1-6. Similarly, the assumptions made on cell thermal conductivity have a small effect on the fin to flange gradient. A study was conducted wherein the thermal conductivity was assumed to vary by approximately 2300% in the parallel to plate direction and 340% in the normal direction (based on variances of values reported in the literature as described in Section 5.2) with very little effect on the thermal gradient.

This baseline packaging scheme was adequate for relatively low (i.e. 40°F) coolant inlet temperatures, but was not adaptable to operation at higher (55°F) coolant temperatures. This lack of compatibility with higher coolant temperatures is due to the inherent inability of a flange-cold rail mounting system to fulfill simultaneously the requirements for high heat rejection rate per inch of rail (approximately 4.5 watts/per inch in our baseline design) and small thermal gradient from flange root to coolant. Even with a flange-root to coolant resistance of 2.5 $\frac{°F\text{-inches}}{watt}$, an 11°F gradient would result due to the baseline design's short contact length with the rail. Since the flange root to coolant resistance is only one of five series thermal paths between the coolant inlet and maximum cell temperature, such a large gradient would make it impossible to maintain cell temperatures below 68°F with inlet coolant temperature as high as 55°F.

Since a battery module capable of accepting a wider range of coolant temperature was desired, further development of the baseline design was stopped and a study of alternate configurations was instituted.

Figure 6.1-10a through 6.1-10c illustrates several interesting concepts first considered. In 6.1-10a, although the flange to coolant thermal path has been improved by doubling the length of the package,

the fact that heat is only removed through one broad face of each cell would cause an undesirable temperature gradient to result across the cell.

In 6.1-10b, the length is again twice as long as in the baseline design, but relatively thick (0.25 inch) thermal conduction fins (when compared to other schemes) would be needed to meet the temperature requirement.

6.1-10c is a design similar in construction to the baseline, except that the use of square planform 100 A-H Ni-Cd cells was considered. In addition to doubling the length of the package (and thus reducing the watt density along the rail), the cell to sidewall contact area more than doubled; increasing the proportion of heat directly entering the sidewall rather than taking the higher resistance path along the thermal fin. Although detailed thermal analysis showed this last design to be very attractive, it had to be dropped since: a) it was based upon a type cell which had never been built, nor funded for development; and b) other concepts appeared capable of meeting the requirements equally well.

Two configurations evolved which were worthy of detailed consideration. These two are discussed below.

The first is a package geometrically similar to the baseline design except that one entire surface is mounted to a flat cold plate. This design is illustrated in Figure 6.1-11 and 6.1-12. The cells are arranged broad side to broad side with thermal conduction plates between them. The heat generated within a cell is transferred through its broad sides, across a kapton tape and epoxy interface to the thermal conduction plates (fins). The heat flows down the fins to the base plate through a brazed or welded interface, and from the base plate to the coolant across the cold plate to base plate interface. In

DISCARDED CONCEPTS

FIGURE 6.1-10

(a)

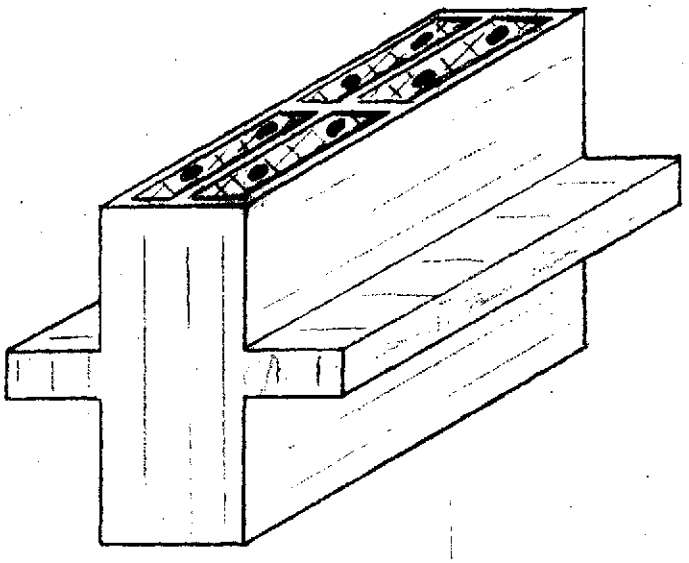

(b)

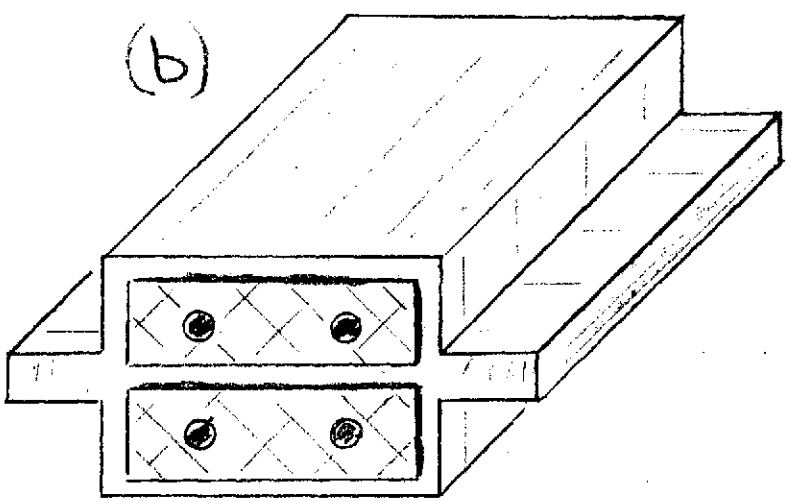

(c)

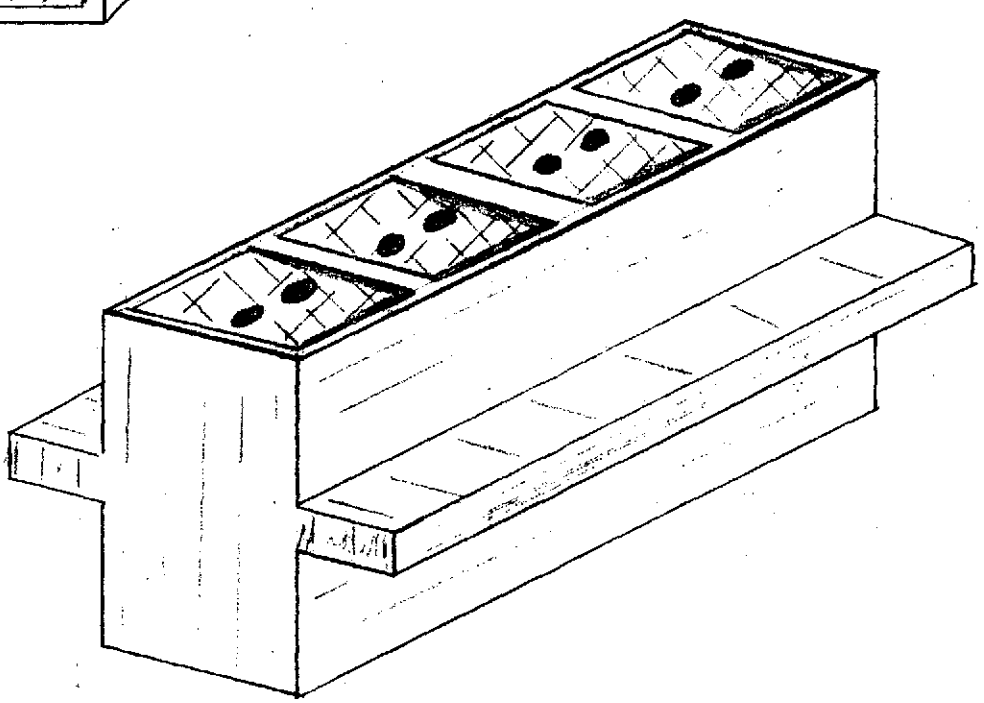

FIGURE 6.1-11

ALTERNATE CONCEPT #1
FLAT COLD PLATE COOLED
BATTERY MODULE DESIGN

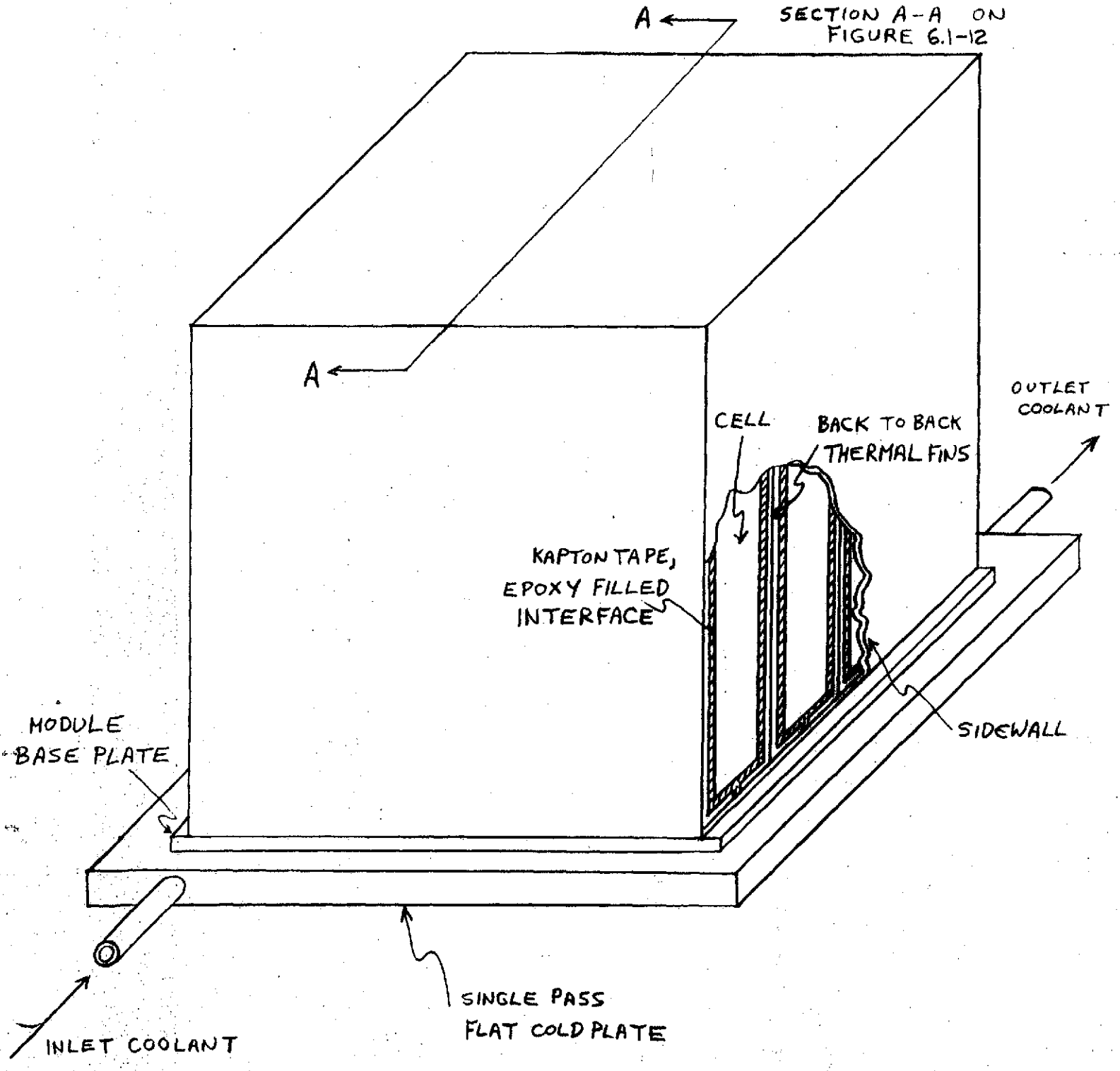

ALTERNATE CONCEPT #1
FLAT COLD PLATE COOLED BATTERY MODULE DESIGN

(SECTION A-A, FIGURE 6.1-11)

FIGURE 6.1-12

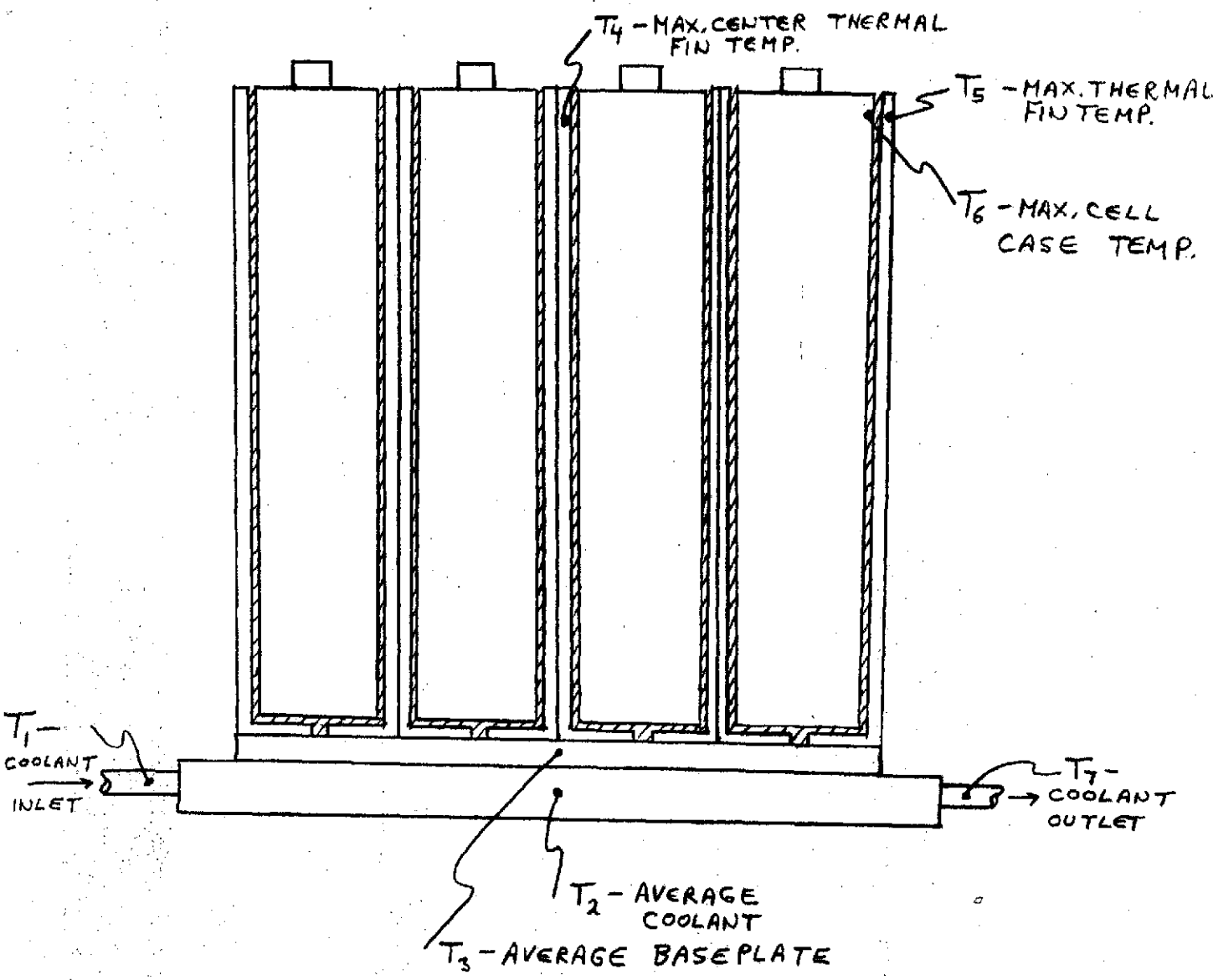

addition, some heat is transferred directly from the bottom face of the cell to the baseplate, and from the narrow sides of the cell to the sidewalls of the module and thence to the base plate.

Figures 6.1-13 through 6.1-18 show the contribution of each of the thermal flow paths to the overall gradient between maximum cell temperature and inlet coolant temperature. As can be seen in the figures, the controlling thermal resistance is no longer at the coolant interface (as in the baseline design), but is now from the "top" of the thermal fin to the base plate ($T_4 - T_3$). Assuming a 30 pound per hour flow rate; 300 Btu/(hr.-ft.^{2}-^{o}F) baseplate to coolant conductance, and a 0.050" epoxy filled gap between the fins and the cell faces, a 5^{o}F (maximum) gradient in Figure 6.1-15 could be tolerated for a 55^{o}F inlet coolant temperature (see Table 6.1-1). Because of the large height of the cell (7.3 inches), a 0.25 inch fin and 0.25 inch baseplate thickness would be required to achieve so small a temperature difference. The fin, base plate, and cold plate weight required for thermal control (assuming 6061 aluminum) would be approximately thirteen (13) pounds (Table 6.1-2)

The chief advantage of this design is that it is compact, almost cubical in shape, minimizing the module's volume. It has two principal disadvantages. The first is its relatively high thermal control weight. (While the fin weight could be reduced to some extent by the use of internal heat pipes in a honeycomb plate, this is not presently recommended due to the orientation constraints thereby imposed, and the added complexity and cost of module fabrication.) The second disadvantage is the large baseplate to cold plate surface area (80 square inches) required for mounting. The larger a package's critical thermal interface, the more its stringent flatness and roughness requirements complicate its fabrication and increase its cost.

FLAT COLD PLATED MODULE DESIGN PARAMETERS

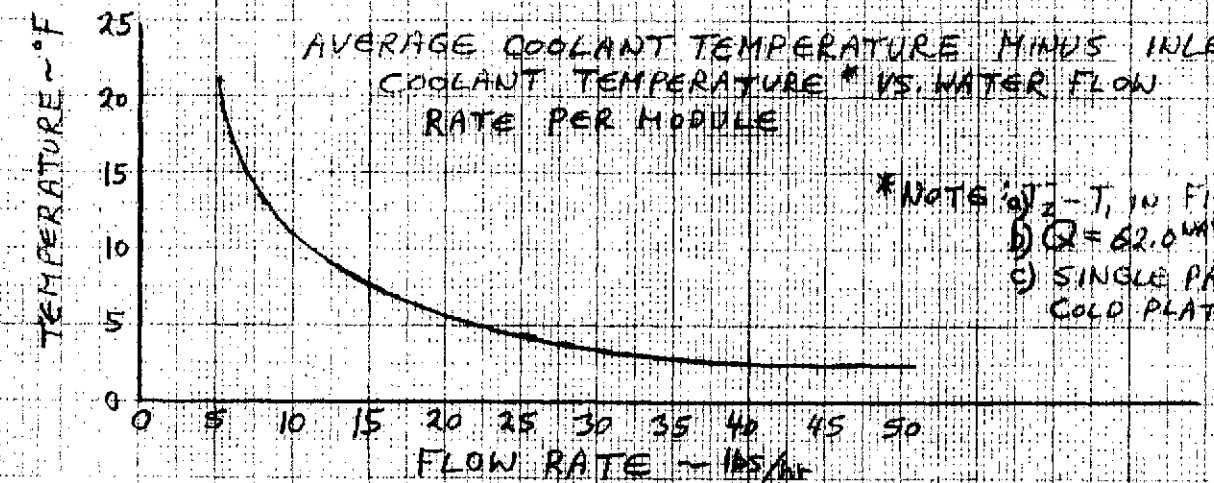

FIGURE 6.1-13

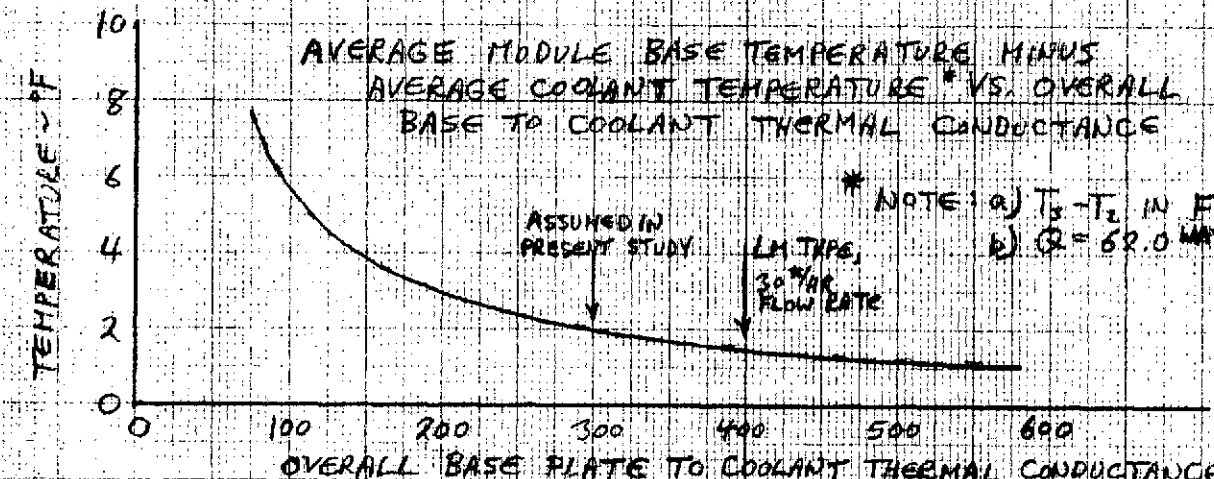

FIGURE 6.1-14

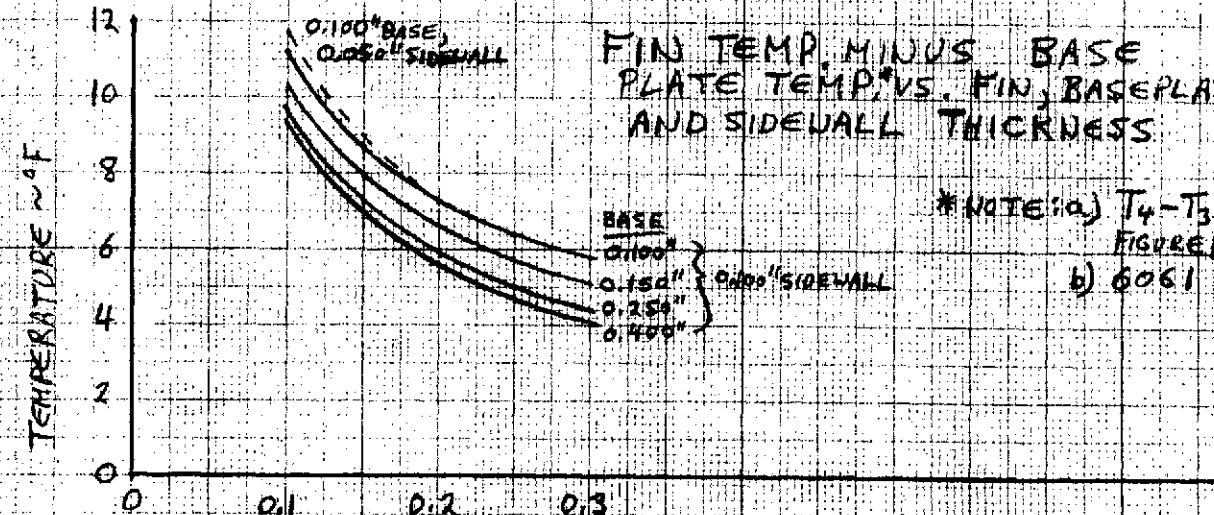

FIGURE 6.1-15

D.L. 11/17/70

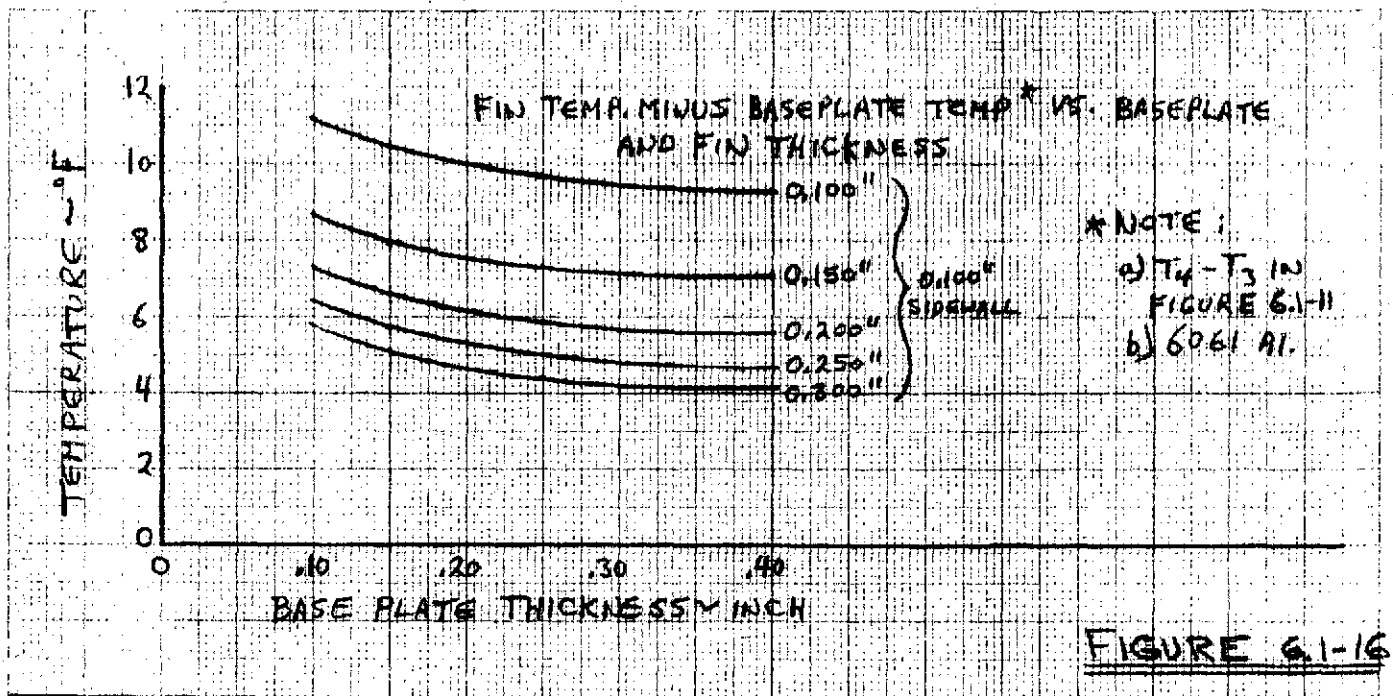

FIGURE 6.1-16

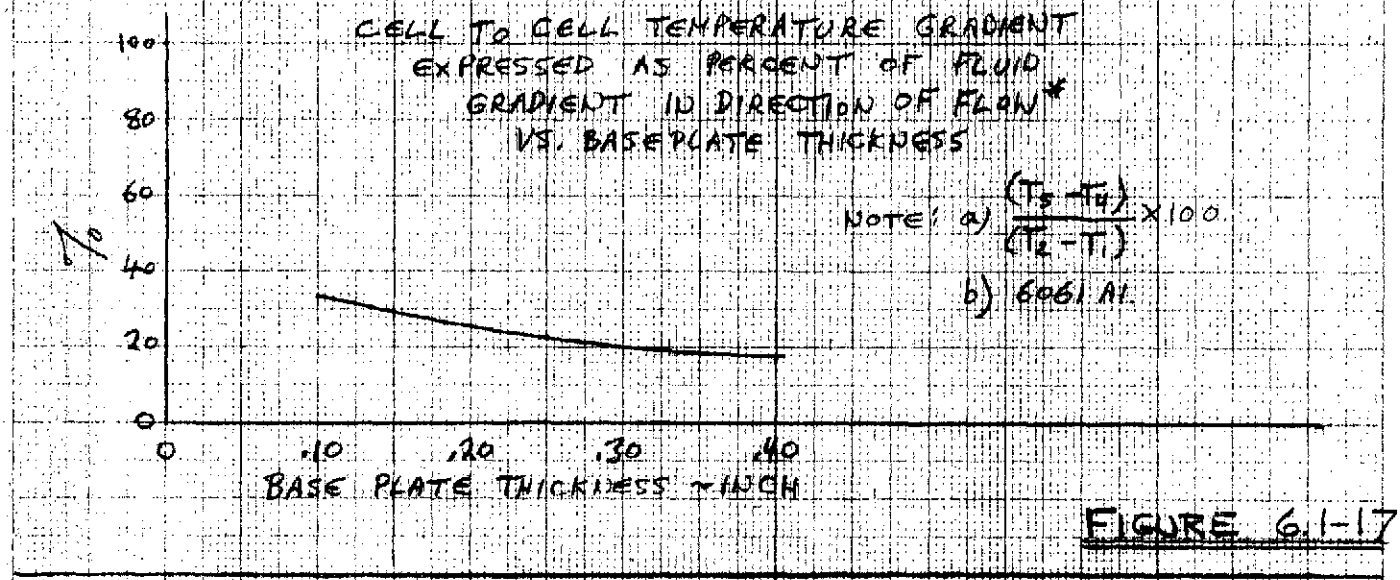

FIGURE 6.1-17

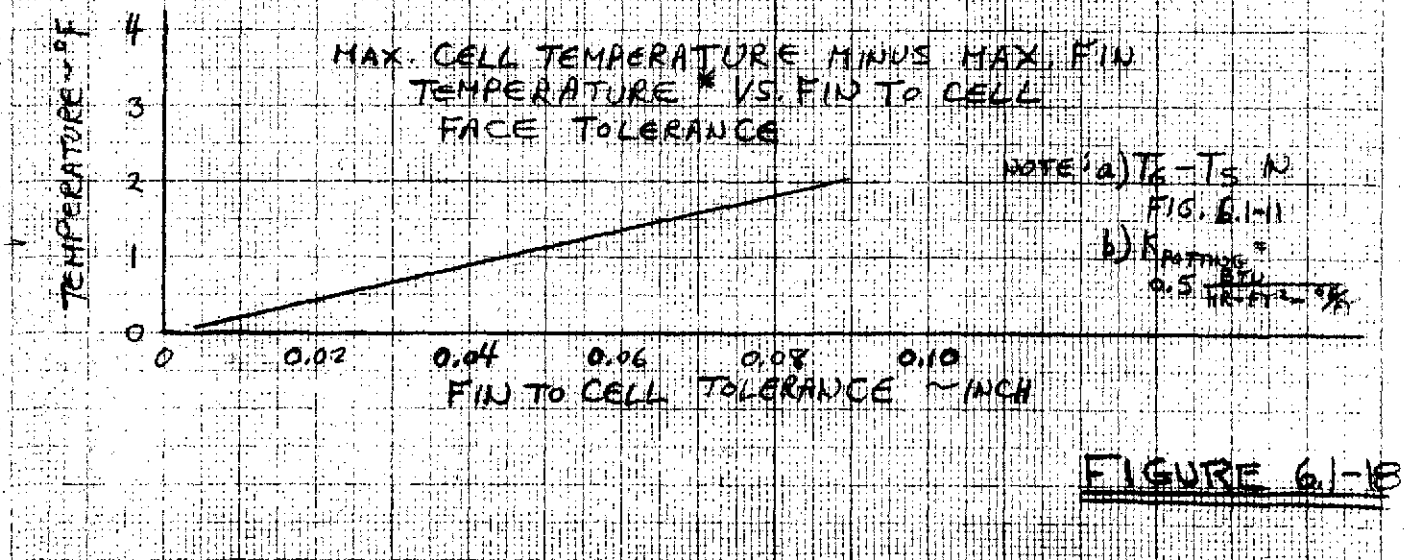

FIGURE 6.1-18

D.L.
11/12/70

Table 6.1-1

Flat Cold Plate Cooled Battery Module:

Fin and Baseplate Thickness Determination

$\triangle T_{1-2}$ = 3.5°F (30 lb./hr. flow rate)

$\triangle T_{2-3}$ = 2.0°F (300. BTU/hr.-ft.^{2} °F baseplate to coolant conductance)

$\triangle T_{4-5}$ = 0.7°F (20% of $\triangle T_{1-2}$)

$\triangle T_{5-6}$ = 1.1°F (0.050 in. (max.) fin to cell epoxy filled gap)

7.3°F (not including environmental input or $\triangle T_{3-4}$)

0.7°F (±10% tolerance to include environmental input)

$\triangle T_{sub-tot.}$ 8.0°F (not including $\triangle T_{3-4}$)

$T_{max.\ cell}$ = 68°F (design requirement)

$T_{max.\ inlet\ coolant}$ = 55°F (design requirement)

$\triangle T_{total}$ = 13°F

$\triangle T_{3-4\ (allowable)}$ - 13.0-8.0 = 5.0°F

From Figure 4: Sidewall thickness = 0.050" (6061 aluminum - structural requirement)
Fin thickness = 0.250" (6061 aluminum)
Baseplate thickness = 0.250" (6061 aluminum)

Flat Cold Plate Cooled Battery Module:

Weight Determination

$A_{sidewalls} = 2 \times 7.3 \times 1.95 \times 4 = 114 \text{ in.}^2$

$A_{baseplate} = 7.3 \times 4 \times 1.95 = 57 \text{ in.}^2$

$A_{fins} = 8 \times 7.3 \times 7.3 = 426 \text{ in.}^2$

$W_{sidewalls} = A_{sidewall} \times$ sidewall thickness $\times$ 0.1 lb./in.^{3} (6061 aluminum)

$W_{sidewalls} = 114 \times 0.050 \times 0.1 = 0.6$ lbs.

$W_{fins} = A_{fins} \times$ fin thickness $\times$ 0.1 lb./in.^{3} (6061 aluminum)

$W_{fins} = 426 \times 0.25 \times 0.1 = 10.6$ lb.

$W_{baseplate} = A_{baseplate} \times$ baseplate thickness $\times$ 0.1 lb./in.^{3} (6061 aluminum)

$W_{baseplate} = 57. \times 0.25 \times 0.1 = 1.4$ lbs.

$W_{total} = 0.6 + 10.6 + 1.4 = 12.6$ lbs. (55°F coolant inlet)

$\left[W_{coldplate} \text{ (LM type)} = 1.0 \text{ lb/ft}^2 \times \frac{60 \text{ in.}^2}{144 \frac{\text{in.}^2}{\text{ft.}^2}} = 0.4 \text{ lbs.}\right]$

The second packaging approach yields a long (30 inch), narrow (3.5 inch) module, dubbed the "flat pack". The "flat pack" is a cold rail mounted design, illustrated in Figure 6.1-19. The cells are arranged four-in-line with their plates parallel to the cold rails. The advantage of this geometry is that the contact length with the cold rail represents a four fold increase over the baseline design. The flange root to coolant temperature gradient is therefore greatly reduced due to the lower watt density along the flange. In addition, no internal thermal fins are required due to the direct thermal path from the cell to the sidewall; and minimal sidewall thicknesses are needed since the flange is located midway up the plate stack.

Figures 6.1-20 through 6.1-24 show the contribution of each of the thermal flow paths to the overall cell to inlet coolant temperature gradient. Assuming a 30 pound per hour flow rate, 2.5 (^{o}F-in/watt) flange root to coolant thermal resistance and a 0.050 inch epoxy filled gap between the cell face and module sidewall, a 3.6^{o}F (maximum) temperature gradient between the cell face and module sidewall could be allowed in Figure 6.1-22.(see Table 6.1-3). A 0.085" sidewall thickness would be required to achieve this temperature difference. The total thermal control weight attributable to sidewalls, mounting flanges and cold rails (assuming 6061 aluminum) would be approximately 5.9 pounds (Table 6.1-4).

This design's principal advantages are

- o Low thermal control weight (without the need for internal heat pipes)
- o Small thermal interface area (45 square inches).

It only potential disadvantage is the larger effective volume it requires compared to a cubical geometry (approximately 850 vs. 650 cubic inches).

ALTERNATE CONCEPT #2

"FLAT PACK", COLD RAIL COOLED BATTERY MODULE DESIGN

FIGURE 6.1-19

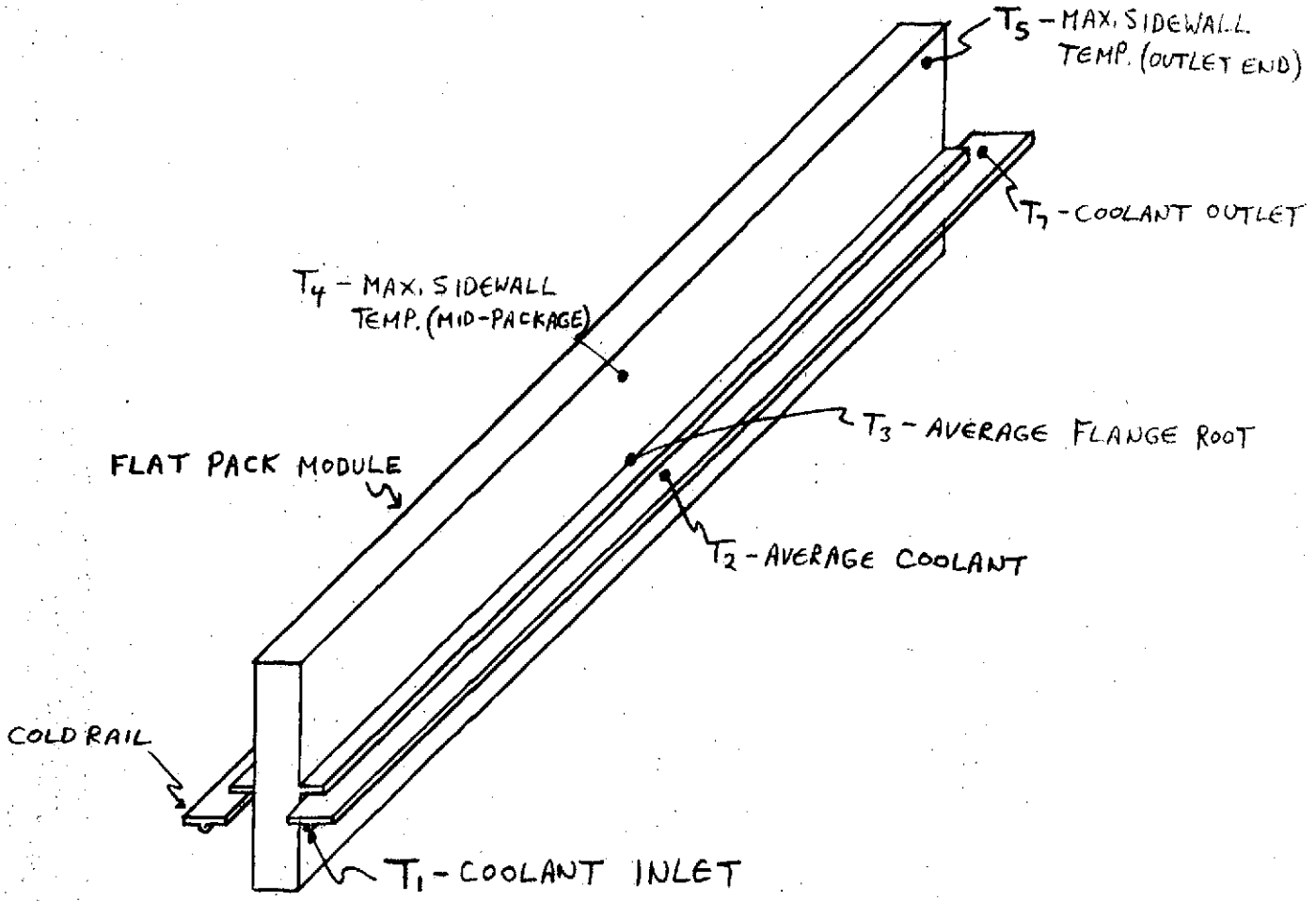

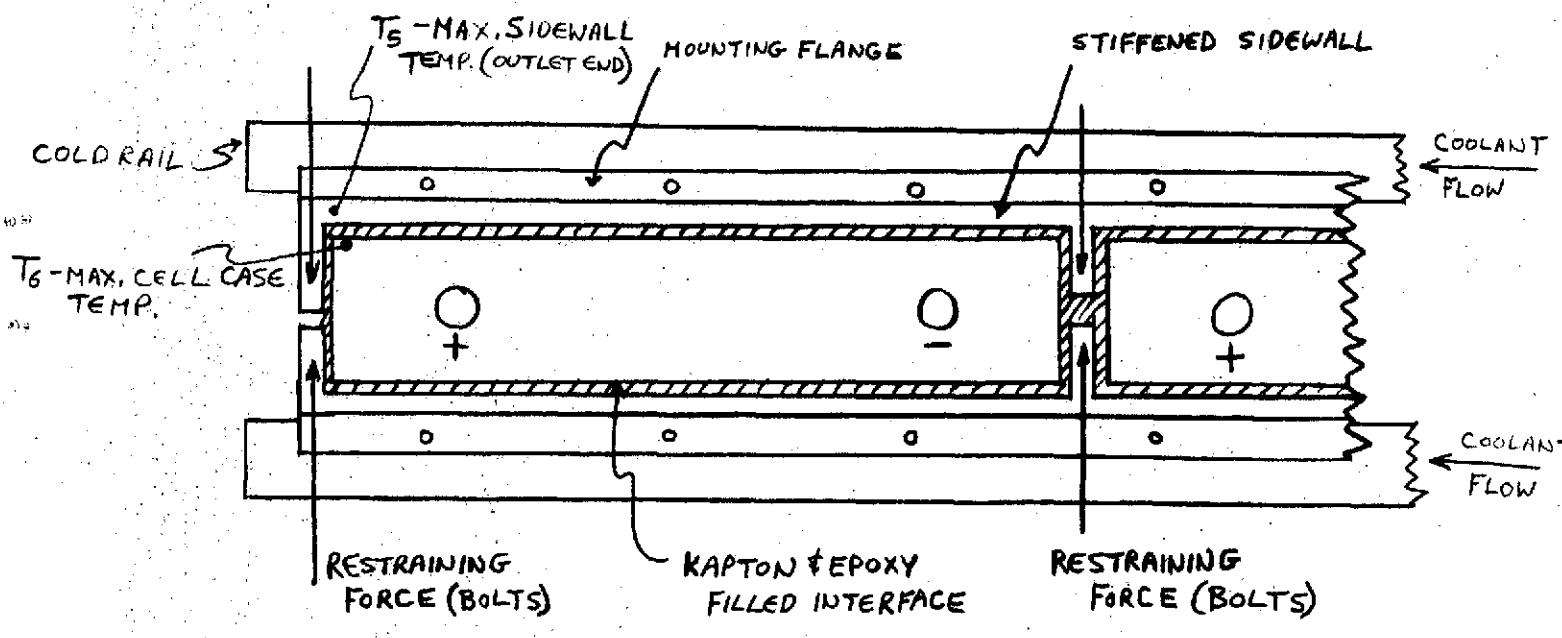

FLAT PACK DESIGN PARAMETERS

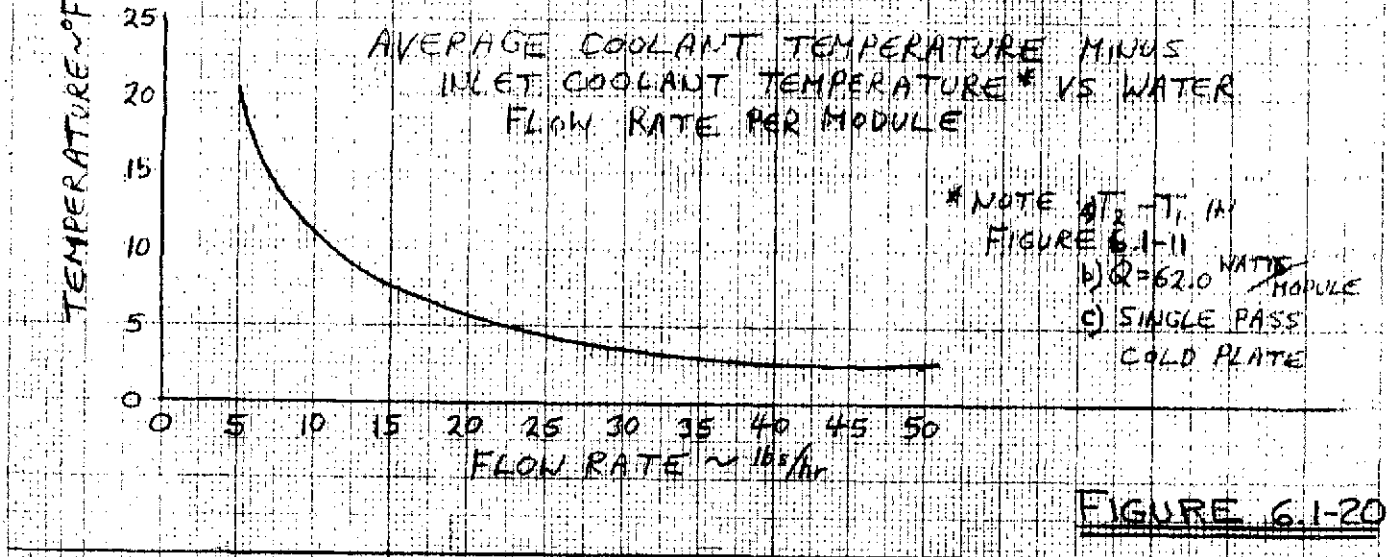

FIGURE 6.1-20

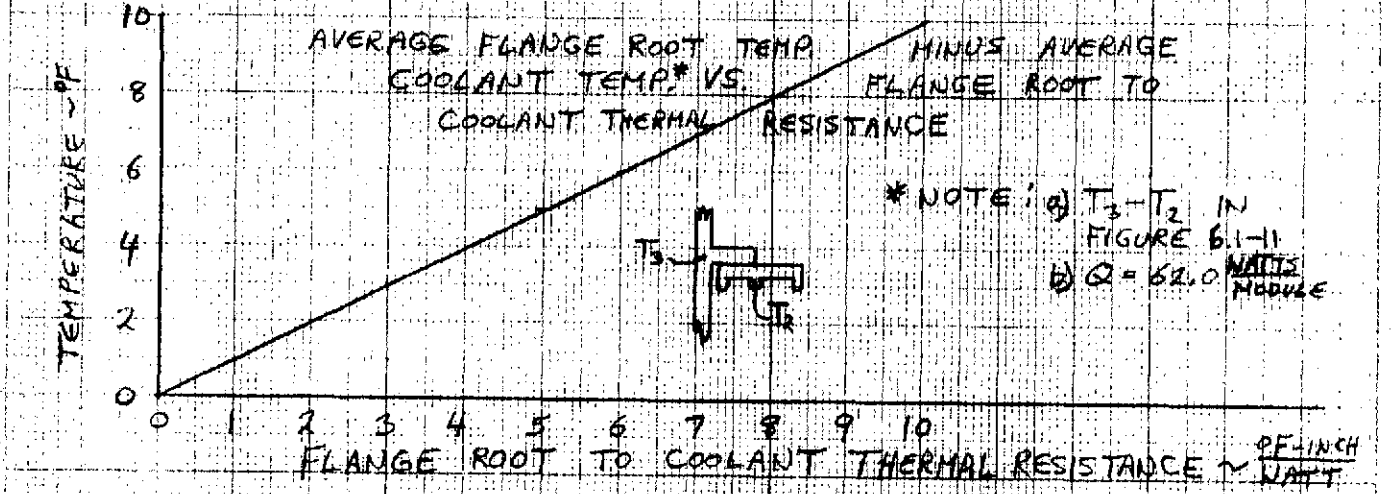

FIGURE 6.1-21

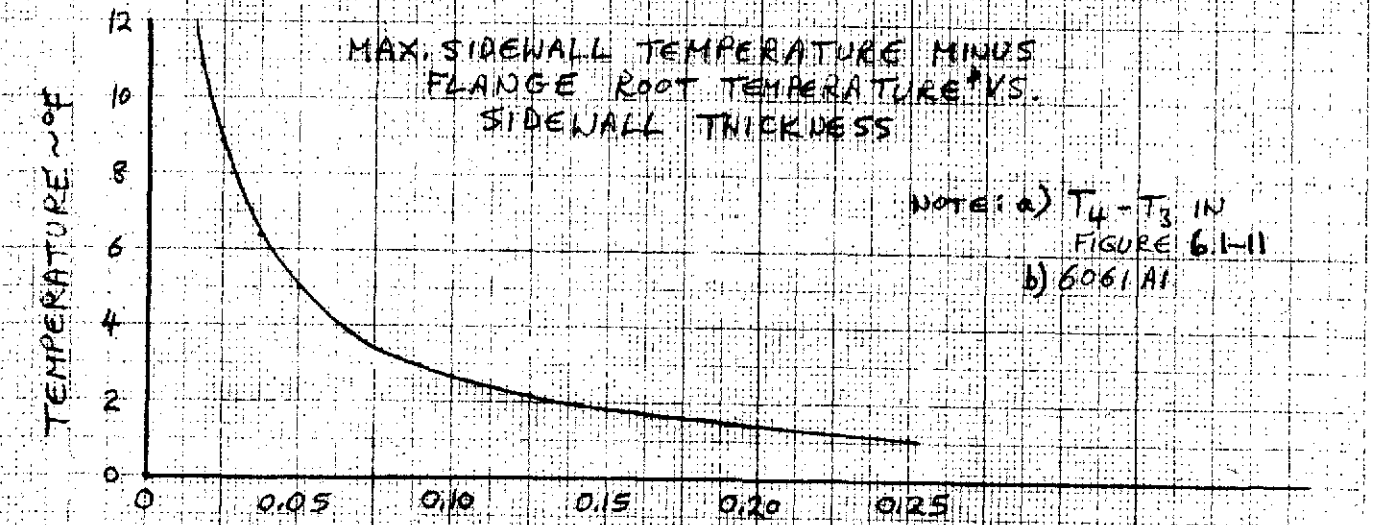

FIGURE 6.1-22

DL
11/11/70

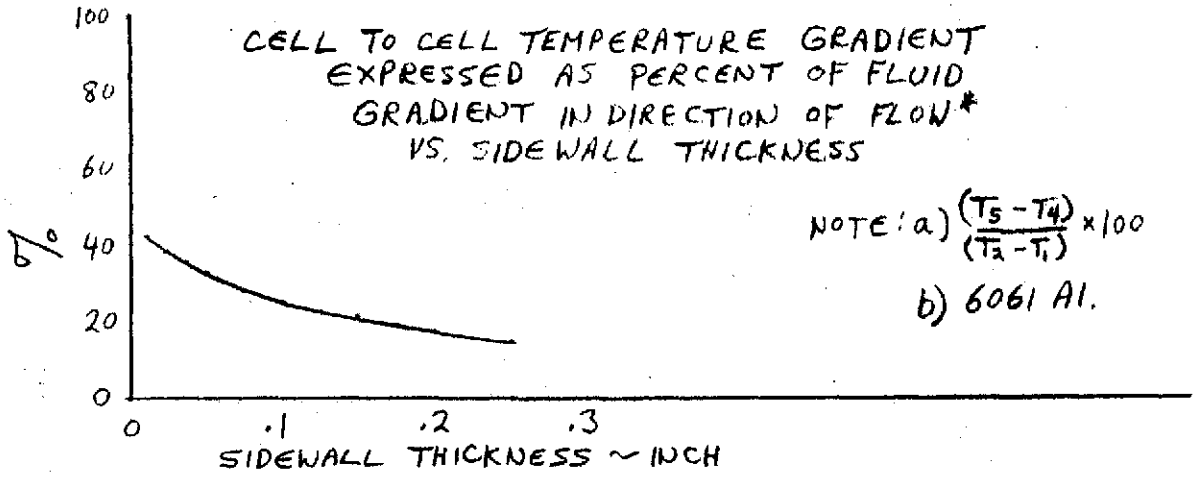

FIGURE 6.1-23

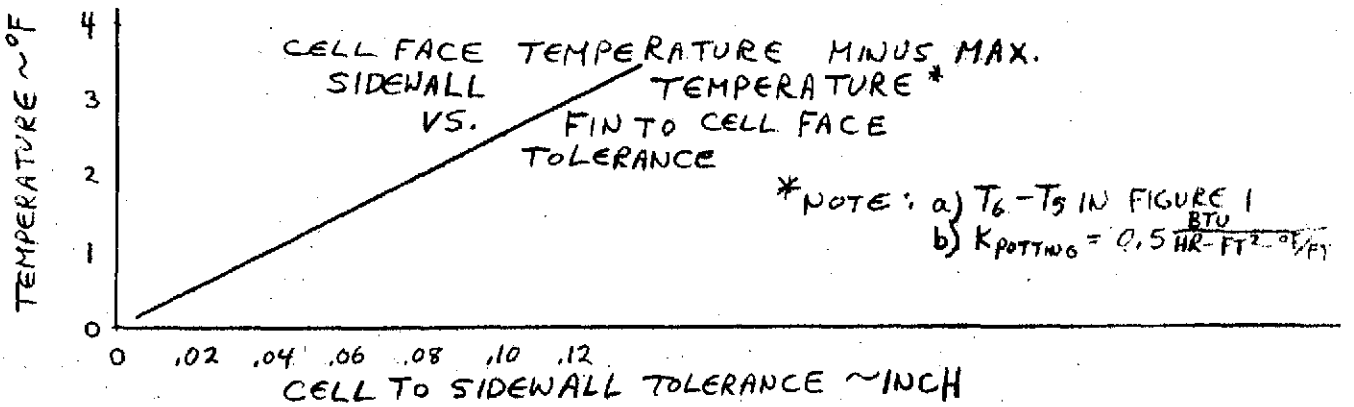

FIGURE 6.1-24

D.L.
11/13/70

Table 6.1-3

"Flat Pack," Cold Rail Cooled Battery Module:

Weight Determination

$A_{sidewalls}$ = 2 x 7.5 x 4 x 7.3 = 440 $in.^2$

$W_{sidewalls}$ = $A_{sidewall}$ x sidewall thickness x 0.1 $lb./in.^3$ (6061 aluminum)

$W_{sidewalls}$ = 440 x 0.085 x 0.1 = 3.7 lbs.

$W_{flanges}$ = Flange width x flange thickness x length x 0.1 $lb./in.^3$ (6061 aluminum)

$W_{flanges}$ = 0.625 x 0.25 x 2 x 30 x 0.1 = 0.93 lbs.

W_{total} = 3.7 + 0.9 = 4.6 lbs. ($55^{\circ}F$ coolant inlet)

[$W^{*}_{cold\ rail}$ = 0.5 lb./ft. x 30 in./ 12 $\frac{in.}{ft.}$ = 1.3 lbs]

*Proposed Cold Rail:

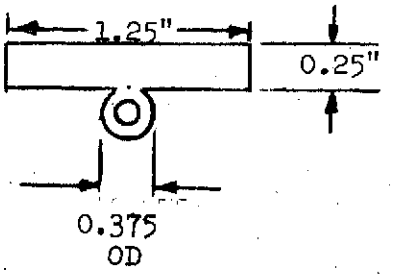

Table 6.1-4

"Flat Pack", Cold Rail Cooled Battery Module:

Required Sidewall Thickness Determination

T_{1-2} = $3.5^{\circ}F$ (30 lb./hr. flow rate)

T_{2-3} = $2.5^{\circ}F$ ($2.5^{\circ}F$-in./watt flange root to coolant resistance)

T_{4-5} = $1.4^{\circ}F$ (40% of T_{1-2})

T_{5-6} = $1.2^{\circ}F$ (0.050 in. (max.) fin to cell epoxy filled gap)
$8.5^{\circ}F$ (not including environmental input or T_{3-4})
$0.8^{\circ}F$ (10% tolerance to include environmental input)

$T_{sub-tot.}$ = $9.4^{\circ}F$ (not including T_{3-4})

$T_{max.\ cell}$ = $68^{\circ}F$ (design requirement)

$T_{max.\ inlet\ coolant}$ = $55^{\circ}F$ (design requirement)

T_{total} = $13^{\circ}F$

$T_{3-4\ (allowable)}$ = 13.0 - 9.4 = $3.6^{\circ}F$

From Figure 4: Sidewall thickness = 0.085" (6061 aluminum)

6.2 Mechanical Design

As stated in 6.1, the "flat pack" design was chosen. The particular version selected was the all welded structure shown in Figure 6.2.2. This configuration meets the structural requirements, is within the weight limits, and is designed with the necessary thermal constraints observed. Studies and analyses leading to this selection are described in 6.2.1 through 6.2.3 below.

6.2.1 Mechanical Design Approach

In addition to the requirements, ground rules and assumptions listed in 4.1, and the material properties constraints shown in 5.1.1 and 5.1.2, the following constraints were observed in studying the baseline and later configurations:

- Minimize volume
- Minimize structural weight
- Constrain cells against 100 psig operating pressure to provide maximum safety margin consistent with other constraints
- Provide for the thermal properties given in 6.1
- Provide for module removal and replacement by one (1) man in zero "g".

The initial baseline configuration (in parallel with the thermal studies), and the subsequent "flat pack" configuration, concentrated on two approaches:

- Honeycomb structure
- All-welded structure

6.2.2 Honeycomb Structure

This design, shown in Figure 6.2-1, appeared, at first, to offer a most attractive solution to the problem of a viable thermal design with light weight and simple fabrication.

The sidewall honeycomb sandwich was designed using 6061-T6 aluminum alloy, 0.080-inch thick inner face sheets (for thermal requirements), and 0.020-inch thick outer skins. The inner and outer sheets were to be adhesive bonded to epoxy impregnated fiberglass honeycomb core. A mounting flange, approximately located at the cells' centers of gravity, was designed for welding or brazing to the inner skin. This flange, of 0.25-inch 6061-T6 alloy, conducts the heat from the inner skin to the cold rails.

Aluminum skin honeycomb spacers were designed to be placed between cells, and were to be held in place by structural bolts. The latter also had the function of breaking up the beam length of the flat pack (31 inches). Sides and bottom were to be fabricated of thin sheet aluminum to retain the cell encapsulant. A fiberglass cover was provided for safety and mechanical protection of the cell terminals.

Flange mounting hardware was to be captive, quick release fasteners spaced on two-inch centers for sufficient mechanical contact to provide a high thermal conductance interface. Provision was made for bosses on the module to accommodate detachable carrying handles. Calculated weight of this design, including cells at 8.0 lb. each, was 42.9 lb.

A review of this design showed its inability to contain the 100 psig maximum internal cell pressure in all directions.. This review demonstrated the necessity to design a pressure vessel which would restrain the cells on all six sides in order to provide adequate safety margins.

6.2.3 All-Welded Structure

This design, shown in Figures 6.2-2 and 6.2-3 (photo) is made entirely of 6061-T6 Aluminum, except for the optional protective dust cover. The case is fabricated in nine (9) parts:

- (2) Sidewalls and mounting flanges

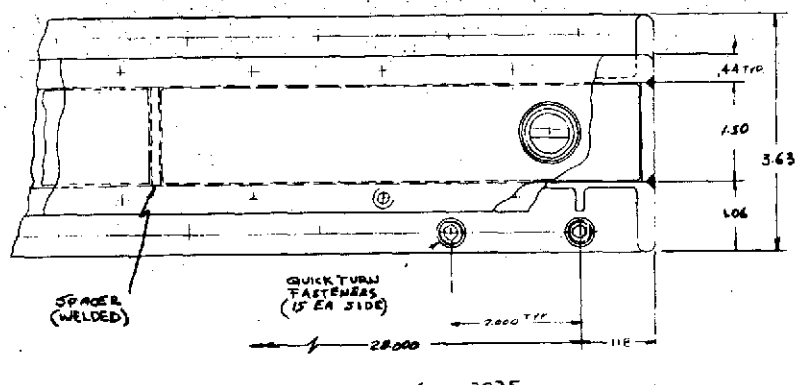

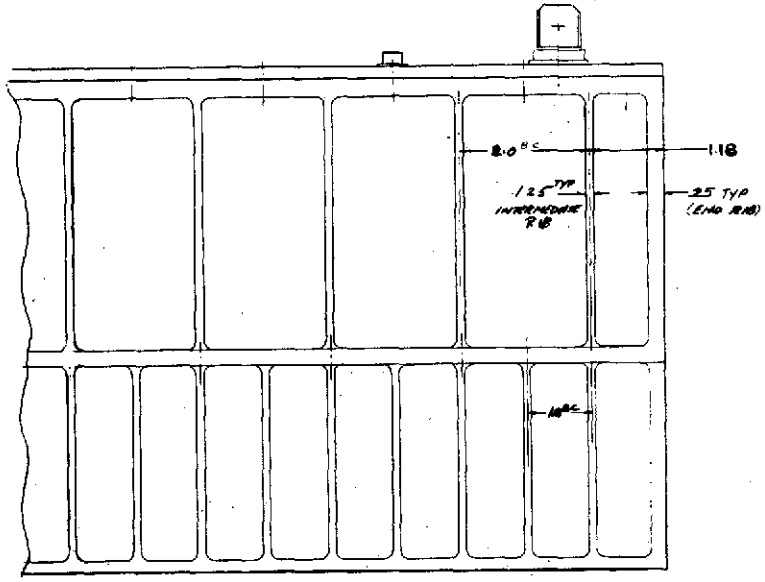

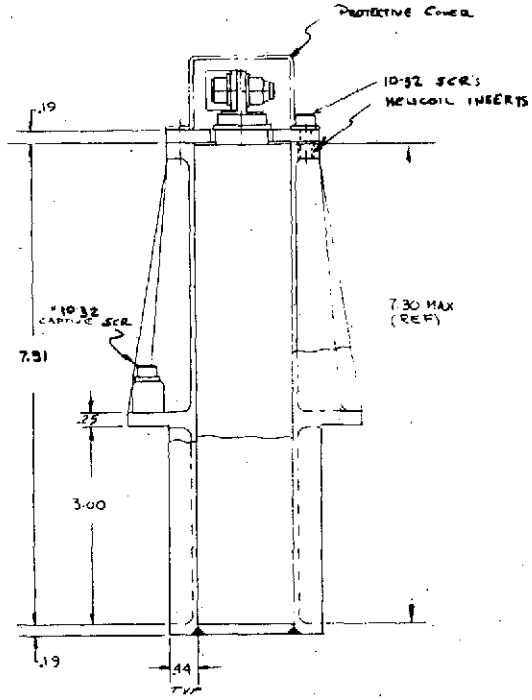

ORIGINAL PAGE IS OF POOR QUALITY

UNLESS OTHERWISE SPECIFIED DIMENSIONS ARE IN INCHES	CONTRACT NO.	GRUMMAN AIRCRAFT ENGINEERING CORPORATION BETHPAGE, NEW YORK 11714
	DRAWN BY	BATTERY MODULE
	LAYOUT BY	100 AMPERE HOUR - N. Cd
	CHECKED BY	(WELDED STRUCTURE)
	QA LEADER	
	MFG. GROUP	
	PROJ. ENGR.	SIZE D / CODE IDENT NO. 26512 / 559-105AV
	CONT. APPR.	SCALE 1:1 / SHEET

FIGURE 6.2-3

ALL WELDED STRUCTURE

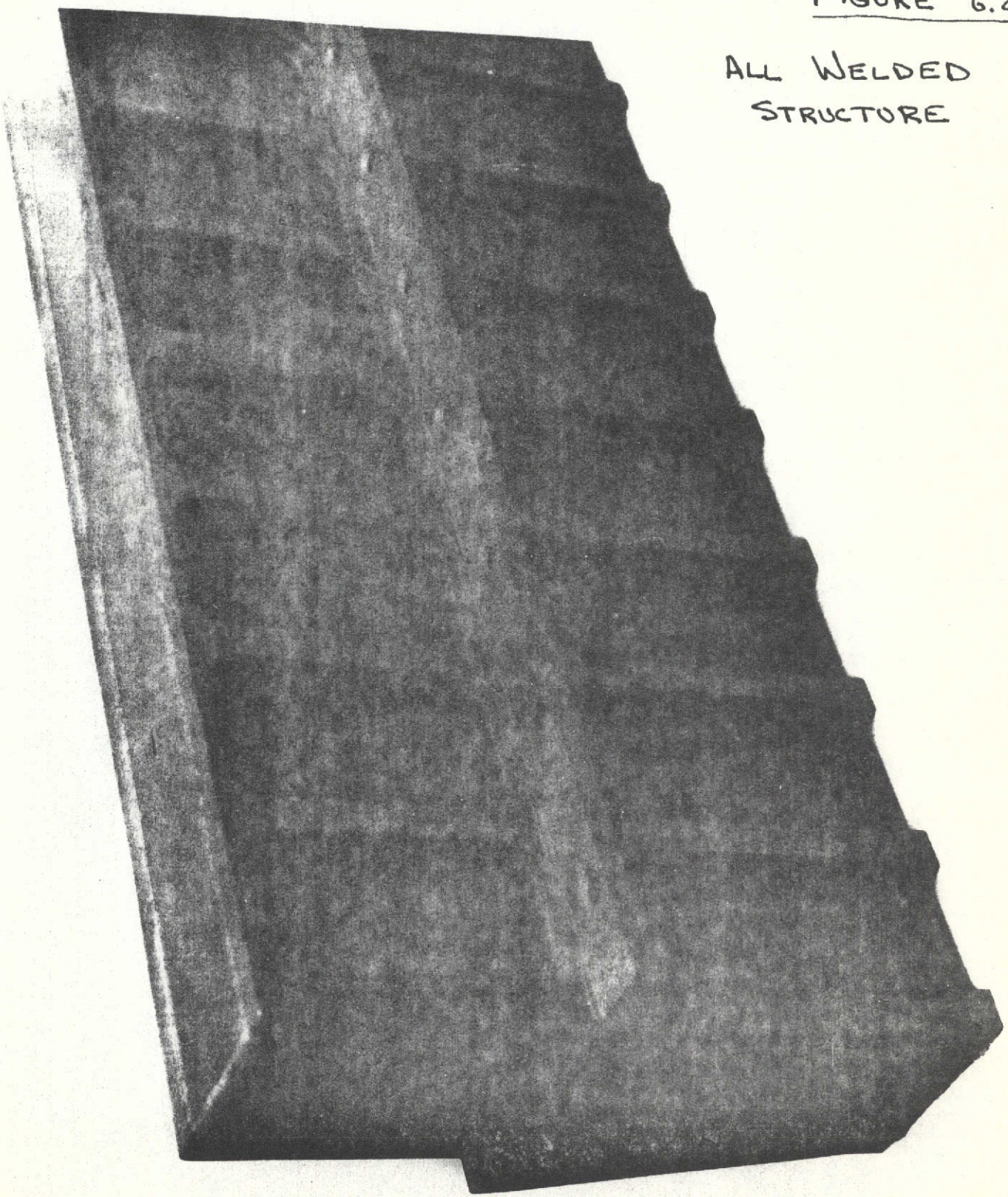

- (2) End plates
- (1) Bottom plate
- (1) Top cover plate
- (3) Bulkheads (cell separators) with welding tabs

The entire assembly, except for the cover plate is tungsten inert gas (TIG) seam welded together to form a unit structure. Following this, weld integrity is verified by the dye penetration (Zy-Glo) method.

Fractures were found on the bulkhead tab welds in the engineering model after proof test. Subsequent examination by metallurgical and electron fractography techniques showed insufficient penetration of the weld leading to an overload in the weld nugget itself. Details of this analysis, and the resulting recommendations and fixes will be found in 7.5 and 10.

6.2.3.1 Design Details

Experience gained from the Lunar Module (LM) program indicate that launch stresses due to acceleration and vibration are not the limiting factors in the structural design. The major load on the structure is caused by the cell internal design pressure of 100 psig, and the form factor is dictated by thermal considerations (6.1). Additional considerations used were:

- Containment of ruptured cells
- Sizing to accommodate cell dimensional tolerances, and achievement of reasonable manufacturing costs.
- Use of high thermal conductivity electrical insulation between cells and case
- Corrosion protection of case materials

The sidewall/mounting flange parts were each fabricated from a single plate using a numerically controlled milling machine. The walls use "T" section rib stiffeners for maximum strength with

minimum weight. The mounting flanges were remilled after welding to the following specifications:

- o Surface -- 32 microinch
- o Flatness -- 0.010 per foot TIR
- o Parallelism -- 0.005 per foot TIR

End plates and bottom plate were cut from standard stock, and the top cover plate was fabricated from 0.19-inch thick material.

Provision is made in the mounting flanges to use fifteen (15) number 10-32 captive screws on two-inch centers to connect each flange to the cold rails. The top cover plate is attached to the weldment with thirty-two (32) number 8-32 screws after the cells are in place and encapsulated.

The cell cavities' internal surfaces were hard-coat anodized in accordance with MIL-A-8625, Type III. External surfaces were alodined to provide both corrosion resistance and low thermal emissivity. The underside of the top cover plate was also hard-coat anodized. It should be noted that the oxide coating resulting from anodizing provides the following benefits:

- o Electrical insulation -- dielectric strength of 300 to 500 volts/mil
- o High thermal conductivity surface
- o Protection from KOH attack

The intercell connecting straps are made of nickel-plated copper, 0.090" thick x 0.625" wide (see 5.1.3). Each connector strap has clearance holes for two #8-32 stainless steel screws for connection to the cell terminals. These holes are on 3-inch centers. Each strap has a stress relief loop in the center. The design considerations used were:

- o Maximum module steady-state current = 100 ampere

- Maximum total voltage drop/module = 20 m V at 100 ampere
- Maximum total dissipation/module = 2 watt at 100 ampere

The strap design yields the following results:

- $J = 1850$ amp/in.^{2}
- $r = 4.94 \times 10^{-6}$ Ω/cm
- $\sum IR = 13$ m V at 100 amp
- $\sum I^2R = 1.3$ watt at 100 amp
- Self-heating -- negligible at 100 ampere ($\simeq 0.00009^{\circ}C/^{\circ}C$)

The terminal design of the heater cells was such that tightening the straps into place to achieve good connection caused a risk of putting undesirable torque on the terminal and the cell-to-terminal seal. Details of a redesign to eliminate this problem are given in 10.

A structural analysis was made on the engineering model. This analysis is reported in detail in Appendix B.. The results are contained in Table 6.2-1. To provide a minimum safety factor of 1.5, 150 psig was used to calculate the margins noted in the table. As long as all results are positive, minimum safety factor requirements are met. The cell divider weld figure, the smallest shown, is for the present stitch weld design. The ultimate design, shown in 10., will have a larger safety margin as an additional benefit, as noted in the table.

Table 6.2-1

STRUCTURAL ANALYSIS

Load Condition	Location and Description	Minimum Margin of Safety Under Load
150 psig	Cell divider stitch weld	+0.06
	Proposed cell divider butt weld (1)	+1.6
	Cold rail flange bending moment	+0.94
	Sidewall "T" stiffener	+1.5
	Sidewall membrane	+0.3
	End plate	+2.6
	End plate weld	+7.8
	Bottom plate	+2.6
	Bottom plate weld	+18
	Top cover bolts - shear stress (bolts)	+0.9
	Top cover bolts - shear out of cover	+0.7

(1) As proposed in Section 10.

6.3 Electrical Design

The module design, using four (4) cells in series, has the following electrical characteristics:

- Average Discharge Voltage = 4.8 volts (to 70% SOC)
- Maximum Charge Voltage (tentative)
  - 6.04 volts at 20°C (68°F)
  - 6.24 volts at 0°C (32°F)
- Total Energy Capacity ≅ 450 watt-hours

The above are based on the following current ratings:

- Maximum Charge Rate = C/1.2
- Maximum Steady-State Discharge Rate = C/1.2

Charging may be done at the individual module level, or with several modules in series or parallel. While specific charge control techniques and levels will be selected from subsequent parametric cycle testing, the present scheme using constant current, step-programmed by temperature modified voltage, and low-level floated by either compensated ampere-hour or third (oxygen sensing) electrode signal, appears to be highly efficient (see 8.3).

The module is capable of accepting cell monitoring and/or reconditioning circuitry by minor modification to the top cover restraining plate. Semiconductors and/or other components can be mounted by adding small "L"-brackets, which can be bolted, brazed or welded on to this plate. Heat thereby added to the module is conducted across the top plate to the sidewalls, and thence to the mounting flanges. Due to the potentially high values of dissipation expected, however, implementation of this method is doubtful.

6.4 Maintainability, Human Factors and Safety

The following demonstrates the manner in which various module features implement the design ground rules of 4.3:

1) Minimize Astronaut Effort and Time

a) No special training required to replace module. The astronaut need only be shown:

- How and where to attach and detach carrying handles
- Location of captive mounting flange hardware
- How to disconnect module electrically

All are simple operations requiring no special tools.

2) Minimize Use of Tools

a) Screwdriver used for flange hardware

b) Two wrenches -- one in each hand -- used for electrical connection hardware (balanced torque)

c) Handles snap in and out of bosses in sidewalls.

3) Design for One-Man Handling

a) Weight $\sim$ 45 lb.

b) Maximum Dimension = 30.25 inches

4) No Venting to Cabin

a) Cells are sealed

b) Modifications to dust cover permit manifolding to space vent

5) Prevent Shock Hazard

a) Module voltage $<$ 6.5 volts max.

b) Module case electrically isolated from cells

c) Dust cover prevents contact with terminals

6) Prevent Module Damage from Dropped Tool

a) Dust cover over terminals

Other design features enhancing maintainability and safety include:

o No interruption of coolant lines. No violation of thermal control integrity by module removal and/or insertion.

o Module capable of containing pressure to 150 psig with positive safety margin -- restraint on all faces.

7.0 MODULE TESTS

7.1 Thermal Evaluation Tests

7.1.1 Objective

The purpose of this test program was to demonstrate the adequacy of the 100 ampere-hour Ni-Cd battery module's thermal design in maintaining cell temperatures at acceptable levels (0-20°C, 32-68°F) while operating at the extremes of the design thermal environment and electrical operating regime. Additionally, the test was to provide engineering data useful in evaluating particular design problems in detail in an effort to further optimize the mechanical and thermal packaging.

7.1.2 General Test Procedures

The test article consisted of four (4) 100 ampere-hour nickel cadmium cells, each containing an internal resistive heater element, packaged in a module housing of the recommended (i.e.: "flat pack") design. Figure 6.2-3 is a photograph of the finished test article, with the top pressure plate not yet mounted.

The "heater" cells are described in Appendix B. They were operated as resistive heaters (known heat sources) during most of the testing, and charged and discharged as actual storage cells during the remainder of the tests.

Each cell contained a pressure gauge on its header, through which the internal cell pressure could be monitored and recorded.

Thermocouples were located on the individual cells prior to encapsulation and on the module exterior prior to test (see Figures 7.1-1 and 7.1-2). These and all other sensors were monitored and recorded continuously by the data system during testing. Figure 7.1-3 shows the Hewlett Packard data system used for all data acquisition.

All testing was performed in the Grumman Battery Laboratory, Plant 14. The module was mounted on a pair of specially modified Lunar Module cold rails through which conditioned coolant (water) was circulated. Figure 7.1-4 details the modifications made to the LM cold rails. Figure 7.1-5 is a photograph showing the module mounted on its cold rails. The inlet coolant temperature and flow

rate through the rails were controlled to predetermined values with the aid of the constant temperature bath shown in Figure 7.1-5 and hose cocks on the inlet and outlet lines. All fluid system parameters (inlet and outlet coolant temperatures and flow rate) were monitored and recorded continuously.

The module was tested under conditions simulating the hot design case (maximum coolant inlet temperature, minimum flow rate, maximum ambient temperatures, 50% DOD, voltage limit charge control) and the cold design case (minimum coolant inlet temperature, maximum flow rate, minimum ambient temperature, 12% DOD, auxiliary electrode charge control). In the above tests, the cells were operated as heaters whose input powers simulated the estimated heat generation rates for the above conditions.

In addition to the runs described, the hot, cold and nominal (30% DOD) design cases were repeated by actually charging and discharging the test cells rather than using them as heaters. During these "live" cell runs, the cold case was imperfectly simulated as voltage limit charge control was used.

7.1.3 Instrumentation

The test instrumentation allocation is described below.

7.1.3.1 Thermocouples

A. Cells (see Figure 7.1-6)

Cells #19 and #31: 18 (9 each)

Cells #20 and #30: 4 (2 each)

B. Module Sidewalls (see Figure 7.1-7)

7 (13 on Side A, 4 on Side B)

C. Module Bottom (see Figure 7.1-7)

2

FIGURE
7.1-1

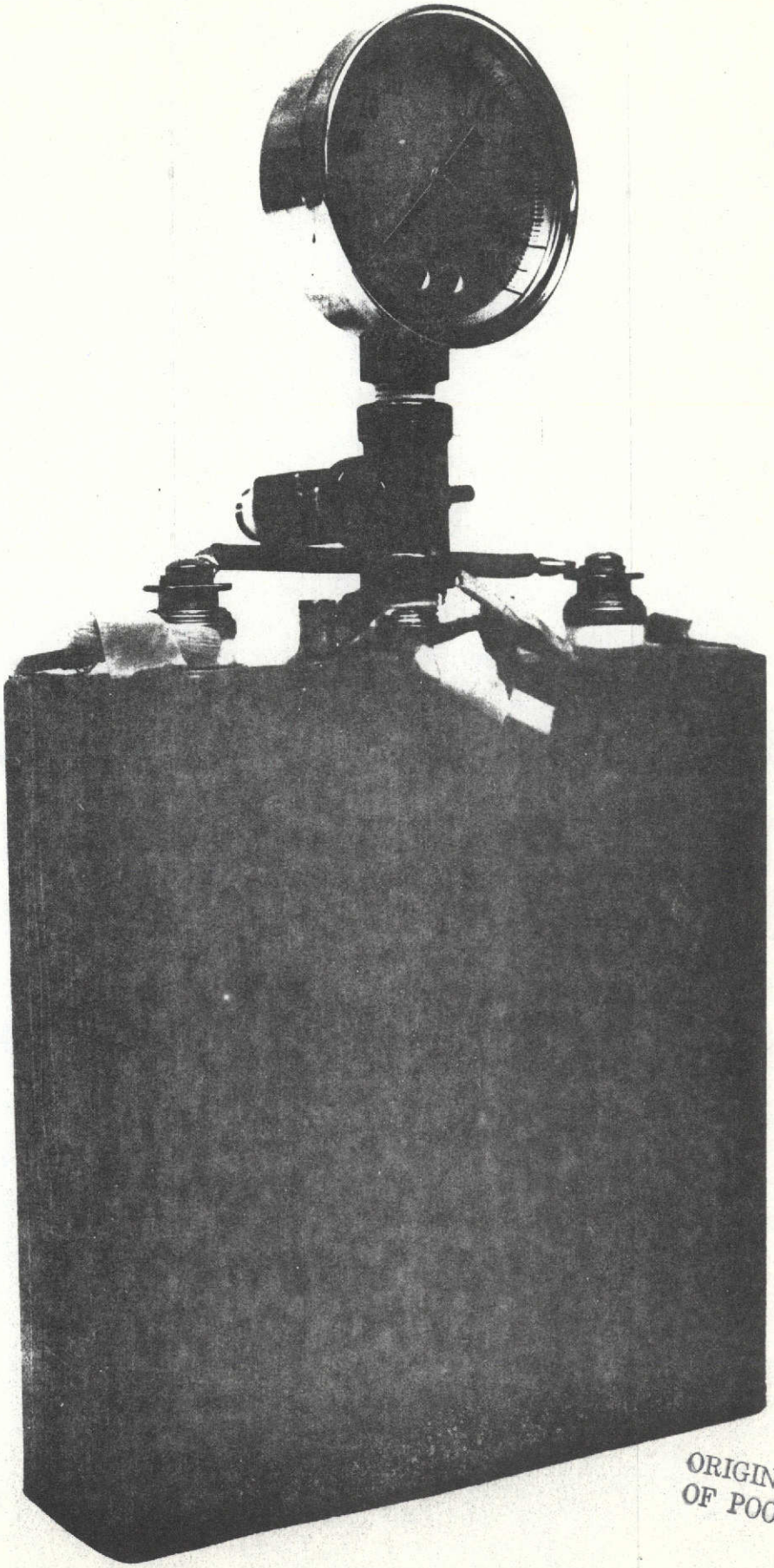

HEATER CELL
WITH
THERMOCOUPLE

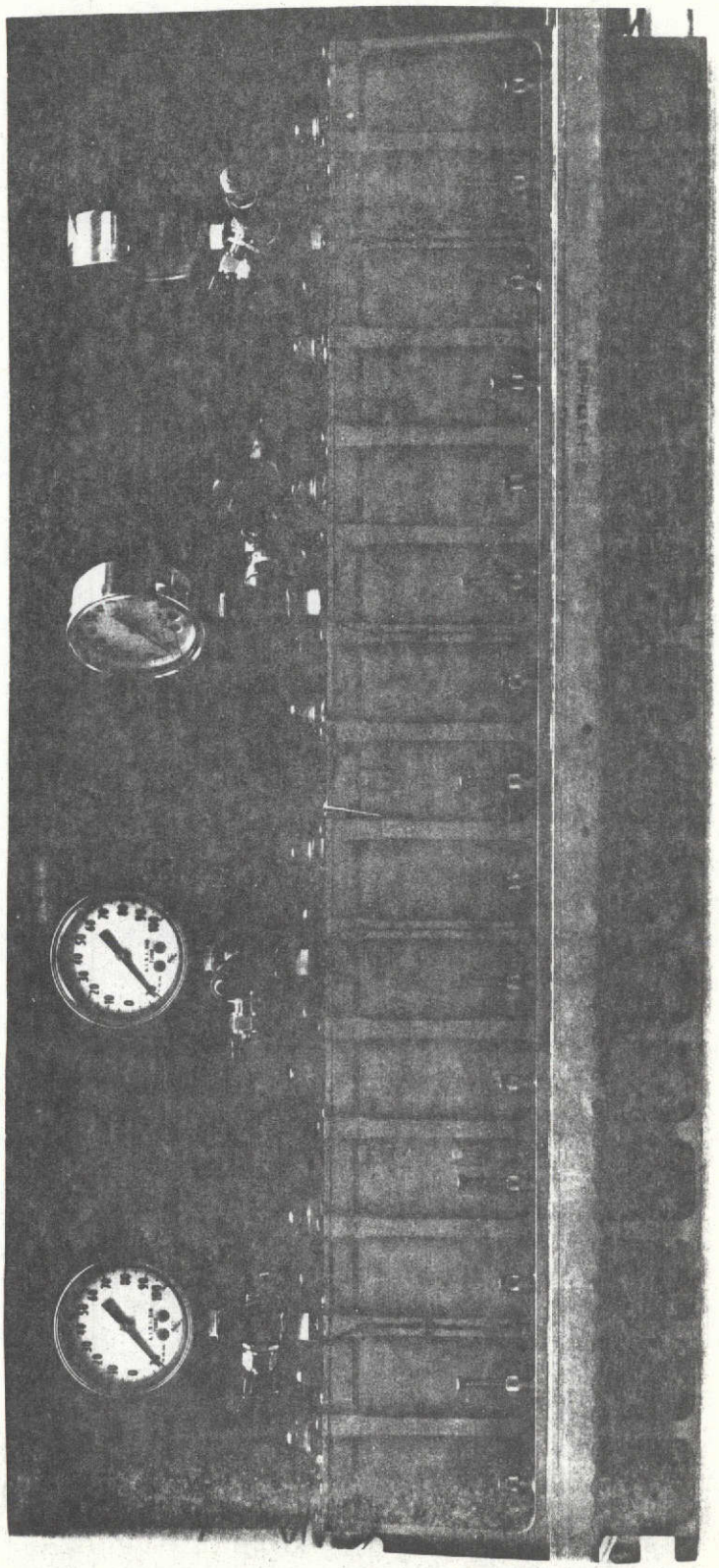

FIGURE 7.1-2

BATTERY MODULE

WITH THERMOCOUPLE

FIGURE 7.1-3

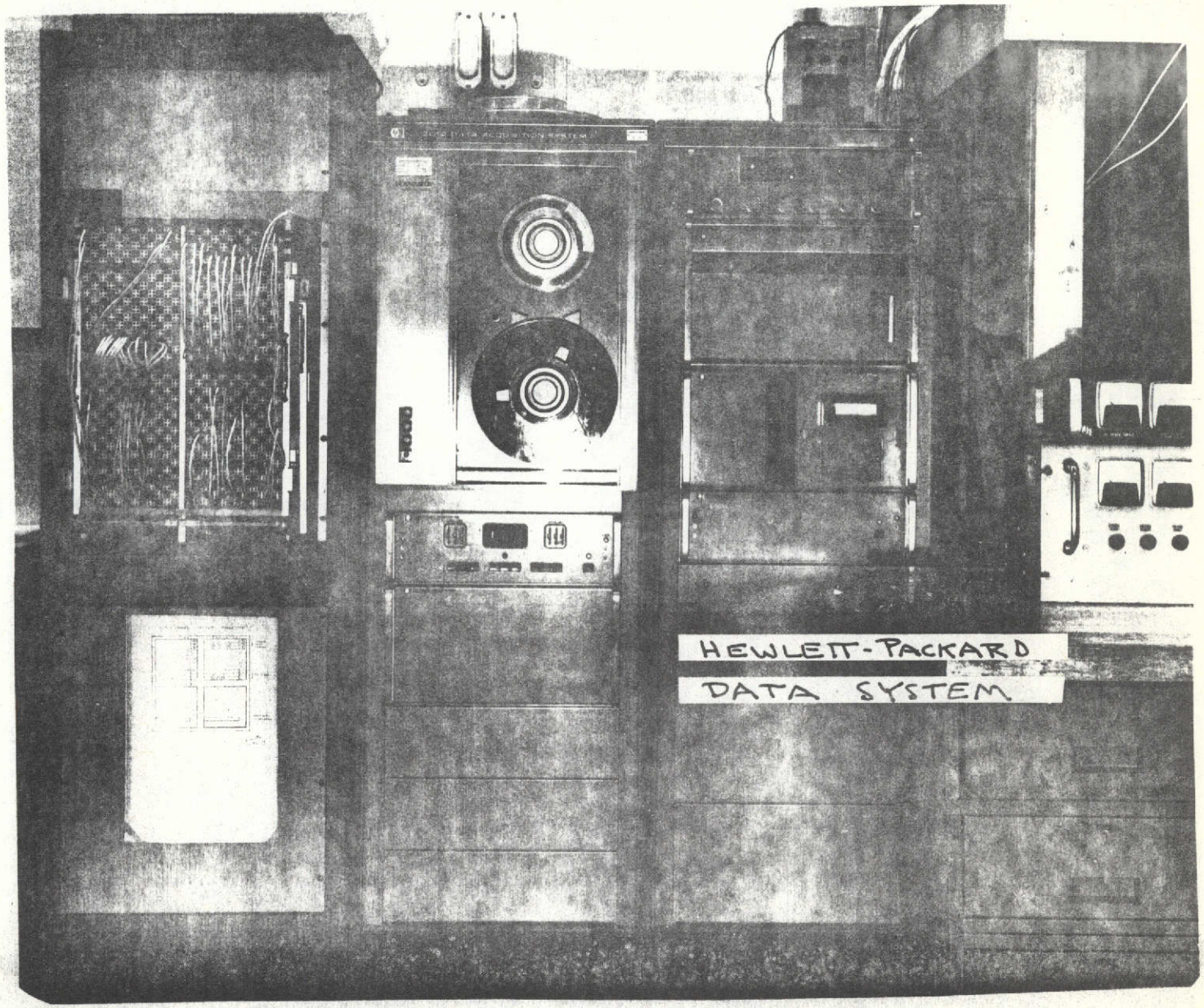

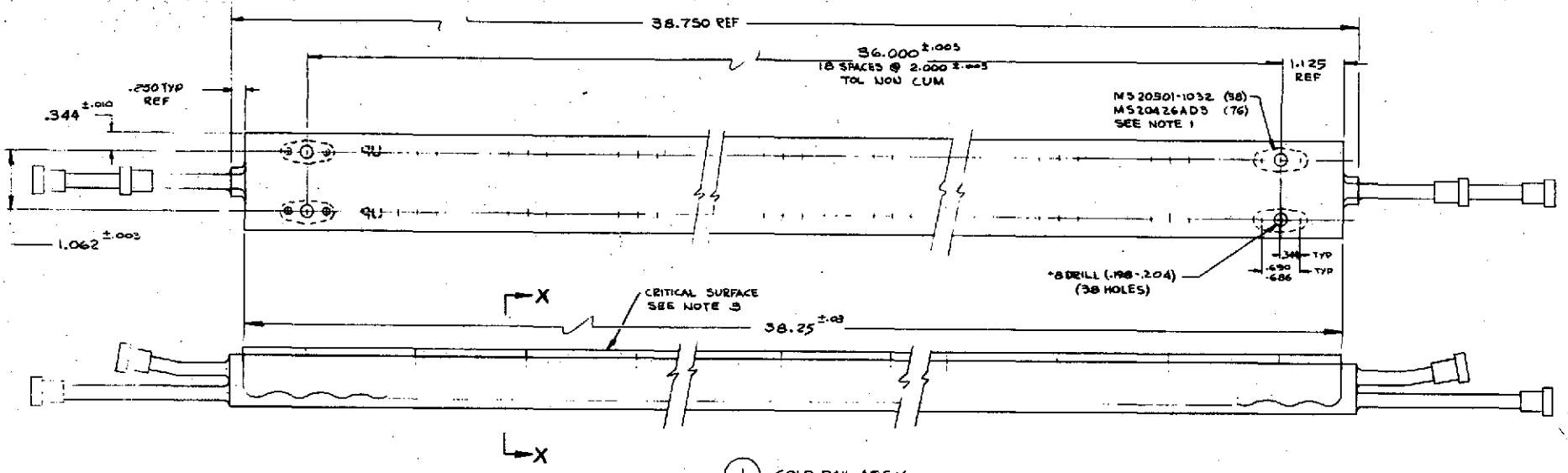

(-1) COLD RAIL ASSY
MAKE FROM LDW330-55054
(TWO REQ'D)

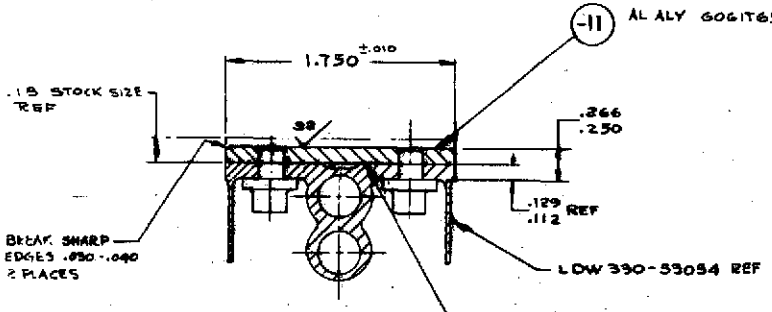

SECTION-XX
SCALE 2/1

NOTES:
1- COUNTERSINK ALL RIVET HEADS FLUSH TO .010 BELOW THE SURFACE OF -11 THERE IS TO BE NO TRIMMING OF RIVETS AFTER ASSEMBLY.
2- MAXIMUM ALLOWABLE DEVIATION FROM STRAIGHT SHALL BE .020 OF AN INCH PER FOOT OF LENGTH AND .50 DEGREE PER FOOT OF LENGTH IN STRAIGHTNESS AND TWIST RESPECTIVELY. MAXIMUM ALLOWABLE DEVIATION FROM FLAT .004 INCHES PER INCH.
3- CRITICAL SURFACE - PROTECT THIS SURFACE WHENEVER POSSIBLE BY TAPING TO PRESERVE ORIGINAL SURFACE FINISH. THE CRITICAL SURFACE SHALL BE SMOOTH AND FREE FROM PROTRUSIONS OF ANY TYPE. GOUGING DUE TO HOLD DOWN TOOLS OR OTHER REASONS NOT PERMITTED.
4- SURFACE OF PART -11 WHICH MATES WITH LDW330-55054 IS A CRITICAL SURFACE AND MUST BE SMOOTH AND FREE FROM PROTRUSIONS AND GOUGINGS WHEN BONDING TOGETHER.

GRUMMAN AEROSPACE
COLD RAIL ASSEMBLY
SCALE: FULL
D.E. 1501 4-27-71
G. Wong 8-17-71
559-114AV

FIGURE 7.1-4

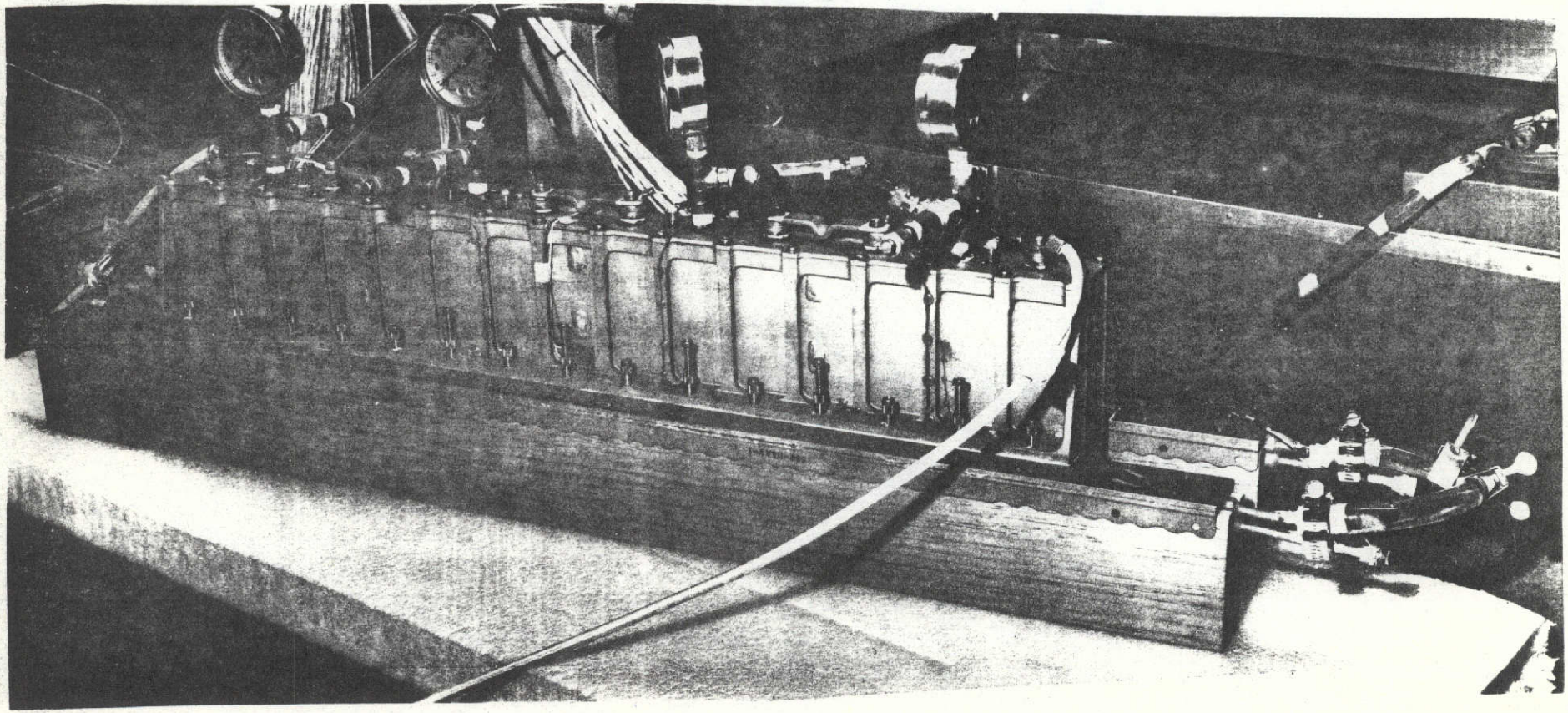

CELL MODULE
MOUNTED ON COLD PLATE

FIGURE 7.1-5

D. Intercell Spacers (see Figure 7.1-7)

1 on spacer #1 facing Cell #19

1 on spacer #3 facing Cell #31

2 total

E. Flange Root (see Figure 7.1-8)

16 (8 per flange)

F. Total Thermocouples on Module: 59

G. Thermocouples on Cooling System (see Figure 7.1-9)

1 pump outlet

2 cold rail inlets

2 cold rail outlets

2 thermopiles (outlets minus inlets)

H. Ambient Air

2 thermocouples at opposite ends of module

All thermocouples were fabricated in the Grumman Thermodynamics Laboratory. They were all 0.005 inch diameter (36 ga) copper-constantan with a one-mil teflon coating; cut to three foot lengths from the same spools of wire. The beads were formed by heliarc welding.

7.1.3.2 Other Instrumentation

A) 4 cell terminal voltages

B) 1 module terminal voltage

C) 1 module current

D) 4 heater voltages

E) 4 heater currents

F) Each cell's pressure was manually recorded from the gauge on its header

G) Time was automatically recorded by the data system from its internal clock

Figure 7.1-6

THERMOCOUPLE LOCATIONS ON* HEATER CELLS

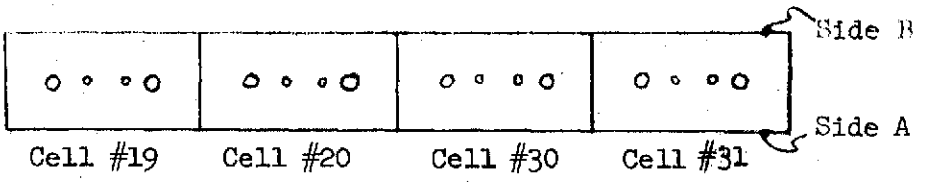

Cells #19, #31: 18 thermocouples (9 on each cell)

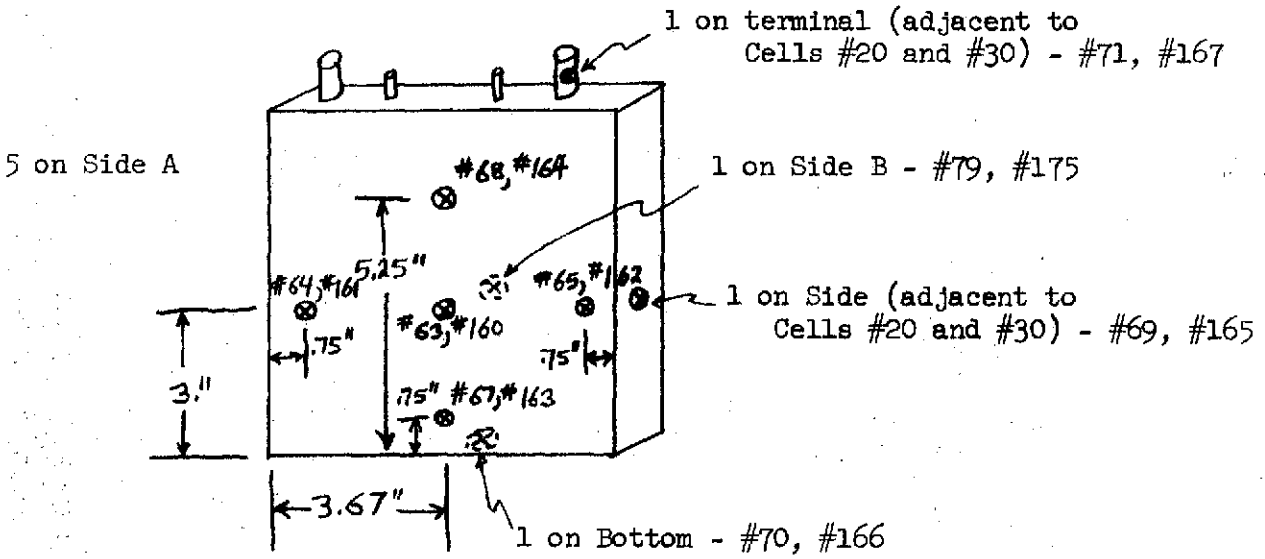

Cells #20, #30: 4 thermocouples (2 on each cell)

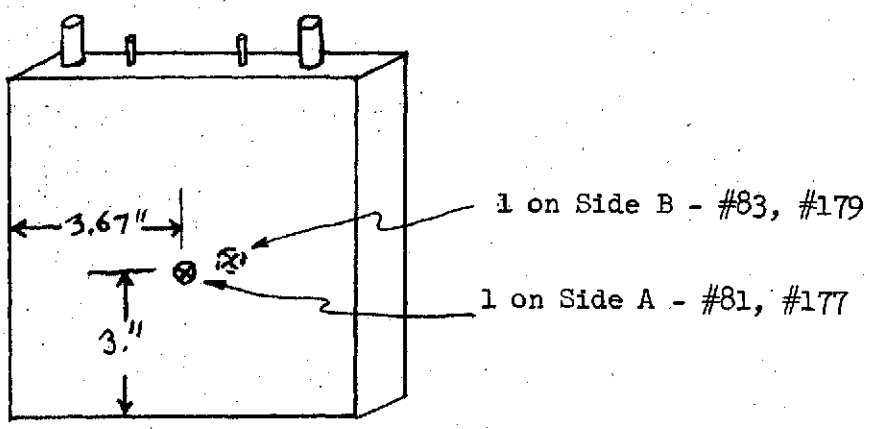

* All thermocouples under the Kapton wrap which covers the five major sides of the cell.

Figure 7.1-7

THERMOCOUPLE LOCATIONS ON WALLS OF MODULE CONTAINER

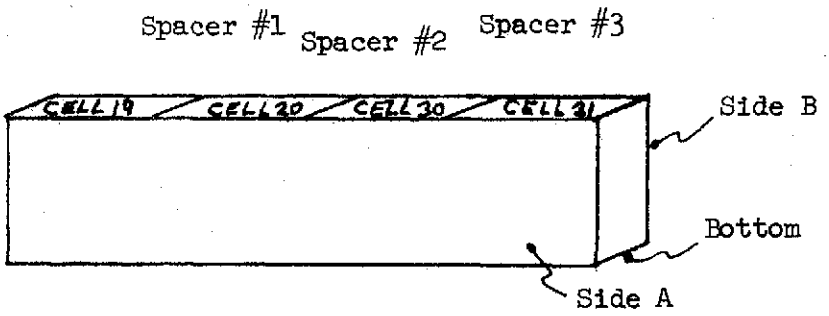

Side A: 13 thermocouples

Exterior View

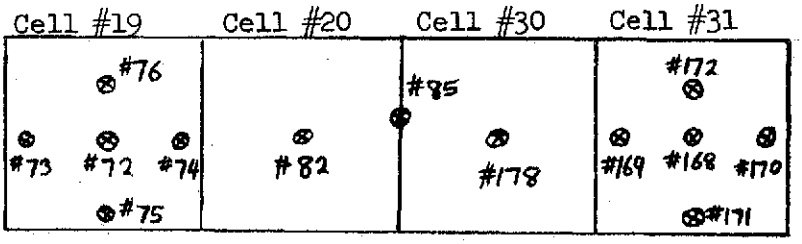

Side B: 4 thermocouples

Exterior View

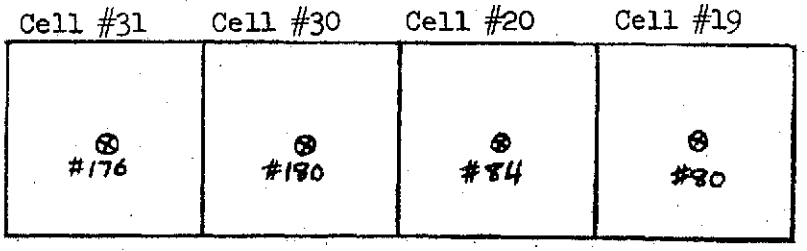

Bottom: 2 thermocouples

Exterior View

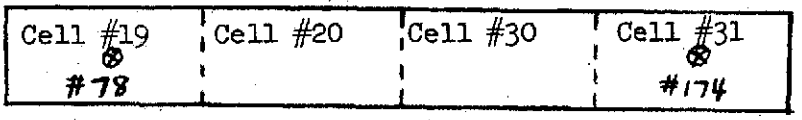

Spacers: 2 thermocouples

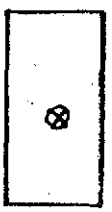

One (1) on spacer #1 facing Cell #19-#77

One (1) on spacer #3 facing Cell #31-#173

Figure 7.1-8

THERMOCOUPLE LOCATIONS ON MODULE MOUNTING FLANGES

16 Thermocouples (8 on each flange)

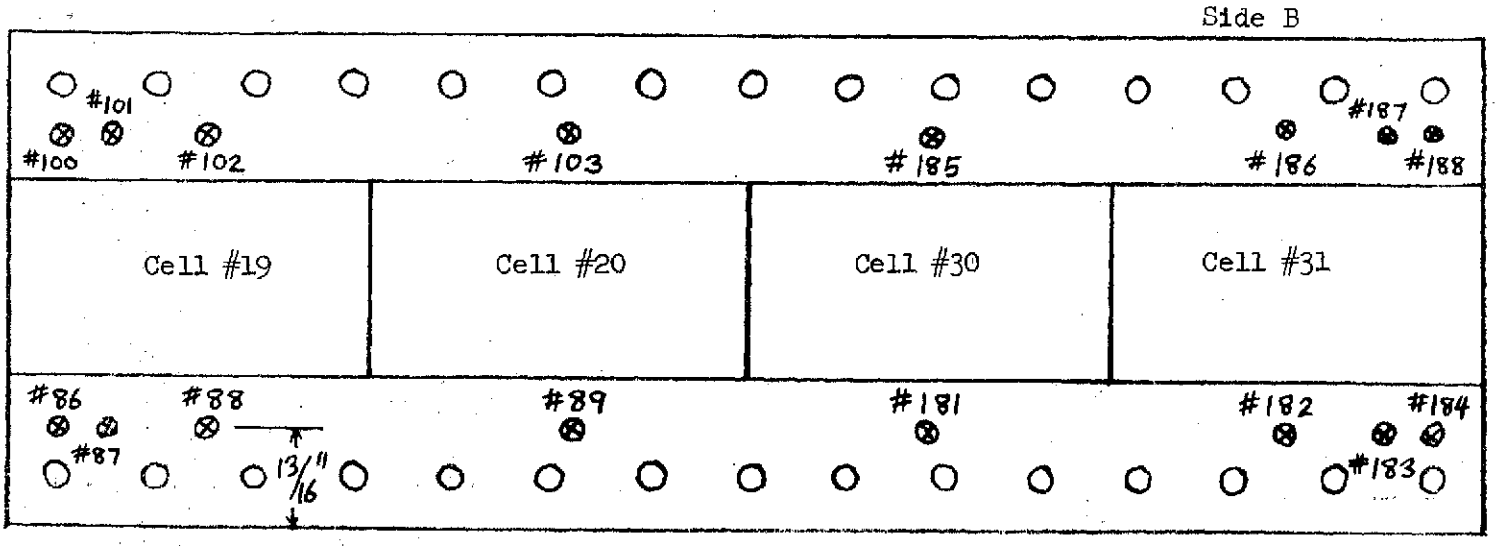

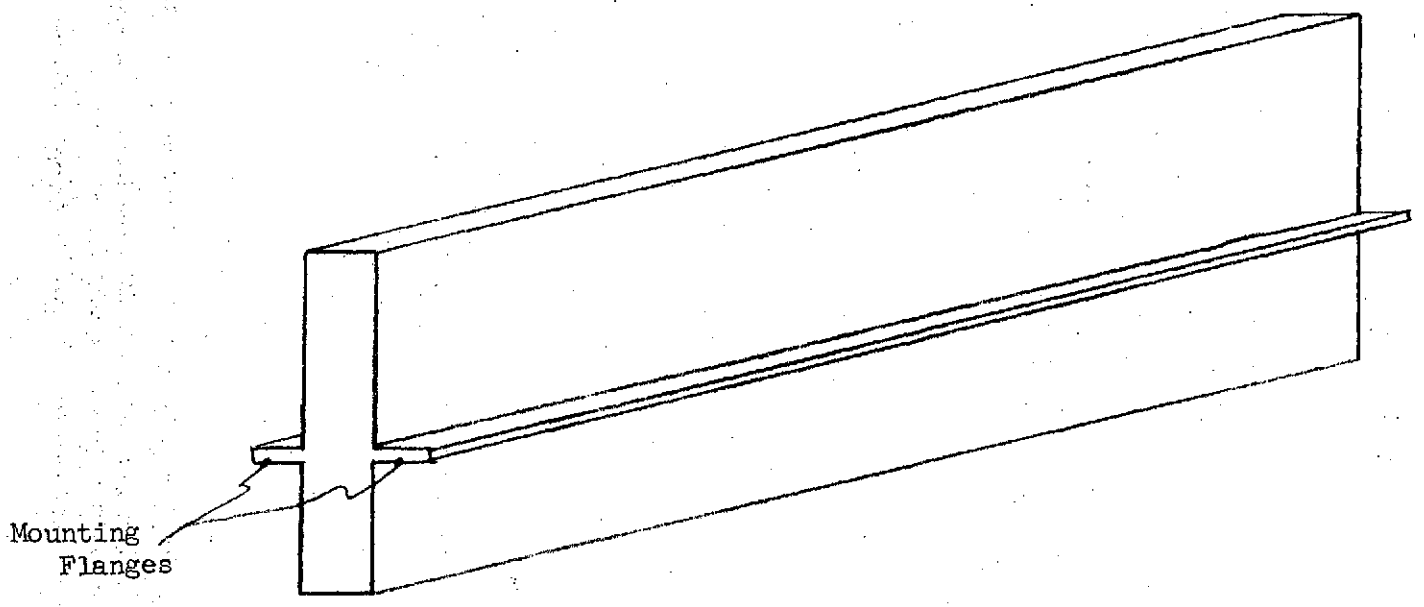

Figure 7.1-9

THERMOCOUPLE LOCATIONS ON COOLING SYSTEM

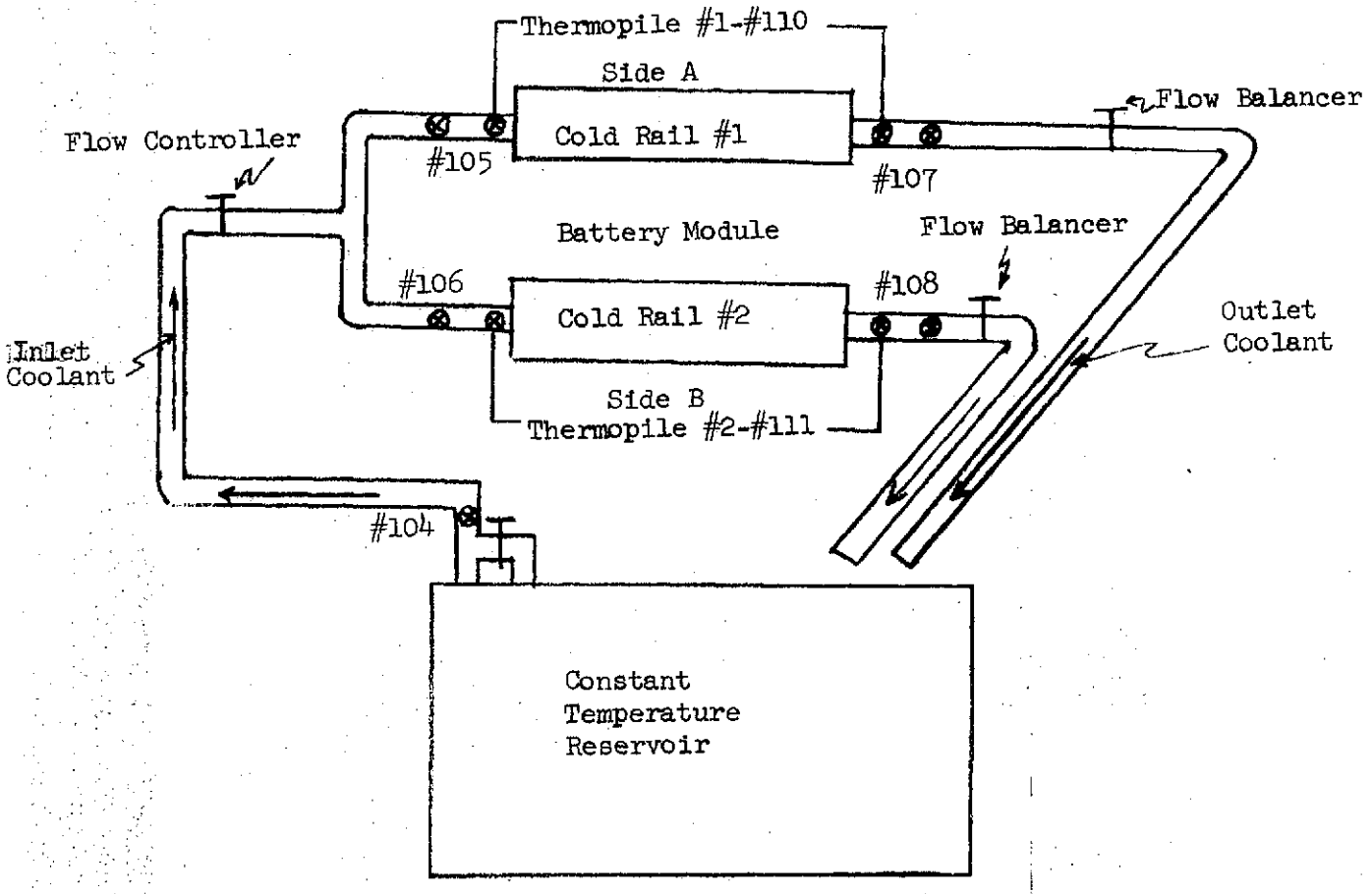

3 thermocouples on inlet coolant (1 common, 2 individual)

2 thermocouples on outlet coolant (2 individual)

2 thermopiles (outlet minus inlet on each coolant leg)

H) Flow rates were monitored by periodically weighing the effluent from each cold rail in a given time period. Adjustments to the total flow were made with a hose-cock on the common inlet tubing, and adjustments in flow balance between the rails were made with hose-cocks on the outlet tubing.

7.1.3.3 Test Equipment

See Table 7.1-1

7.1.3.4 Data System Channel Allocations

See Table 7.1-2

7.1.4 Test Control Circuitry

The "heater" tests (Runs 3-9, 7.1.5 below) were run using individually controlled constant current sources for each cell heater. A schematic for one of these sources is shown in Figure 7.1-10. In the figure, the heater current is monitored in a 20 ampere, 50 mV shunt. The signal across this shunt is compared to a buffered reference voltage tapped from a 0.100 volt source. Comparison and voltage amplification is accomplished in differencing amplifier A2 and the following two (2) NPN transistor stages. Heater current level is directly controlled by the 2N174A power transistors. The 50K, multiturn potentiometer acts as a current level adjustment by varying the actual reference voltage used. The selected currents were:

- o Hot case -- 16 watts/cell -- 20 ampere
- o Cold case -- 3.9 watts/cell -- 9.88 ampere

based on a heater resistance nominal of 0.04 ohm. Actual values for each heater were subject to minor adjustment to allow for tolerance variation and drift.

The "live cell" tests (Runs 10 through 17) were made using Grumman's Test Controller. Since each element of this device

Table 7.1-1

Test Equipment

Item #	Description	Manufacturer	Model #	# Required
1	200 (3-wire) channel, Data Acquisition System	Hewlett-Packard	2012B	(1)
2	Heater Power Supply, 40 V, 125 amp	Sorensen	DCR40-125A	(1)
3	Module Power Supply, 100 amp, 10 volt	Sorensen	SRL-10-100A	(1)
4	Discharge/Charge Control Circuitry	Grumman		(1)
5	Heater Power Control Circuitry	Grumman		(1)
6	Refrigerated/Heated Constant Temperature Bath (Reservoir)	Lab-Line Instruments	3324-x	(1)
7	Temperature Regulator	"	3202	(1)
8	50 Channel, Copper-Constantin, 0°C Reference Junction	Jos. Kaye & Co.		(2)

Table 7.1-2

Data System Channel Allocations

Data Channel #	Scale	Type	Measurement Description
60	100 MV	Temperature	Spare Channel
61			Spare Channel
62			Room temperature, outlet end
63			Cell #19, side A, center
64			(a)*Cell #19, side A, left
65			Spare
66			Cell #19, side A, right
67			Cell #19, side A, lower
68			Cell #19, side A, upper
69			Cell #19, narrow side adj. to Cell#2(
70			Cell #19, bottom
71			Cell #19, neg. terminal
72			Side A, opposite #63
73			Side A, opposite #64
74			Side A, opposite #66
75			Side A, opposite #67
76			Side A, opposite #68
77			(a)*Space #, opposite #69
78			Bottom, opposite #70
79			Cell #19, side B, center
80			Side B, opposite #79
81			Cell #20, side A, center
82			Side A, opposite #81
83			Cell #20, side B, center
84			Side B, opposite #83
85			Side A, temperature of 200 temperature sensing resistor
86			Side A, flange root, end bolt adj. to cell #19
87			Side A, Flange root, 1" in from #86
88			Side A, flange root, center of #19
89			Side A, Flange root, center of #20
100			Side B, flange root, end bolt adj. to cell #19
101			Side B, flange root, 1" in from #100
102			Side B, flange root, center of #19
103			Side B, flange root, center of #20
104			(b) Pump outlet
105			Rail #1 inlet (battery Side A)
106			Rail #2 inlet (battery Side B)
107			(c) Rail #1 outlet (battery side A)
108			Rail #2 outlet (battery Side B)
109			Spare
110			Cu-Cm thermopile #1 (rail #1)
111	100 MV	Temperature	Cu-CM thermopile #2 (rail #2)
112		Shunt Voltage	Heater current, cell #19
113			Heater current, cell #20
114			Heater current, cell #30
115			Heater current, cell #31
116		Calibration	Shorted channel
117	10V	Calibration	Standard cell
118	10V	Calibration	Standard cell

Table 7.1-2

(Continued)

Data Channel #	Scale	Type	Measurement Description
119	10V	Voltage	Heater voltage, cell #19
120			Heater voltage, cell #20
121			Heater voltage, cell #30
122			Heater voltage, cell #31
123			Terminal voltage, cell #31
124			Terminal voltage, cell #30
125			Terminal voltage, cell #20
126			Terminal voltage, cell #19
127			String current
128			Shorted channel (calibration)
129	10V	Voltage	Module voltage
160	100 MV	Temperature	*Cell #31, side A, center
161			*Cell #31, side A, left
162			Cell #31, side A, right
163			Cell #31, side A, lower
164			Cell #31, side B, upper
165			Cell #31, narrow side adj. to cell#30
166			Cell #31, bottom
167			Cell #31, pos. terminal
168			Side A, opposite #160
169			Side A, opposite #161
170			Side A, opposite #162
171			Side A, opposite #163
172			Side A, opposite #164
173			Spacer #3, opposite #165
174			Bottom, opposite #166
175			Cell #31, side B, center
176			Side B, opposite #175
177			Cell #30, side A, center
178			Side A, opposite #178
179			Cell #30, side B, center
180			Side B, opposite #179
181			Side A, flange root, center of #30
182			Side A, flange root, center of #31
183			Side A, flange root, 1" in from end bottom adj. to cell #31
184			Side A, flange root, end bolt adj. to cell #31
185			Side B, flange root, center cell #30
186			Side B, flange root, center of 31
187			Side B, flange root, 1" in from end bolt adj. to cell #31
188			Side B, flange root, end bolt adj. to cell #31
189	100 MV	Temperature	Room temperature, inlet end
190		Internal Calibration	
191		Internal Calibration	

a) Thermocouples number 64, 77, 160 and 161 (all within the module)were found to be open circuited after fabrication. These channels were shorted at the reference junction input hence they read room temperature.

b) Thermocouple #104 was accidentally open circuited after run # 9 and not replaced since it was not a critical measurement. In following runs it read room temperature.

(Concluded)

c) Thermocouple #107 was accidentally lost while repairing a leak in the coolant loop prior to run # 10 . It could not be conveniently shorted out and was left open circuited.

d) Channels 60 through 109 on reference junction #1, channels 160 through 189 on reference junction 2.

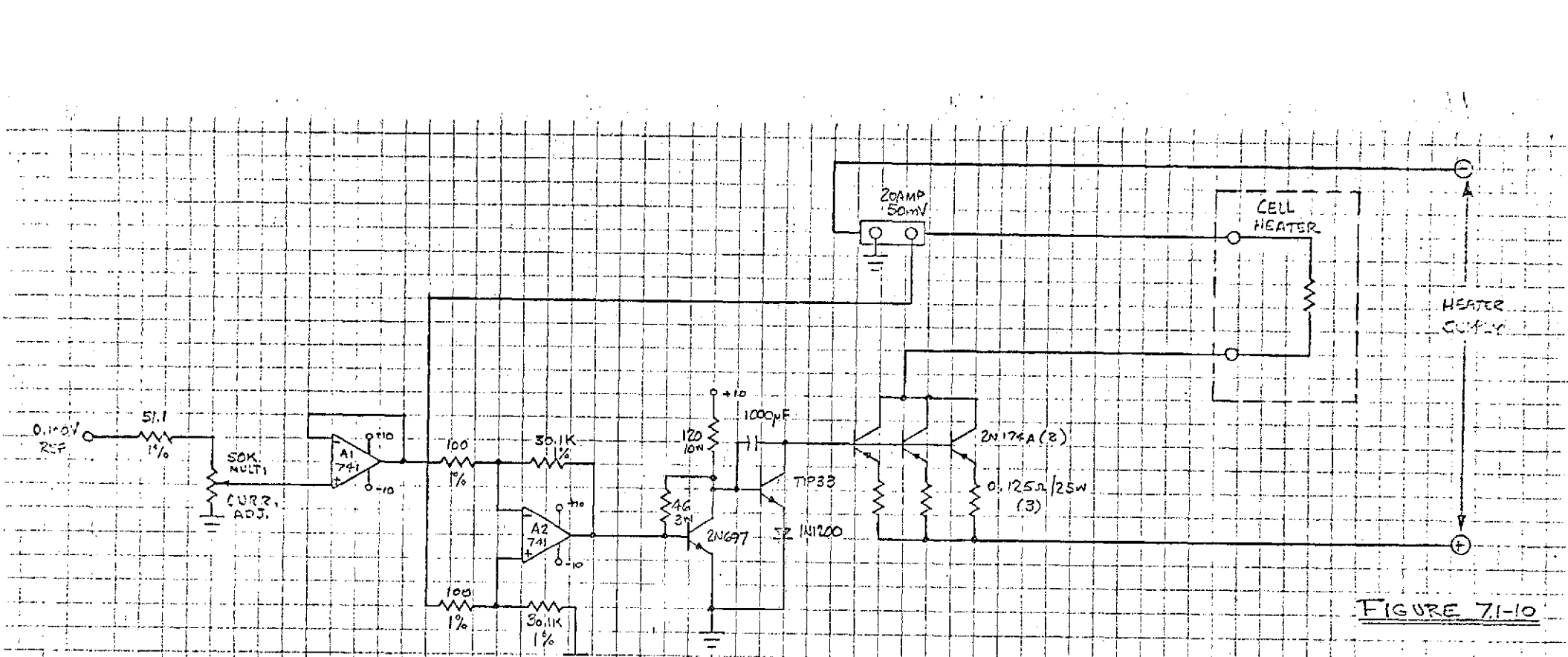

FIGURE 7.1-10

MODULE TEST SET-UP
CELL HEATER CURRENT CONTROL
CELL THERMAL TESTS

TW 10/14/71

has been previously described in detail in Monthly Progress Reports, a block diagram showing the electrical test set up is included as Figure 7.1-11. In this diagram, the functional interrelationships of the various elements is clearly demonstrated as follows:

a) The test begins with the module's cells fully charged

b) When bias power is applied, and a manual RESET command is issued, contactors K1 and K2 will be closed, placing the system in CHARGE mode until the next timing pulse occurs.

c) The next timing pulse (count 1--generated by the relay closure in the DDAS, and buffered by the "Relay Logic Interface") causes a DISCHARGE command to be issued by the "Counter-Coincidence Gates" block. This starts a chain of events which result in the opening of K1 and K2, and the closing of K3 and K4, configuring in DISCHARGE mode.

d) DISCHARGE mode continues until count 37 is reached (36-minute interval), at which time a CHARGE command is issued. K3 and K4 open, K1 and K2 close, and CHARGE mode is enabled.

e) At count 94, the counter is reset to zero. At the next pulse, count 1, the cycle repeats.

f) In the DISCHARGE mode, the discharge-side reference portion of the "Charge-Discharge Current Control" controls the main power current. The value of this current -- set by precision resistor networks on plug-in sub-boards -- depends on the desired depth of discharge, and is as follows:

12% DOD -- 20 amperes (C/5)

30% DOD -- 50 amperes (C/2)

50% DOD -- 83.3 amperes (C/1.2)

For this mode, the "Volt-Temp. Detector" is inoperative. Control is exerted through the current programming terminals of the "Charge-Discharge Power Supply".

g) In the CHARGE mode, operation always begins at 83.3 amperes (C/1.2). When the "Volt-Temp. Detector" senses that the module voltage has reached its preset limit, the current is stepped down to 50 amperes (C/2), resulting in a reduction of module voltage. When module voltage again rises to limit, current is reduced to 20 amperes (C/5); and the last reduction is to 5 amperes (C/20). The module voltage limit during charge is a linear relationship between the following two points:

$0^{\circ}C$ -- 6.24 volts (1.56 V/cell av.)

$20^{\circ}C$ -- 6.04 volts (1.51 V/cell av.)

This relationship is established by mixing the resistance change of the positive temperature coefficient (PTC) resistor (mounted on the module) with the sensed voltage.

It should be noted that, in the process of eliminating various "bugs" from the original Test Controller design, considerable condensation and simplification has occurred. The final design, to be reported fully elsewhere, is a simple, reliable system, requiring only the safety circuitry (for fail-safe unattended operation) to be complete. A further simplification will be made by using the DDAS's time signal instead of the relay closure for future tests.

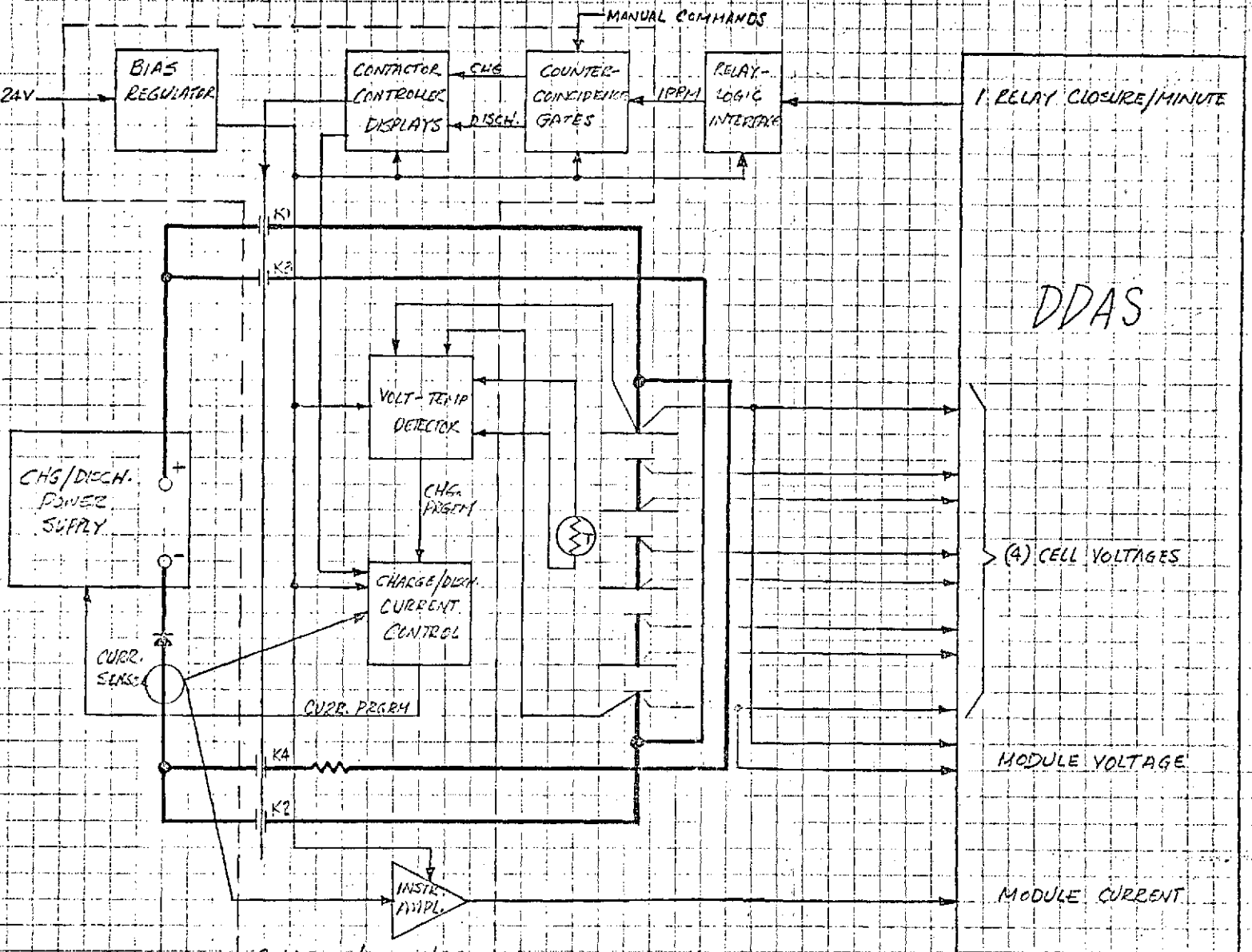

FIGURE 7.1-11

BLOCK DIAGRAM
MODULE ELECTRICAL TEST SET-UP
ACTIVE CELL TESTS

10/12/11

7.1.5 Test Run Log

Run #	Date	Type Run	Description
	11 June 1971	Checkout	Unpowered coolant/data system checkout
	15 June 1971	Checkout	Heater control circuit checkout
	16 June 1971	Heater	16 watts per cell (50% DOD simulation), 55°F coolant inlet, 15 lb. (hr. rail) flow rate. Cells evacuated, all mounting bolts secured.
A	17 June 1971	Heater	16 watts per cell (50% DOD simulation), 55°F coolant inlet, 15 lb/(hr-rail) flow rate. Cell pressurized with N2 for three cycles; 100 psig for 58 minutes, 0 psig for 36 minutes
B	17 June 1971	Heater	Repeat of run #4A except 150 lb/(hr-rail) flow rate
	18 June 1971	Heater	3.9 watts per cell (12% DOD simulation), 32°F coolant inlet, 150 lb./(hr-rail) flow rate. Cells at 0 psig N2.
	22 June 1971	Heater	16 watts per cell (50% DOD simulation), 55°F coolant inlet, 15 lb/(hr-rail) flow rate. Cells at 0 psig N2.
A	23 June 1971	Heater	Repeat of run #6 with cells evacuated.
B	23 June 1971	Heater	Repeat of run #7A with 150 lb/(hr-rail) flow rate
	24 June 1971	Heater	Repeat of run #7A with two pass cooling configuration
	25 June 1971	Heater	Repeat of run #8
)	20 August 1971	Checkout	Checkout of orbital control circuitry
L	24 August 1971	Live	4-50% DOD cycles, 55°F coolant inlet, 15 lb/(hr-rail)
2	25 August 1971	Live	Repeat of run #11 with 5 complete orbits
3	27 August 1971	Live	4-12% DOD cycles, 32°F coolant inlet, 25 lb/(hr-rail) flow rate
4	1 Sept. 1971	Live	5-30% DOD cycles, 45°F coolant inlet, 15 lb/(hr-rail) flow rate
5	3 Sept. 1971	Live	Same as run #14 with 6 orbital cycles
6	9 Sept. 1971	Checkout	Checkout of 12% DOD controls
7	10 Sept. 1971	Live	Repeat of run #13 with 6 orbital cycles.

7.2 Heater Test Results

7.2.1 Heater Test Series

Test runs 1 through 9 comprise the heater powered series of runs. Each of these is described in 7.2.1.1 below, and the pertinent data from each is presented. A discussion of the data is found in 7.2.1.2.

7.2.1.1 Heater Test Data

Runs #1 and #2:

Runs number 1 and 2 were checkout runs in which the proper operation of the control circuitry, instrumentation, data acquisition system and the cooling system were verified. No data is presented for these two runs.

Run #3:

In run number 3, the insulated, unpowered module was supplied with 55°F coolant (water) at a flow rate of 15 pounds per hour per cold rail. All mounting bolts were secured and only one coolant passage per cold rail was active. The temperatures in the system were monitored until stabilization had occurred. Figure 7.2-1 is a temperature map of all the module and coolant system thermocouples following stabilization. As can be seen in the figure, there is a 1°F temperature rise in the coolant reflecting the environmental heat leak into the system. The module thermocouples show that near isothermal conditions exist throughout the module.

Following unpowered stabilization, power was supplied to each heater at a nominal rate of 16 watts per cell until equilibrium was re-established.

Figure 7.2-2 shows the total power to the module vs. time beginning with the time power was initially applied. The figure also shows the change in temperature of a selected thermocouple (#85 - the temperature sensing resistor's (TSR) temperature) from which one may see when equilibrium was achieved, and the variation of inlet coolant temperature during the run.

Figure 7.2-3 is a temperature map of the module at "powered equilibrium".

MODULE STEADY STATE TEMPERATURE DISTRIBUTION

RUN NO. 3

SIDE A

SIDE B

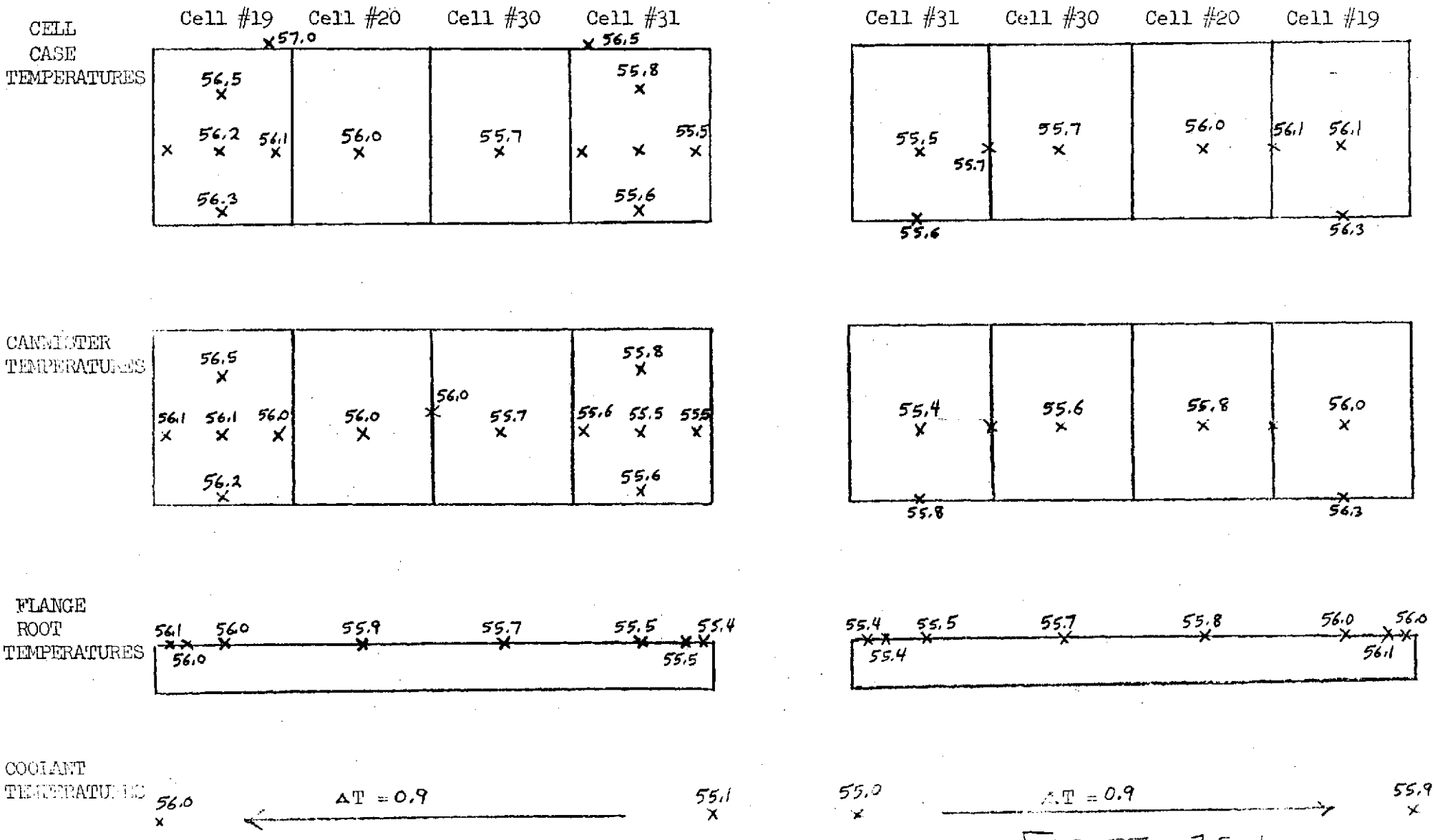

FIGURE 7.2-1

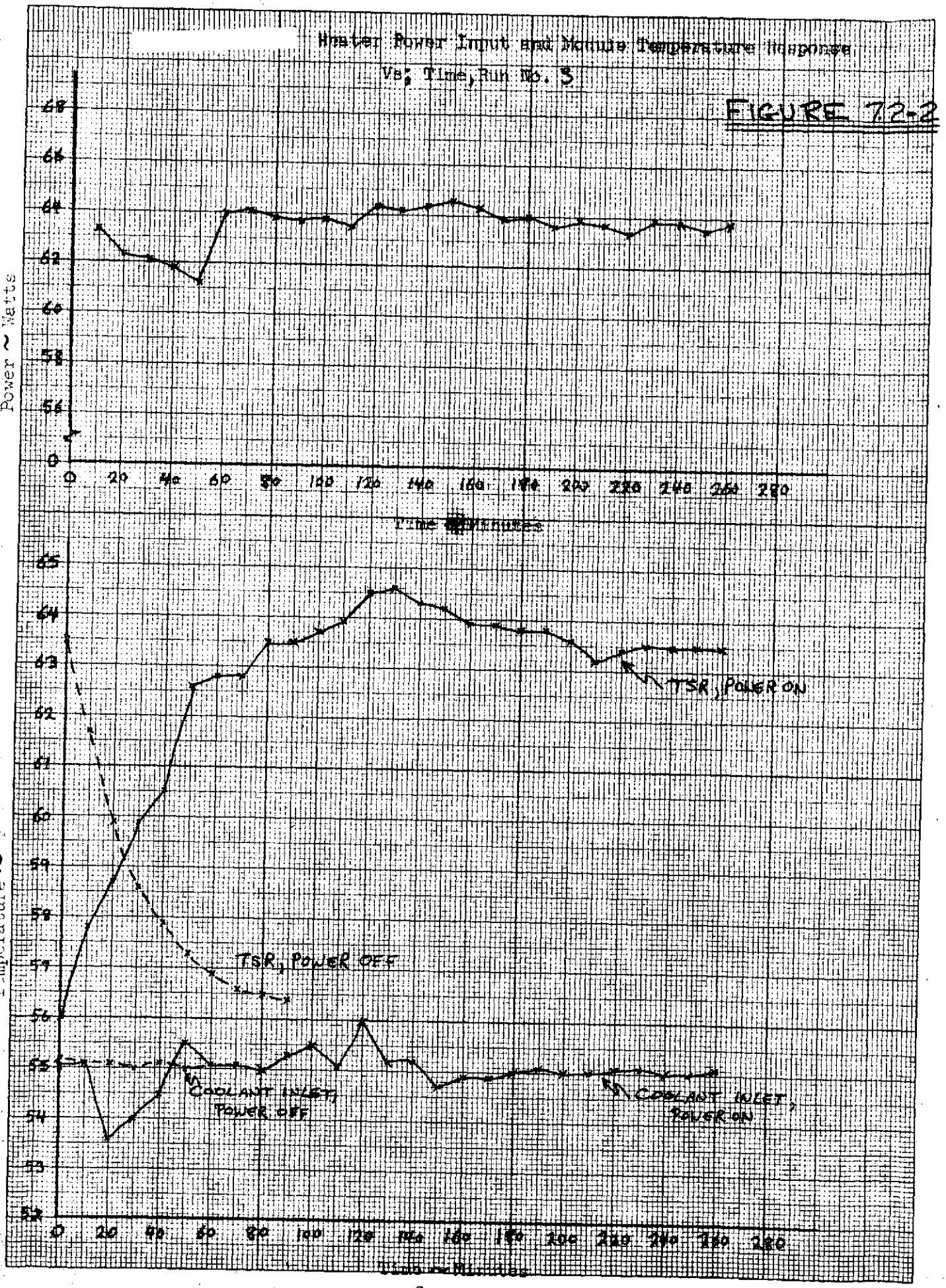

FIGURE 7.2-2

MODULE STEADY STATE TEMPERATURE DISTRIBUTION

RUN NO. 3

SIDE A

SIDE B

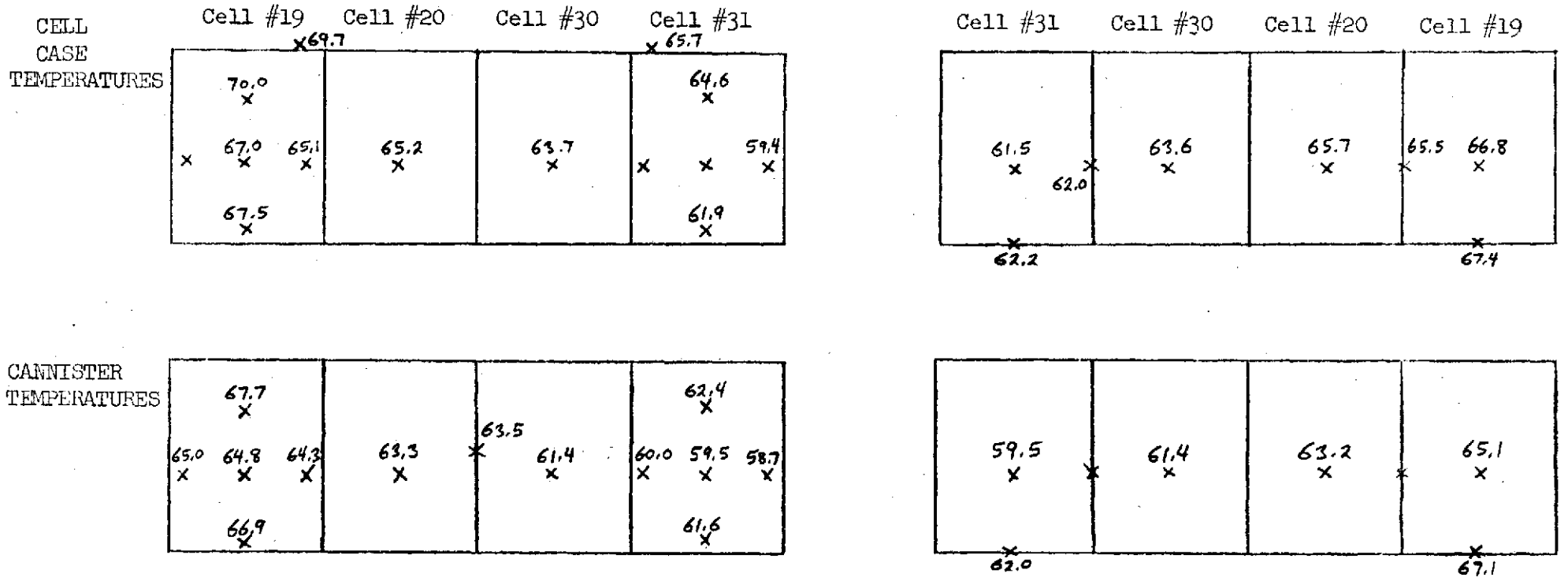

FIGURE 7.2-3

Figure 7.2-4 is a plot of coolant temperature, flange root temperature, center cell face (cell reference) temperature, maximum cell temperature (top of broad face), and center of cell face temperature versus distance along the module.

Following stabilization, power to the heaters was cut and the module allowed to re-stabilize at the coolant temperatures. Figure 7.2-2 also contains a plot of the TSR and coolant inlet temperatures from the time heater power was interrupted. This data was used to determine the thermal time constant for the system.

Runs #4A and #4B

Run number 4A was a repeat of run #3 with the exception that the intercell connectors were installed prior to the test, and the pressure in the cells was cycled from 0 to 100 psig with dry nitrogen.

Equilibrium conditions on the unpowered module were first established at a coolant inlet temperature of 55°F and a flow rate of 15 pounds per hour per rail. Figure 7.2-5 is a temperature map of the module prior to the application of heater power.

Power was then supplied to the heaters at a nominal rate of 16 watts per cell. Figure 7.2-6 shows the response of thermocouple #85 vs. time for the powered portion of the run. Additionally, the inlet coolant temperature and power input to the module are plotted vs. time. The cell pressurization schedule is superimposed on the timeline.

Figure 7.2-7 is a temperature map of the module after equilibrium had been reached. Figure 7.2-8 is a plot of coolant temperature, flange root temperature, cell reference temperature and maximum cell temperature vs. distance along the module.

Run #4B was a repetition of 4A, except flow rate to the

FIGURE 7.2-4

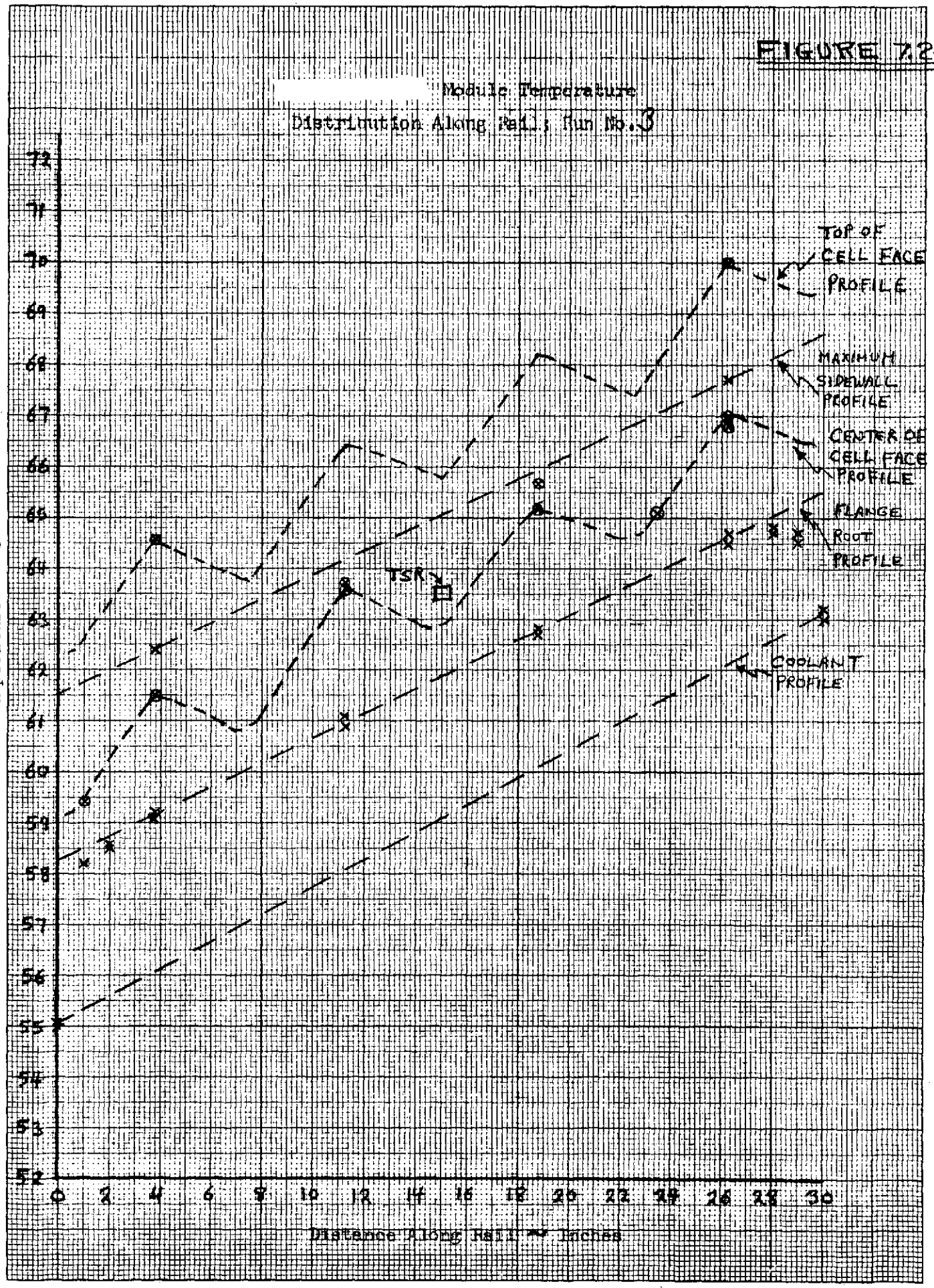

MODULE STEADY STATE TEMPERATURE DISTRIBUTION

RUN NO. 4A

SIDE A

SIDE B

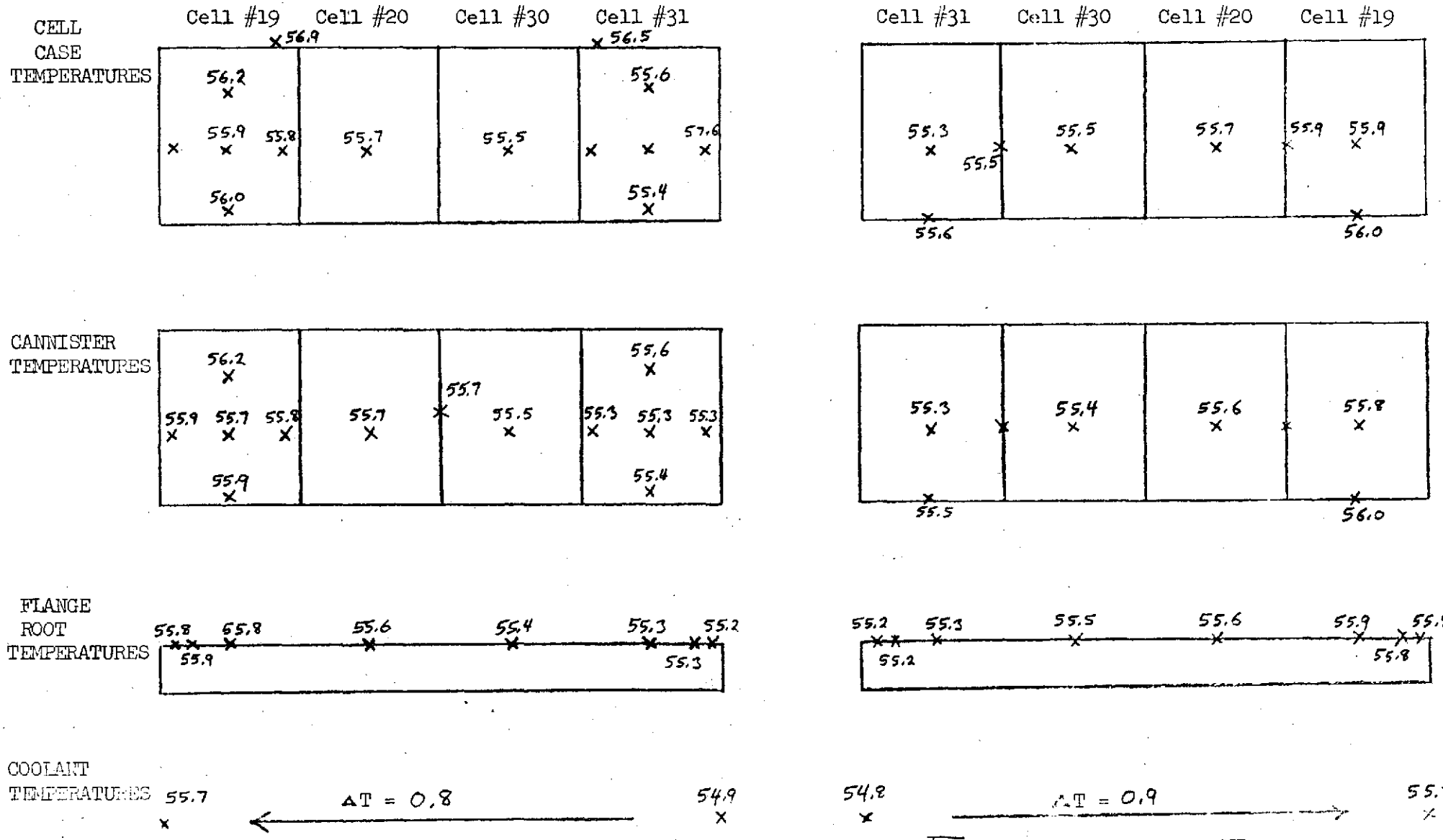

FIGURE 7.2-5

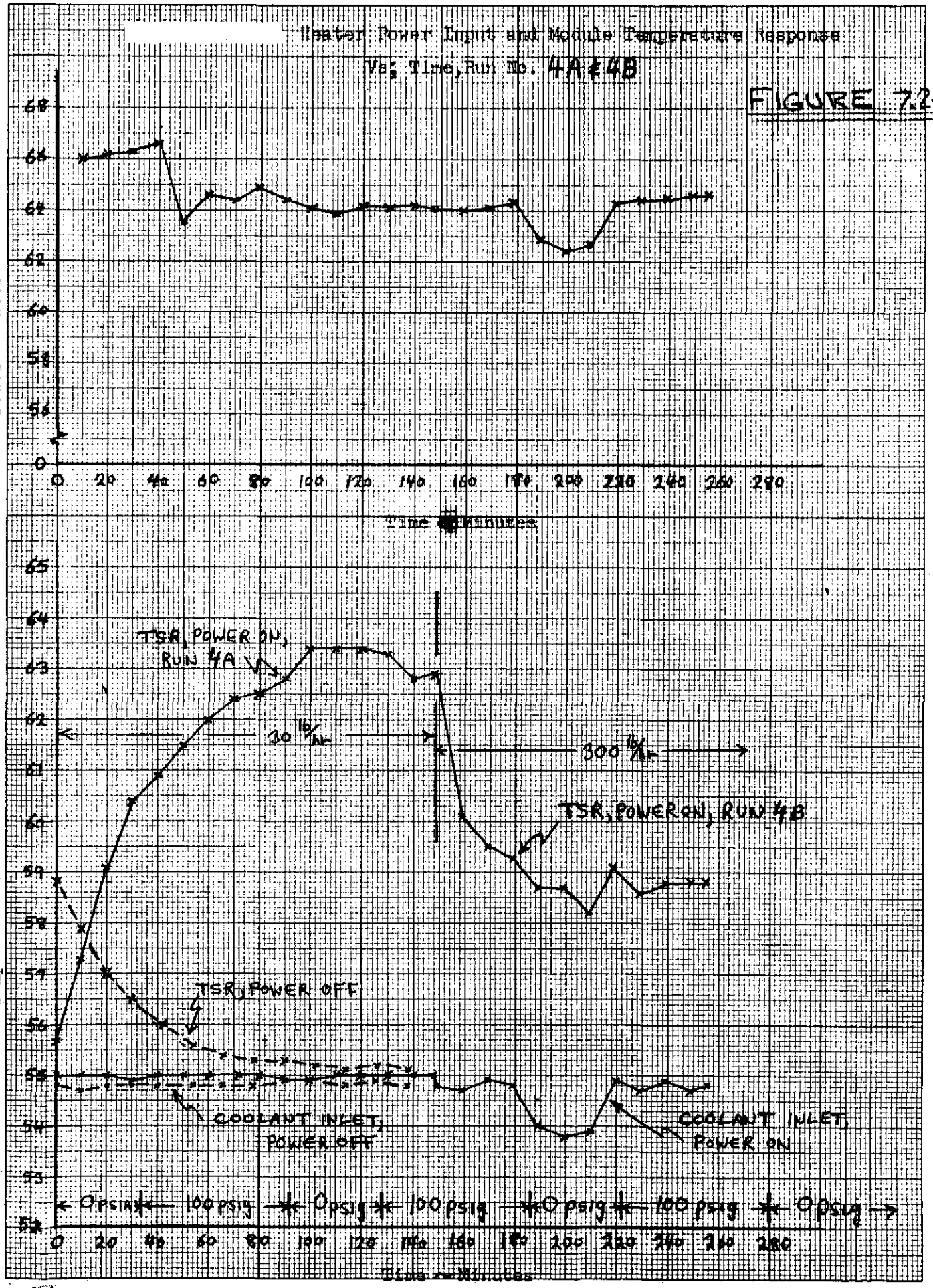

FIGURE 7.2-6

C-2

MODULE STEADY STATE TEMPERATURE DISTRIBUTION

RUN NO. 4A

SIDE A

SIDE B

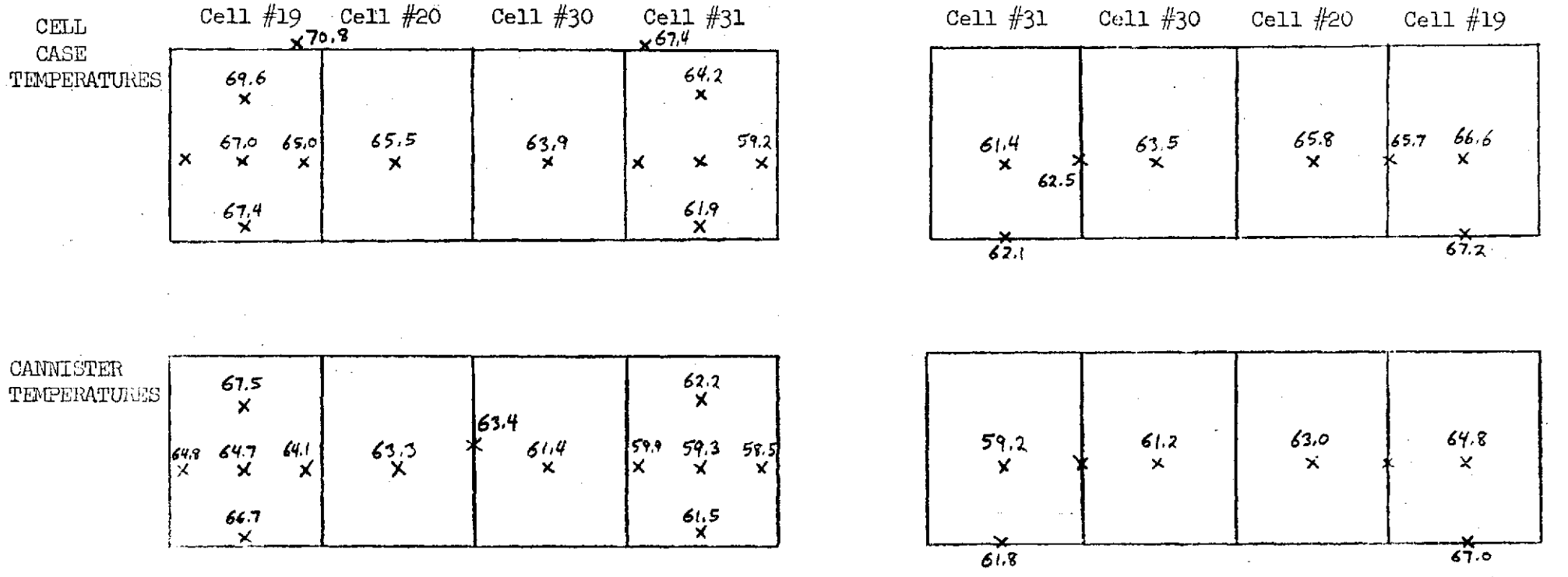

FIGURE 7.2-7

FIGURE 72-8

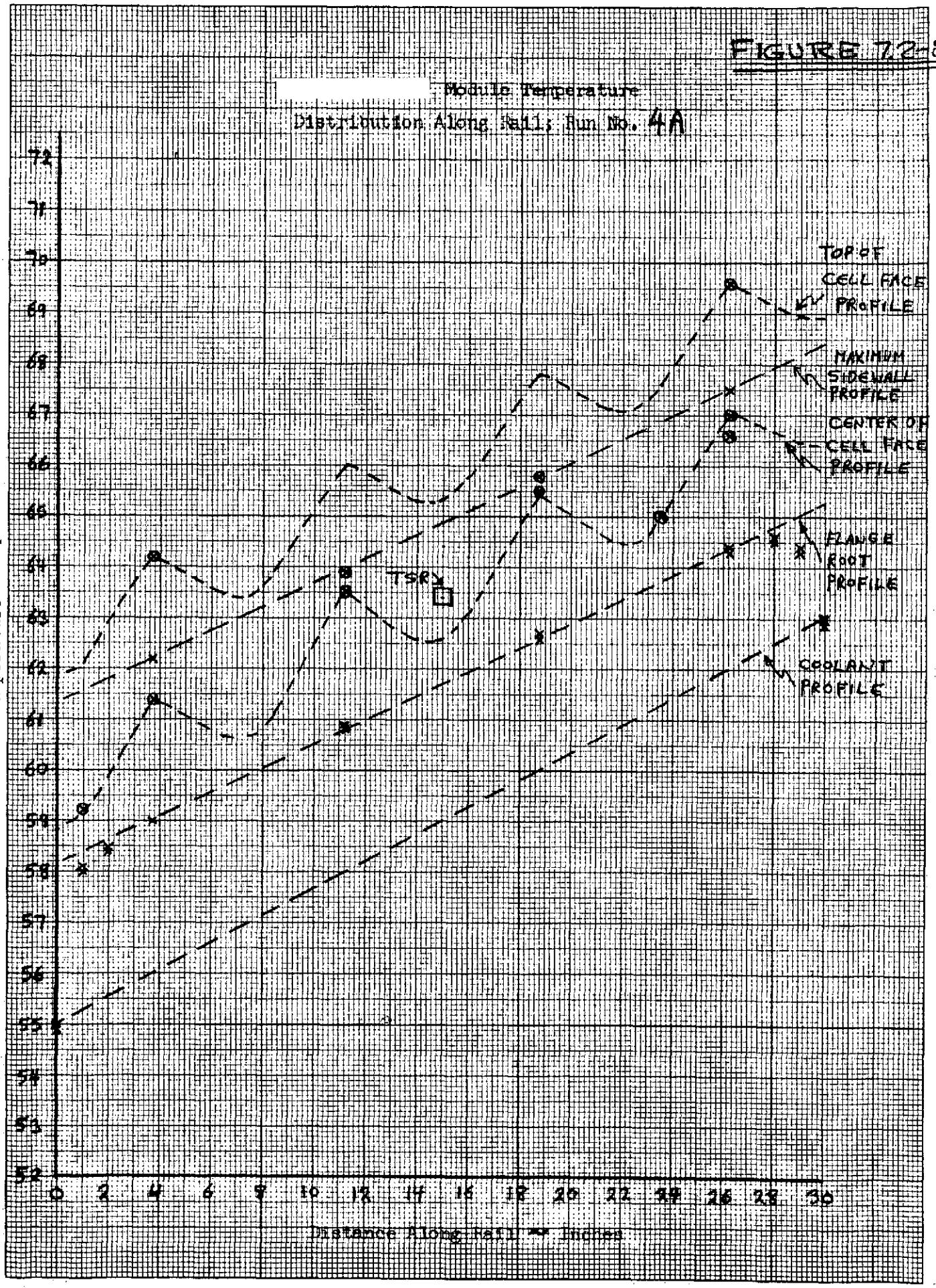

module was increased to the maximum achievable with the pumping system. The maximum flow rate was 300 pounds per hour (150 lb/hr-rail). The power input, inlet coolant temperature and TSR temperature are shown plotted against time in Figure 7.2-6.

Figure 7.2-9 is a temperature map of the module following equilibration at the 16 watt per cell, 300 pound per hour condition. Figure 7.2-10 is a plot of coolant, flange root, cell reference and maximum cell temperature vs. distance along the module.

Figure 7.2-6 also contains a plot of the TSR and inlet coolant temperature vs. time following interruption of heater power to the cells.

Run #5

Run number 5 was conducted on the insulated module at an inlet coolant temperature of 32°F; a high flow rate (approximately 150 pounds per hour per rail); and a heater input of 3.9 watts per cell. This run simulated the cold design case (12% depth of discharge).

Figure 7.2-11 shows a temperature map of the module at equilibrium prior to the application of heater power.

Figure 7.2-12 shows the TSR temperature, power input to the heaters, and the inlet coolant temperature profiles during the run.

Figure 7.2-13 is a temperature map of the module at equilibrium while powered; while Figure 7.2-14 is a plot of coolant temperature, flange root temperature, cell reference temperature and maximum cell temperature vs. distance along the module.

The temperature decay of the system following cessation of heater power was not monitored.

Run #6

Prior to run number 6, the captive bolts holding the module

MODULE STEADY STATE TEMPERATURE DISTRIBUTION

RUN NO. 4B

SIDE A

SIDE B

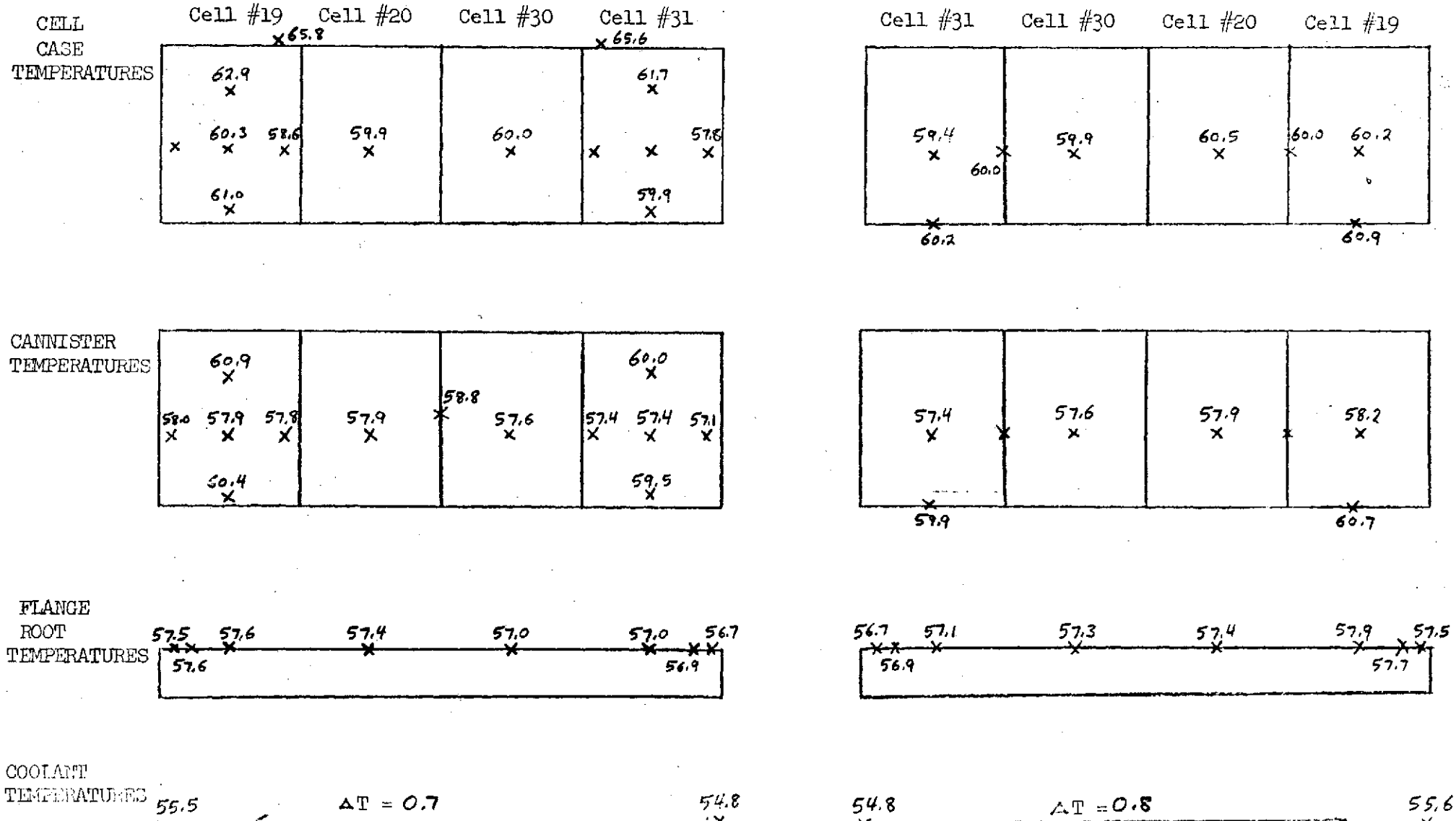

FIGURE 7.2-9

FIGURE 7.2-10

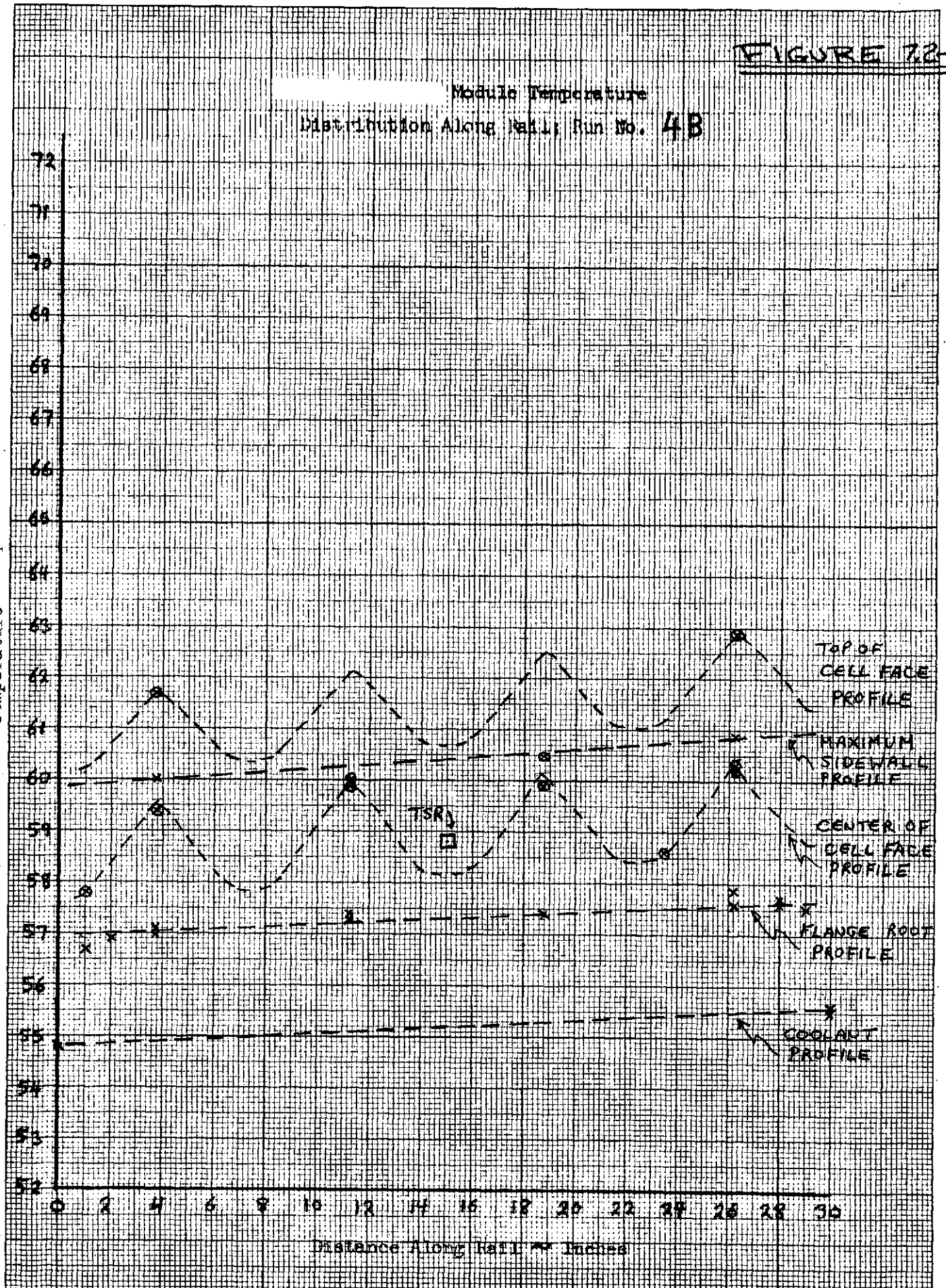

MODULE STEADY STATE TEMPERATURE DISTRIBUTION

RUN NO. 5

SIDE A

SIDE B

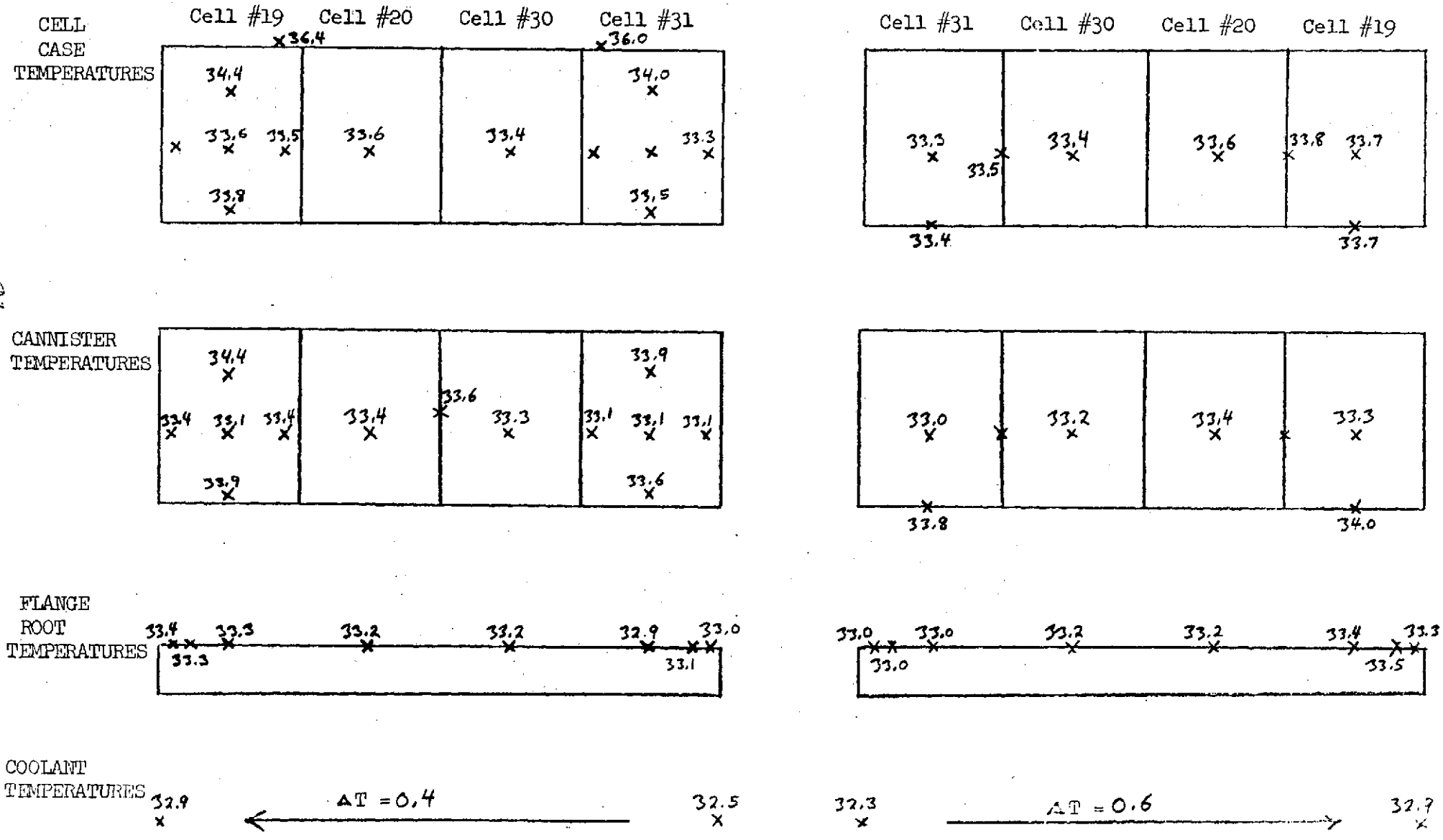

FIGURE 7.2-11

FIGURE 22-12

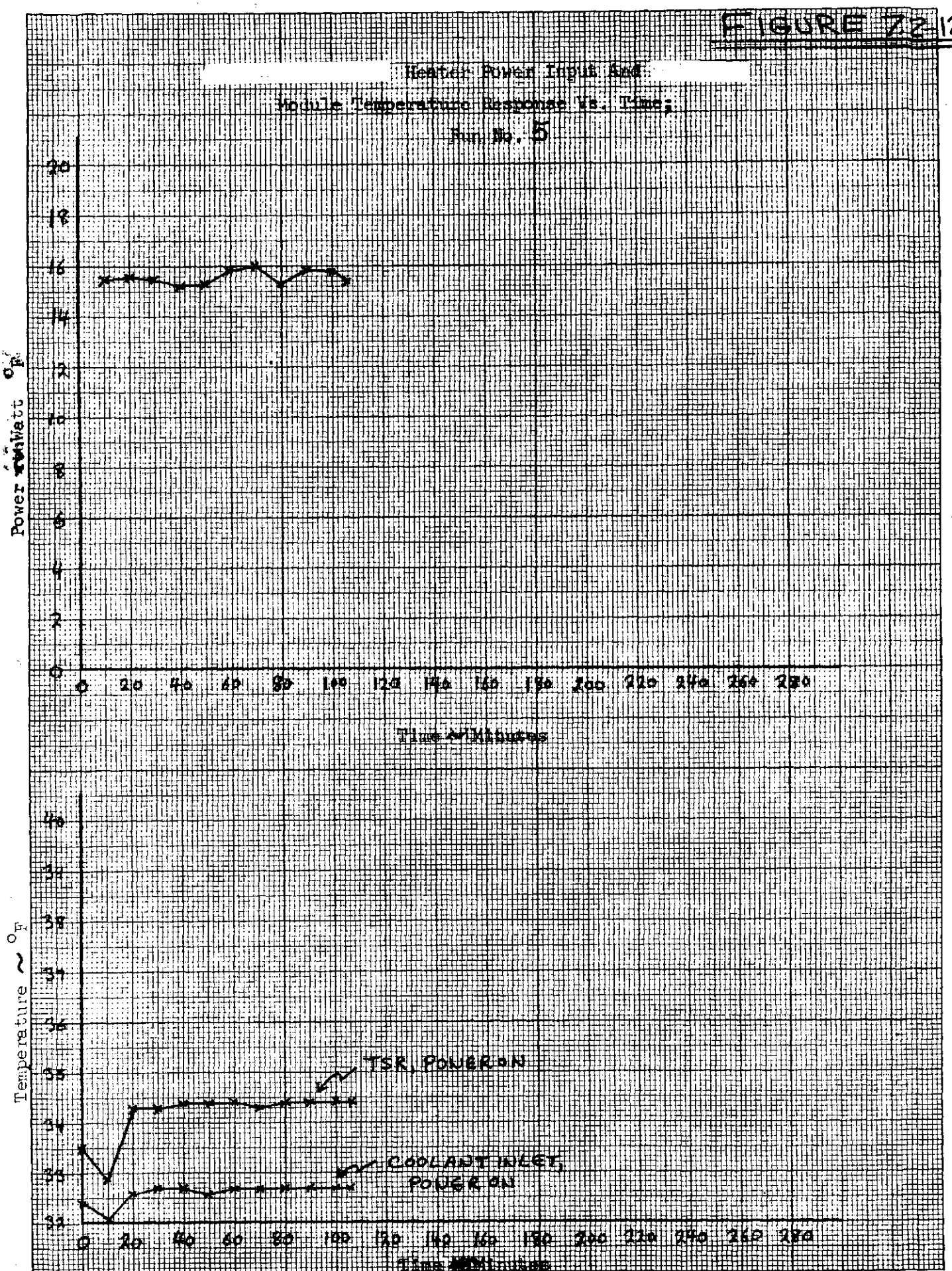
Heater Power Input And
Nodule Temperature Response Vs. Time;
Run No. 5
Power ~ Watt
Time ~ Minutes
Temperature ~ °F
TSR, POWER ON
COOLANT INLET, POWER ON
Time ~ Minutes

MODULE STEADY STATE TEMPERATURE DISTRIBUTION RUN NO. 5

SIDE A

SIDE B

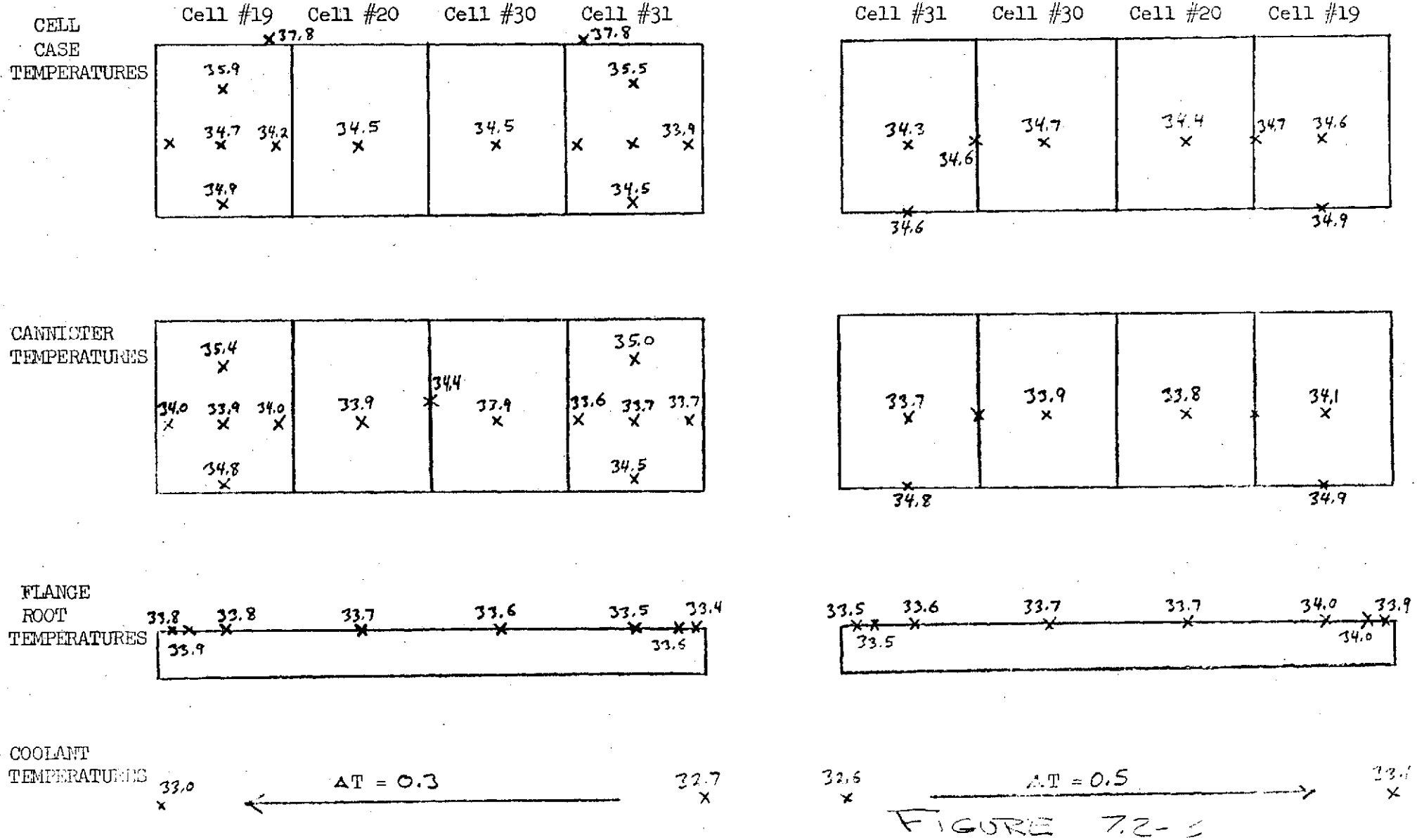

FIGURE 7.2-5

FIGURE 7.2-14

Module Temperature

Distribution Along Rail; Run No. 5

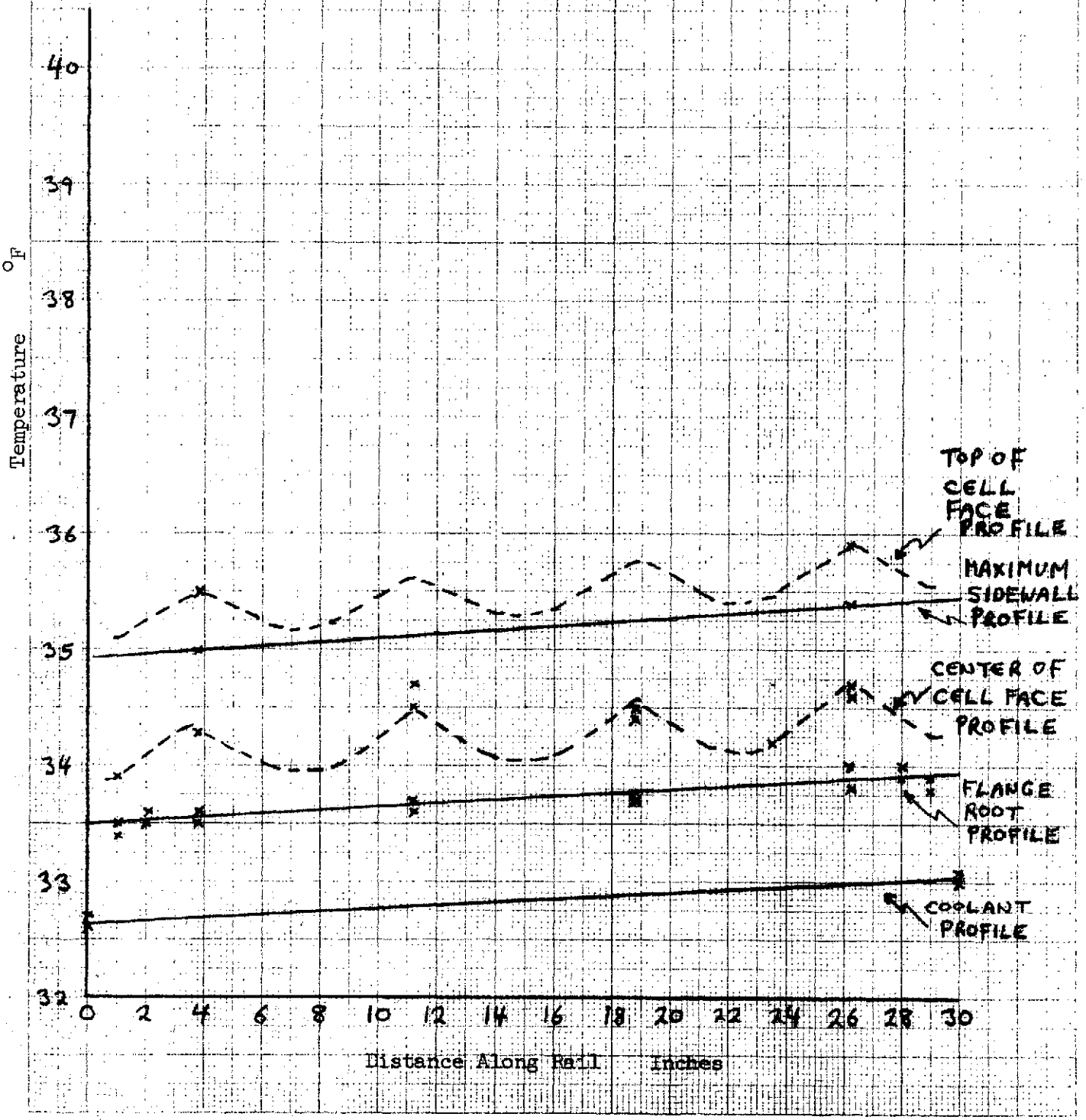

to the cold rail were all opened and the module was unseated. The module was then reseated on its rails and every other bolt torqued down. The bolt to bolt span was thus increased from 2 to 4 inches.

In this run, power was supplied to the cell's heaters without first equilibrating the module to the coolant temperatures. The module was supplied with coolant at a flow rate of 15 pounds per hour per rail at an inlet temperature of 55°F. The heaters were powered at 16 watts each.

Figure 7.2-15 shows the power, TSR temperature and inlet coolant temperature profiles for the run. As can be seen from the TSR temperature response, true thermal equilibrium was not achieved; therefore no temperature map is supplied for the run. The run was repeated the following day (Run #7A).

Runs 7A and 7B

Run 7A is a repeat of run #6. Figure 7.2-16 is a map showing the temperature distribution within the module prior to the powered portion of run 7A.

Figure 7.2-17 shows the TSR, inlet coolant and power profiles during the run. As can be seen, thermal equilibrium was achieved.

Figure 7.2-18 is a temperature map of the module at equilibrium while powered and while cooled with a flow of 15 pounds per hour per rail.

Figure 7.2-19 shows the coolant temperature, flange root temperature, cell reference temperature and maximum cell temperature profiles along the module at equilibrium.

Run 7B was a continuation of 7A in which flow rate to the module was increased from a total of 30 pounds per hour to approximately 300 pounds per hour.

The TSR, inlet coolant, and power profiles for run 7B are

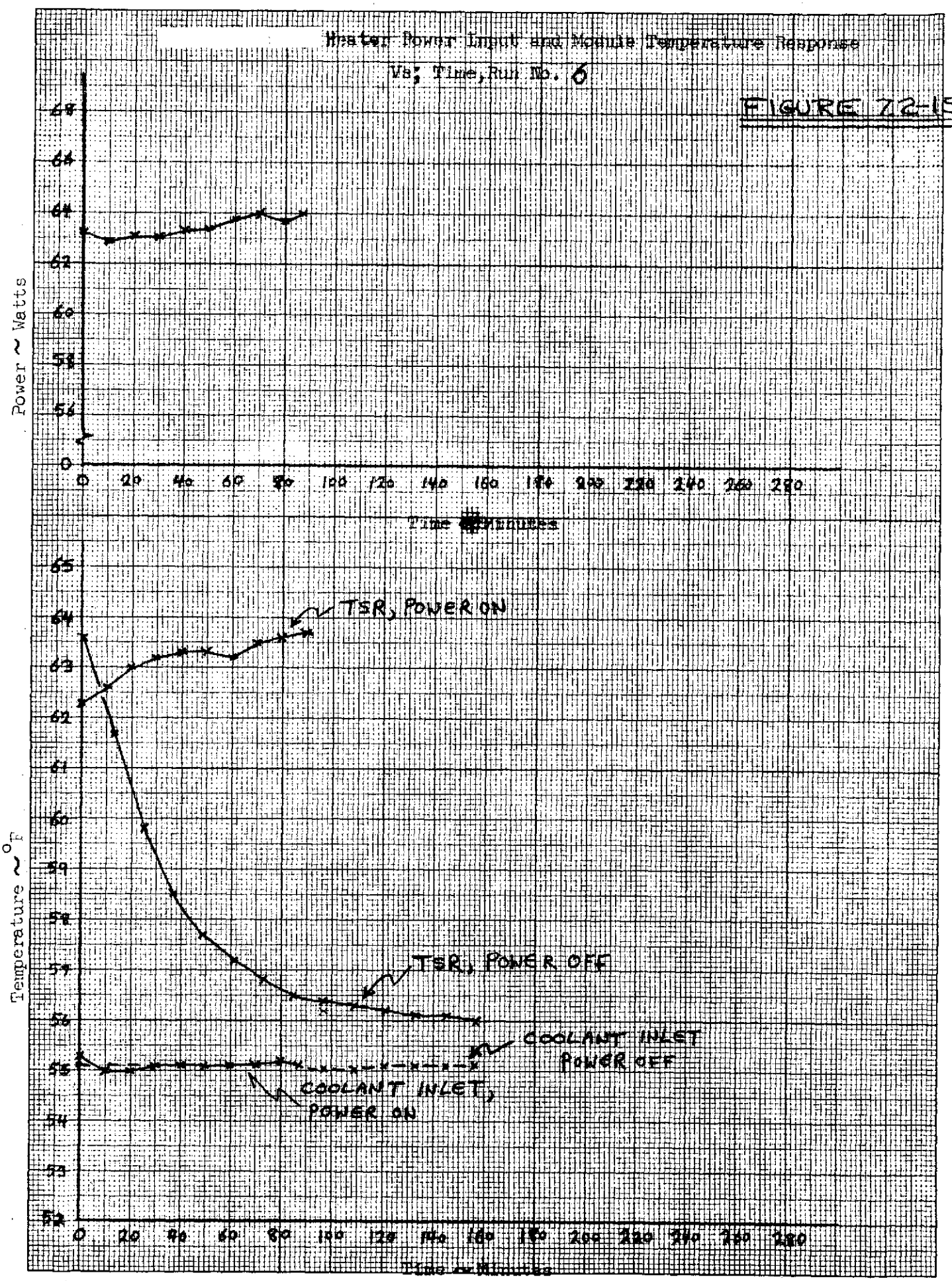
Heater Power Input and Module Temperature Response
Vs; Time, Run No. 6
FIGURE 7.2-15
Power ~ Watts
Time ~ Minutes
Temperature ~ °F
TSR, POWER ON
TSR, POWER OFF
COOLANT INLET POWER OFF
COOLANT INLET, POWER ON

MODULE STEADY STATE TEMPERATURE DISTRIBUTION

RUN NO. 7A

SIDE A

SIDE B

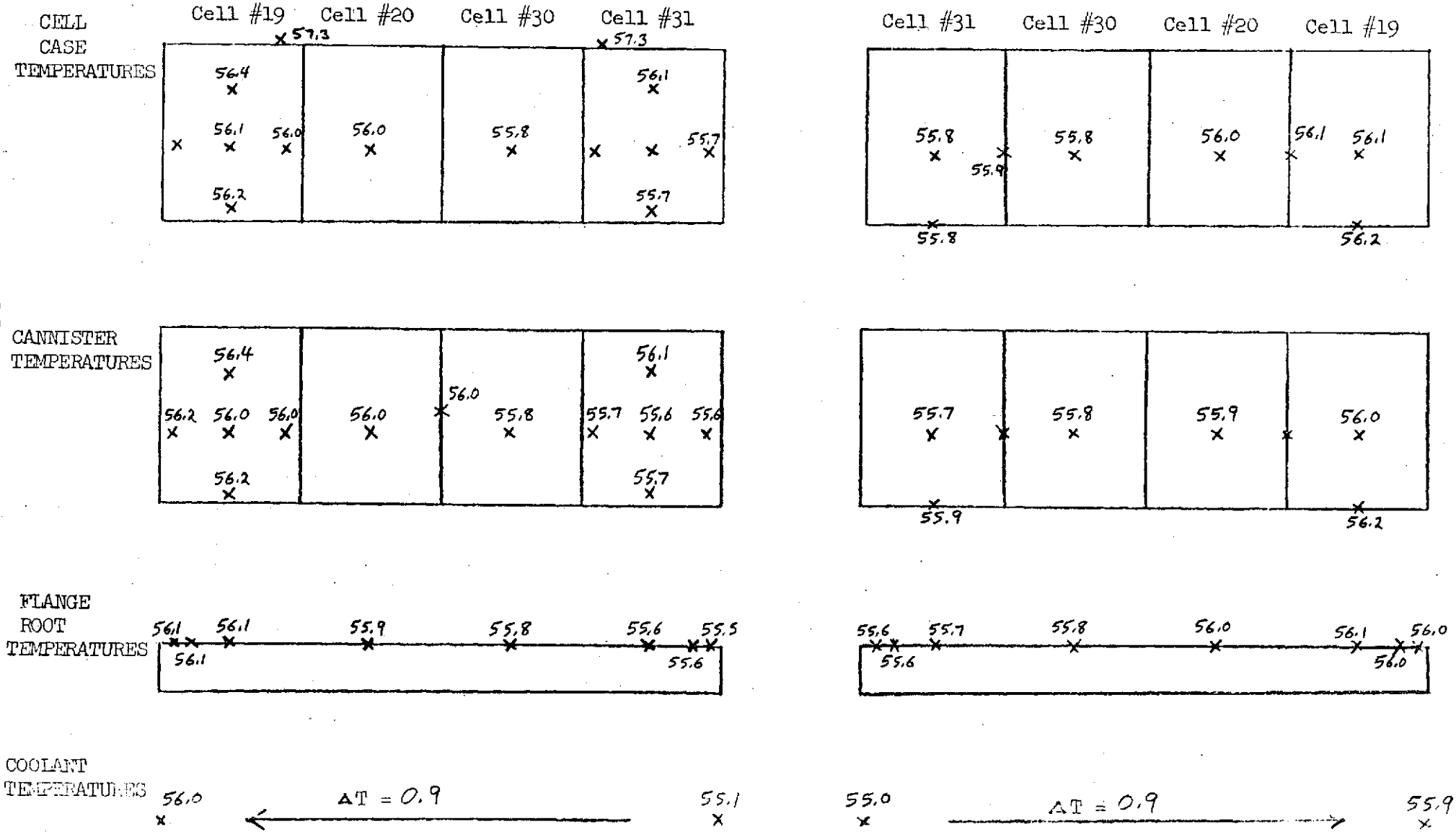

FIGURE 7.2.16

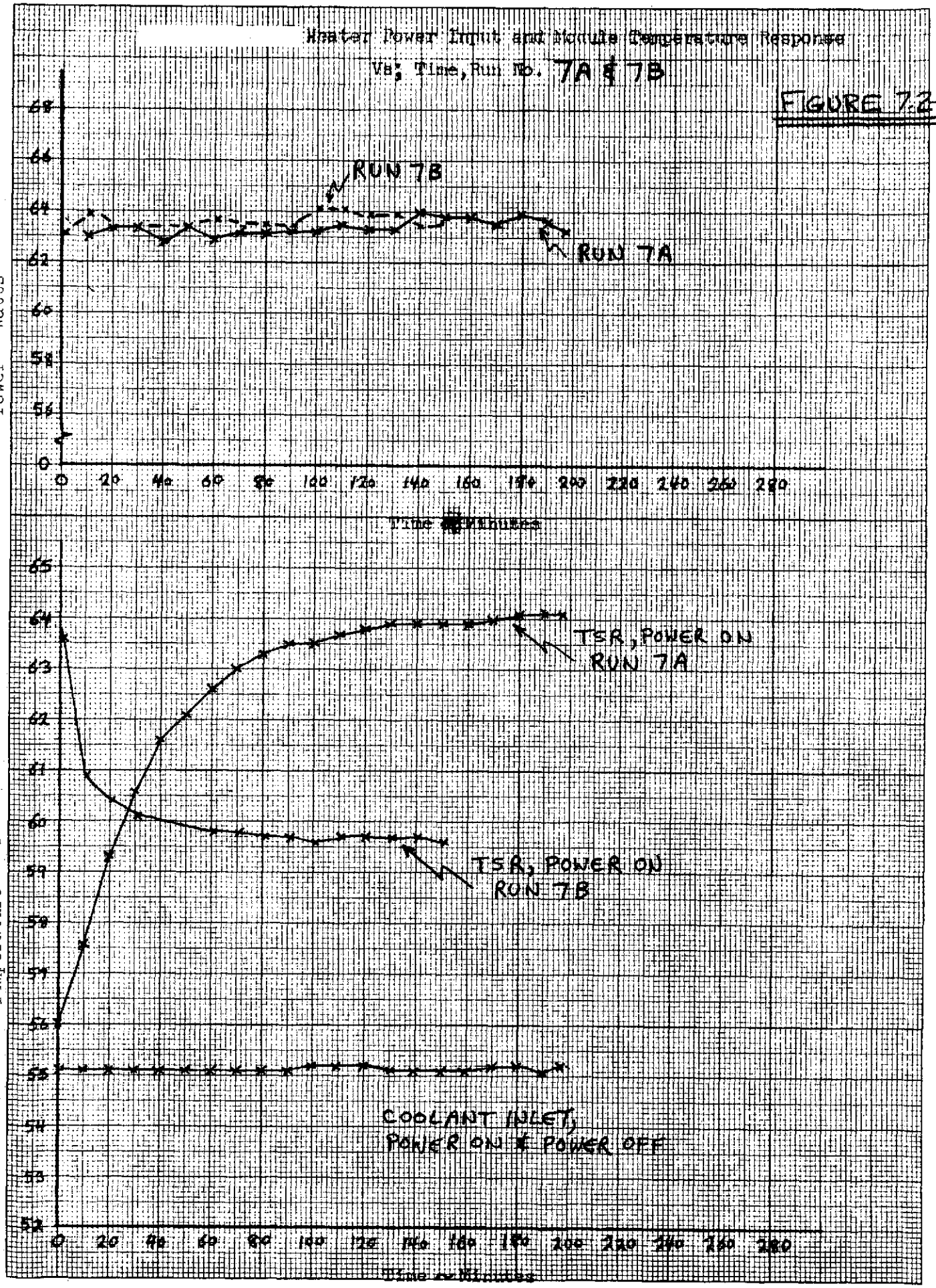

FIGURE 7.2-17

MODULE STEADY STATE TEMPERATURE DISTRIBUTION

RUN NO. 7A

SIDE A

SIDE B

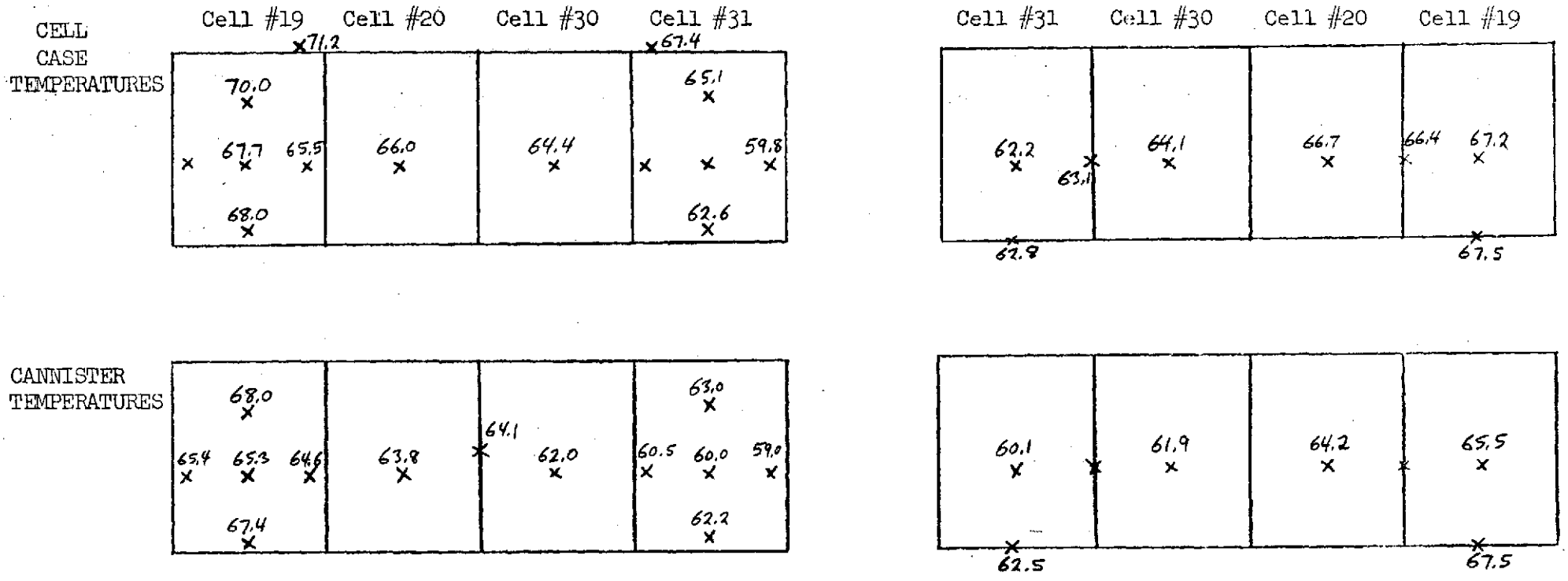

FIGURE 7.2-18

FIGURE 7.2-K

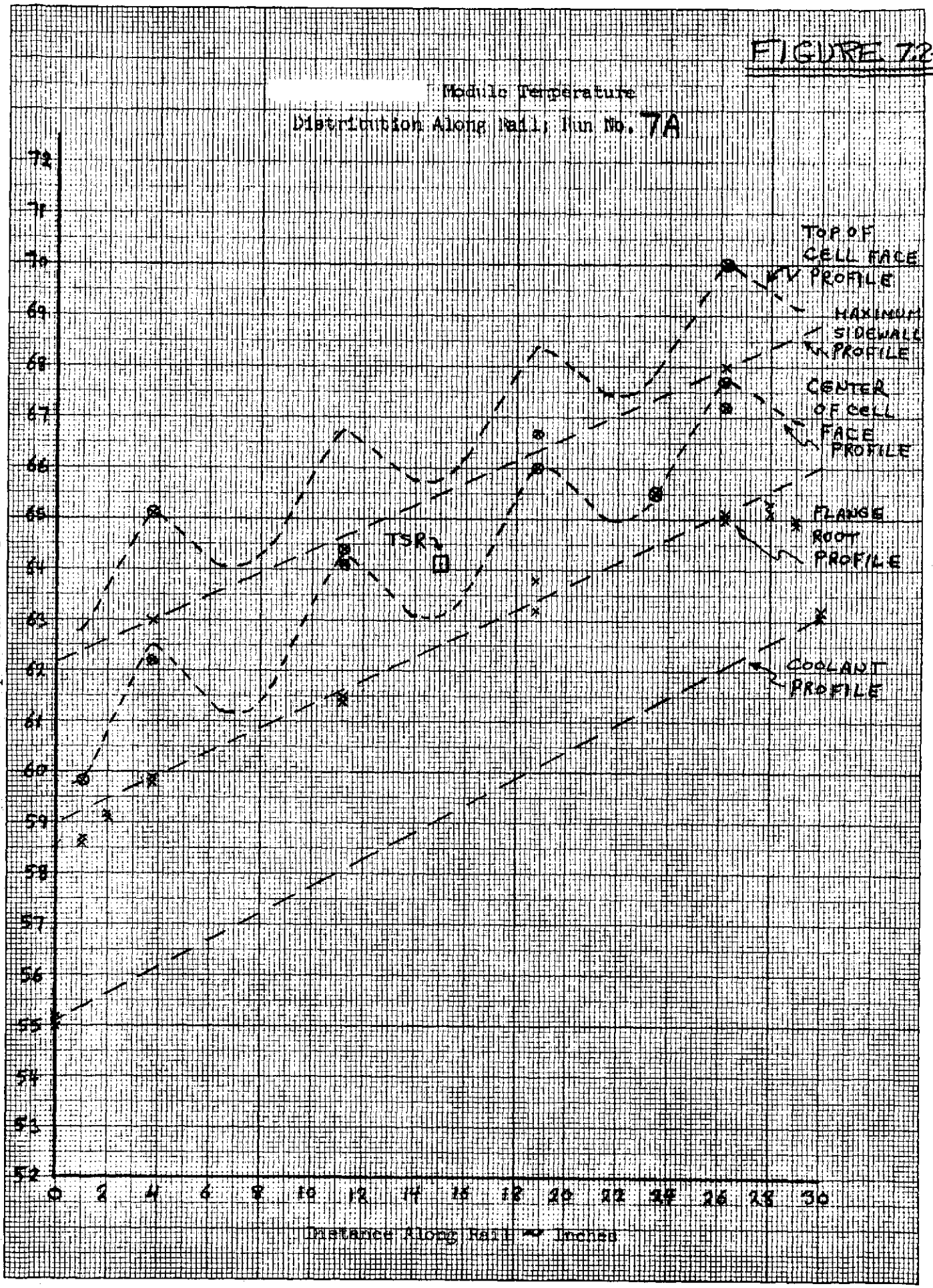

shown in Figure 7.2-17.

A temperature map of the module following stabilization at the 300 pound per hour flow rate is shown in Figure 7.2-20.

Figure 7.2-21 shows the variation of coolant, flange root, cell reference and maximum cell temperatures along the module at equilibrium.

The temperature decay of the system following interruption of power was not monitored.

Run #8

Prior to run number 8, the cooling system was reconfigured from a "one-pass" to a "two-pass" system. The sketch below shows a cross-section of the cold rail to which the module was mounted.

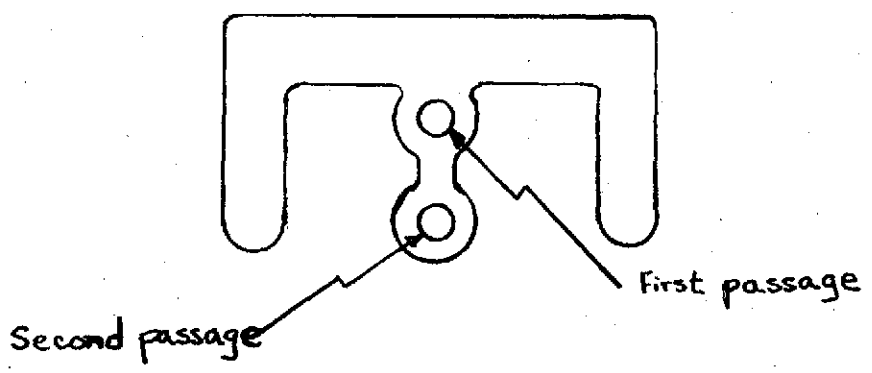

In previous runs, coolant was run through the first passage only. In this run, the effluent coolant from the first passage was brought back to the inlet of the second passage and run through again.

The flow rate, as before was 15 pounds per hour per rail, and the inlet temperature was 55°F. The cells were powered at 16 watts each.

MODULE STEADY STATE TEMPERATURE DISTRIBUTION

RUN NO. 7B

SIDE A

SIDE B

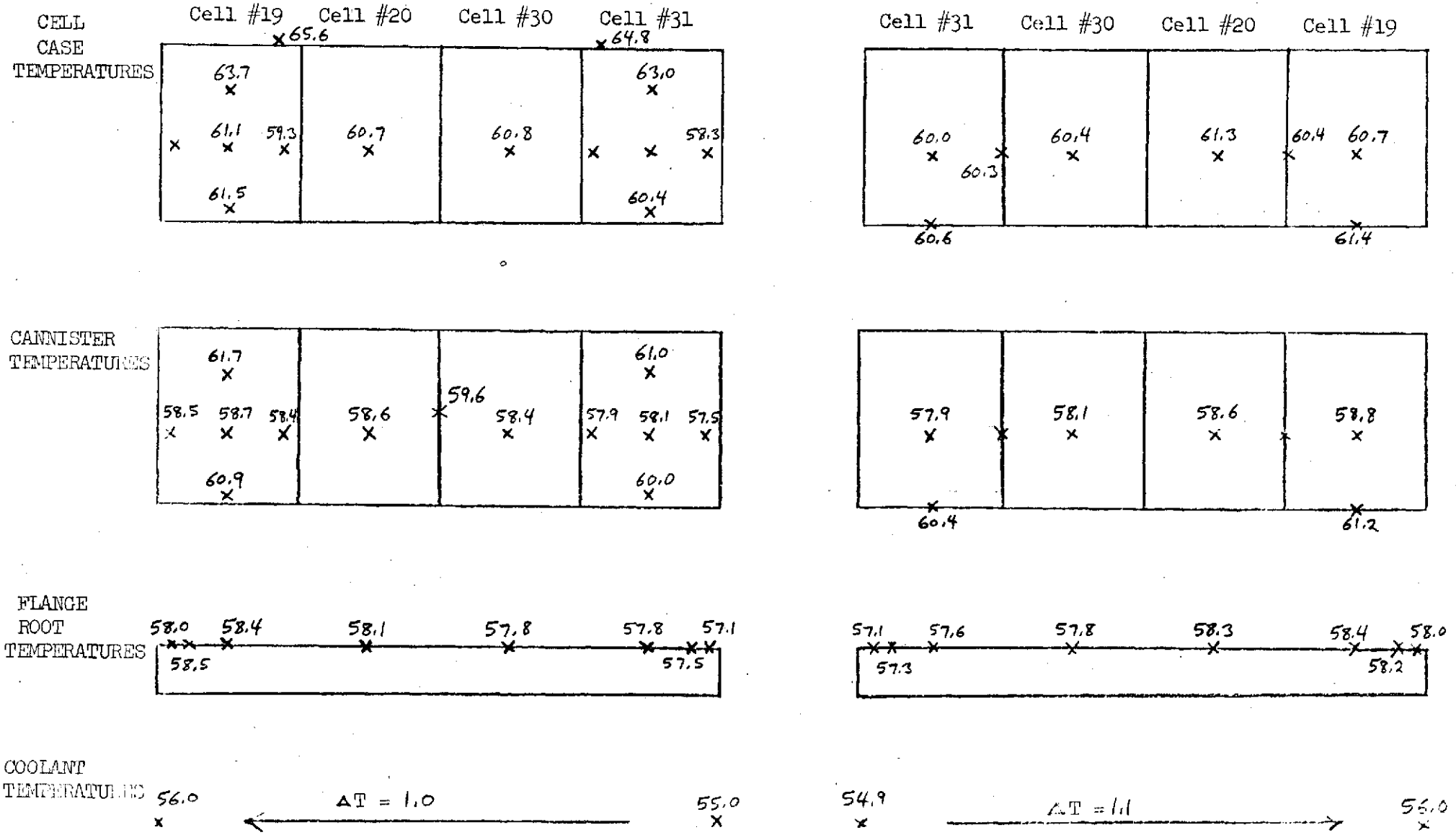

FIGURE 7.2-20

FIGURE 72-21

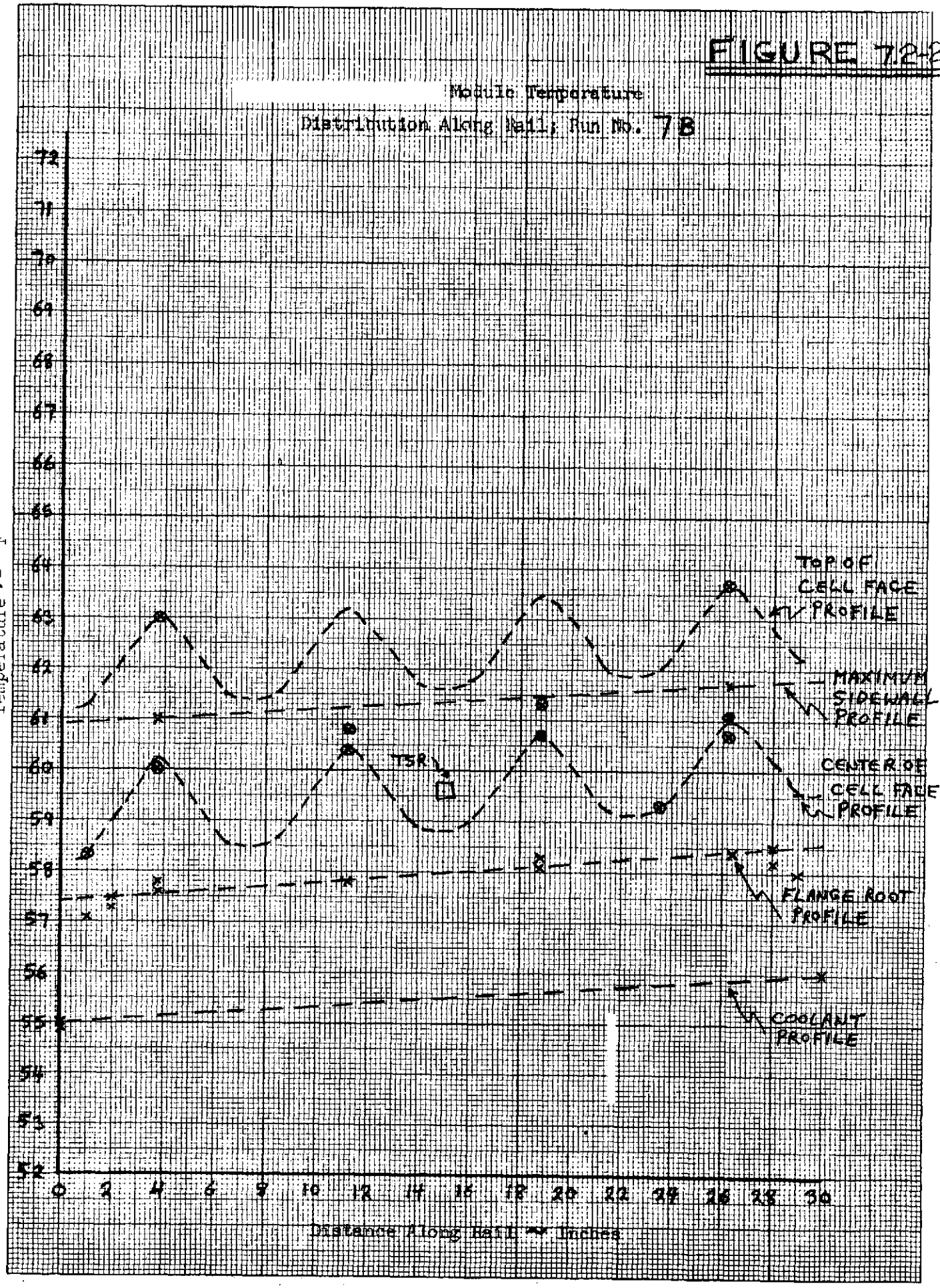

As can be seen from the response of the TSR in Figure 7.2-22, equilibrium had not quite been achieved when the run was terminated. The run was therefore repeated the next day (run #9).

Run #9

Run number 9 was a repeat of two pass cooling condition conducted in run number 8.

Figure 7.2-23 is a temperature map of the module prior to power-up.

Figure 7.2-24 shows the TSR, inlet coolant and heater power profiles for the run. As canbe seen, equilibrium was achieved.

Figure 7.2-25 is a temperature map of the module under load at equilibrium.

Figure 7.2-26 shows the variation of coolant temperature, flange root temperature, cell reference temperature and maximum cell temperature along the module's length.

Figure 7.2-24 also contains a plot of the temperature decay of the TSR following interruption of power to the module.

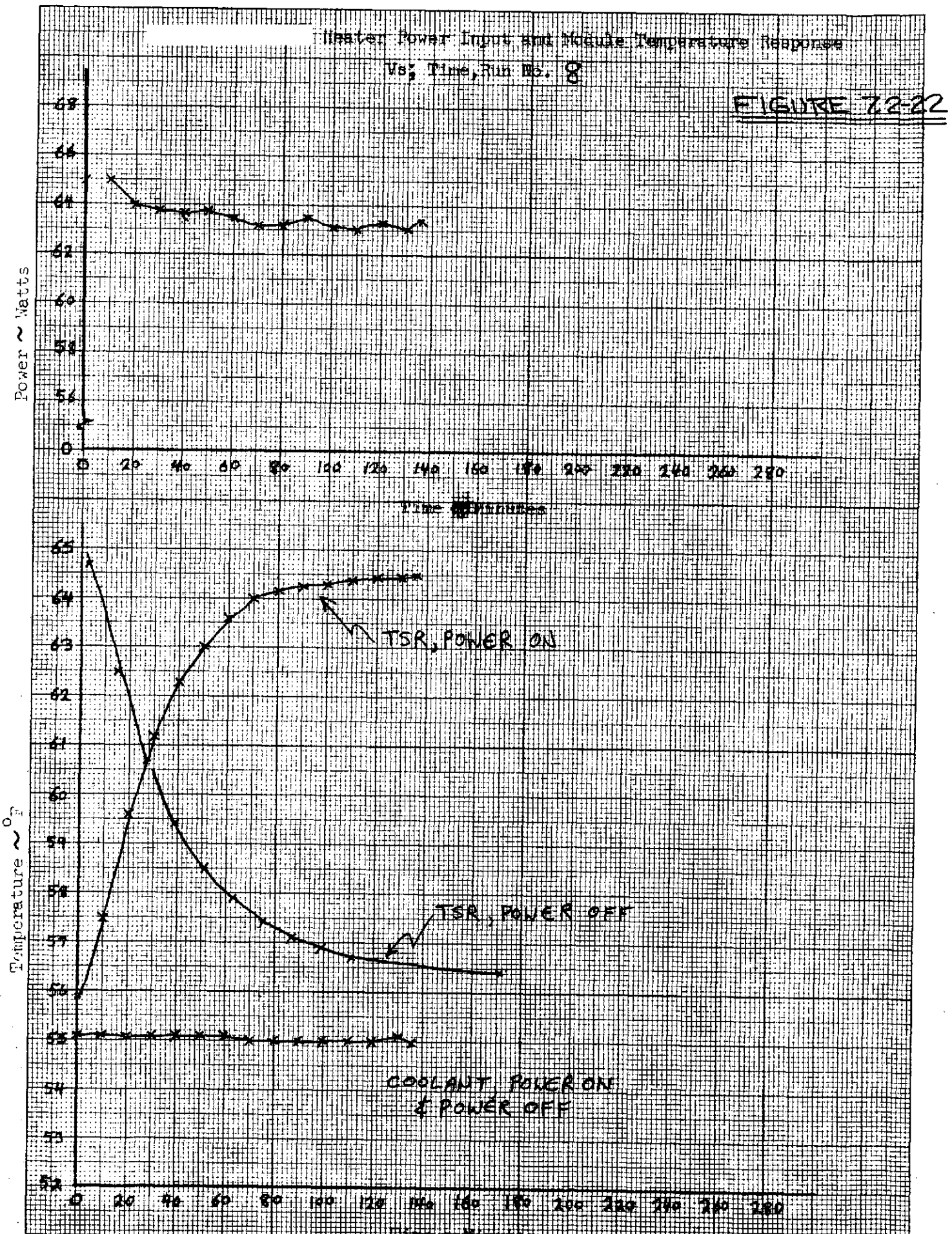

FIGURE 22-22

MODULE STEADY STATE TEMPERATURE DISTRIBUTION

RUN NO. 9

SIDE A

SIDE B

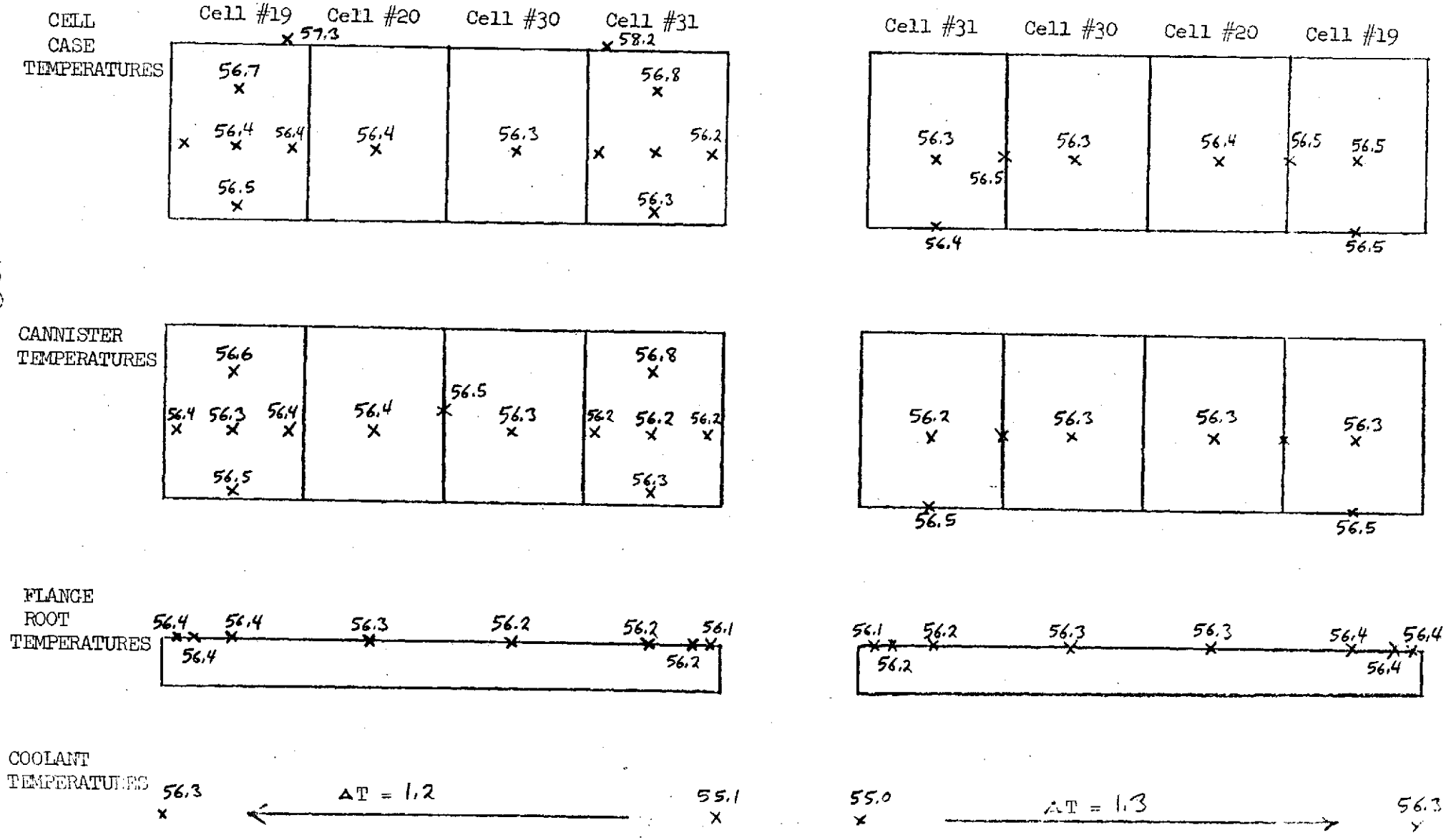

FIGURE 72-23

Heater Power Input and Module Temperature Response
Vs. Time, Run No. 9

FIGURE 7224

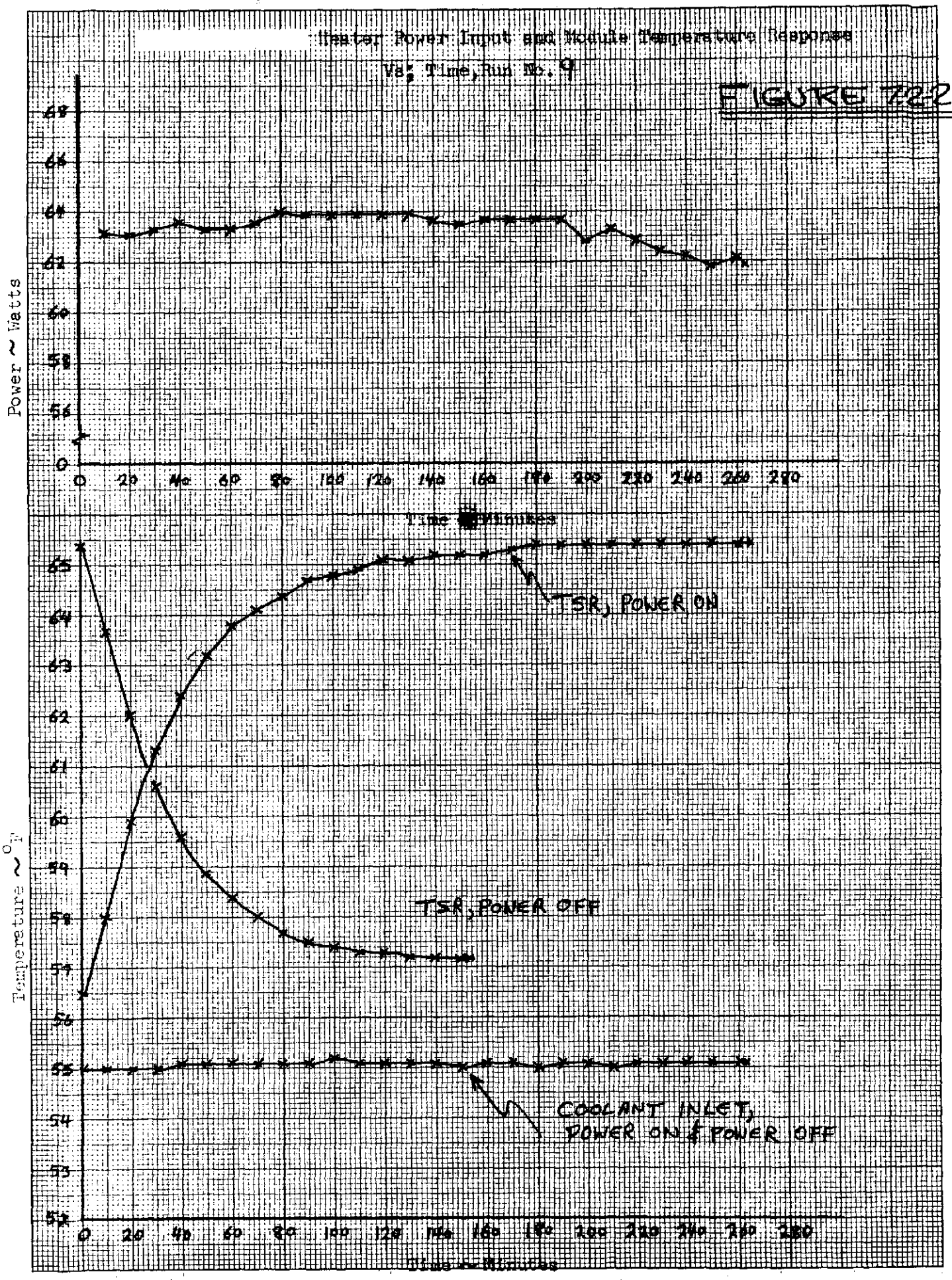

MODULE STEADY STATE TEMPERATURE DISTRIBUTION

RUN NO. 9

SIDE A

SIDE B

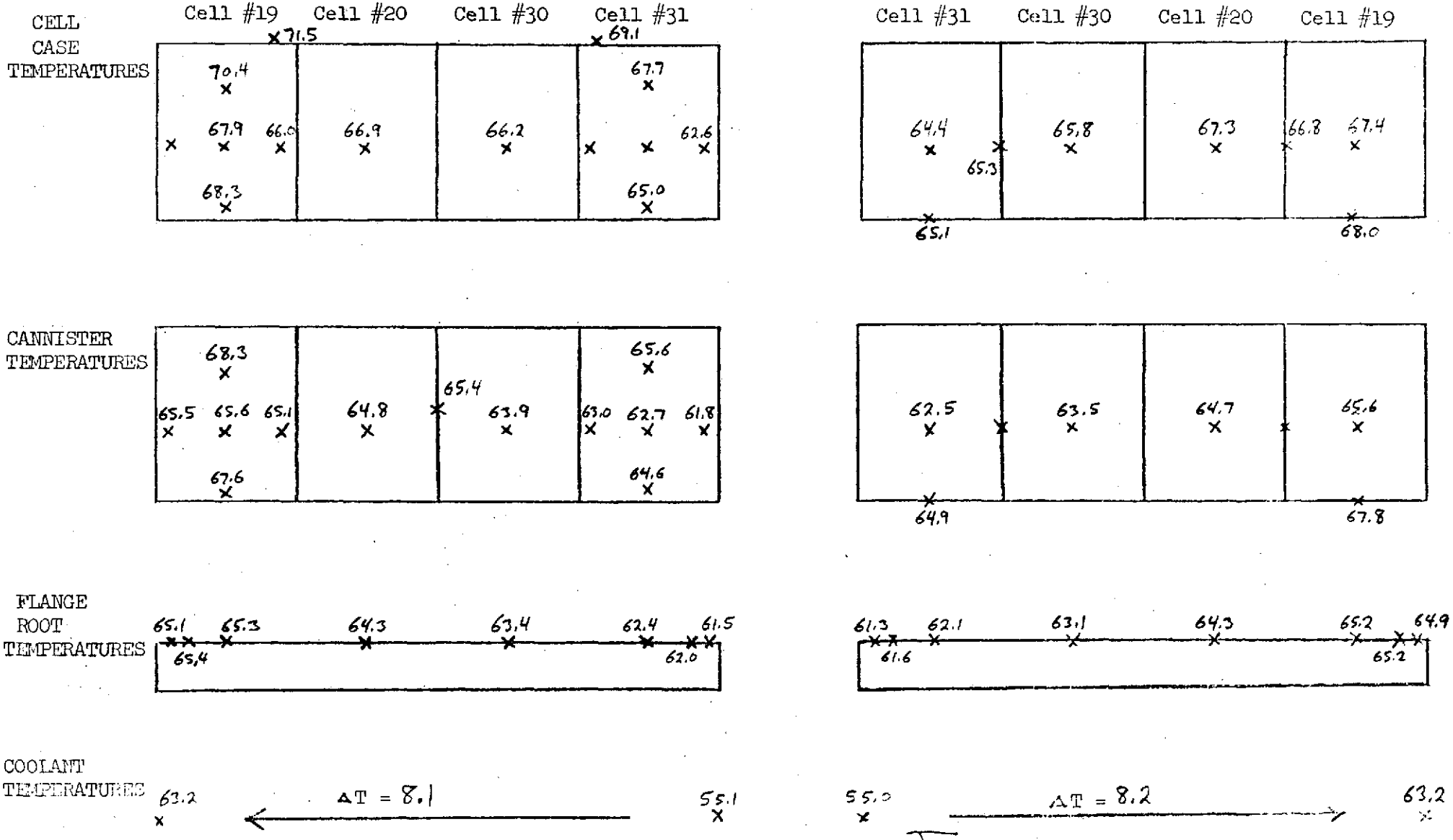

FIGURE 7.2-25

FIGURE 7.2-26

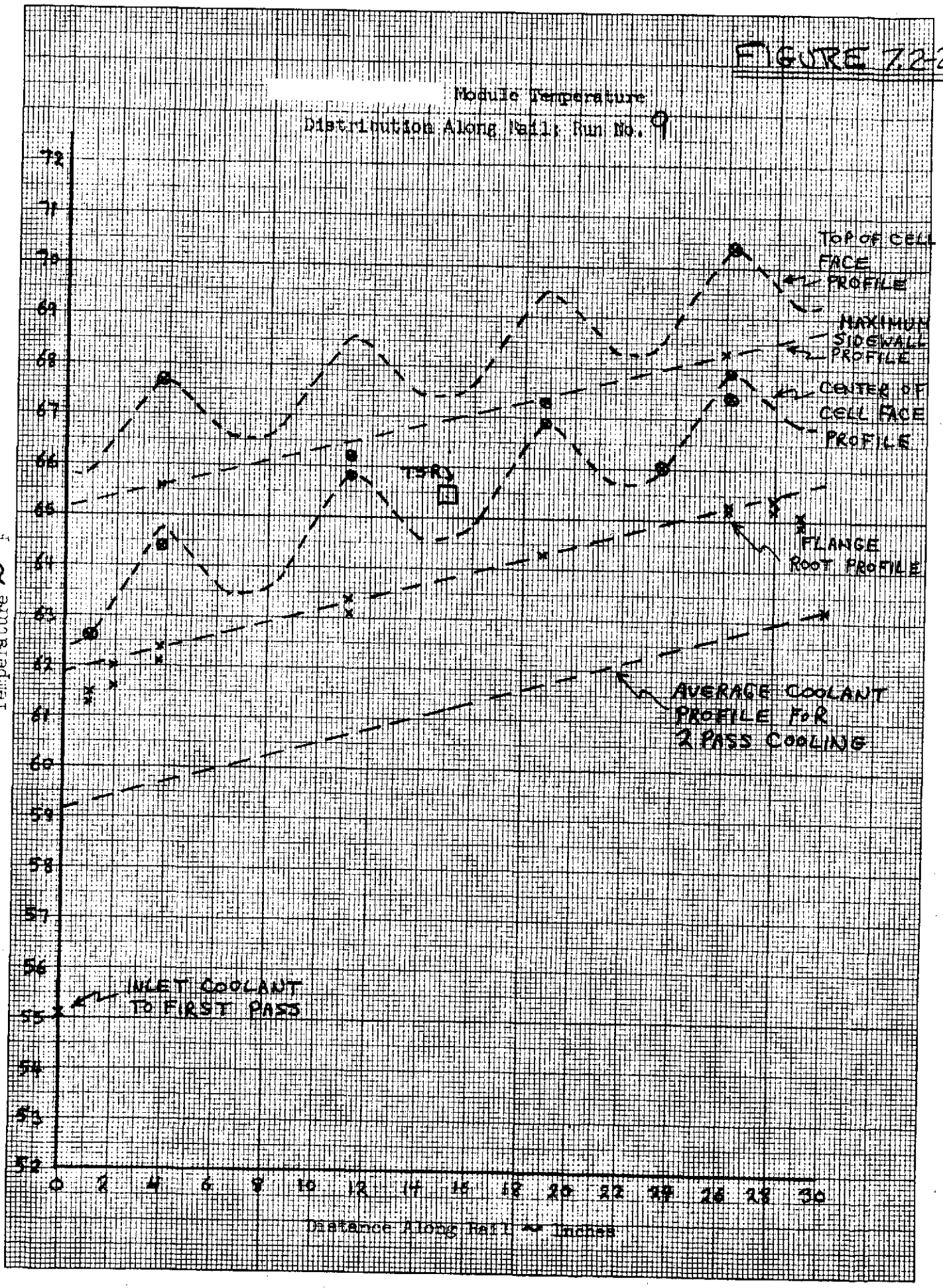

7.2.1.2 Discussion of Heater Test Results

The basic purpose of the heater cell tests was comparison of the expected temperature distribution and levels within the module (from analysis) with actual values measured during test. In order to do this reference must be made to the sketch below where key location temperatures on the module/cold rail are identified.

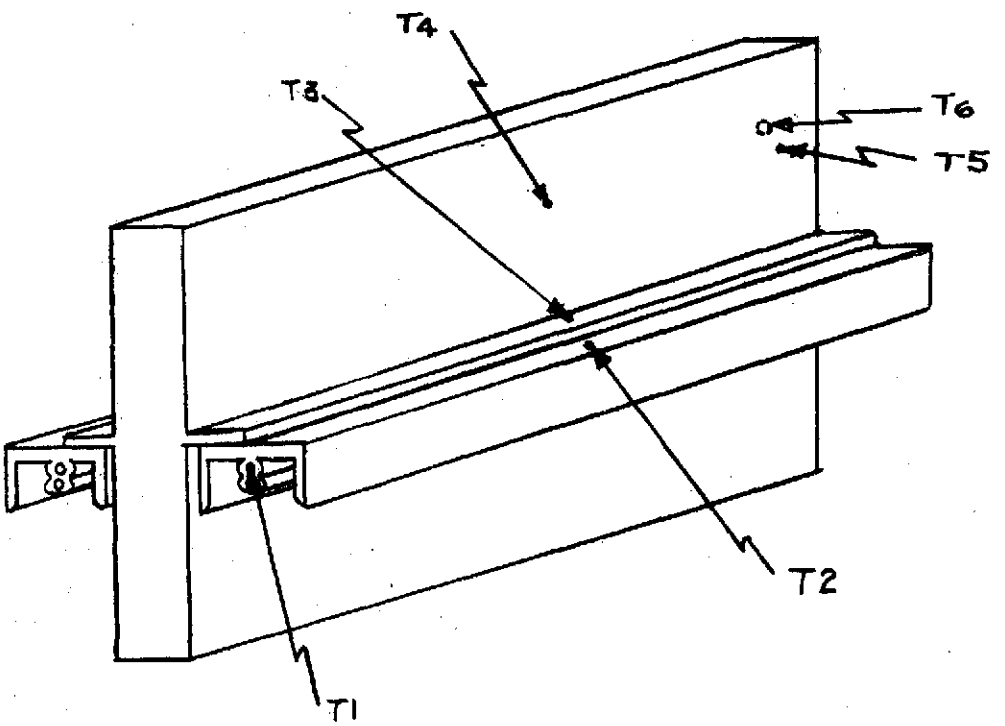

In the sketch, T6 represents the maximum cell face temperature in the module. The design goal was maintenance of T6 below 68°F for a coolant inlet temperature of 55°F, a flow rate of 15 pounds per hour per rail, and a total heat generation rate of 64 watts.

Runs #3 and #4A simulated this design case. Run #7 was made to the same conditions with the single exception that the module was secured to the cold rails by every other mounting bolt (a 4-inch rather than a 2-inch bolt spacing).

Run #9, in which two-pass cooling at 15 lb./hr. per rail was demonstrated is included in the comparison.

Table 7.2-1 below compares the predicted temperature gradients with those demonstrated during testing.

As can be seen from an inspection of Table 7.2-1, the difference between the maximum cell face temperature in run 4A and the inlet coolant temperature was 14.5°F compared to 13.0°F for the design predictions. This would mean that, with a 55°F coolant inlet, the maximum cell face temperature would be 69.5°F compared to the design goal of 68°F. The difference can be traced to two basic causes:

a) the gradient across the potting interface between the cell and module sidewall was 2.1°F instead of the expected 1.2°F, resulting in a 0.9°F higher cell temperature.

b) the measured axial gradient along the module is 65% of the coolant gradient instead of the expected 40%. This causes a 1°F higher maximum cell temperature.

The value of 1.2°F predicted for the temperature gradient across the potting assumed a .001 inch layer of kapton tape and a 0.050 inch thickness of encapsulant. A calculation of the actual potting thickness around the cells (based on weight and surface area) showed that the average was approximately 0.090 inches.

Table 7.3-1

Predicted vs. Actual

Temperature Gradients

Temperature Gradient	Predicted	Run #3	Run #4A	Run #7A	Run #9
Average coolant-inlet coolant (T2-T1)	4.1	4.0	4.0	4.0	6.1
Average flange root-average coolant (T3-T2)	2.5	2.8	2.7	3.4	2.6
Maximum sidewall at midsection-average flange root (T4-T3)	3.6	3.2	3.2	3.0	3.1
Maximum sidewall at outlet-maximum sidewall at midsection (T5-T4)	1.6	2.6	2.5	2.5	1.4
Maximum outlet cell face-maximum sidewall at outlet (T6-T5)	1.2	2.3	2.1	2.0	2.1
TOTAL (T6-T1)	13.0	14.9	14.5	14.9	15.3

Both weight and temperature gradients will be improved in the future by

a) eliminating the kapton tape layer around the cell; adequate electrical isolation between the cell and canister is supplied by both the anodizing on the walls of the cell cavities and the dielectric strength of the encapsulant;

b) respecifying canister dimensions to accept a cell with overall dimensional tolerances of $\pm$0.010 inches rather than $\pm$0.030 inches.

It is estimated that these two changes will result in an encapsulant weight savings of 0.8 pounds and a temperature reduction of 0.6°F. This, in turn, would result in a reduction of the maximum cell case temperature for the design condition to 69°F.

As previously stated, the module under test exhibited a 1°F higher axial gradient than anticipated; resulting in a maximum cell temperature 1°F higher than desired. While this 1°F difference is not a serious problem, the fact serves to introduce a general discussion of the axial (cell to cell) temperature distribution within the module.

Figure 7.2-27 presents a comparison of the cell temperature distributions which would result for three different cold rail concepts.

Figure 7.2-27(a) illustrates the baseline concept of a single pass cold rail supplying coolant at a flow rate of 15 pounds per hour per rail. This conditions was tested in runs 3 and 4A. As can be seen from the figure, the variation between corresponding points on the cells is 5.6°F. The superimposed oscillatory temperature variation is due to the fact that, on any single cell, the

center of the broad face is hotter than edges of the face. This effect cannot be eliminated since these surfaces are concave inward when evacuated, resulting in a substantially larger potting thickness between the cell and the module canister at the center of the face. (The heater cells used in the module were particularly bad in the reppect since the case thickness was less than usual due to the removal of three plates to accomodate the heaters.) Additionally, the presence of the intercell aluminum spacers (which form the cell cavities) in the module canister provide an alternate conduction path for heat leaving the narrow sides of the cell; contributing to the non-uniformity of the temperature across the broad face.

Figure 7.2-27(b) illustrates the axial temperature distribution which results from two pass cooling at the same 15 pounds per hour per rail. This is one method of reducing the axial gradient along the module without increasing the flow rate.

Figure 7.2-27(c) shows the highly desirable axial temperature distribution which would result from using a heat pipe cold rail. The cell to cell variation in temperature is virtually eliminated with such a design. (This same effect could be achieved by supplying a very high flow rate to the baseline type cold rail. However, the quantity of flow available for battery cooling within the space station cooling system is limited.) The subject of integrating the Grumman battery module design into the space station is covered in Section 10.0. More information on the heat pipe cold rail concept is presented in that section.

FIGURE 22-27

Comparison of Axial Temperature (Cell to Cell) Distributions for Three Cold Rail Concepts

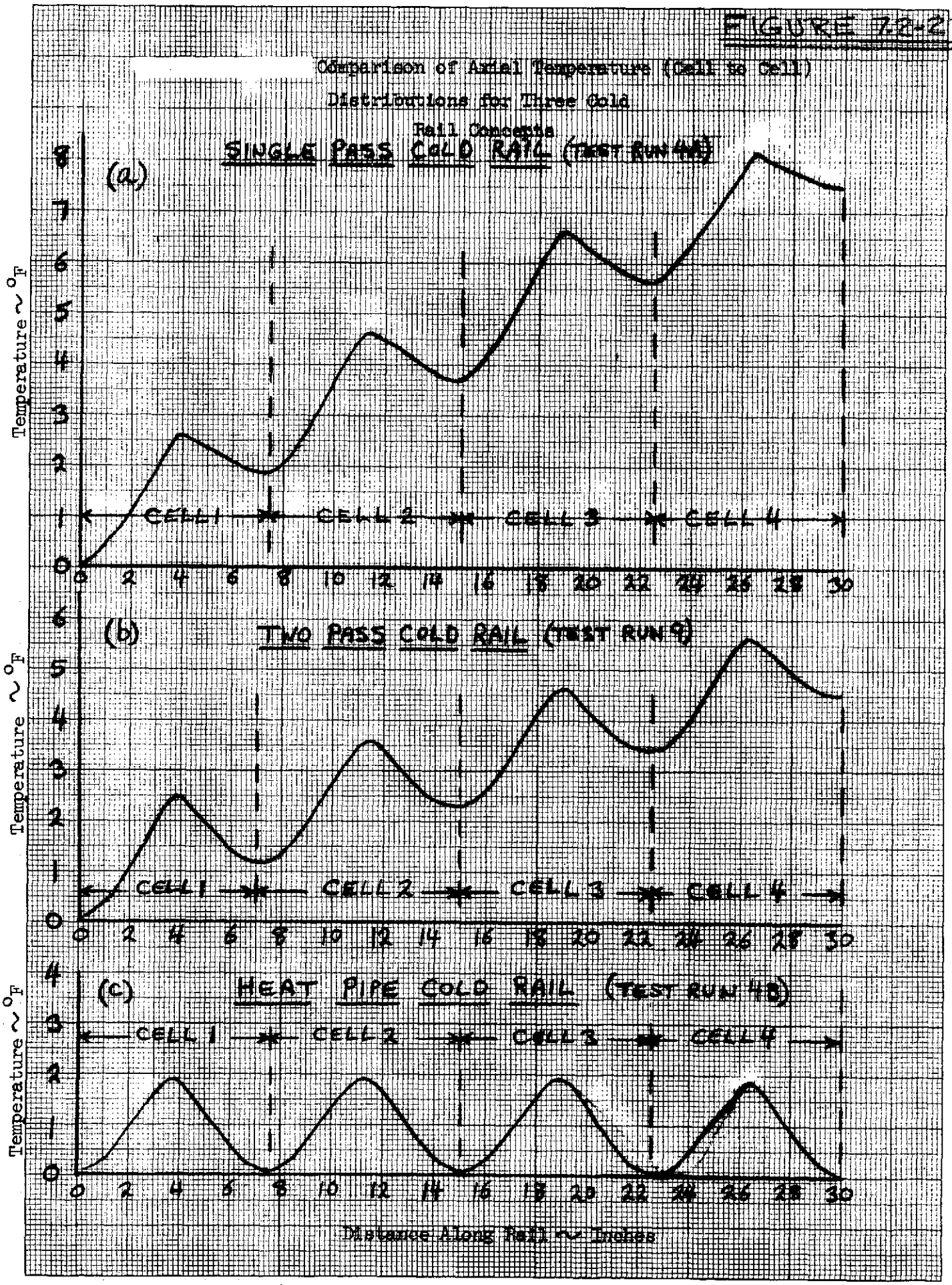

7.2.1.2.1 Discussion of Bolt Spacing Effects

Run 6, and all subsequent tests were performed with a bolt spacing of four (4) inches, instead of the original two (2) inches. Although optimum thermally, two-inch spacing requires too many bolts (30) for good maintainability. Four-inch spacing was simple to test, as it merely required removal of every other bolt. The resulting increase in thermal resistance, mounting flange to coolant, of 2.3°F-in/watt to 2.9°F-in/watt was encouraging, especially since all live cell runs showed maximum cell case temperatures well within allowable limits. It was concluded that three (3)-inch spacing could be safely recommended for the final design. This compromise would even allow for anticipated degradation of thermal performance in the mounting interface under vacuum conditions.

Data used to calculate thermal resistance values were taken from Runs 4A and 7A primarily. Other tests showed confirmatory numbers within limits of accuracy.

7.3 Live Cell Test Results

Test runs 10 through 17 comprise the live cell series, in which the cells were discharged and charged under control of the prototype Test Controller. During this series, minor timing errors occurred, especially at end of charge (shortened by up to 8 minutes). Additionally, certain problems were found, and later solved, with the charge rate level control logic. (These phenomena will be thoroughly discussed in the Test Controller report.) Usefulness of the data was not impaired by these facts. Test runs 12 (50% DOD, 55°F coolant), 15 (30% DOD, 45°F coolant), and 17 (12% DOD, 32°F coolant) are the significant tests, and only their data is reported. (See 7.1.5, Test Run Log.)

7.3.1 Live Cell Test Data

7.3.1.1 Temperature -

Figures 7.3-1 and 7.3-2 present temperature maps of the module at the end of discharge and end of charge respectively of orbit #5 of run #12. The thermal conditions under which the run was made correspond exactly to run #7A. The only difference was that run #7A was a heater run simulating a 50% DOD with a heat generation rate of 16. watts per cell while run #12 was a live 50% DOD run.

The highest module temperatures during orbital cycling were found to occur, as expected, at the end of the discharge portion of the orbit. A comparison of Figures 7.2-18 (run #7A) and 7.3-1 and 7.3-2 (run #12) shows that the maximum cell temperatures reached during run #12 were less than those in run #7A. The maximum cell face temperature in run #12 was 66.8°F, and the maximum temperature rise in the coolant was 6.4°F compared to a cell face temperature of 70.0°F and a coolant gradient of 8.2°F in run 7A.

The lower temperatures exhibited in run #12 are due to the effects of the inherent thermal lag of the module and the fact that the 16 watts per cell orbital average heat generation rate assumed for the module design and used during the heater tests was a convervative figure.

MODULE STEADY STATE TEMPERATURE DISTRIBUTION

RUN NO. 12

50% DoD ORBIT NO. 5

END OF DISCHARGE

SIDE A

SIDE B

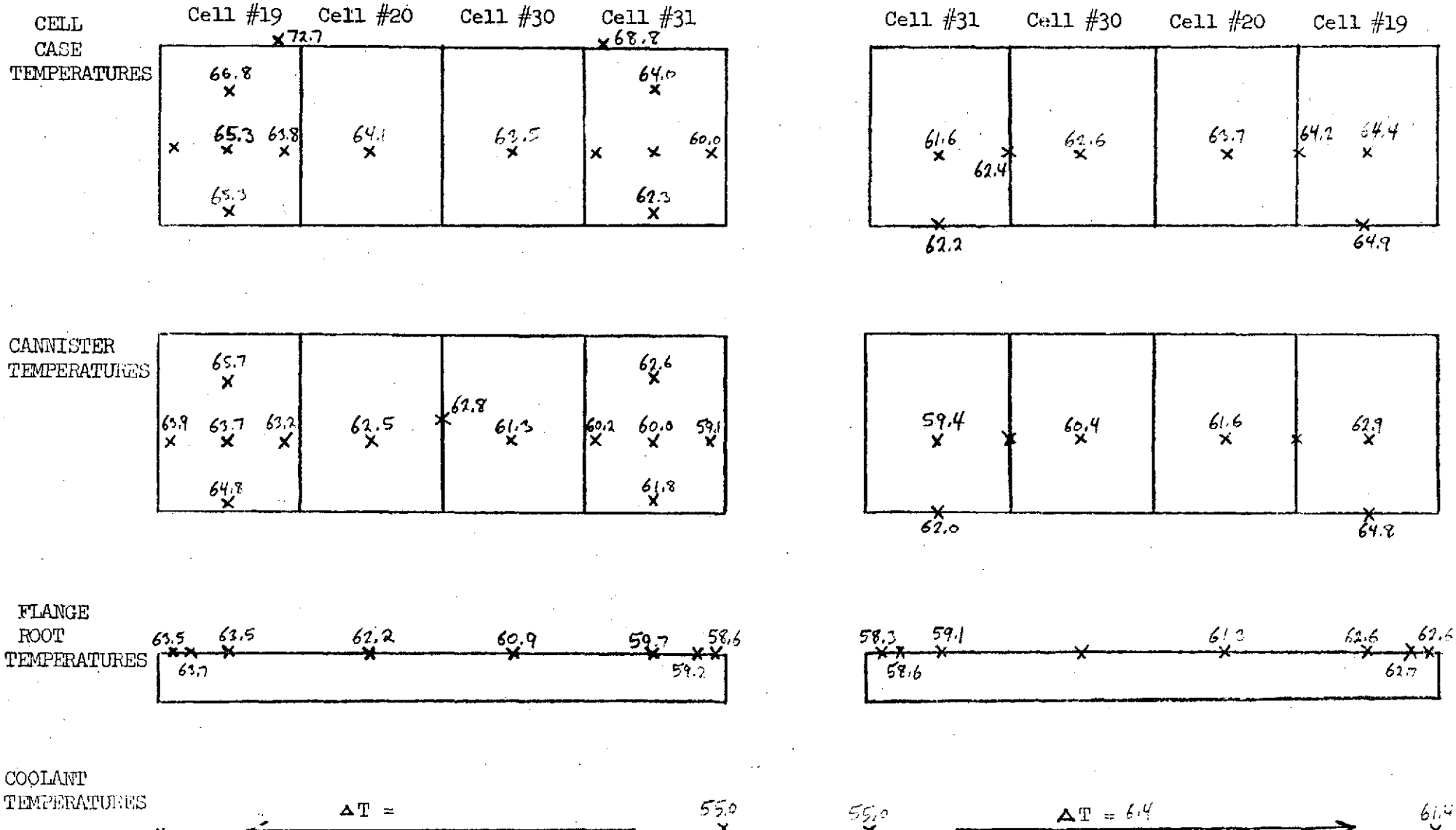

FIGURE 7.3-1

MODULE STEADY STATE TEMPERATURE DISTRIBUTION

RUN NO. 12

50 % DOD ORBIT NO. 5

END OF CHARGE

SIDE A

SIDE B

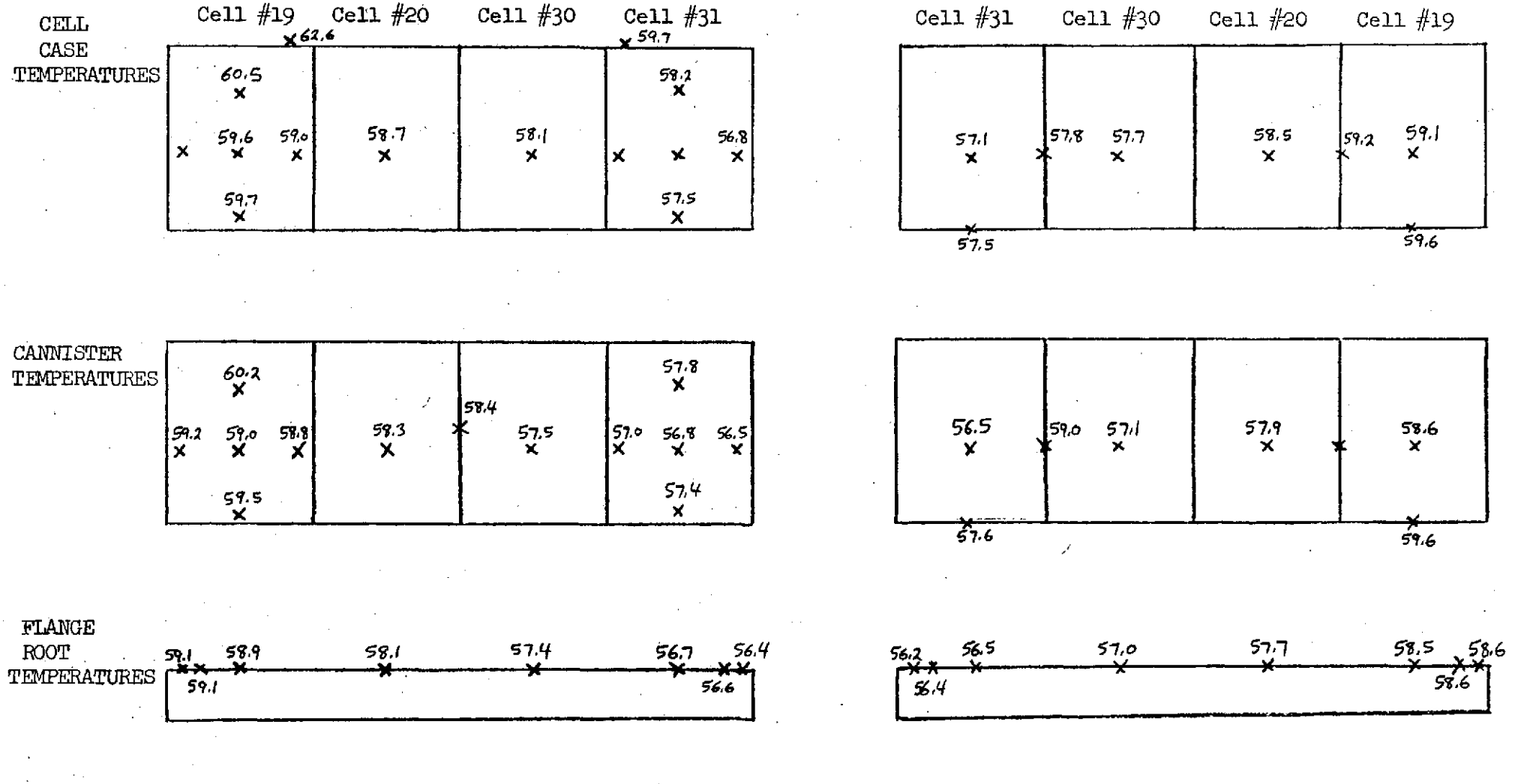

FIGURE 7.3-2

Figures 7.3-3 and 7.3-4 show the temperatures within the module at the end of discharge and end of charge respectively of orbit #6 of run #17. These data may be compared with the data from heater run #5.

Figures 7.3-5 and 7.3-6 are the temperature distribution within the module at the end of discharge and end of charge, respectively of run #15. This 30% DOD run (not simulated as a heater run) was performed to see the sort of temperature distribution which might be expected under a "nominal" electrical and thermal operating regime. As can be seen in the figures, the cell case temperatures along the module are very nearly isothermal and the total temperature rise from maximum cell case to fluid inlet is only 8.4°F (Figure 7.3-5) compared with the 50% DOD allowable design value of 13.0°F.

Figures 7.3-7 through 7.3-8 show typical inlet and outlet coolant temperature versus time for each of the three runs. Figures 7.3-9 through 7.3-11 show average module temperatures versus time. Figures 7.3-12 through 7.3-14 show typical cell center face temperatures versus time. Table 7.3-1 summarizes the important data from these figures. Figure 7.3-15 demonstrates the relationship between apparent depth of discharge (see Appendix A, 4.0) and module and maximum cell temperature rise.

7.3.1.2 Electrical

Module voltages are given in Figures 7.3-16 through 7.3-18. Note the current programming error (orbit 4 charge, Figure 7.3-17) resulting in excessive voltage momentarily. Note also the apparently missing current step (50 amp, orbit 4 charge, Figure 7.3-18). The raw data showed the presence of this step on one reading only (the module voltage rose to the next programming point in less than one minute), resulting in no rise-of-voltage readout from the step. It was typical of the 12% DOD runs that most higher rate charging was at C/5 (20 amp).

MODULE STEADY STATE TEMPERATURE DISTRIBUTION

RUN NO. 17

12 % DOD ORBIT NO. 6

END OF DISCHARGE

SIDE A

SIDE B

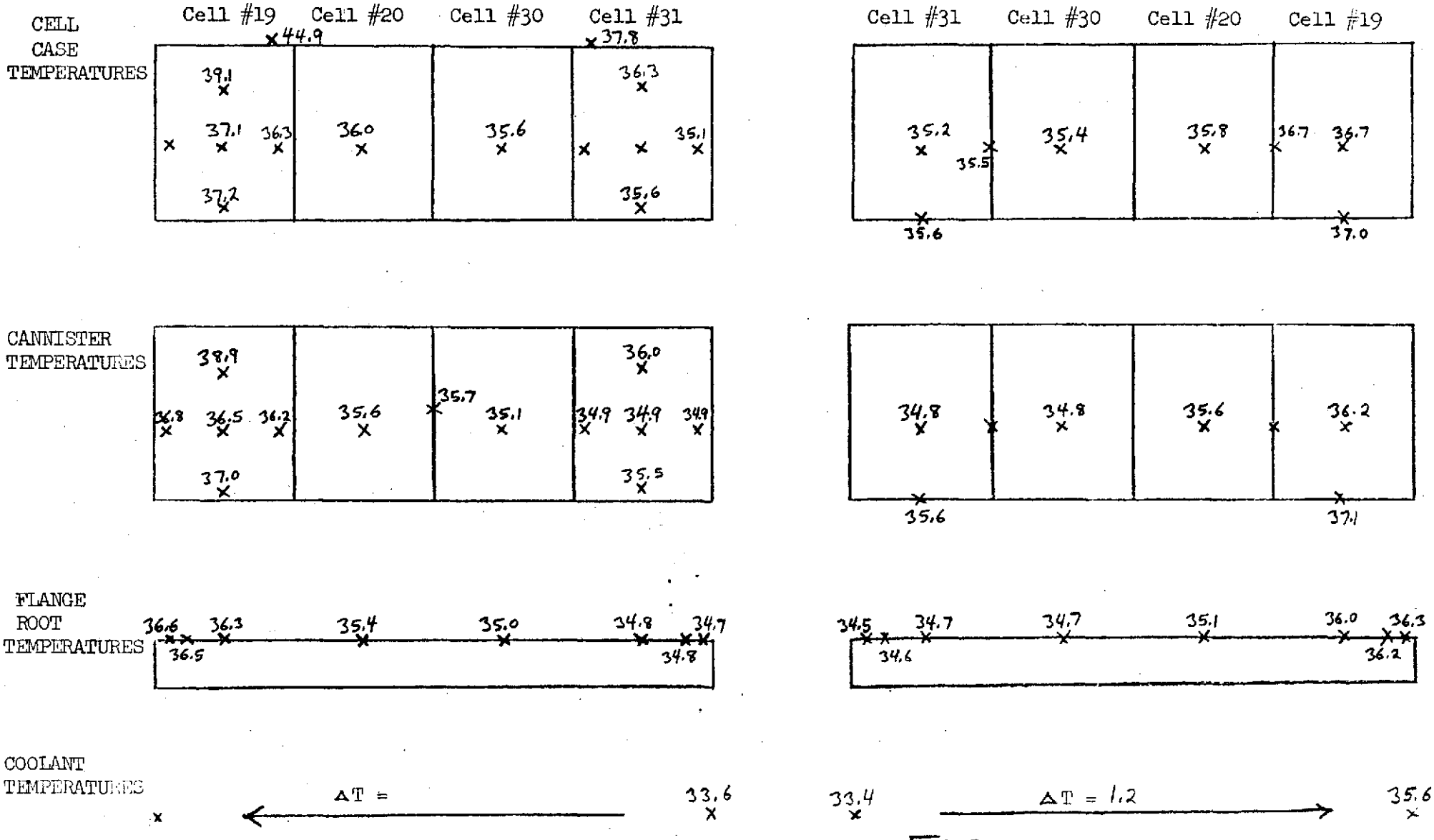

FIGURE 7.33

MODULE STEADY STATE TEMPERATURE DISTRIBUTION

RUN NO. 17

12 %, DoD ORBIT NO. 6

END OF CHARGE

SIDE A

SIDE B

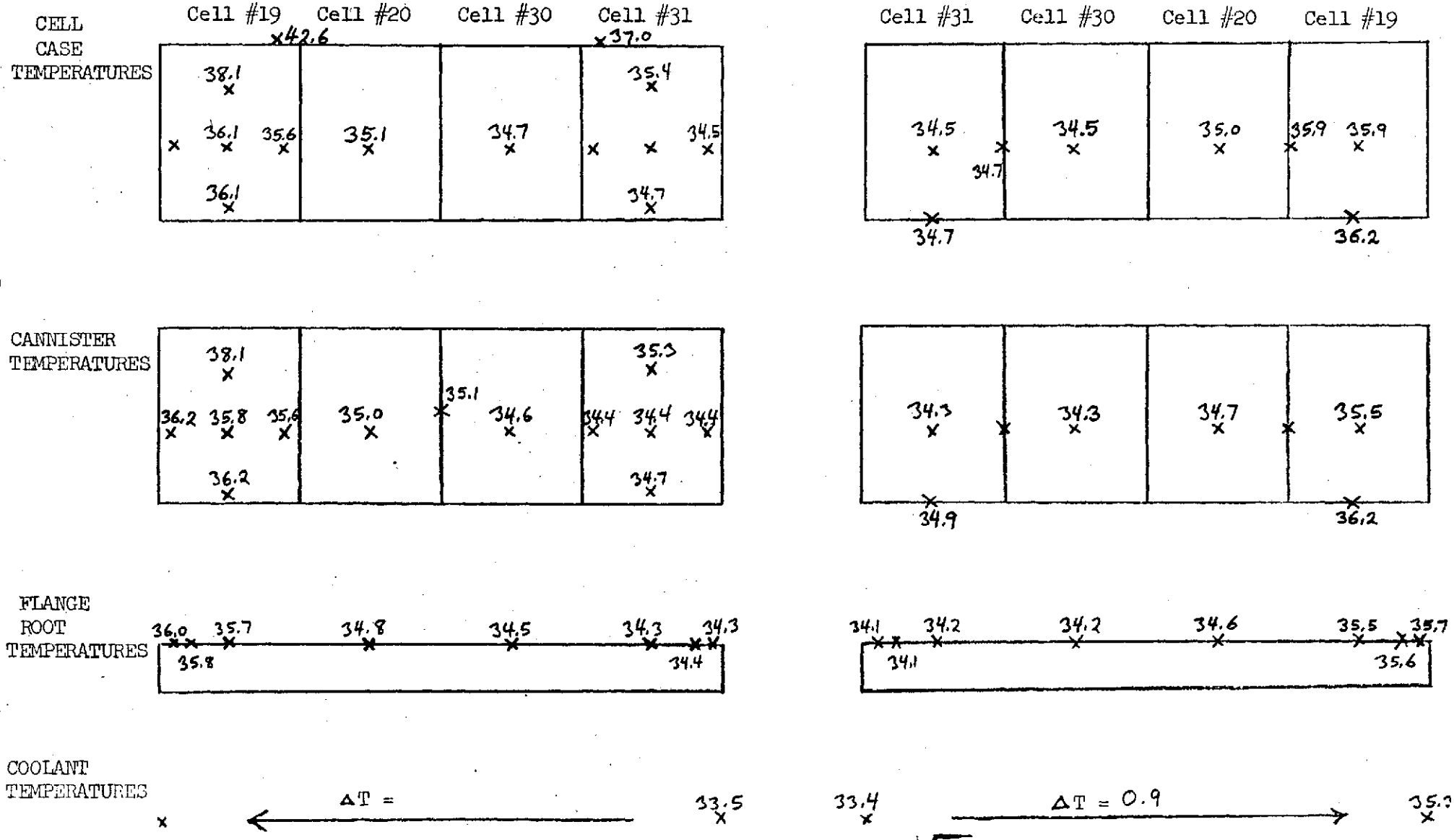

124.

FIGURE 7.3-4

MODULE STEADY STATE TEMPERATURE DISTRIBUTION

RUN NO. 15

30% DOD ORBIT NO. 6

END OF DISCHARGE

SIDE A

SIDE B

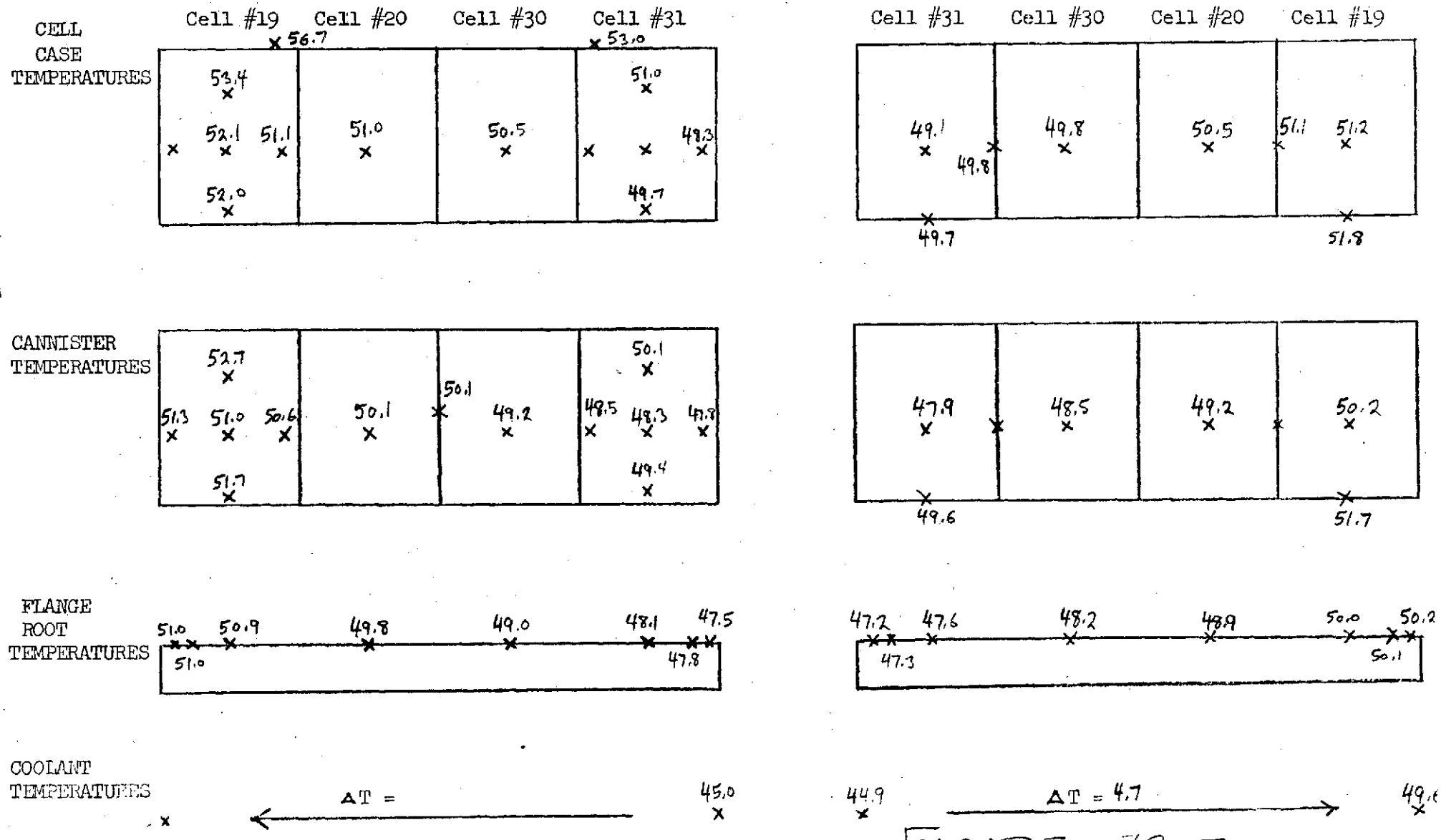

125.

FIGURE 7.3-5

MODULE STEADY STATE TEMPERATURE DISTRIBUTION

RUN NO. 15

30% DoD ORBIT NO. 6

END OF CHARGE

SIDE A

SIDE B

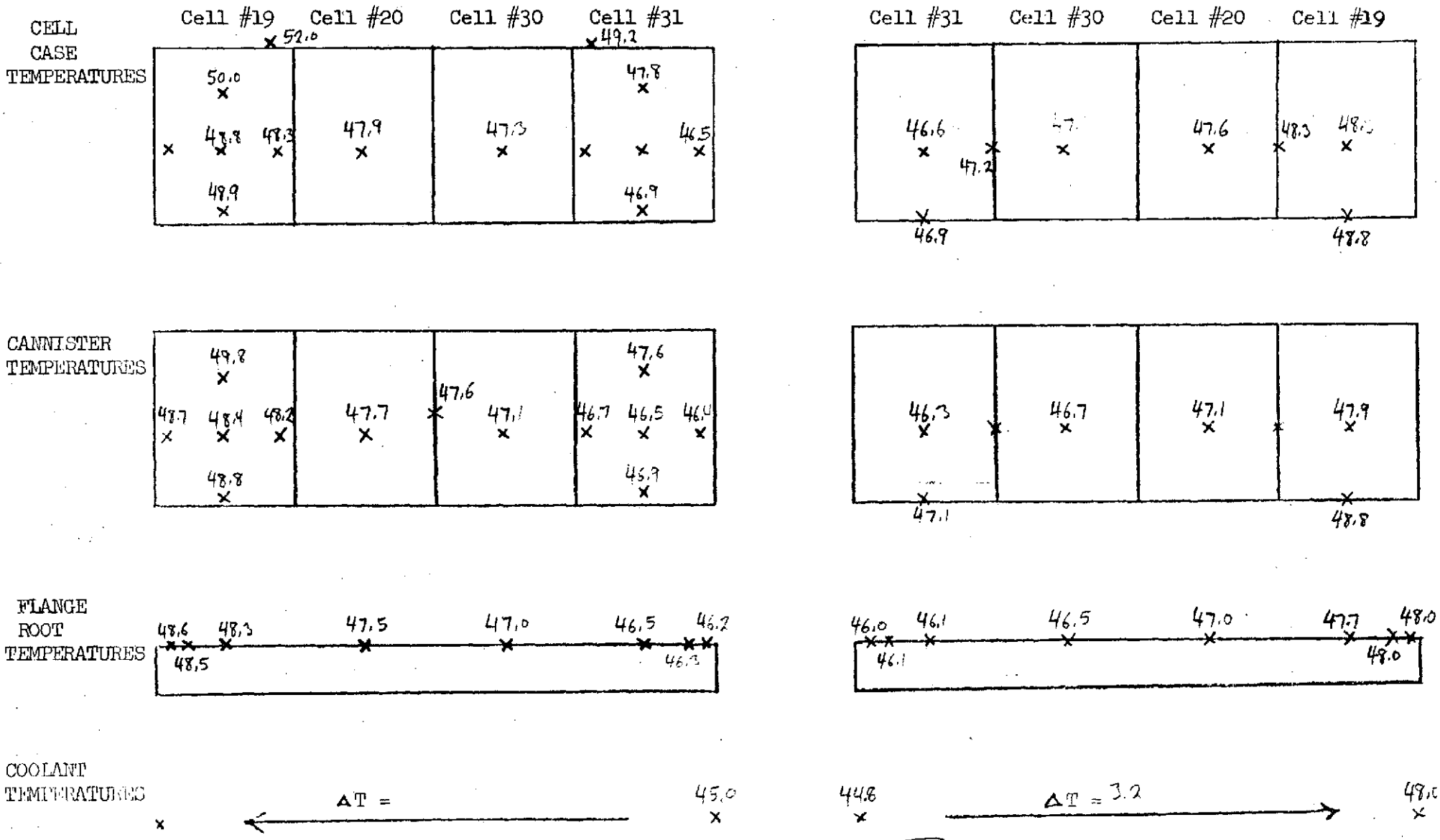

126.

FIGURE 7.3-6

FIGURE 73-7

PLOT 2

COOLANT TEMP. VS. TIME

DEPTH OF DISCH. : 50%
TEMP. : 55°F
ORBITS : 3+4
DATE OF TEST : 8-25-71

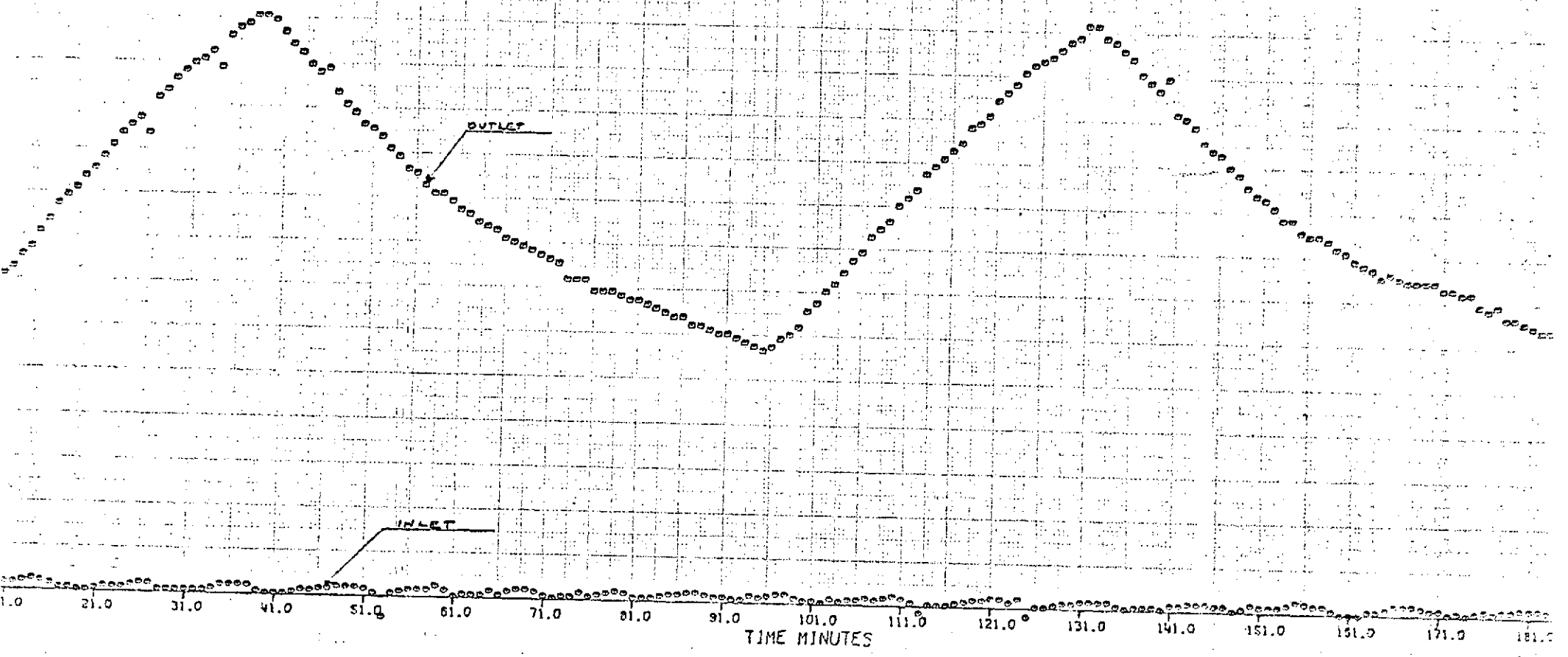

FIGURE 73-5

PLOT 2

COOLANT TEMP. VS. TIME

DEPTH OF DISCH: 30%
TEMP : 45°F
ORBITS : 3 & 4
DATE OF TEST : 9-3-71

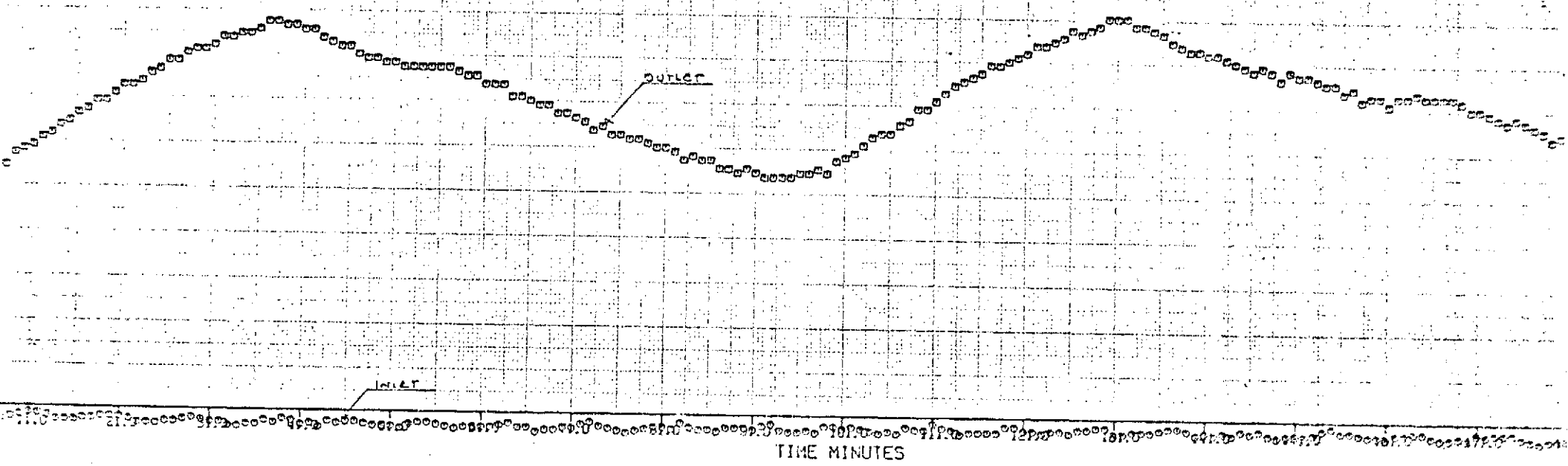

OR

FIGURE 7.3-7

PLOT 2

COOLANT TEMP. VS. TIME

DEPTH OF DISCH : 12 %
TEMP. : 32° F
ORBITS : 3 + 4
DATE OF TEST : 9-10-71

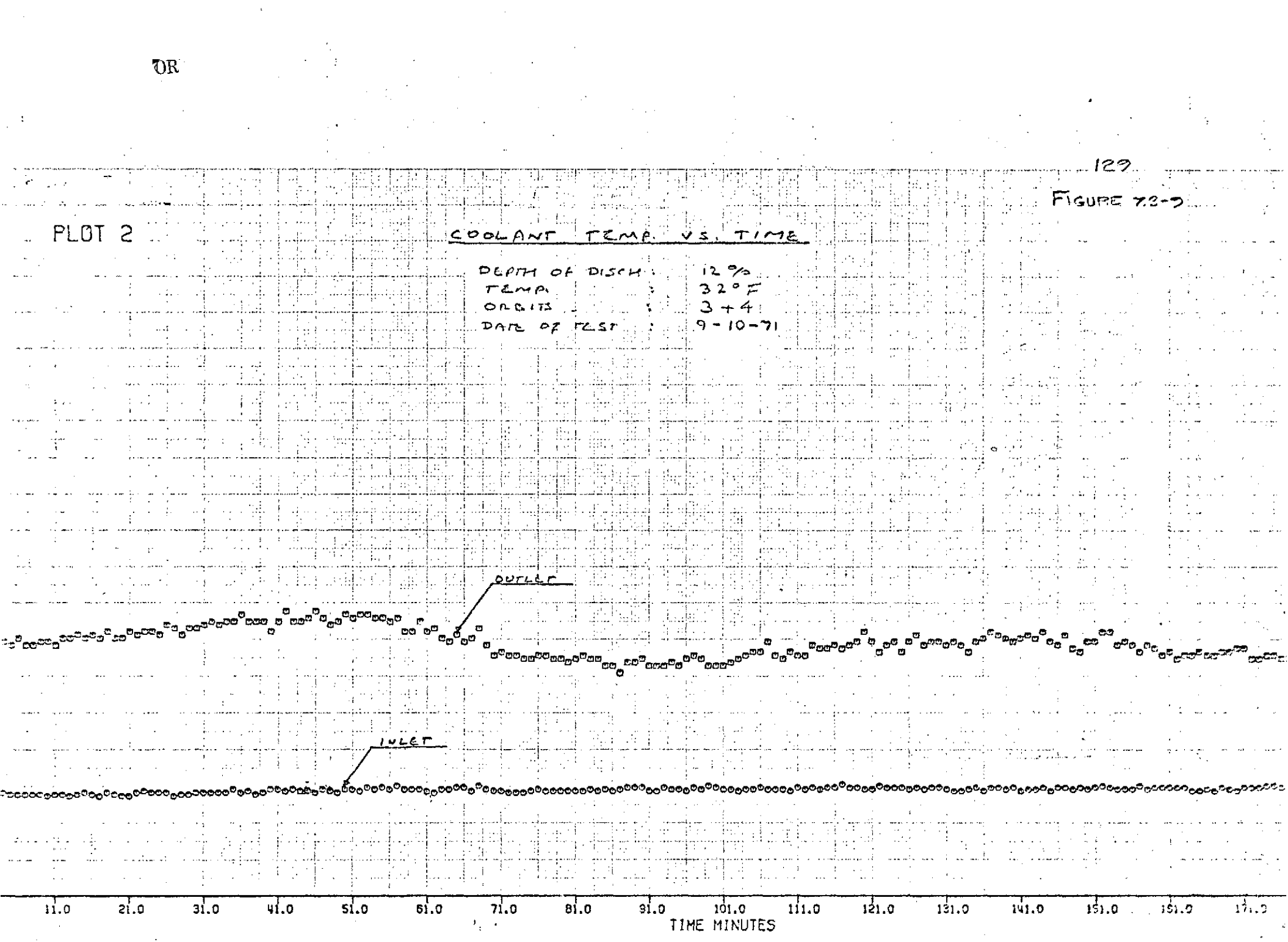

BATTERY MODULE TEST
PHASE I - ENG. UNIT

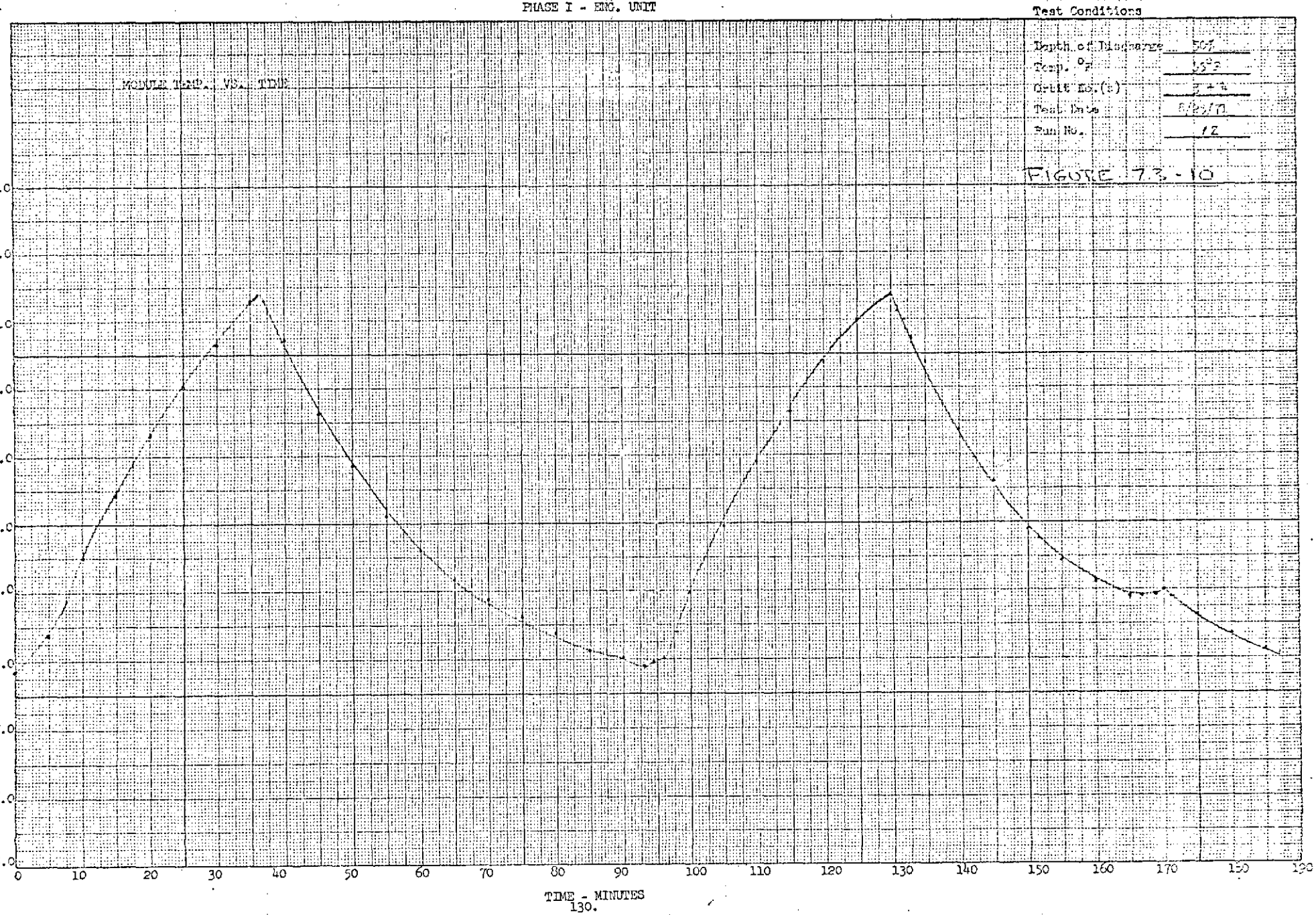

BATTERY MODULE TEST
PHASE I - ENG. UNIT

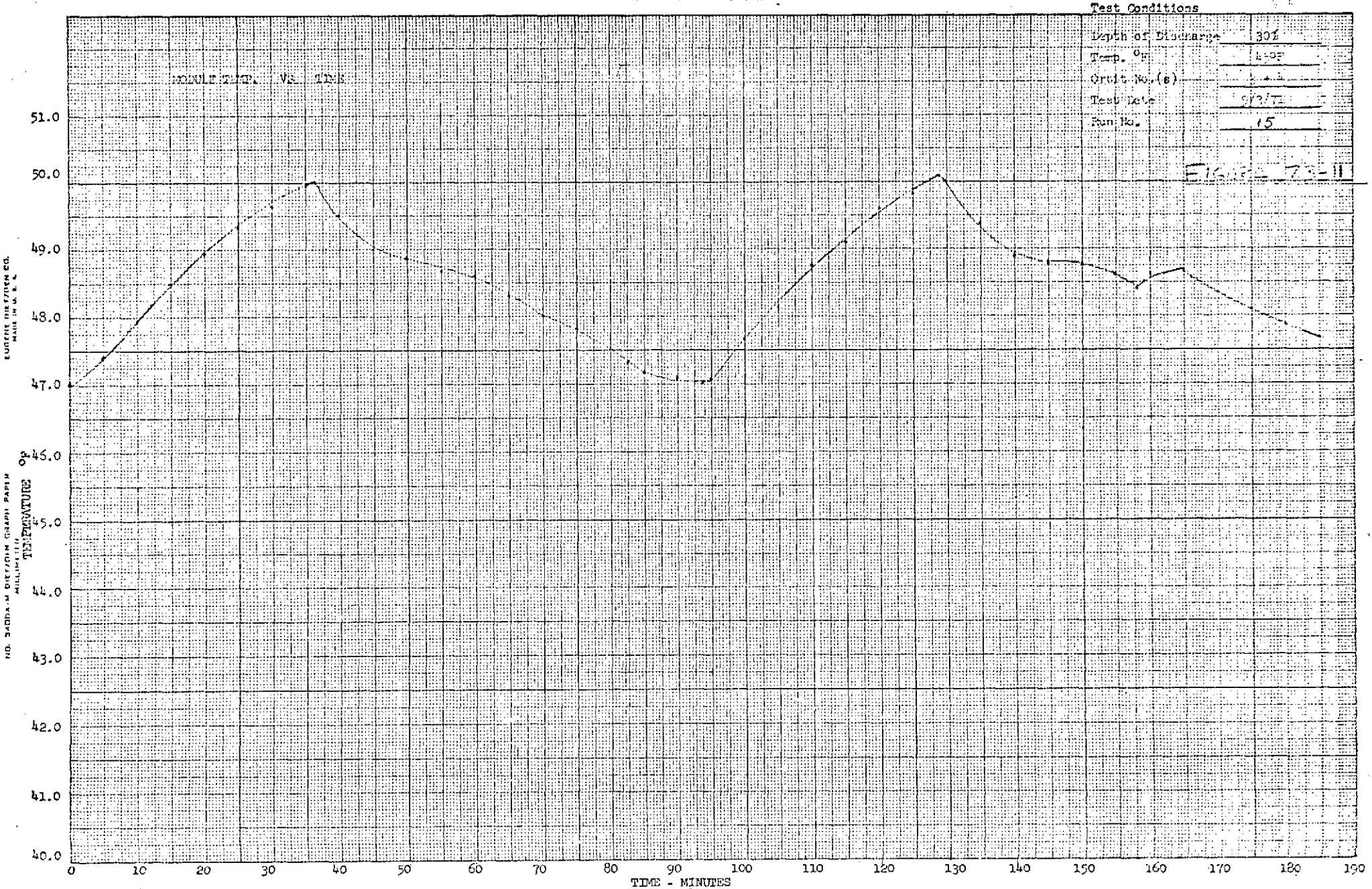

BATTERY MODULE TEST
PHASE I - ENG. UNIT

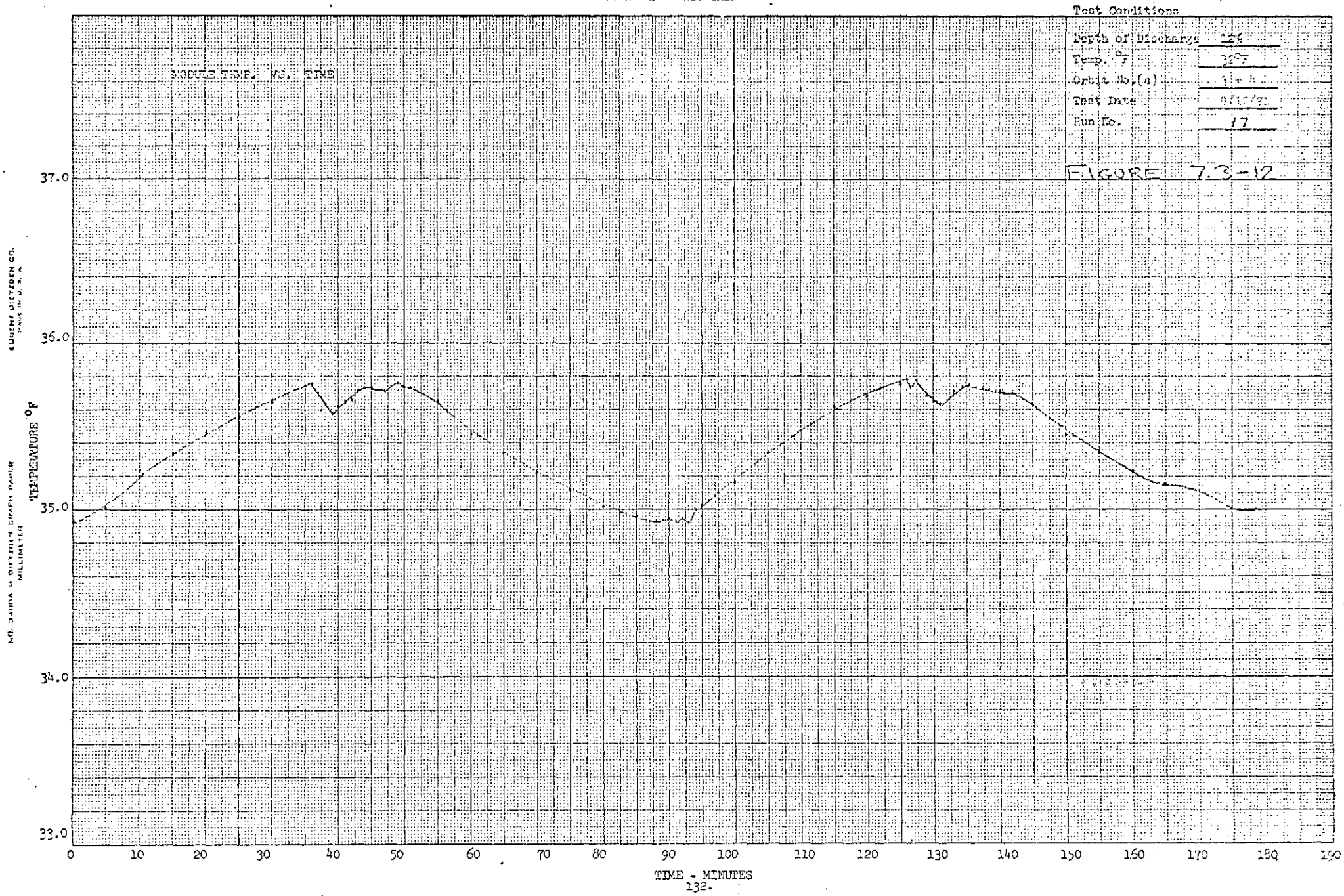

FIGURE 7.3-13

PLOT 1

CELL TEMP. VS. TIME

DEPTH OF DISCH. : 50%
TEMP. : 55°F
ORBITS : 3+4
DATE OF TEST : 8-25-71

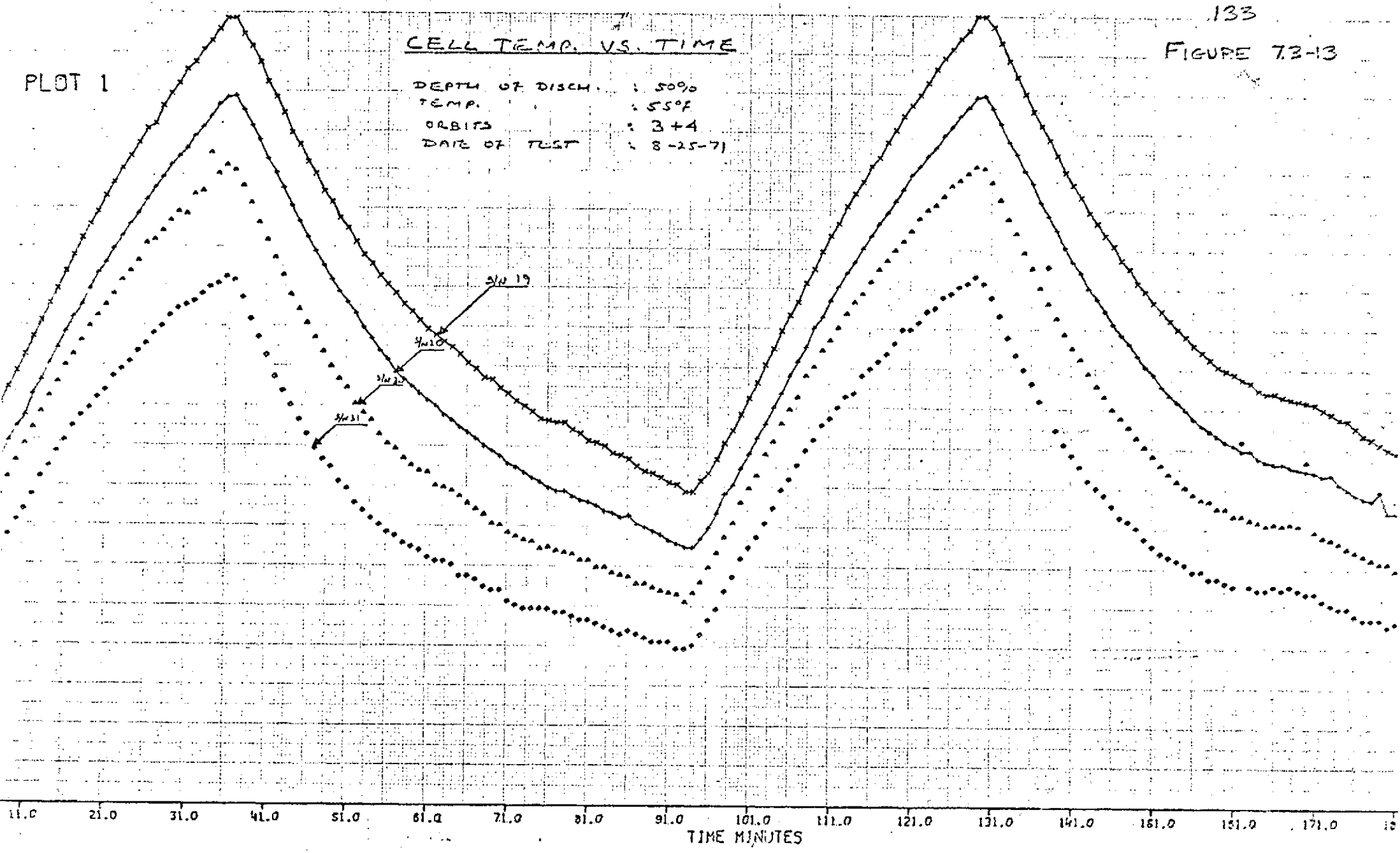

FIGURE 7.3-14

PLOT 1

CELL TEMP. VS. TIME

DEPTH OF DISCH : 30%
TEMP. : 45°F
ORBITS : 3 + 4
DATE OF TEST : 9-3-71

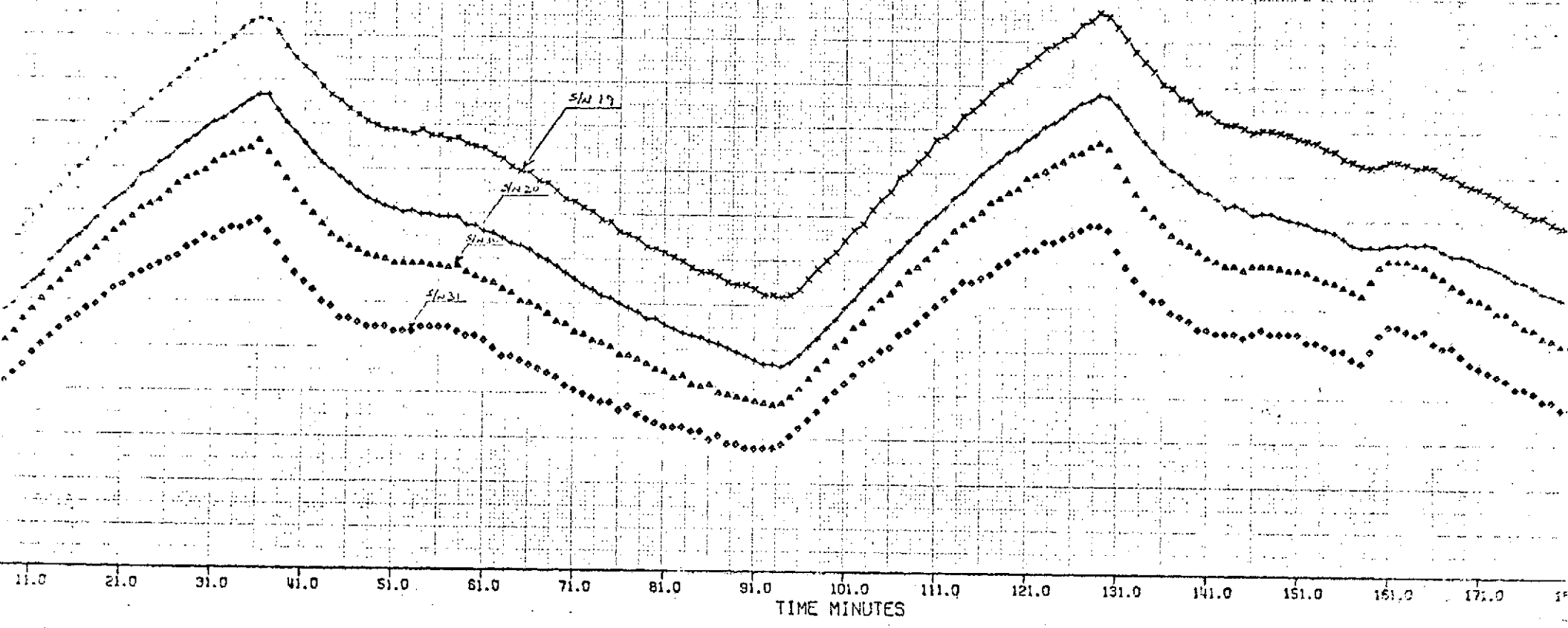

SUMMARY OF TEMP. DATA, LIVE CELL RUNS

Test Condition	Coolant Temp. (°F)		Average Module Temp. (°F)		Max. Cell Center-Face Temp (°F		
	Range	Spread	Range	Spread	Range	Spread	(1) ΔT
50% DOD, 55°F	In.: 55.0-55.3	0.3	57.5-63.5	6.0	58.9-65.0	6.1	9.9
	Out.: 55.7-61.6	5.9					
30% DOD, 45°F	In.: 44.8-45.0	0.2	46.7-50.4	3.7	48.1-51.3	3.2	6.4
	Out.: 47.5-49.6	2.0					
12% DOD, 32°F	In.: 33.3-33.5	0.2	34.8-35.9	1.1	35.8-36.8	1.0	3.4
	Out.: 35.1-35.9	0.8					

NOTES:

(1) ΔT is defined as max. cell center-face temp. minus average coolant inlet.

TABLE 7.3-1

FIGURE 7.2-15

PLOT 1

CELL TEMP. VS. TIME

DEPTH OF DISCH.	: 12%
TEMP	: 32°F
ORBITS	: 3+4
DATE OF TEST	: 9-10-71

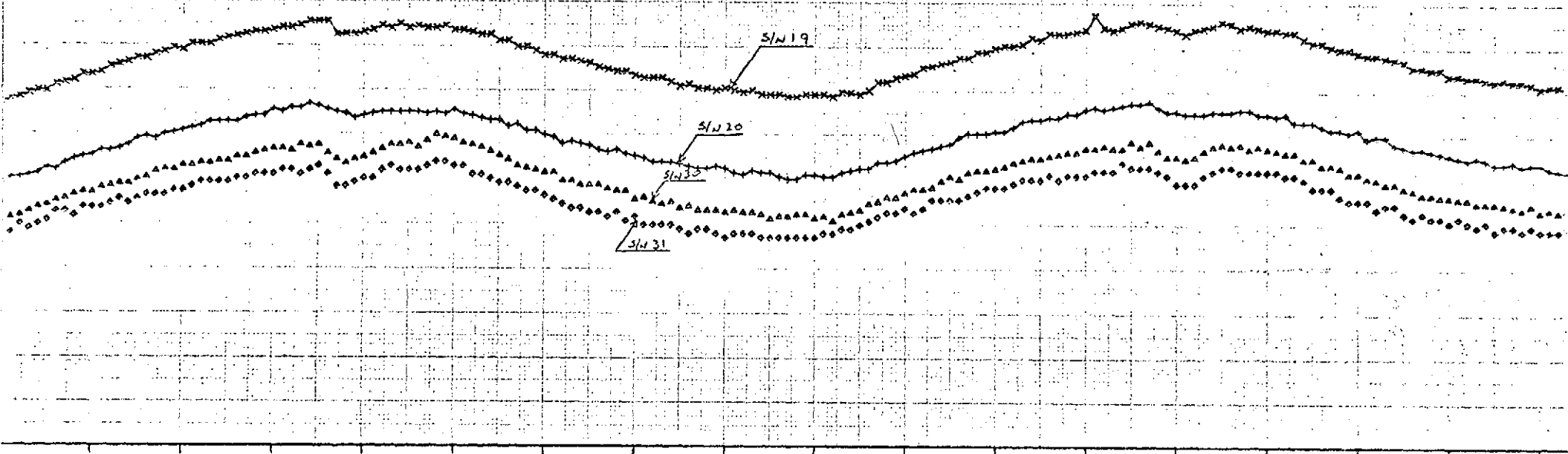

1.0 11.0 21.0 31.0 41.0 51.0 61.0 71.0 81.0 91.0 101.0 111.0 121.0 131.0 141.0 151.0 161.0 171.0

TIME MINUTES

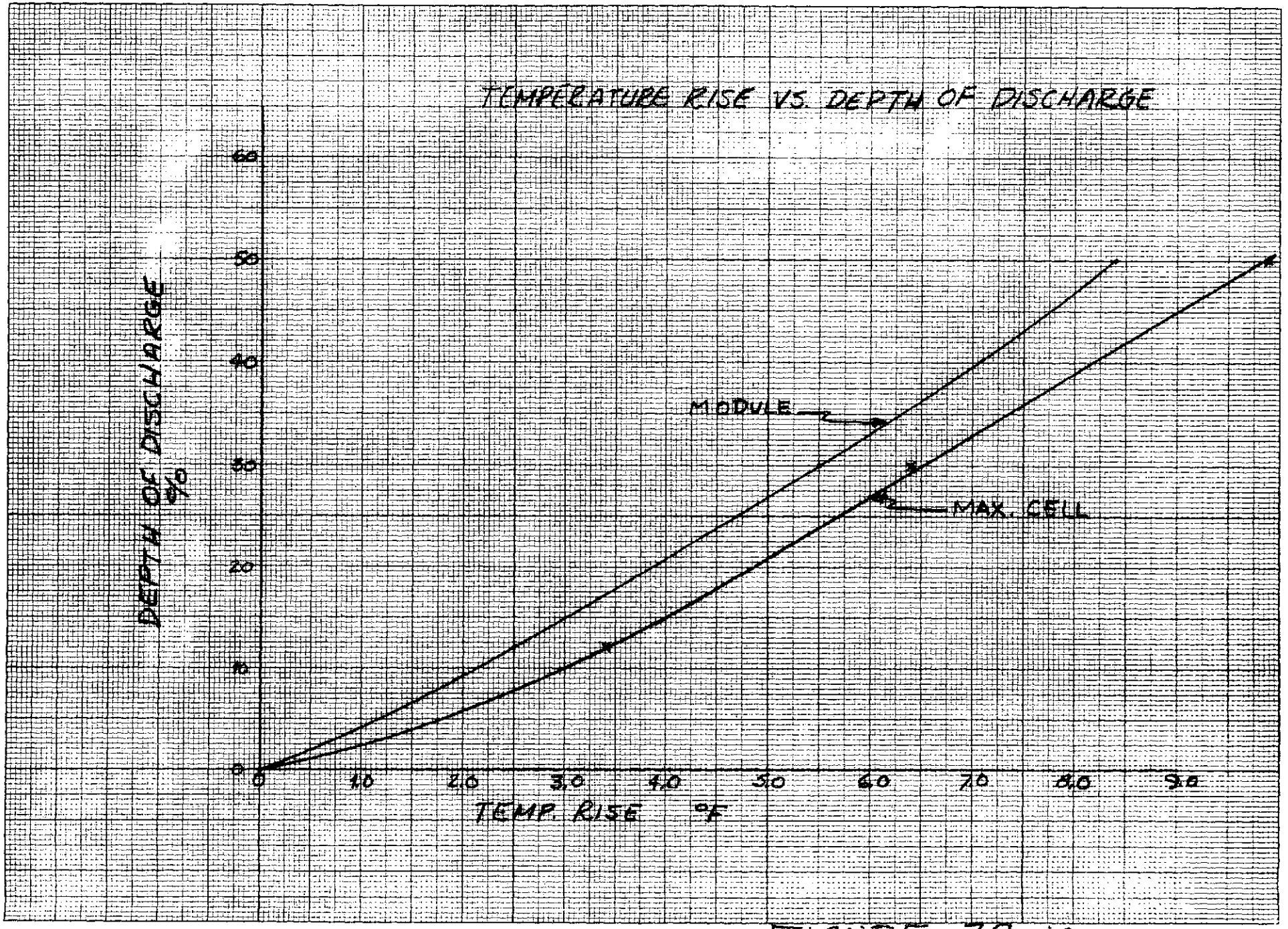

FIGURE 7.3-16

FIGURE 73-17

PLOT 4

DEPTH OF DISCH : 50%
TEMP. : 55°F
ORBITS : 3 + 4
DATE OF TEST : 8-25-71

MODULE VOLTAGE VS. TIME

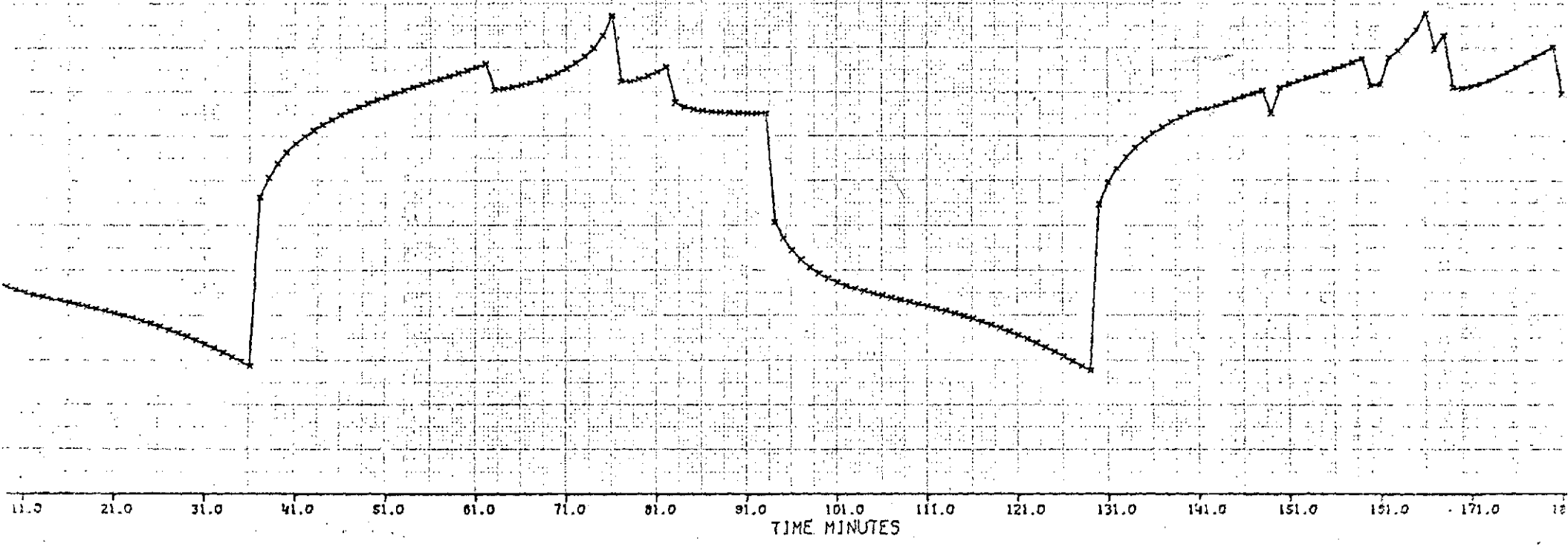

FIGURE 73-13

PLOT 4

MODULE VOLTAGE VS. TIME

DEPTH OF DISCH: 30%
TEMP. : 45°F
ORBITS : 3+4
DATE OF TEST : 9-3-71

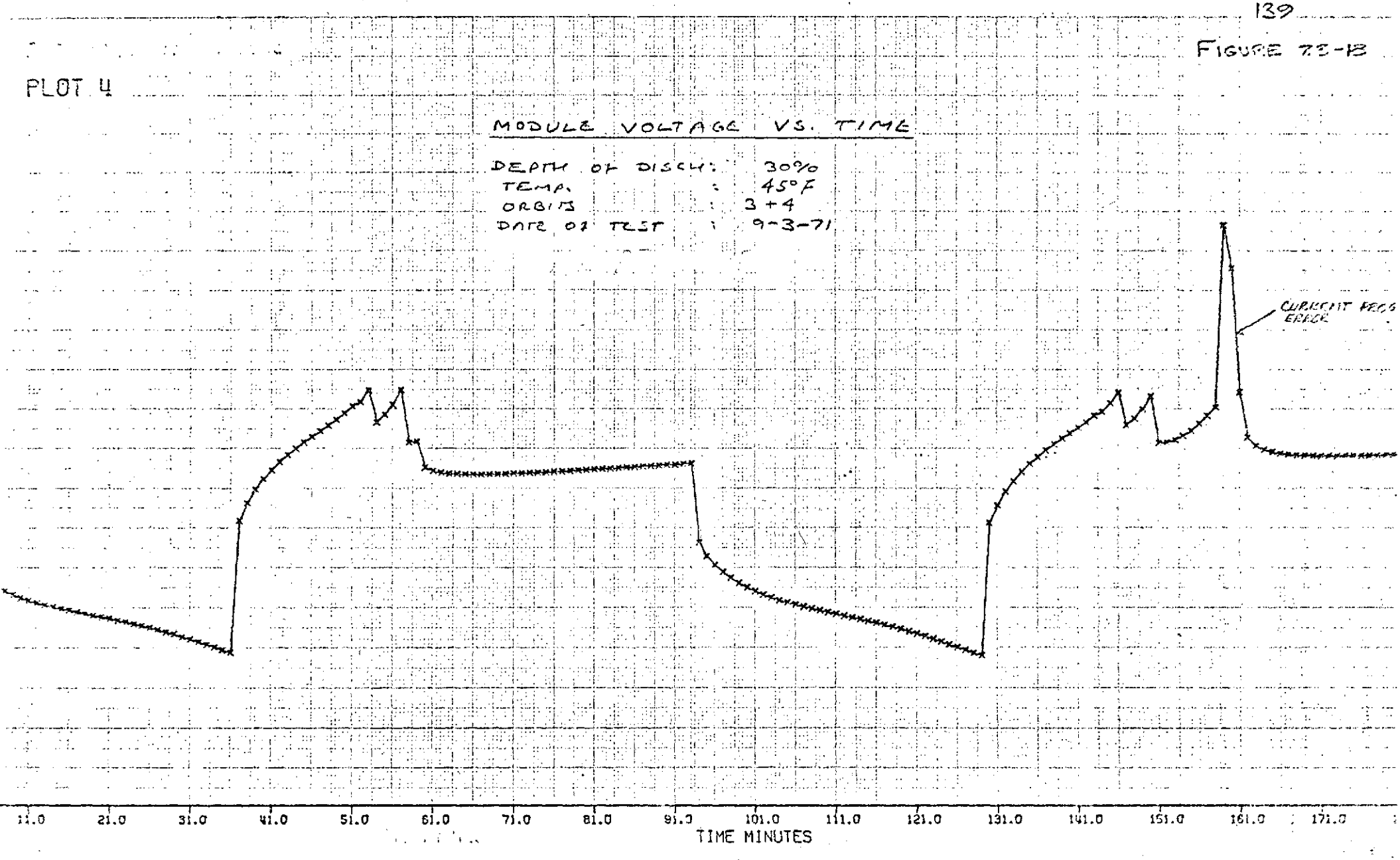

Cell pressures for each run may be found in Figures 7.3-19 through 7.3-21. The generally increasing trend indicates some overcharge in each orbit, and that even by the last orbit, pressure was not stable. The divergence between S/N 19, 20 on the one hand, and S/N 30, 31 on the other, again suggests the difficulty with operating two different types of cell in the same series string with common voltage limit, Although little or no hydrogen appeared to have been generated (recombination during discharge was quick, and there was no indication of leakage), a lower level voltage limit could have reduced or eliminated the rising trend while still permitting full charge. Similarly, later tests with usable oxygen-sensing auxiliary electrode signal charge termination, should show earlier pressure stabilization, and good recharge fractions. (See Appendix for cell description.)

End-of-charge and end-of-discharge voltage are plotted by orbit number in Figure 7.3-22. Both show again the difference between the two cell groups, especially in end-of-discharge. End-of-discharge also shows a rising trend for each of the three runs, indicating the cells were closer to actual full charge as the run progressed. Except for the 50% DOD run, no similar decreasing trend to show higher charge efficiency developed from the end-of-charge voltage data.

Figure 7.3-23 is a breakdown of percent total return (ampere-hours) at each charge rate. As anticipated, the highest percentage at high rates occurred during the 50% DOD run. The 30% and 12% DOD runs show progressively higher percentages at lower rates.

FIGURE 73-19

PLOT 4

MODULE VOLTAGE VS. TIME

DEPTH OF DISCH.	12%
TEMP.	32°F
ORBITS	3 + 9
DATE OF TEST	9-10-71

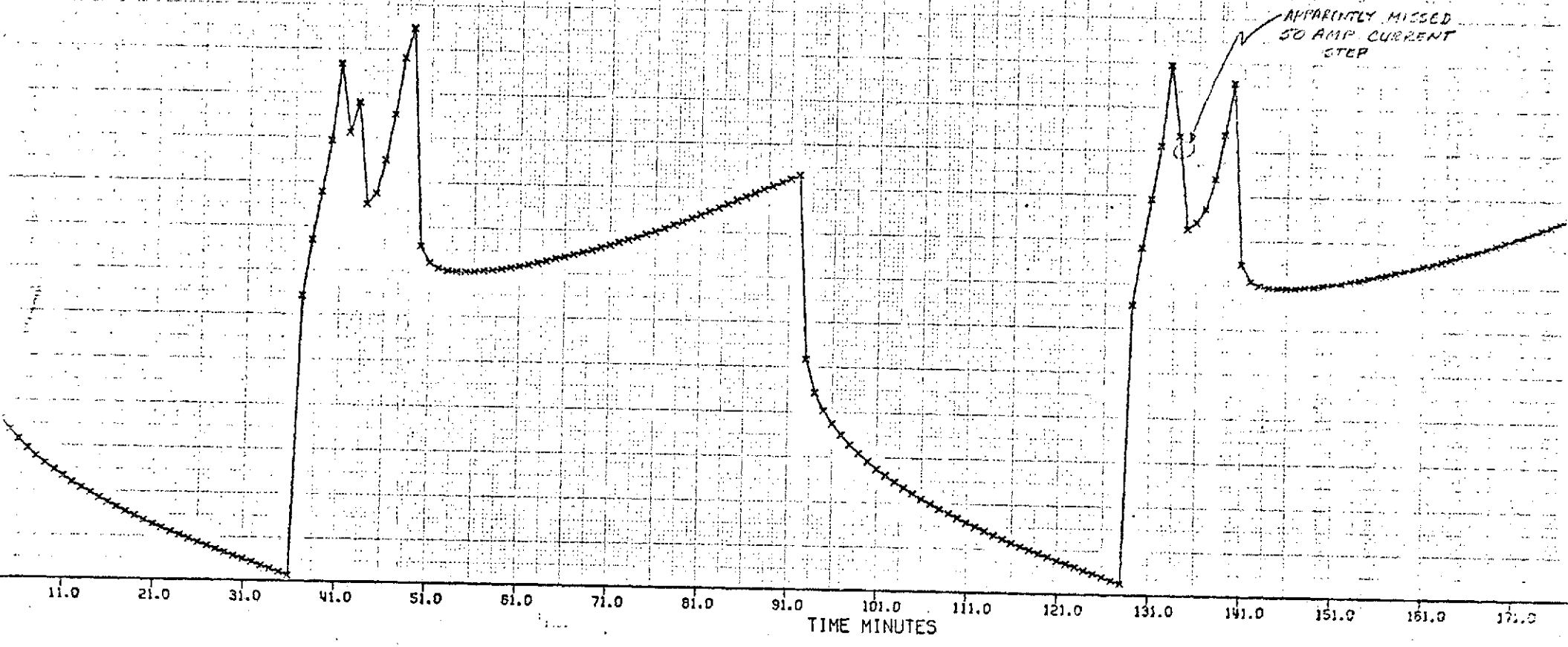

FIGURE 7.3-20

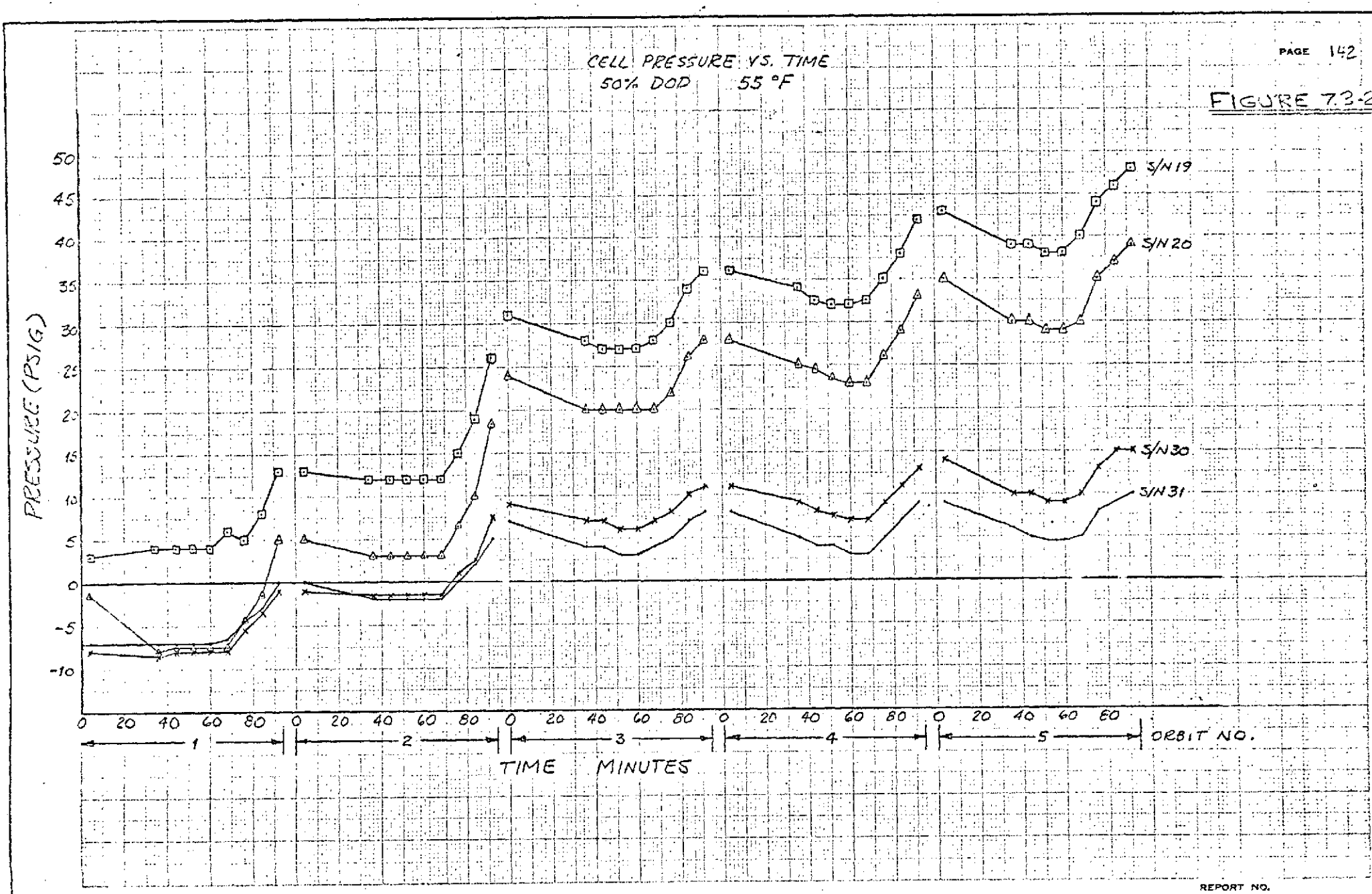
CELL PRESSURE VS. TIME
50% DOD 55 °F
PRESSURE (PSIG)
50
45
40
35
30
25
20
15
10
5
0
-5
-10
S/N 19
S/N 20
S/N 30
S/N 31
0 20 40 60 80 0 20 40 60 80 0 20 40 60 80 0 20 40 60 80 0 20 40 60 80
1
2
3
4
5
ORBIT NO.
TIME MINUTES

FIGURE 7.3-21

REPORT NO.

FIGURE 7.3-22

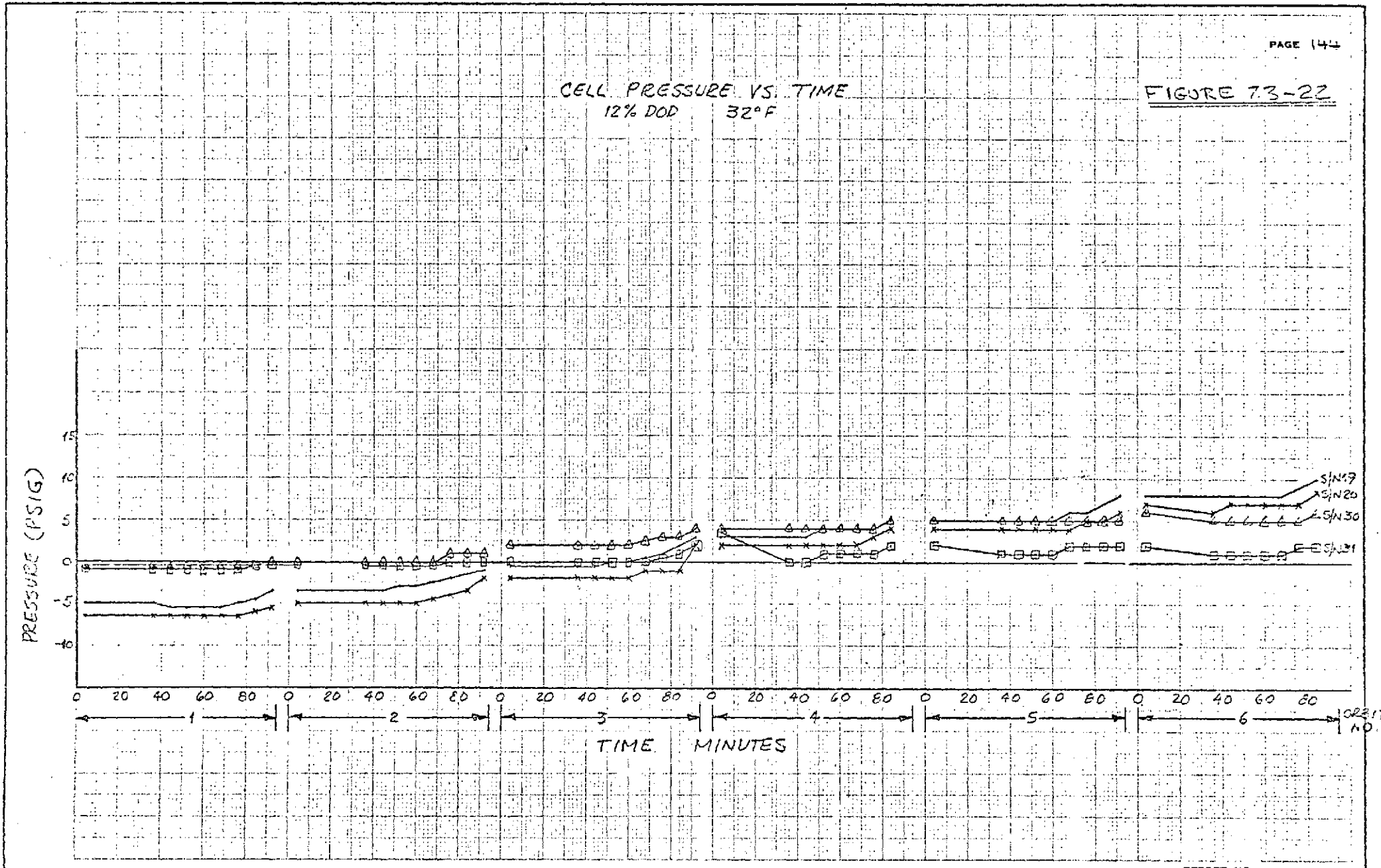
CELL PRESSURE VS. TIME
12% DOD 32°F
PRESSURE (PSIG)
15
10
5
0
-5
-10
S/N 27
S/N 20
S/N 30
S/N 31
0 20 40 60 80
1
2
3
4
5
6
ORBIT NO.
TIME MINUTES

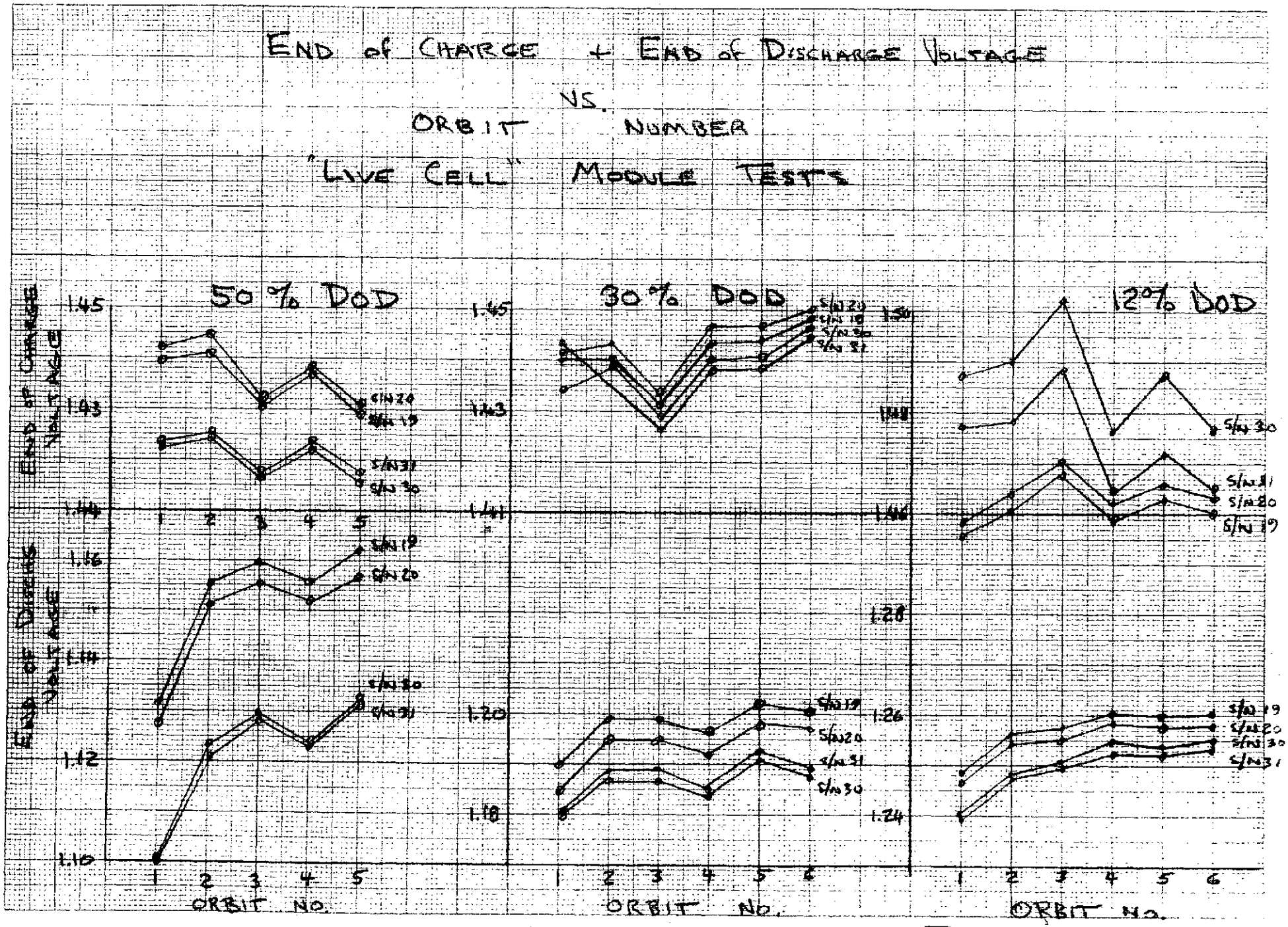
END of CHARGE + END of DISCHARGE VOLTAGE
VS.
ORBIT NUMBER
"LIVE CELL" MODULE TESTS
50 % DoD
30 % DoD
12% DoD
S/N 20
S/N 19
S/N 31
S/N 30
S/N 81
S/N 80
S/N 79
ORBIT NO.
ORBIT NO.
ORBIT NO.

FIGURE 7.3-23

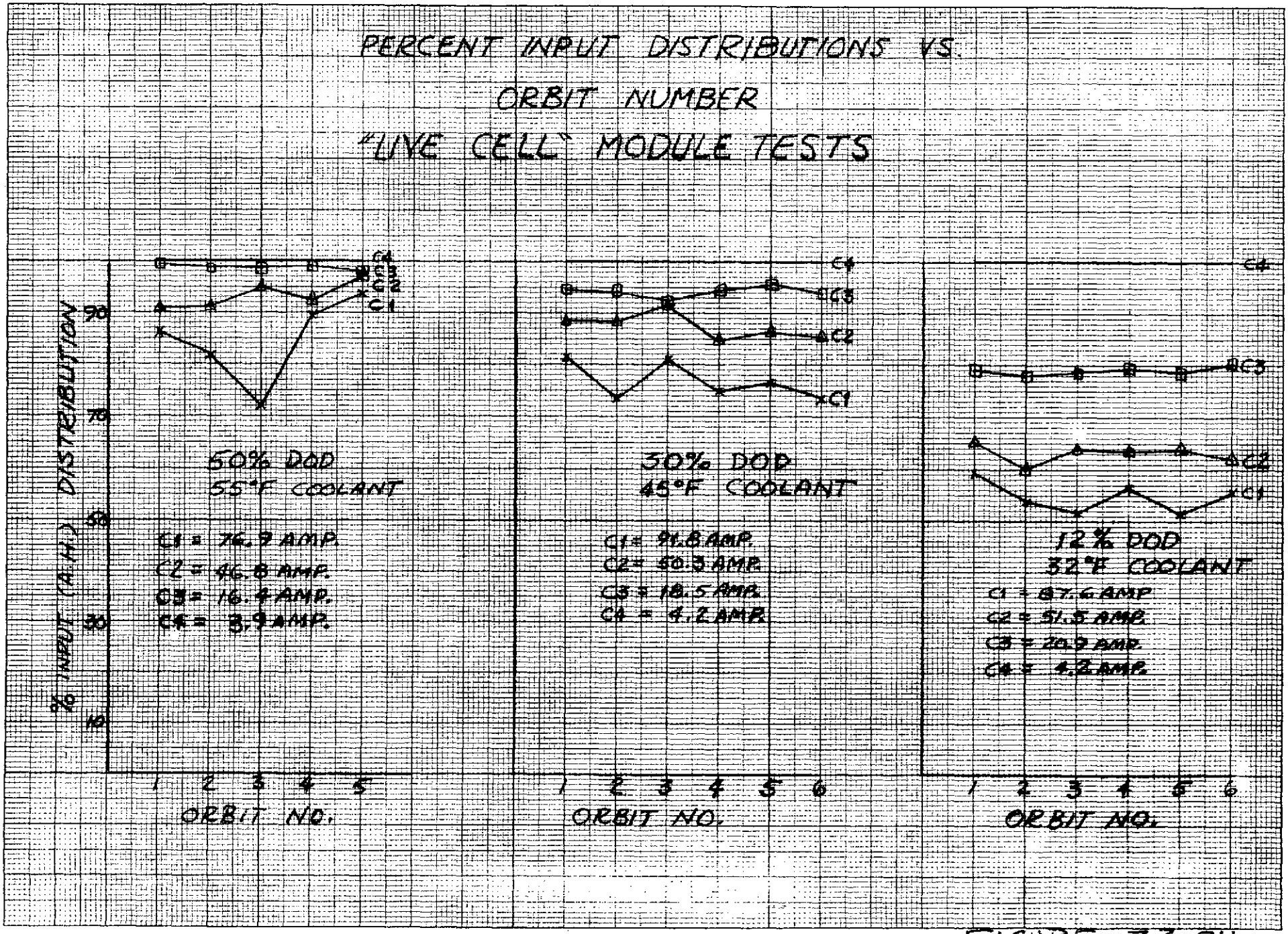

FIGURE 7.3-24

Watt-hour and ampere-hour return ratios are shown in Figure 7.3-25. There is, apparently, a cyclic characteristic evident about an average; i.e.: a below average fraction is followed by one above average, and so forth. Furthermore, the trend of the averages (108% for 50% DOD, 115% for 30% DOD, and 113% for 12% DOD) may possibly indicate achievement of somewhat higher charge efficiency by the time of the 12% DOD cycles. This may have been caused by the earlier runs' acting as "burn-in".

7.3.1.2.1 General Comments

As data from these live cell runs were reviewed, it became quickly evident that performance was not indicative of that to be expected of full capacity cells. This is traceable to two (2) primary causes:

- The cells never had 100 amp-hour capacity due to removal of electrodes to provide space for heater grids.
- There are two distinct types of cell; S/N 19 and 20 is one, and S/N 30 and 31 is the other. (See Appendix .)

From this, it is obvious that thermal data in the heater runs is representative of a worst case test of thermal control. Ultimately, full capacity cells can be expected to generate less heat, allowing both cells and module to run cooler. Such cells will also probably have higher end-of-discharge voltages, and lower return fractions.

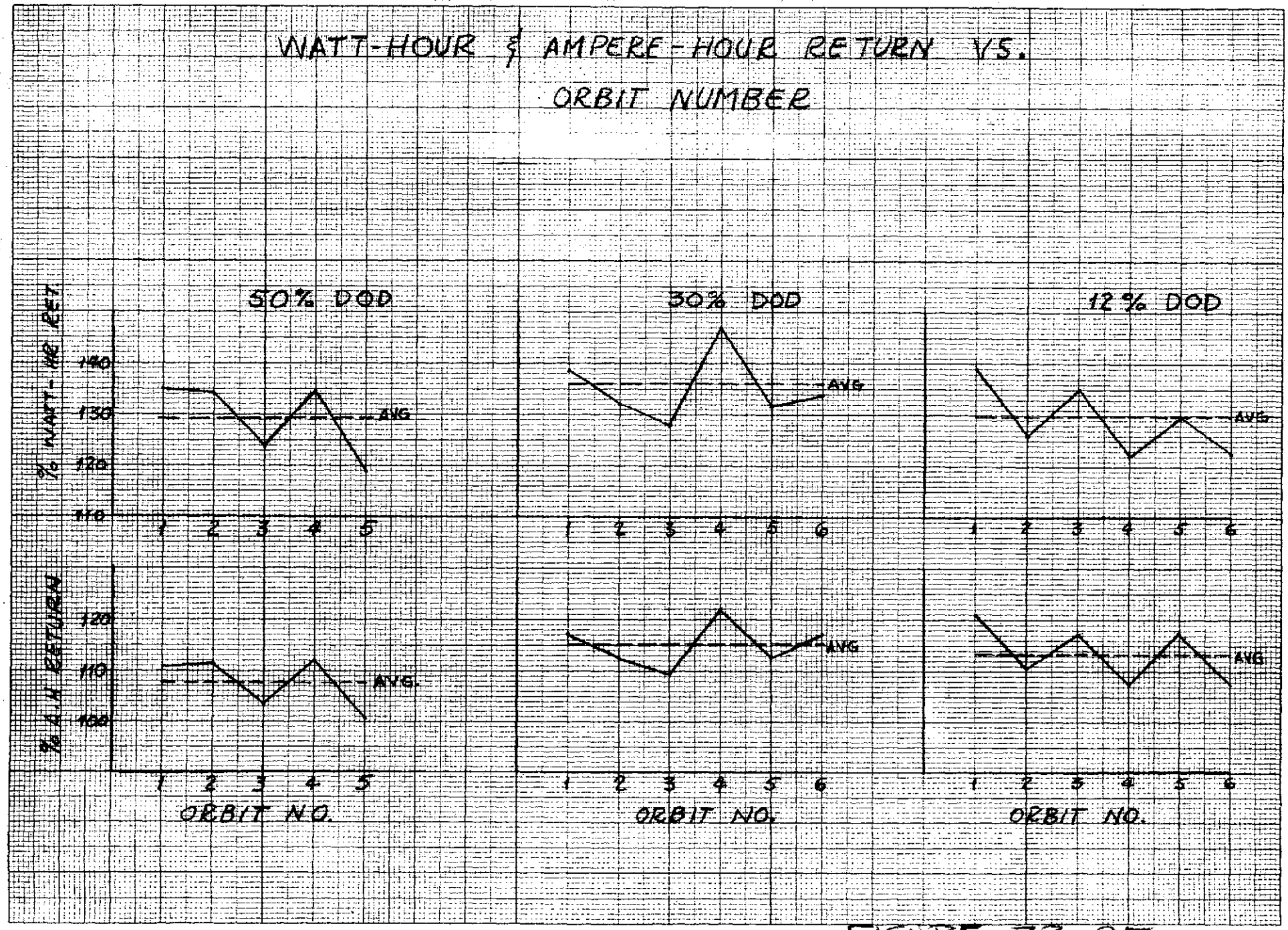

FIGURE 7.3-25

7.4 Proof Pressure Tests

7.4.1 Objective

This test was conducted to assure the adequacy of stress safety margin in the module structure. The module was designed to contain the cells safely under internal pressure conditions of 100 psig. Calculations (see 6.2.3.1) had indicated positive safety margins at 150 psig. The test was conducted at 140 psig.

7.4.2 Test Procedure

After all other tests were complete, the battery was removed to the structural laboratory. Here each cell was pressurized after instrumentation at sea level and room ambient of approximately 72°F. The test was performed as follows:

- Before and after attachment of strain gauges, the module was examined carefully for visible cracks
- The module was instrumented with strain gauges in accordance with Figure 7.4-1
- Pressure lines from stored nitrogen gas tanks were attached to each cell
- The module was placed in a covered pit for personnel safety after connecting the strain gauge outputs to recorders
- The cell pressures were raised to 140 psig at a linear rate over a period of two (2) minutes
- 140 psig pressure was held for 45 seconds
- The cells were depressurized to 0 psig at a linear rate over a period of two (2) minutes
- The module was removed from the pit, disconnected from the pressure lines and instrumentation, and carefully examined again.

FIGURE 7.4-1

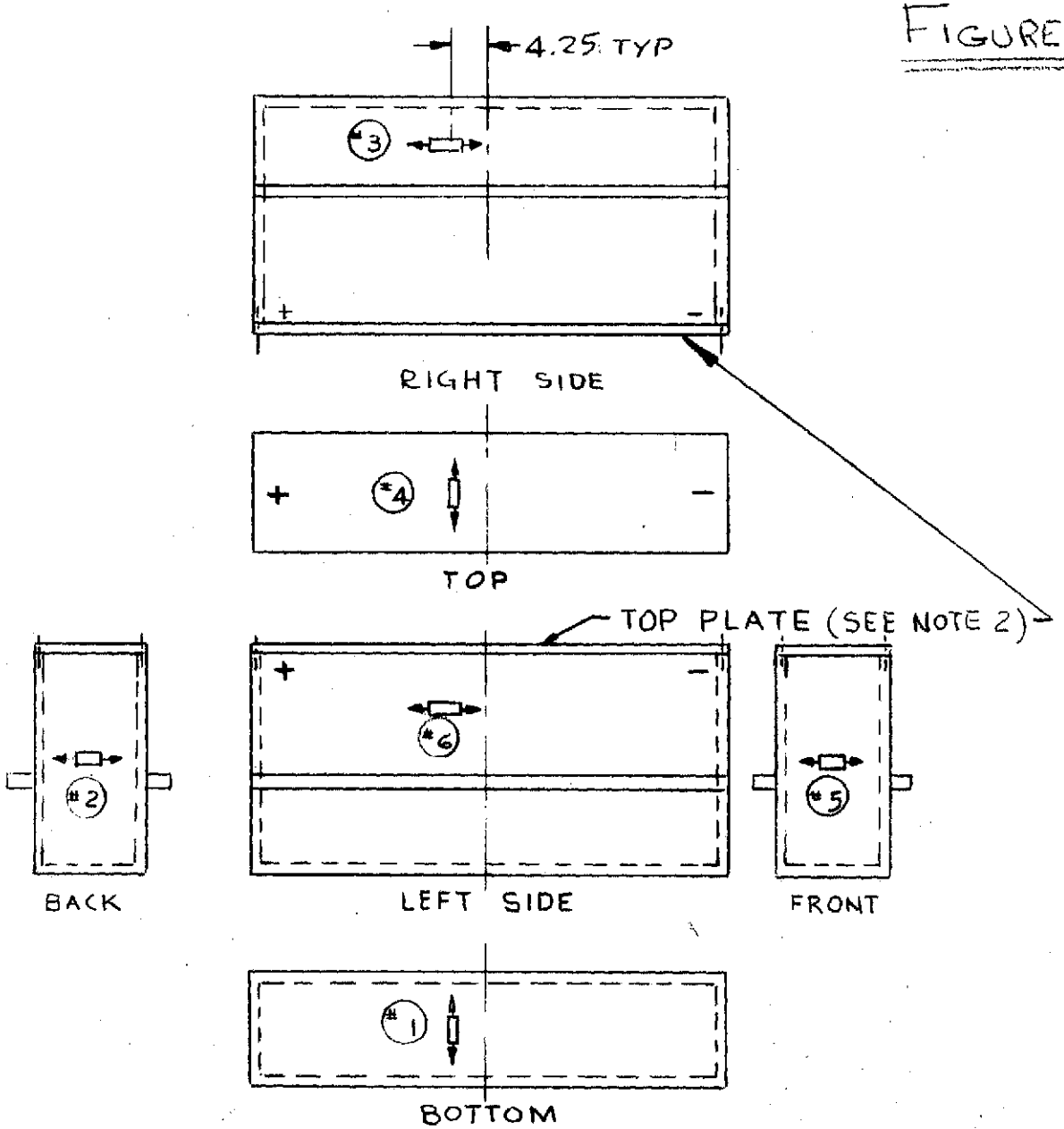

NOTES:

1- ALL STRAIN GAGES ARE TENSION AXIAL GAGES.

2-TOP PLATE IS SECURED TO MODULE CASE WITH SCREWS

LOCATION OF STRAIN GAGES ON BATTERY MODULE

The test was witnessed by Grumman Engineering representatives, Grumman Quality Control,and NAVPRO Quality Control.

7.5 Proof Pressure Test Results

7.5.1 Visual

Six welded bulkhead tabs near the bottom of the mounting flanges showed cracks in the weld. A typical crack is shown in Figure 7.5-1. The module was accordingly submitted to the Metallurgy and Welding Department for analysis.

To determine the failure mode, one weld was sectioned and examined metallographically and by electron fractography. The photograph, Figure 7.5-2, shows the weld section. The weld crown is on the left, and the crack can be seen running into the weld to a depth of approximately 0.055 inch, at which point the fusion zone ended. The metallurgical examination also showed a dark oxide coating at the weld-tab surface interface, indicating the possibility that pre-weld cleaning may have been inadequate. The fracture was shown to be entirely within the weld nugget, demonstrating that the module's own structural properties are adequate. In addition, there was no evidence of shrinkage cracking.

An electron fractograph of the fracture surface, Figure 7.5-3, confirmed that insufficient weld penetration had caused the nugget to be overloaded. The penetration assumed for calculation was 0.085 inch (see Appendix) and yielded a positive, though inadequate, safety margin at 150 psig. Actual penetration was found to be about 0.055 inch. The Metallurgy and Welding Department recommended increasing penetration depth; and improving cleaning procedures as a result of their analysis. The actual solution to this problem, though somewhat different, takes these suggestions into account (see 10).

7.5.2 Stress

The battery module was instrumented with six tension axial strain gauges located as shown in Figure 7.4-1. For identification purposes, the gauges were numbered as follows:

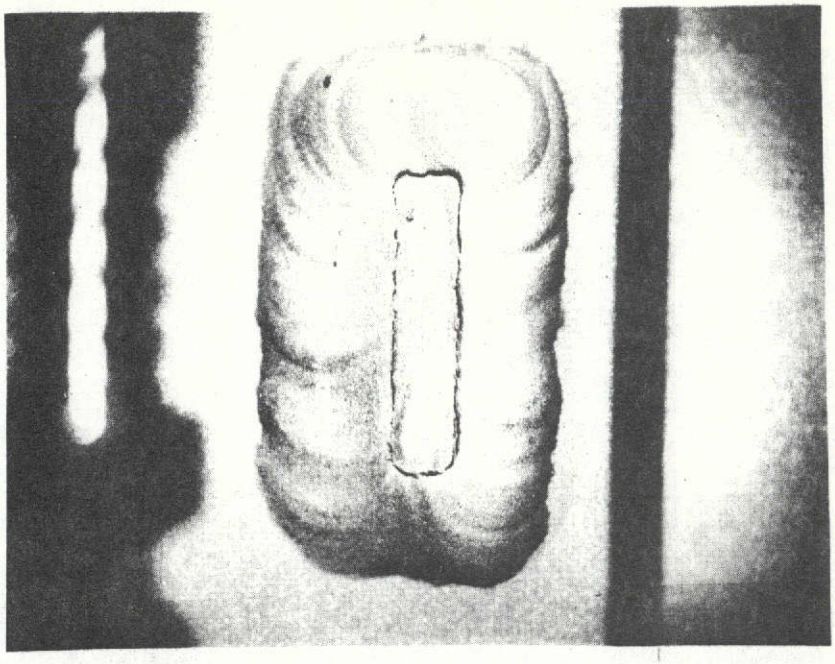

FIGURE 7.5-1

MAG: 3X Typical Cracked Weld Nugget

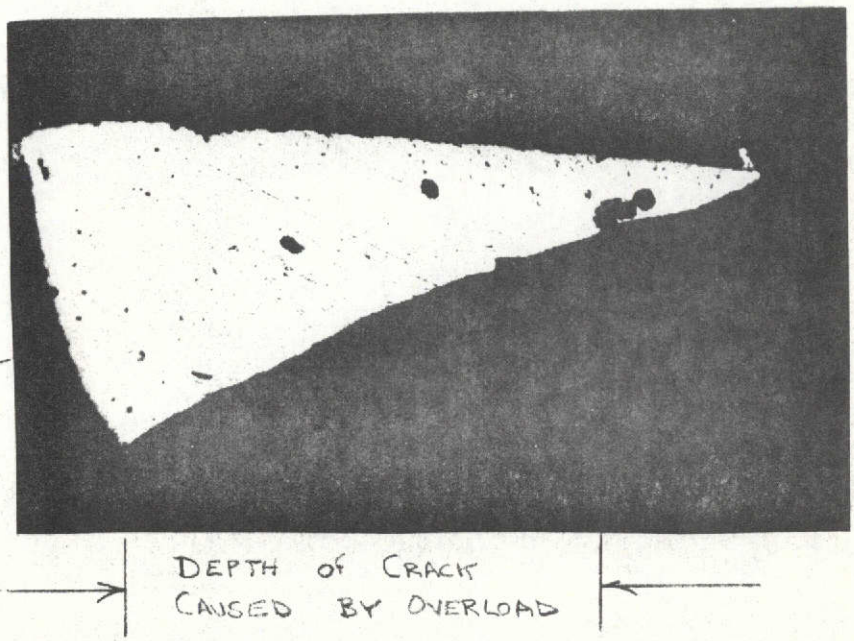

FIGURE 7.5-2

MAG: 50X Section of Nugget Showing Crack Penetration and Oxide Layer

FIGURE 7.5-3

Electron Fractograph of Crack Surface Showing Overload Mechanism

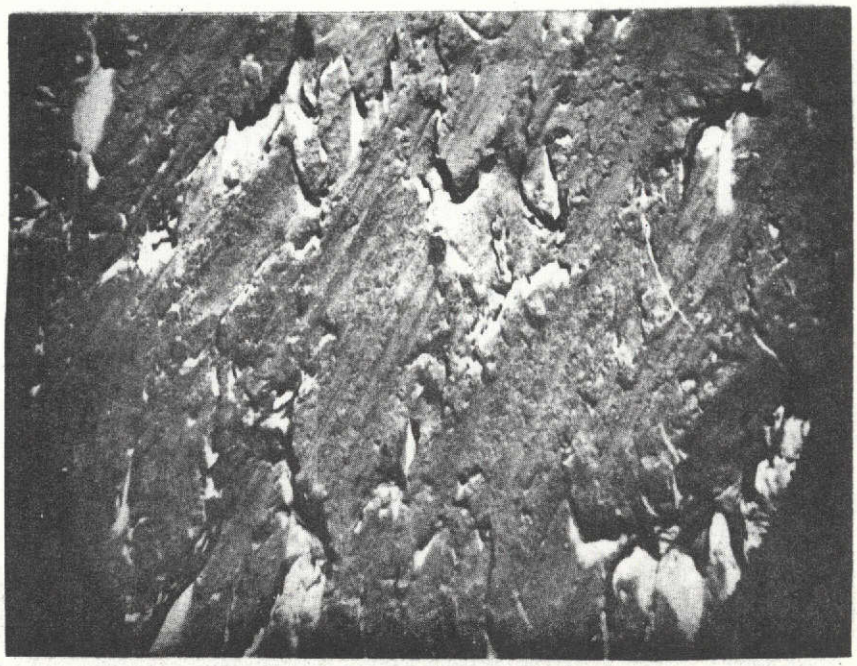

#1 - Bottom of module

#2 - Back side

#3 - Right side

#4 - Top cover

#5 - Front Side

#6 - Left side

The gauge on the right side of the module was located below the mounting flange, and that on the left side was located above the mounting flange.

Figure 7.5-4 shows the plotted values obtained from strain gauges #3 (right side) and #6 (left side), grouped together for comparison. Plotted values of gauges #1, 2, 4 and 5 are shown in Figure 7.5-5. The strain values were plotted for pressures 0-140 psig and 140-0 psig.

7.5.2.1 Discussion of Stress Data

Before discussing the stress data, the basic construction of the module must be reviewed. As shown in Figure 7.4-1, the module outer case is a five sided welded aluminum container with three partitions welded on the inside to divide it into four equal compartments. The top plate is secured to the case with thirty-two (32) #10-32 stainless steel screws. The largest strain recorded was on the left side of the module (strain gauge #6). This value was approximately 525 micro inches per inch.

The strain sustained by the back and front end of the module (strain gauges #2 and #5) was of approximately equal magnitude, 450 microinches per inch. Strain gauge #3, which measured the strain of the right side of the module, recorded 225 microinches per inch. This is 42% of that recorded for the left side. This difference can be attributed to the fact that the gauge on the right side was located between the mounting flange and the welded base of the case resulting in a more rigid section, while that on the left side was located between the mounting flange and the bolted top plate of the case. The strain on the top plate of the module, (gauge #4) also indicated a

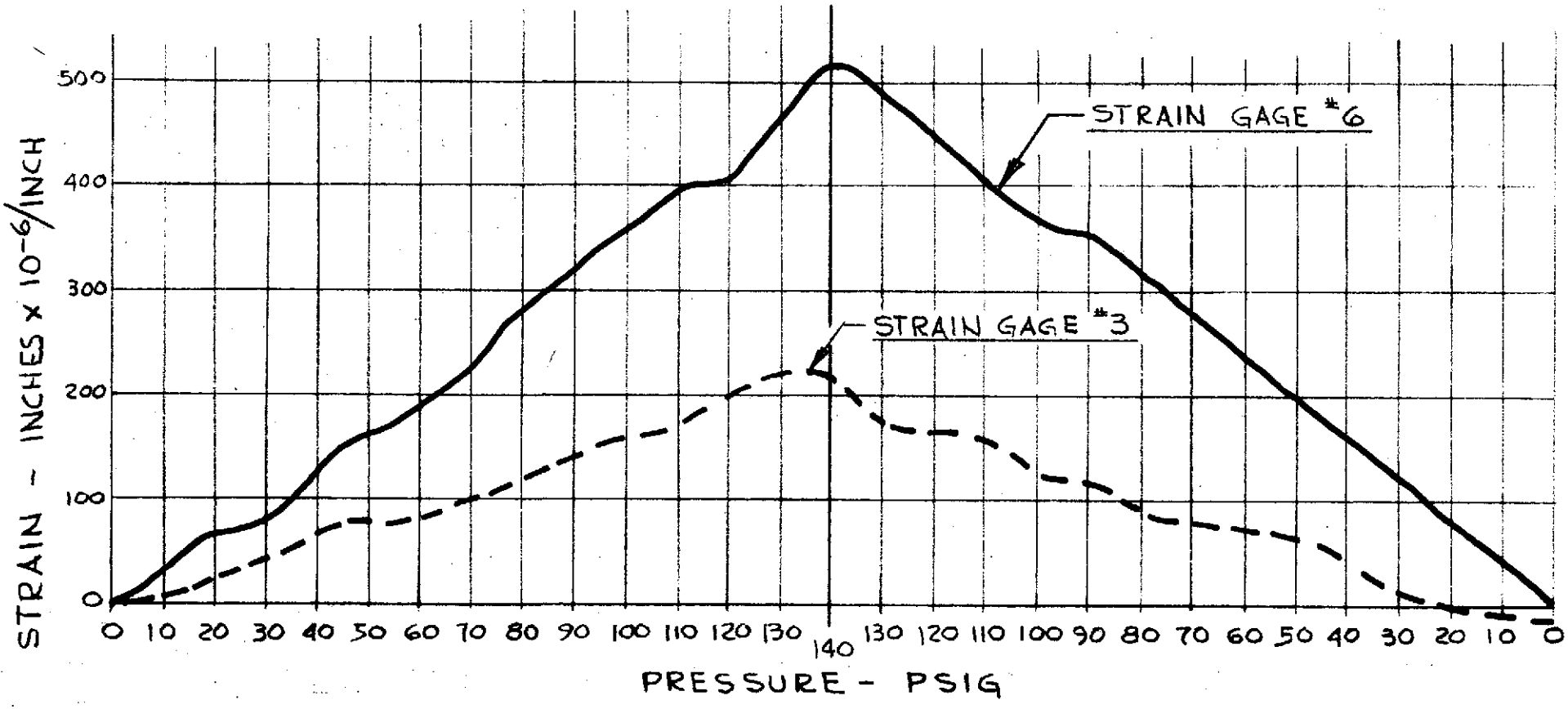

Ni-Cd BATTERY MODULE PROOF PRESSURE TEST

FIGURE 7.5-4

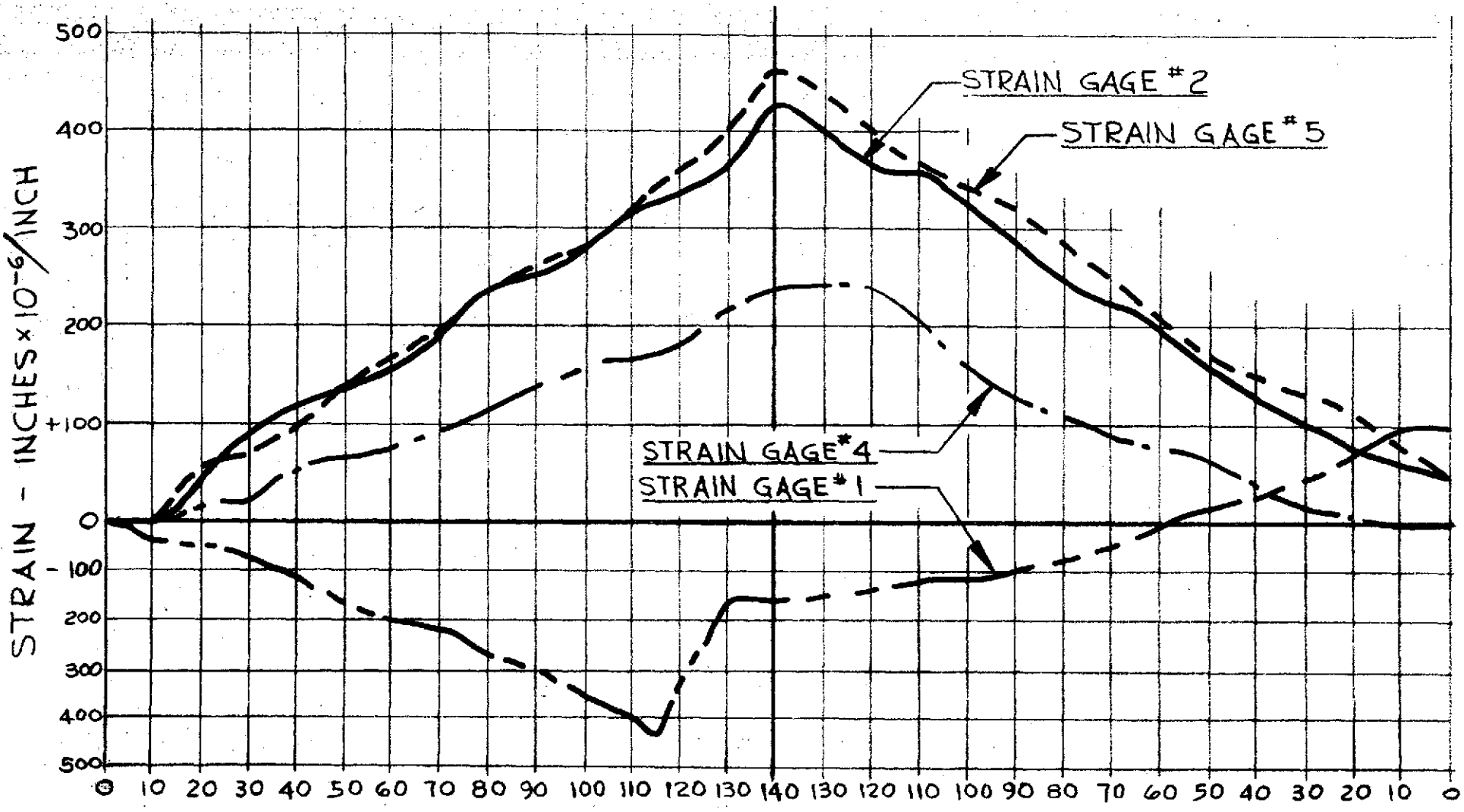

Ni-Cd BATTERY MODULE PROOF PRESSURE TEST

FIGURE 7.5-5

a low magnitude, 250 microinches per inch.

Unlike the four sides described above, the strain recorded for the bottom of the case, gauge #1, resulted in a negative value. In addition, there was a distinct jump from negative 425 to negative 150 microinches per inch. This occurred between 115 and 130 psig internal pressure. The negative value indicates that the stress induced in the gauge side of the bottom was in compression rather than tension. This may be explained by the fact that the base of the case is welded all around. The high internal pressures acting against the two sides of the case thus caused a pivoting action at the welded joint. The discontinuity of strain values (from negative 425 to negative 150 microinches) can be attributed to the fact that two of the welded tabs on each of the three bulkheads failed as a result of insufficient weld penetration. (see 7.5.1 above). The flexing of the sides as a result of the weld failure relieved the stress which was being applied to the base, causing it to jump. As can be seen from the above results, the strain imparted to all sides of the module under an internal pressure of 140 psig is minimal, and well within the design safety margins for actual internal pressures of 100 psig.

8.0 SYSTEM INTEGRATION CONSIDERATIONS

8.1 Thermal

In a Ni-Cd battery system, it is desirable to have all the cells in the system at the same temperature since cell performance during both charge and discharge is temperature dependent.

During charge, all the cells in a string should be at the same temperature so that they are all equally restored to the same state of charge when the "first cell up" signals termination of charge (charge efficiency being temperature dependent).

Similarly, all cells in a string should be at the same temperature during discharge so that the same total energy (thermal plus electrical) is removed from each cell. Since discharge efficiency is temperature dependent, isothermicity would guarantee that the true discharge depth would be the same for each cell.

In addition, battery strings which discharge in parallel should be at the same temperature so that they load share equally. Since it is well established that orbital life decreases with increasing discharge depth, maximum system life (minimum replacement) occurs when all batteries in a system load share equally.

The rejection system available for battery thermal control (as envisioned by both Phase B Space Station contractors) is an actively circulating coolant (water) loop (Figure 8.1-1) which accumulates waste heat within the station and rejects it to a space radiator (which radiates the heat to space). As in any such system, the total coolant flow rate is optimized based on the total vehicle heat load, variation of space radiator weight with heat rejection temperature and variation of subsystem weights with coolant temperature. The point being illustrated is that the available flow in a space vehicles' active cooling system is limited, and is determined from overall vehicle trade-offs.

Figure 8.1-1

TYPICAL LARGE SPACE STATION

HEAT TRANSPORT/REJECTION LOOP CONFIGURATION

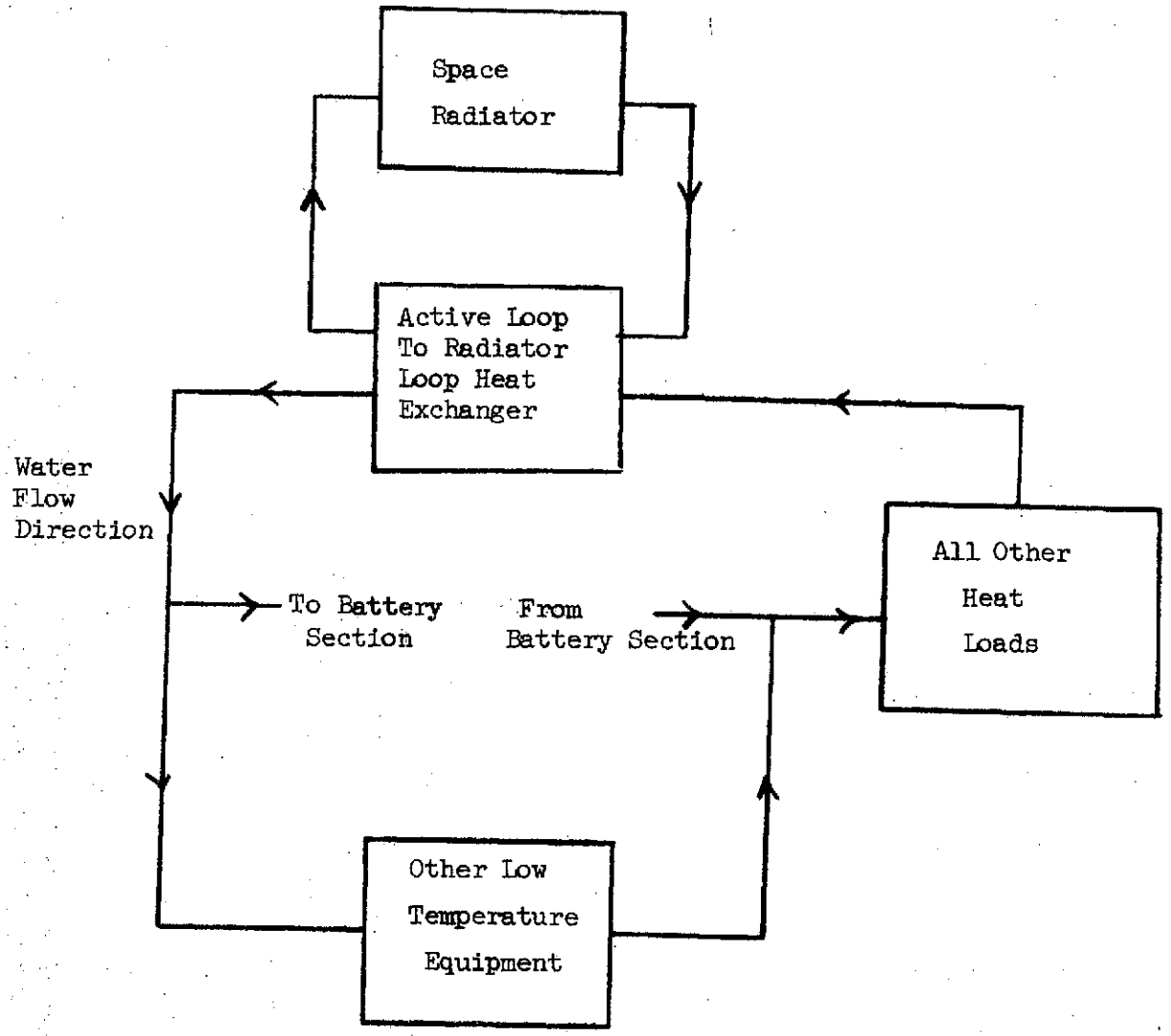

The problem of achieving equal cell temperatures in a limited flow rate system is greatly complicated as the number of cells in the system is increased. Information made available to Grumman by the Phase B contractors indicates that a typical 25 KW system would be comprised of 168 four-cell modules (672 cells). The total flow rate in the active cooling loop is understood to be on the order of 2500 pounds per hour. Several approaches to maintaining all the cells in the battery system at equal temperatures are discussed below.

Any system configuring the battery modules in series on the coolant loop inherently results in unequal cooling and unequal temperatures among the modules. Temperature rise of the coolant due to flow past a module reflects as higher inlet temperature to the next one in line, and so on.

The most obvious way to attempt providing equal cooling and isothermal conditions among modules is to arrange all 168 units in parallel on the loop (Figure 8.1-2) on single pass cold rails (Figure 8.1-3, I). The drawbacks of this approach are obvious:

a) Even if the entire vehicle's flow rate were diverted to the batteries, less than 15 pounds per hour would be available to cool each module. Each module, however requires a minimum of 30 pounds per hour of flow to keep the cell to cell temperature gradient along the direction of flow within acceptable (although not optimum) limits

b) Attempting to equally divide the flow among more than 168 separate paths is a formidable task to be avoided if possible.

A variation of this approach would be an all parallel arrangement as before using multi-pass cold rails. That is, the coolant would flow through the modules once, be brought back to the entrance, and flow through a second passage in the cold rails (see Figure 8.1-3, II).

BATTERY SYSTEM PORTION OF

ACTIVE LOOP- ALL MODULES ON PARALLEL LEGS

FIGURE 8.1-2

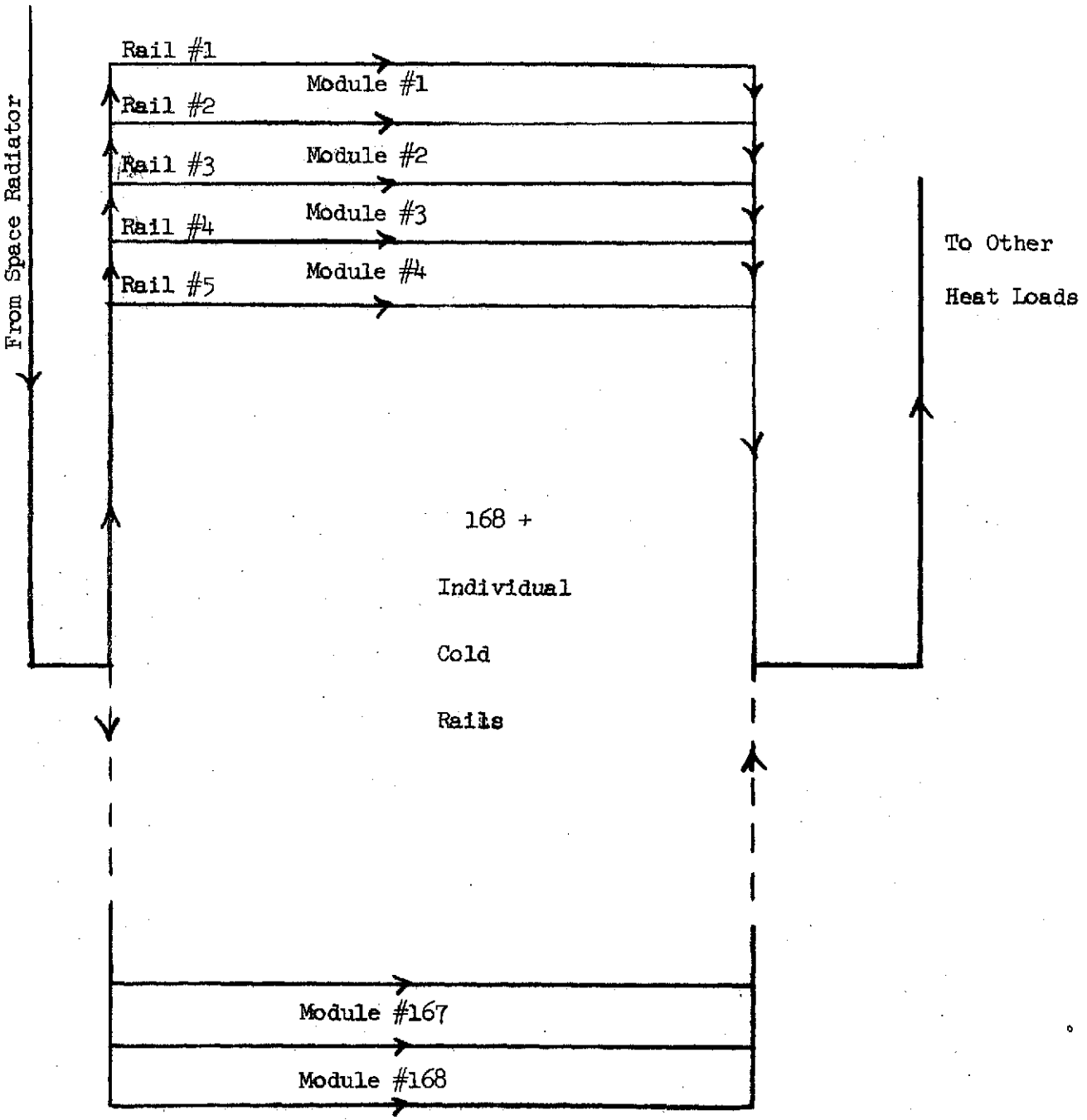

TYPICAL COLD RAIL CONCEPTS

FIGURE 8.1-3

I. Single Pass Coolant Flow

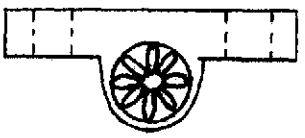

II. Dual Pass Coolant Flow

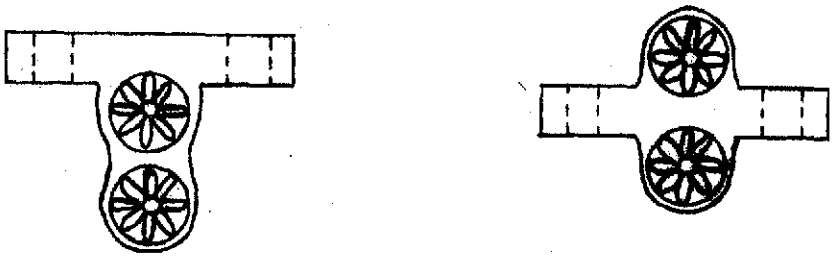

III. Coolant Flow Heat Pipe Augmented

Shown with redundant coolant paths

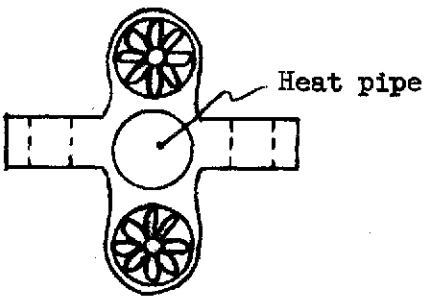

NOTE:

a) All coolant passages have extended surface inserts
b) All heat pipes are isothermalizers charged with water and are of the Grumman spiral artery design

IV. Heat Pipe Cold Rail

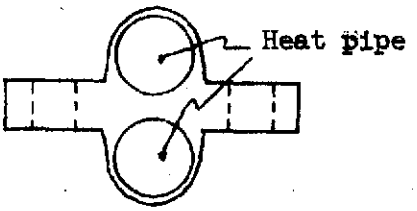

Such a two-pass arrangement with a flow rate of 15 pounds per hour per module would result in a cell to cell temperature variation approximating that achieved with a 30 pound per hour flow rate. This configuration would provide equal cooling to each module with an acceptable (not optimum) cell to cell temperature gradient within the module. Its disadvantages are:

a) A highly complex plumbing system due to the flow balancing and lines routing required, and

b) A great increase (doubling) of the pressure drop in the lines over the single pass scheme.

A second variation to the all parallel approach would be a single pass, all parallel arrangement as before with an isothermalizer heat pipe on each of the module's mounting flanges to eliminate the cell to cell axial temperature variation which would otherwise result. The drawbacks to this scheme are:

a) Complex flow balancing and flow routing between modules is still required

b) The heat pipes are used on the replaceable, rather than the permanent, part of the system. That is, over a ten year space station lifetime, the battery modules would have to be replaced several times, discarding the heat pipes each time (while the cold rails remain in the system permanently).

Another possible variation would be an all parallel system with an isothermalizer heat pipe built into the cold rail (see Figure 8.1-2, III). This configuration still has the disadvantage of requiring flow balancing and routing to each module. However, its heat pipe does eliminate the problem of cell to cell gradients within the module due to the low flow rates while retaining the heat pipe as an integral, permanent (rather than expendable) part of the cooling system.

The last scheme proposed is one which potentially eliminates the complexities of flow distribution to each battery module. In this approach, the modules would be mounted on heat pipe cold rails (see Figure 8.1-3, IV). No actual vehicle coolant would flow through these rails. Instead, the heat picked up from each module would be transported by its heat pipe (with a negligible temperature gradient developed along the module's length) to its condenser ends. The condenser ends from large numbers of heat pipe cold rails would be routed to a single central heat exchanger from which the summed heat would be dissipated to the coolant loop. Typically, in a six battery power system arrangement, one-sixth (1/6) of the available coolant flow could be routed to each of six parallel, heat exchangers (located near each battery). All the heat pipes from a particular battery's cold rails would be routed to the same heat exchanger. The flow balancing within the system becomes simplified, requiring only equal division of the available coolant among 6, instead of 168, flow paths. Coolant routing, in general, would be much less complex. In addition, the presence of the heat pipe in the cold rail eliminates cell to cell temperature variations within the battery module without compromising the basic simplicity desirable for the design of the replaceable battery module itself. This system is the one recommended in 10.

8.2 Mechanical Considerations

Since both thermal and electrical considerations (discussed in 8.1 and 8.3, respectively) are the primary impacts on the form taken by any suggested mechanical configuration, it is necessary to review them before proceeding further. Effects due to maintainability, safety and other elements may then be discussed.

8.2.1 Thermal Impacts

Type of cooling system, size (in terms of number of modules), and isothermicity are all major considerations to be handled. For a Space Station, using a pumped liquid (water) coolant with cold rails, these involve problems and tradeoffs in cold rail design (size, weight, fabrication, structural integration); plumbing design (routing, subsystem compatibility, complexity), and structural compatibility with other subsystem components.

8.2.2 Electrical Impacts

Size of battery, charge control implementation, and bus voltage and distribution all affect mechanical design. Between the two prime Phase B contractors, Grumman's information indicates there are only two similar items. Both studies concluded that bus voltage should be approximately 112 to 120V nominal, and both use 672-cell, 168-module systems. Other parameters appear to be as indicated in 8.3 below. The use of 21-module (North American Rockwell-NAR) and 28-module (McDonnell Douglas-MDAC) batteries, however, suggest a 7-module rack configuration as shown in 8.2-1, since both the above numbers are divisible by seven (7). For the former, then, each battery would contain three (3) racks; while the latter would consist of four (4).

The configuration must be designed with an intermodule electrical connection system compatible with both the intercell connectors (6.2.3.1) and maintainability (4.3 and 6.4). Basically, the implications are:

- o Quick disconnect with captive hardware
- o Sufficient conductor cross-section
- o Short length

Finally, it is desirable to incorporate charge control, requisite monitoring and control/protection electronics in the mounting with the

modules. (This, and associated problems, is discussed further in 8.3.) This technique minimizes wiring, reduces control problems, and improves EMC in a large, complex vehicle such as Space Station.

8.2.3 Other Impacts

Maintainability effects include:

- o Captive hardware use for mounting
- o All hardware to accept standard tools
- o Easy module accessibility
- o Quick disconnects

Safety demands consideration for venting of gases and/or electrolyte (KOH) vapors escaping from damaged cell seals to space, or, at least, out of occupied areas.

8.2.4 Structural Considerations

Whereas internal cell pressure is the limiting constraint for module design, the mounting/integration structure must also withstand: (see 4.1)

- o Vibration
- o Shock
- o Acceleration

while supporting the requisite quantity of modules, and associated electrical and thermal hardware. A 7-module configuration which shows promise of meeting all the considerations and impacts noted above is shown in Figure 8.2-1 without electronics. This arrangement has the following advantages:

- o Before connection to coolant plumbing, it is relatively mobile, allowing location flexibility
- o Compatible with other equipment mountings
- o Low weight and volume penalties for structure
- o Easy maintainability
- o Easily expandable to handle more modules or other equipment

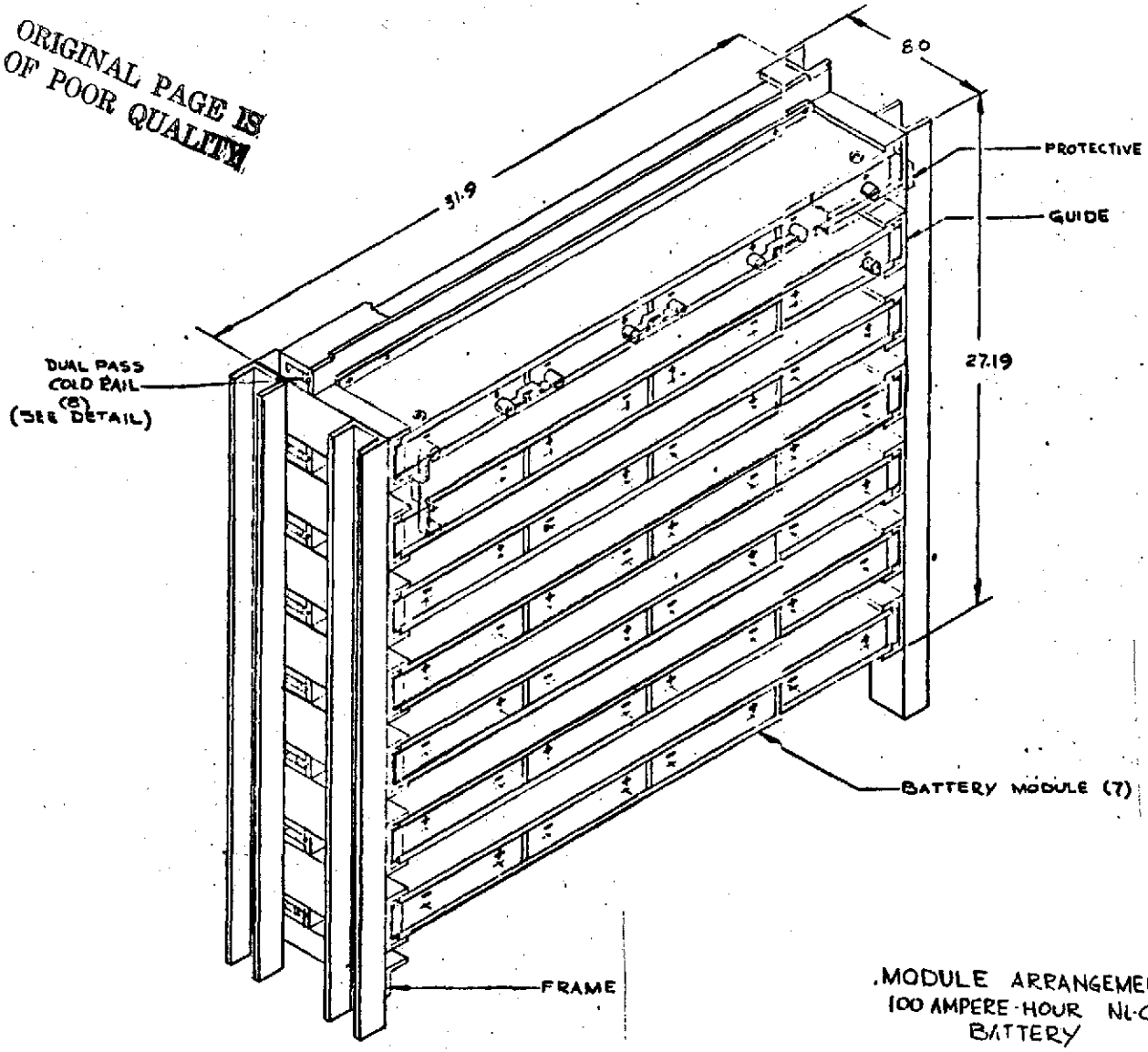

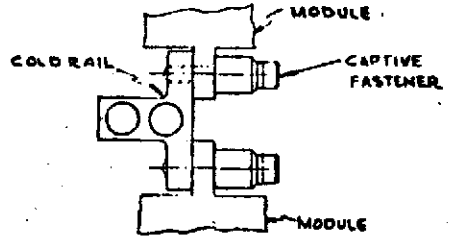

DUAL PASS COLD RAIL

MODULE ARRANGEMENT
100 AMPERE-HOUR Ni-Cd
BATTERY

Figure 8.2-1

8.3 Electrical Considerations

As noted in 8.2.2, the Phase B Study Contractors, NAR and MDAC, have been contacted several times for their inputs and comments. (Parenthetically, Messrs Nussberger and Murray have regularly received copies of Grumman reports on this program.) Table 8.3-1 summarizes the information derived to date from these exchanges. It can be seen the two designs are quite different. The only similarities lie in the general voltage range and the total cell-module complement. Although, as noted in 8.2, Grumman feels a configuration like the 7-module rack (Figure 8.2-1) is preferable, no final recommendation can be made until a system design is selected. There are, in fact, certain characteristics of both NAR's and MDAC's systems mitigating against use of such a rack. Some of these are briefly discussed below.

In NAR's system, the fact that only about 100 cells (25 modules) at a time can be high rate charged complicates the switching and control hardware extensively. There exists the question of which group(s) to select for full charge during any light period, the ancillary problem of which group(s) should receive the remainder of the charging energy, and in what sequence or by what criteria such selection is made. Finally, there is the question of whether the selection and sequence should be astronaut controlled, computer controlled or both.

In MDAC's system, the problem basically concerns the parallel-charge, series-discharge scheme. It is difficult to see exactly how this can be implemented. The impact on integration configuration is impossible to predict without further very detailed study. MDAC's charge control scheme is close to the original Grumman proposal.

A summary of a suggested alternate battery configuration is shown in Table 8.3-2. The following key items are noted:

Table 8.3-1

PHASE B STUDY INFORMATION SUMMARY

Item	NAR	MDAC
Bus Voltage	+112V nominal, 3-wire	120 V nominal
Number of Busses (Main)	4	2
Number of Cells (total)	672	672
Number of Modules (total)	168	168
Number of Batteries/Bus (note 4)	2	3
Number of Cells/Battery	84 (note 1)	112 (note 2)
Charging Configuration	(1) charger per group	(4) groups in parallel
Discharge Configuration	-- (note 3)	(4) groups in series
Charge Rate Data	~ 83 amp to ~ 100 cells Depends on solar array cap.	C/2 to C/5
Recharge to 100% SOC	~ Once/8-9 orbits	~ Once/day
Depth of Discharge/Orbit	~ 6% (Crew Night) - 11% (Crew Day)	15% Av., 35% Max.
Charge Control	Not Stated	V/T, each cell, First cell up Reversal only
Monitoring/Reconditioning	Part of Charger	
Misc. Data	o Loads = 19.6 KW/24 Hr. Av. 15 KW/24 Hr. Min. 14-hr. Crew Day 25.3 KW-Sun 19.9 KW-Eclipse 10-hr. Crew Rest 16.5 KW-Sun 11.1 KW-Eclipse o ±112 V array construction o ~ 2500 ft.^{2} (16-17 KW) avail. for charging o $2\frac{1}{2}$-yr. life o Excess array capability switched to other cells after end of high rate charge	o Array norm. to sun-two-gimbal system o Charge termination on V/T limit o Charger tests batt. for V/T limit every 30 sec. after termination while in sun. o Solar Array Capability ~ 2X peak load o Cell sampling rate: 1-5 minutes o Array has logic-controlled partial shunt reg.

NOTES:

1. Consists of (3) 20-cell groups and (1) 24-cell group
2. Consists of (4) 28-cell groups
3. Batteries are permanently tied to bus
4. 100% redundancy noted by both groups.

SUGGESTED ALTERNATE BATTERY SYSTEM

Item	Description	Remarks
Bus Voltage	120 V - 145 V	112 V min. equip.
Number of Busses (Main)	2	
Number of Cells (Total)	576	1/3 redundancy
Number of Modules (Total)	144	
Number of Batteries/Bus	3	Each battery consists
Number of Groups/Battery	4	of (4) 6-module groups
Charging Configuration	1 Charger/Group	
Discharge Configuration	Same as Charge	
Charge Rates	83.3A (C/1.2) max.	Step-Programmed
	50A (C/2)	Const. Curr.
	20A (C/5)	C/20 considered out
	5A (C/20)	off
Recharge to 100% SOC (1)	Every orbit (2)	115% min. return
Depth of Discharge (1)	22.5%	33.5% for 2 batt/bus
Charge Control	V/T each group	V/T steps to next lower curr
	Aux. Electrode Each Cell	1st aux. elect. up
		steps to cut off
Monitoring/Reconditioning	Part of Charger	As Required
Charge Power Requirements(1)	25 KW (12.5 KW/bus)	Non-diss shunt switching regulator

NOTES:

1. Based on 25 KW Space Station Load, measured at user equipment
2. One battery charged at a time at max. rate. As current steps, excess capability is released to next battery. Computer used to monitor and control excess array switching, and to program chargers to accomodate.

- o Full recharge occurs each orbit without undue solar array sizing penalty (Array same size as MDAC's, and only ~ 20% larger than NAR's)
- o Smaller cell-module complement for lighter weight
  - Maximum depth of discharge (DOD) less than average design figure for this program
  - Maximum DOD for loss of two batteries less than design limit.

This system uses the preferred mechanical configuration, but in a 6-module rack. Each rack would contain its own charge control electronics and such other circuitry (monitoring, reconditioning) as may hereafter be found necessary. A central computer routs the available solar energy to each battery and battery group as previous batteries/groups free its. A more detailed explanation of this is shown in 9, where this system is recommended.

9.0 CONCLUSIONS

It is concluded that a 4-cell, 100 Ampere-Hour, Nickel-Cadmium battery module can be built, and integrated with Space Station Electric Power Systems and Environmental Control Systems (for cooling). It is further concluded that such a module may be mounted with charge electronics built and configured consistent with the recommendations of NASA/MSC Contract NAS 9-10411, "Evaluation of New Approaches to Packaging of Power Assemblies for Use in a Space Environment".

9.1 Specific Findings

Of the basic ground-rules, only one -- weight--is still in question. The present module design, in its final form, with cells installed will weigh 43 pounds, 3 pounds above the design goal.

The assumption of 16 watts/cell worst case orbital average heat generation rate appears high. From the data, actual "live cell" temperature rises were only about 2/3 of the worst case predictions. Final cell data will be obtained from Parametric and Life Cycle Tests.

It was decided that incorporation of reconditioning hardware onto the module would impose too severe a thermal problem, and might impair module reliability if the permanently connected circuitry were to fail. A better choice seemed to be to utilize centralized reconditioning, either on-board, or in ground support facilities. Reconditioning them becomes a maintenance procedure, and requirements would be determined from the results of Life Cycle Tests.

Since the completion of the initial work on this module, it has been found that auxiliary, oxygen-sensing electrode control is probably not feasible for cells of this size, since no adequate electrode design exists. Alternative methods are being explored, and will be reported in the cell development and charge control reports. It will be a constraint on these alternatives that there be no major effect on module structure or cell heat generation.

The package selected was the "Flat-Pack", long, thin design (see Figure 6.1-19, et al). This design meets the thermal, mechanical, electrical and integration requirements generally. Exceptions, minor in nature, are noted in the body of this report.

APPENDIX

HEATER CELL DESIGN

1.0 BACKGROUND - Originally the heater cells were to be devices similar in thermal resistance and mass, and physical size to actual 100 A.H. cells, but which were not electrochemically active. It was finally decided to use the present design herein described since the live cell with embedded heater could more accurately reflect the thermal properties of real cells.

2.0 DESIGN DESCRIPTION - Four (4) cells (S/N 18 through 21), and, later, two (2) additional cells (S/N 30 and 31), were built in accordance with the design layout shown in Figure A1. This sketch shows how 8-mil Inconel 601 expanded (mesh) material was interwoven among the active plates to form the heater. Also shown is the manner in which the heater material is connected to two 25-Ampere terminal seal assemblies. Except for the necessary reduction in plate quantity to allow for the heater, the cell design was the same as the baseline design, Development Group I.

Each heater was carefully adjusted so that maximum voltage drop at maximum required power (25.0 watt/cell) would be less than 1.00 volt to avoid electrochemical activity when only the heater was used. This requirement resulted in a nominal design heater resistance of 0.04 Ω ($25\ \text{amp}^2 \times 0.04\ \Omega = 25$ watt; $25\ \text{amp} \times 0.04\ \Omega = 1.00$ Volt). Actual values for the cells used in the battery module are given below:

Cell S/N	Heater Resistance, ohm
19	0.03880
20	0.03880
30	0.03805
31	0.04155

(Values were measured using a Kelvin double bridge, and verified by VOI measurements during heater tests.)

Typical overall cell dimensions are shown in Figure A2.

HEATER CELL INTERNAL SCHEMATIC

A. ARRANGEMENT OF PLATES, HEATERS AND SEPARATOR

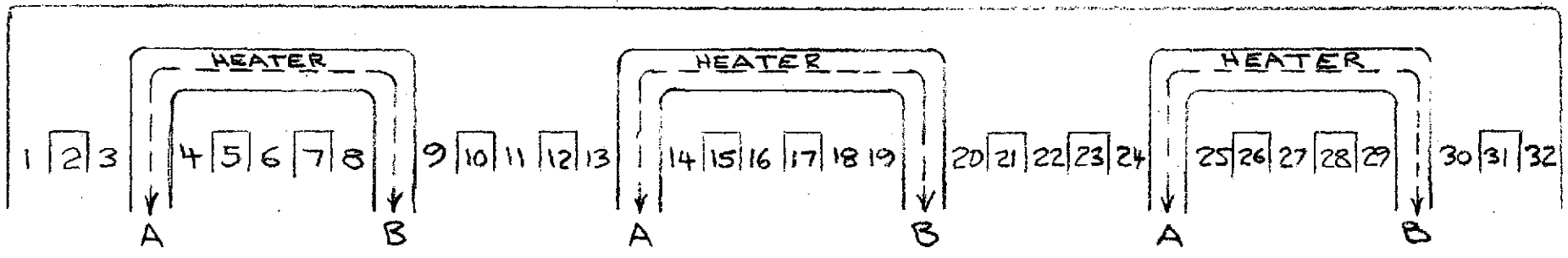

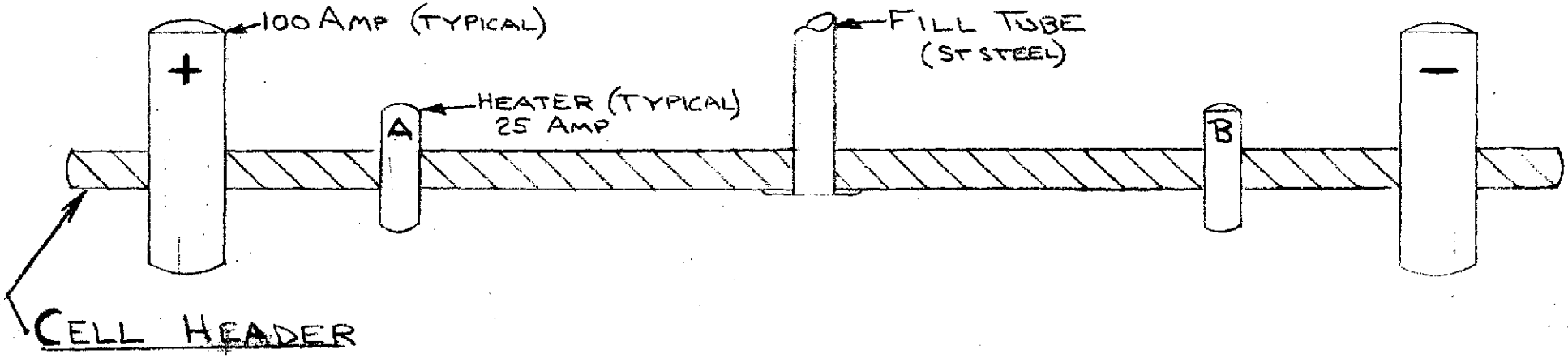

B. ARRANGEMENT OF HEADER AND TERMINALS

174

NOTES:

1. ODD NUMBERS ARE NEGATIVE PLATES
2. EVEN NUMBERS ARE POSITIVE PLATES
3. SOLID LINES ARE SEPERATOR
4. HEATER SEPERATOR MATERIAL - FT 2140 POLYPROP
5. PLATE AND CAN SEPERATOR MATERIAL - 250S NYLON PELLON
6. SEPARATOR THICKNESS = 0.010 INCH
7. PLATE THICKNESS -- 0.028 INCH
8. HEATER THICKNESS -- 0.008 INCH (EXPANDED INCONEL)

FIGURE A:

HEATER CELL

TYP. DIMENSIONS

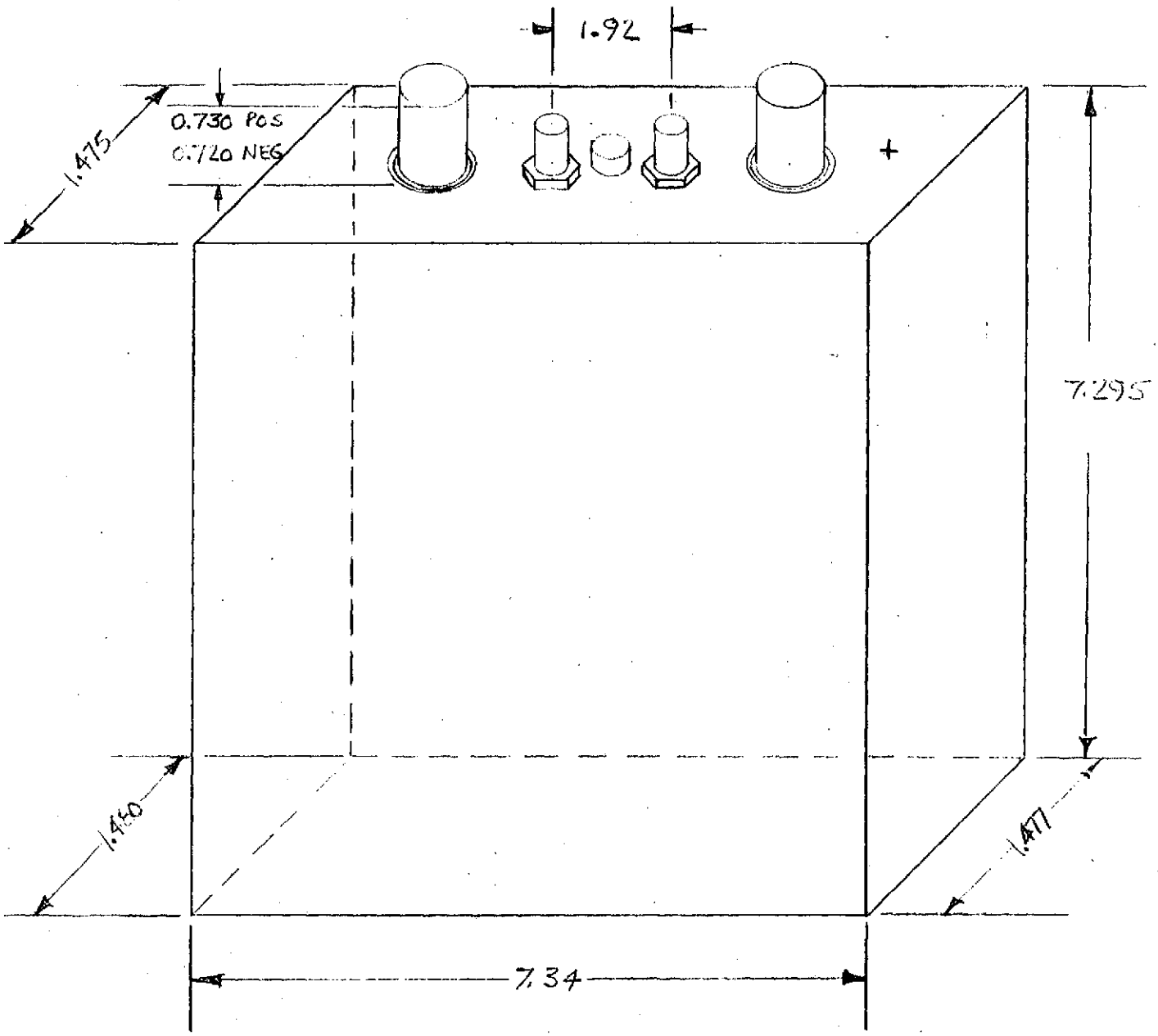

FIGURE A-2

APPENDIX

3.0 HISTORY - Although six (6) cells were constructed, only four were used in the engineering model of the 100 A.H. Battery Module. S/N 21 showed very poor performance during the seller's tests, and was accordingly not shipped. S/N 18 was damaged beyond repair in shipment due to improper packaging. (The fill tube seal was broken, allowing contamination.) This latter unit was returned to the seller.

S/N 30 and 31 were built to replace S/N 18 and 21. Table I shows this resulted in sizable differences in:

- Active Material Weight
- Negative to Positive Ratio
- Electrolyte Ratio

The module was thus fabricated with two distinctly different cell designs. For thermal testing, this fact is not especially important. However, electrical data validity is considerably impaired, especially in the module (see 7.3). Neither the later Design Verification Test model, nor any subsequent modules will be built with this kind of initial difference among cells.

4.0 ELECTRICAL DATA (OTHER THAN CYCLING TESTS) - Table II contains a summary of all electrical data taken at the seller's facility, and non-cyclic data taken at Grumman. (Cyclic data is reported in 7.3.) It should be noted that initial capacity is only 75 to 85 Ampere-Hours. Thus, "50%" depth-of-discharge (DOD), based on 100 Ampere-Hours, is actually 59 to 67%. Similar statement are true for "30%" and "12%" DOD's.

TABLE I

TABULATION OF HEATER CELL DESIGN DATA

Description	Unit	Cell S/N			
		19	20	30	31
Date of first discharge at seller		2/26/71	2/26/71	5/14/71	5/14/71
Positive group weight	Gram	962	962	999	999
Negative group weight	Gram	1204	1204	1140	1140
Positive active material	Gram	419	419	456	456
Negative active material	Gram	603	603	496	496
Ratio of neg. to pos. active material	--	1.44	1.44	1.09	1.09
Core weight	Gram	2369	2366	2306	2305
Electrolyte	Gram	474	474	418	418
Electrolyte	CC	362	362	319	319
Elect. ratio (wt. elect./wt. core x 100)	%	20	20	18.1	18.1

177

TABLE I

TABLE II

HEATER CELLS ELECTRICAL DATA

TABLE II

CHARGE

Cell S/N	Date	Current Amp	Pressure (PSIG) Start	End	Δ P	Volt (Final)	Temperature Start	End	Δ F	Input AH	Remarks
19	-	-	-	-	-	-		-	-	-	Electrical operation starts with A discharge
20	-	-	-	-	-	-		-	-	-	
30	-	-	-	-	-	-		-	-	-	
31	-	-	-	-	-	-		-	-	-	
19	3/1/71	30.0	-	-	-	1.50	75	(Amb)	-	120.0	
20	3/1/71	30.0	-	-	-	1.51	75	(Amb)	-	120.0	
30	5/15/71	30.0	-	-	-	1.68	69	86	+17	120.0	
31	5/15/71	30.0	-	-	-	1.69	69	86	+17	120.0	
19	3/9/71	30.0	-	-	-	1.43	75	(Amb)	-	135.0	
20	3/9/71	30.0	-	-	-	1.43	75	(Amb)	-	135.0	
30	5/18/71	30.0	-15	-3	+12	1.41	75	112	+37	105.0	
31	5/18/71	30.0	-15	-3	+12	1.41	75	106	+31	105.0	
19	5/5/71	10.0	-15	+15	+30	1.47	75	78	+3	135.0	
20	5/5/71	10.0	-15	+17	+32	1.47	75	78	+3	135.0	
30	5/27/71	10.0	-15	-7	+8	1.45	79	84	+5	140.0	
31	5/27/71	10.0	-15	-9	+6	1.45	79	88	+9	140.0	
19	5/10/71	OCV	-	-15	-	1.226	-	74	-		OCV after 0.2 Ah drain → 16 hours taken after 24 hours at OCV
20	5/10/71	OCV	-	-14	-	1.221	-	74	-		
30	5/28/71	OCV	-	-15	-	1.234	-	73	-		
31	5/28/71	OCV	-	-15	-	1.235	-	73	-		

AFTER INCORPORATION IN MODULE

IN FULL CAPACITY CYCLES ONLY

19	6/26-6/28/71	10.0	-14	-1	+13	1.517	75	79	+4	157.8	
20	6/26-6/28/71	10.0	-15	-10	+14	1.471	75	79	+4	157.8	
30	6/26-6/28/71	10.0	-15	+3	+18	1.463	75	79	+4	128.6	
31	6/26-6/28/71	10.0	-15	+3	+18	1.461	75	79	+4	128.6	
19	7/15-7/19/71	10.0	-13	-6	+7	1.479	77	81	+4	118.0	
20	7/15-7/19/71	10.0	-15	-5	+10	1.477	77	81	+4	118.0	
30	7/15-7/19/71	10.0	-15	+6	+9	1.510	77	81	+4	118.0	
31	7/15-7/19/71	10.0	-15	0	+15	1.505	77	81	+4	118.0	
19	8/17-8/18/71	10.0	-13	+12	+25	1.502	75	80	+5	95.0	
20	8/17-8/18/71	10.0	-15	+19	+34	1.500	75	80	+5	95.0	
30	8/17-8/18/71	10.0	-14	+12	+26	1.510	75	80	+5	95.0	
31	8/17-8/18/71	10.0	-15	+8	+23	1.501	75	80	+5	95.0	

DISCHARGE

Cell S/N	Date	Current Amp	Pressure (PSIG) Start	End	Δ P	Output To 1.0 V	to 0.9 V	Temperature (°F) Start	End	Δ F	Remarks
19	2/26/71	50.0	-	-	-	-	37.4(*)	70 (Amb.)		-	Discharge after activation
20	2/26/71	50.0	-	-	-	-	37.4(*)	70 (Amb.)		-	
30	5/14/71	50.0	-	-	-	-	26.6(*)	70 (Amb.)		-	*Not full capacity at seller
31	5/14/71	50.0	-	-	-	-	23.4(*)	70 (Amb.)		-	
19	3/1/71	50.0	-	-	-	75.0	-	75 (Amb.)		-	Cap. cycle #1
20	3/1/71	50.0	-	-	-	75.0	-	75 (Amb.)		-	Cap. cycle #1
30	5/15/71	50.0	-	-	-	-	75.8	85	97	+12	At Seller
31	5/15/71	50.0	-	-	-	-	76.5	85	95	+10	
19	3/9/71	50.0	-	-	-	86.0	-	75 (Amb.)		-	Capacity test
20	3/9/71	50.0	-	-	-	85.0	-	75 (Amb)		-	Capacity test
30	5/17/71	50.0	-13	-15	-2	-	78.0	100	103	+3	At Seller
31	5/17/71	50.0	-13	-15	-2	-	76.5	94	102	+8	
19	5/7/71	50.0	-7	-11	-4	87.5	-	80	94	+14	Conditioning
20	5/7/71	50.0	-4	-8	-4	87.5	-	80	93	+13	and capacity
30	5/27/71	50.0	-9	-14	-5	80.0	81.5	90	98	+8	check at
31	5/27/71	50.0	-10	-14	-4	80.0	81.5	87	97	+10	Grumman
19											
20											
30											
31											
19	7/14/71										
20	7/14/71										Was Not
30	7/14/71										Determined
31	7/14/71										
19	8/16/71	50.0	-13	-13	0	0.900 V		55	55	0	After 28 days on open circuit stand
20	8/16/71	50.0	-15	-15	0	1.035 V	59.0	55	55	0	
30	8/16/71	50.0	-13	-13	0	1.156 V	A.H.	55	55	0	
31	8/16/71	50.0	-14	-14	0	1.157 V		55	55	0	
19	9/16/71	50.0	-13	-13	0	0.973 V		33.7	33.9	+.2	After 29 days on orbital cycling and open circuit stand
20	9/16/71	50.0	-13	-13	0	0.897 V	59.0	33.7	33.9	+.2	
30	9/16/71	50.0	-10	-10	0	1.116 V	A.H.	33.7	33.9	+.2	
31	9/16/71	50.0	-8	-13	-5	1.126 V		33.7	33.9	+.2	
19,20, 30,31	9/16/71	0.2 Ah drain/cell to zero volts. Then each cell shorted with short wire.									To conduct proof press test

APPENDIX

The design details for the four (4) heater cells used in the prototype battery module thermal bench tests are described below.

These cells are each "live" 100 A.H. size Ni-Cd cells which include a 25 watt, 1 volt dc inconel heater assembly. Four of these cells were fabricated by Eagle-Picher for Grumman. The cells are basically EP RSN 110B cells which have been modified to permit their operation with a dc heater. These modifications include:

a) the addition of an expanded Inconel heater assembly (refer to Figure and the discussion below),

b) the addition of two 25 ampere rated terminals to the normal 100 A.H. header assembly to accomodate the heater leads,

c) the addition of a stainless steel pressure tap and gauge to the normal header assembly,

d) the removal of one (1) positive plate and two (2) negative plates to dimensionally permit the inclusion of the heater assembly, and,

e) the net addition of three (3) layers of 1^{o} mil separator material.

Inconel 601 was selected as the heater material for its inertness to KOH, low variation of resistance with temperature, and ready availability. Expanded 8 mil thick Inconel 601 sheet (fabricated by the Exmet Corporation, Bridgeport, Connecticut) was purchased by Eagle Picher per Grumman's direction.

The sheet stock was expanded to a pattern which would provide the necessary unit resistance required by the heater design. This

unit resistance was chosen such that the resistance of a 6 inch wide by 12 3/8 inch long strip would be 0.120 ohms in the long direction. Each of these strips are folded so as to form two 6 inch x 6 inch heater plates (See Figure A1). Three of these U-shaped heater elements are then electrically paralleled to form the final heater assembly with a total impedance of 0.040 ohms (consistent with 25 watts at 1 volt). This low voltage capability was required to preclude the possiblity of electrolyzing the electrolyte.

The heater elements are spaced within the cell as shown in Figure A1 so that the generated heat will be distributed uniformly within the plate stack.

Table II lists the serial numbers of each of the completed heater cells, its measured dc impedance (on a four lead Kelvin bridge), and the electrical capacities obtained in bench tests during check-out cycling at Grumman.

TABLE III

Heater Cell

Data

Serial #	Impedance, ohms	Capacity (C/2)
19	.03880	87.5
20	.03880	87.5
30	.03805	80.0
31	.04155	80.0